Development and Characterization of Inhibitors of the *E. coli* Methionine Aminopeptidase

Dissertation

zur Erlangung des Grades des Doktors der Naturwissenschaften der
Naturwissenschaftlich-Technischen Fakultät III
- Chemie, Pharmazie, Bio- und Werkstoffwissenschaften -
der Universität des Saarlandes

vorgelegt von

Rolf Schiffmann

Saarbrücken 2005

Tag des Kolloqiums:	19.05.2006
Dekan:	Prof. Dr. K. Hegetschweiler
Berichterstatter:	Prof. Dr. R. W. Hartmann
	Dr. C. D. Klein

MEINEN ELTERN

IN DANKBARKEIT

Man findet oftmals mehr, als man zu finden glaubt...

Pierre Corneille

Diese Arbeit entstand unter der Anleitung von Prof. Dr. R. W. Hartmann und Dr. C. D. Klein in der Fachrichtung Pharmazeutische und Medizinische Chemie der Universität des Saarlandes von Mai 2002 bis November 2005.

So far, the content of this thesis has been partly published in or submitted to the following journals:

Klein, C. D.; Schiffmann, R.; Folkers, G.; Piana, S.; Rothlisberger, U., Protonation states of methionine aminopeptidase and their relevance for inhibitor binding and catalytic activity. Journal of Biological Chemistry 2003, 278, (48), 47862-47867.

(chapter 4.3.3)

Schiffmann, R.; Heine, A.; Klebe, G.; Klein, C. D., Metal Ions as Cofactors for the Binding of Inhibitors to Methionine Aminopeptidase: A Critical View of the Relevance of *In Vitro* Metalloenzyme Assays.

Angewandte Chemie Int Ed Engl 2005, 44, (23), 3620-3623.

(chapters 4.5, 4.6)

Schiffmann, R.; Neugebauer, A.; Klein, C. D., Metal-Mediated Inhibition of *E. coli* Methionine Aminopeptidase: Structure-Activity Relationships and Development of a Novel Scoring Function for Metal-Ligand Interactions.

Journal of Medicinal Chemistry 2006, 49, (2), 511-522

(chapter 4.4.5)

TABLE OF CONTENTS

1 Introduction

Infectious and parasitic diseases like HIV/AIDS, hepatitis, tuberculosis and malaria represent the second highest cause of death and are responsible for 20 % of the mortality worldwide[1]. In Africa, this proportion even increases to 65 %. The communicable diseases mentioned are followed by malignant neoplasms (13 % worldwide). In spite of the development of new and the improvement of existing drugs, these diseases together account for every third death worldwide, equal to cardiovascular diseases. In addition, the emergence of antibiotic-resistant and multi-drug resistant bacteria makes the situation worse and is nowadays a serious challenge to the clinical treatment of infections, particularly in hospitals. Many genera of gram-positive and gram-negative bacteria have developed resistance to commonly used drugs such as ß-lactams, quinolones, aminoglycosides and macrolides. Especially *Streptococcus pneumoniae*, *enterococci*-strains and *Staphylococcus aureus* are problematic bacteria.

The problem of drug-resistance also appears in the treatment of cancer. Therefore, new targets in drug development are clearly needed. As different as these diseases are, there is an ubiquitous enzyme related to all of them: The methionine aminopeptidase (MetAP). This metal-dependent enzyme is involved in the N-terminal processing of proteins and essential for every organism, making it a target for the development of new antibiotic, antifungal or antiparasitic drugs. Besides, certain inhibitors of the MetAP can inhibit angiogenesis, an important step in cancer growth. This underlines the important role of this enzyme for the proper functioning of proteins and thus of whole cells. Insight into the mode of action of these inhibitors and characterization of the enzyme will not only be useful for the further development of anti-cancer drugs but will also lead to a better understanding of the physiological processes involved in the development of cancer and in cancer growth.

Another aspect showing the importance of this enzyme is its use in the biotechnology industry: Often, large amounts of purified proteins are required for further testing (for example granulocyte-colony-stimulating factor, G-CSF[2]) or are to be produced as drugs in the pharmaceutical industry like insulin. Many of the recombinant proteins for therapeutic uses are based on the secretory products from mammalian cells. An intracellular heterologous production of these proteins in *E. coli* may result in a product with an unphysiological methionine at the N-terminus. This methionine should be removed in order to avoid potential immunogenicity. Chemical removal with cyanogen bromide under relatively strong acidic conditions essentially allows any residue to be adjacent to the methionine. Unfortunately, this

reaction is not terminal specific and therefore limited to proteins without an internal methionine. Another option is the use of exopeptidases that cleave amino acids sequentially from the N-terminal end of proteins. However, proteolysis and digestion of the rest of the protein are unwanted side effects in this case. Here, the use of MetAP is clearly useful. This can be done either by overexpression of MetAP with the protein of interest in the same cell (thus ensuring removal of methionine *in situ*) or treatment of the protein with purified MetAP after expression and isolation. The success of these methods was demonstrated with interleukin-1ß[3], interleukin-2 and ricin A both *in vitro* and *in vivo*[4]. Insufficient N-terminal processing due to the substrate specificity of the MetAP can be adjusted with certain mutations, used for example in the production of human haemoglobin[5]. Even MetAPs stable against heat and chemical denaturants are already known[6].

The diverse aspects clearly show the high potential of MetAPs and the relevance and importance of research done with these enzymes. This work will hopefully be useful for the further characterisation of the enzyme and especially for the development of inhibitors as potential drugs.

2 The Target: Methionine Aminopeptidase (MetAP)

Enzymatic activities that remove amino-terminal residues of methionine from certain proteins have been observed in both prokaryotes[7, 8] and eukaryotes[9-11]. It became evident that certain enzymes, the methionine aminopeptidases, play a much more important role than other unspecific exopeptidases and are responsible for the largest part of N-terminal methionine-removal. Lower and higher eukaryotes as well as bacteria seem to share a similar N-terminal protein processing machinery, indicating universality of this system[12].

2.1 Classification of MetAPs

MetAPs exist in two forms (type-I and type-II) that can be further distinguished (see Fig. 2-1). Whereas eubacteria express only type-I and archaeabacteria only type-II MetAPs, eukaryots posess both types.

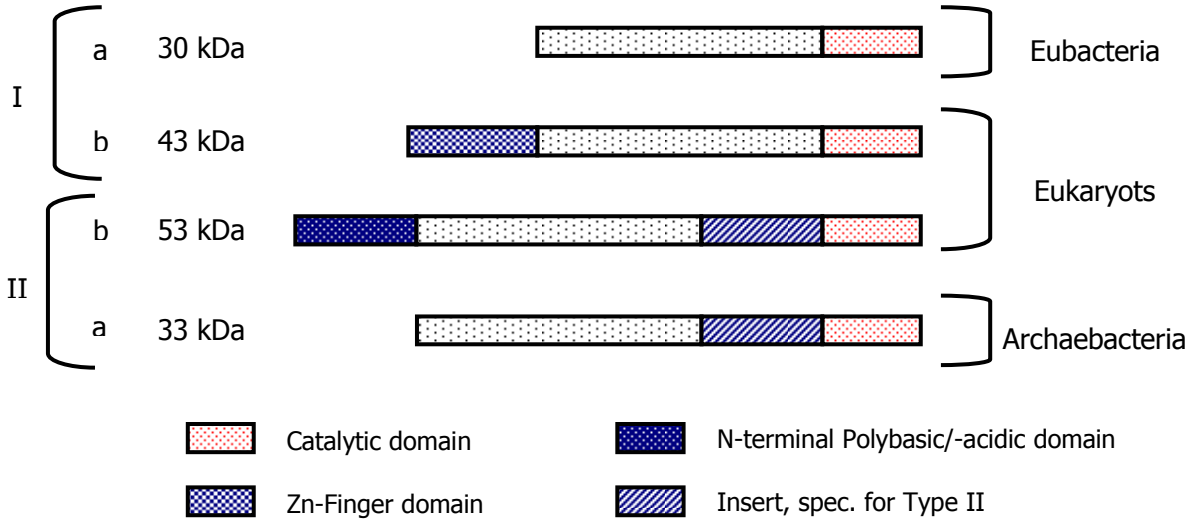

Fig. 2-1 Classification of MetAPs

Type-I and type-II can be distinguished by an insert of about 60 amino acids, forming a helical subdomain whose function is still unknown. Thus, enzymes resembling the eubacterial form lacking this insert are designated type-I, while those with the insert (thus related to the

first porcine MetAP described) are designated type-II. Moreover, MetAPs exist with and without an N-terminal extension, whose presence is the basis for additional differentiation: To further distinguish the eukaryotic MetAPs with the extension from those MetAPs without, those enzymes with the extension are labeled as type-Ib and type-IIb. Thus, eubacterial MetAPs (without the extension) have been designated type-Ia while archaebacterial MetAPs (also without the extension) are designated -IIa.

2.1.1 N-terminal Extensions

Some type-I and type-II MetAPs display large N-terminal extensions that contain either zinc-finger motifs or poly-lysine and aspartic acid blocks[13-15]. The N-terminal extension of yeast MetAP-I (yMetAP) for example displays a sequence resembling zinc-finger domains. This indicates a possible protein-nucleic acid or protein-protein interaction and is believed to have a function in association with ribosomes[16]. In contrast, the human enzyme lacks the consensus zinc-finger sequence and instead contains the extended runs of basic and acidic residues. These N-terminal extensions are not required for *in vitro* enzymatic/catalytic activity but are important for the *in vivo* function. The N-terminal domains of the type-II enzyme seem to regulate the level of protein synthesis. MetAP-II(b) is a glycoprotein and was initially described in mammalian cells as p67[17], a cellular protein that associates with (and inhibits phosphorylation of) the eukaryotic translation initiation factor 2α (eIF2α). eIF2 is required for protein synthesis[18]: The formation of the initiation complex plays a significant part in the initiation of peptide chain synthesis. This process is blocked when eIF2 is phosphorylated, which happens in various stress-related situations and leads to a down regulation of the cellular protein synthesis. Phosphorylation of eIF2α blocks the initiation of translation and inhibition of this phosphorylation consequently stimulates the initiation[15]. The inhibition of this phosphorylation is a function of the N-terminal domain of MetAPs. The presence of terminal carbohydrate moieties is required for the “POEP-” (protection of eIF2α phosphorylation) activity of MetAP. The protecting property can be modulated by p67-deglycosylase (p67-DG). Imbalance of p67 and p67-DG (a protein controlling the activity of p67 by removal of the p67- necessary glycosyl moiety) can lead to either cancerous growth or cell death[19] and the balance between MetAP and p67-DG will possibly determine the fate of the cells whether they will grow or induce apoptosis[19]. In summary, MetAP-II is a

bifunctional protein which catalyzes the cleavage of N-terminal methionine from nascent polypeptides and affects translational initiation through its ability to associate with eIF2α[20].

The N-terminus of MetAP-II is also able to interact with other proteins such as S100A4, a protein that regulates tumor metastasis and a variety of cellular processes. The binding of S100A4 does not affect *in vitro* MetAP activity but could modulate the N-terminal processing of nascent substrates by changing their localization[21].

The presence of the N-terminal domains in the eukaryotic isoforms implies that these enzymes have (perhaps additional and not yet known) functions that are not required in prokaryotes. Although many efforts have been made to understand the functional differences of the two types of MetAPs (see 2.3.5.2 Yeast MetAPs), the role of each type of MetAP is not yet entirely clear. *In vivo* substrate differences as well as interactions with other proteins have been described. Although the type-I MetAP seems to play a more important role in methionine metabolism, the two types of MetAPs can generally substitute each other.

2.1.2 Evolution of Different MetAPs

The phylogenetic tree shows that the present-day type-I and type-II enzymes of eukaryotes are more closely related to the eubacterial and archaeal forms, respectively, than they are to each other. Due to the phylogenetical closeness of bacterial and eukaryotic MetAP-I (see Fig. 2-2), it seems likely that the eukaryotic MetAP-I has developed from eubacterial MetAP-I in the course of evolution according to the endosymbiont-theory.

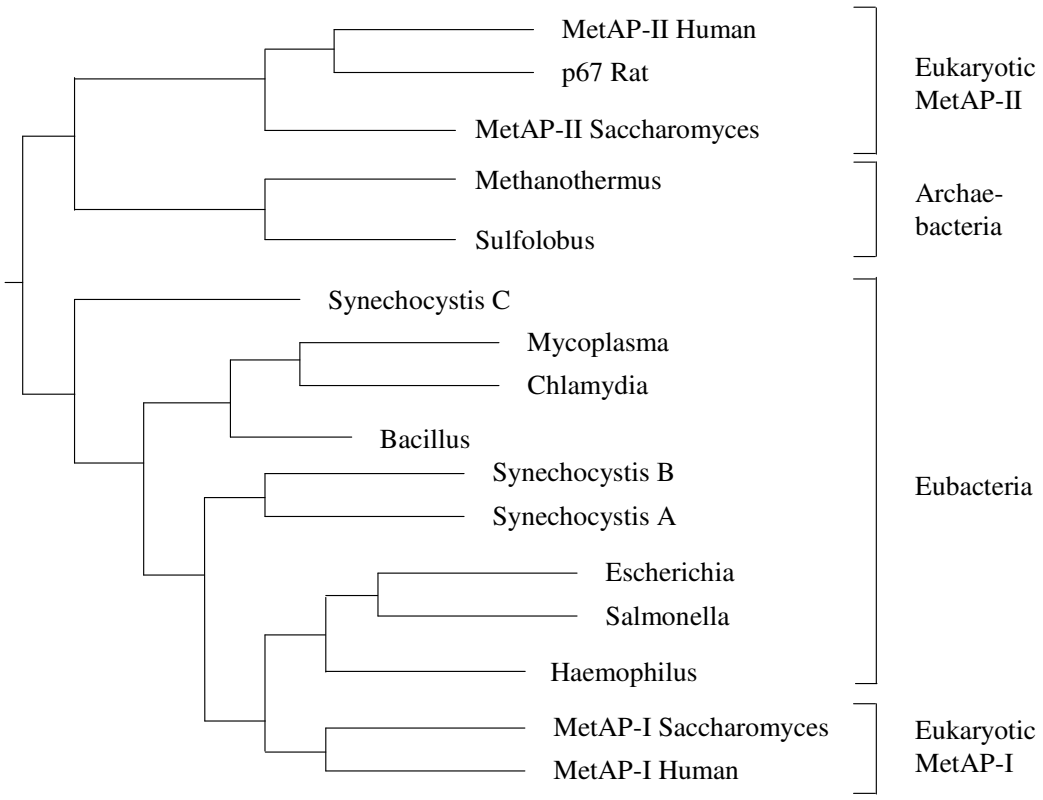

Fig. 2-2 Evolutionary tree of MetAPs[22]

2.2 Physiological Role of MetAPs

2.2.1 Protein Synthesis in Eukaryotic and Prokaryotic Cells

Although there are natural differences between eukaryotic and prokaryotic protein synthesis such as the size of ribosomes (for a review see Ref.[23]), the cellular machinery for protein

synthesis has been highly conserved and a common principle exists: Proteins are specified by mRNA after transcription of DNA and synthesized on ribosomes as depicted in Fig. 2-3.

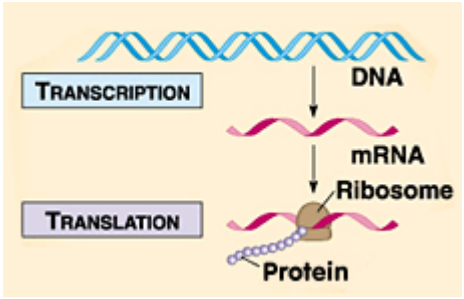

Fig. 2-3 Schematic protein synthesis (©1999, Addison Wesley Longman Inc.)

Protein synthesis is normally initiated with the AUG codon that encodes for methionine (in the cytosol of eukaryotes) or formyl-methionine (in prokaryotes, mitochondria, and chloroplasts). Rare exceptions are, for example, the initiation with phenylalanine or tryptophane in prokaryotes[24, 25] or with glutamine both in prokaryotes and eukaryotes[26, 27]. The amino acids are transported to the ribosomes via activated tRNAs carrying the corresponding anticodons. After initiation of the complex, the polypeptide chain is elongated according to the coding sequence of the mRNA as shown in Fig. 2-4.

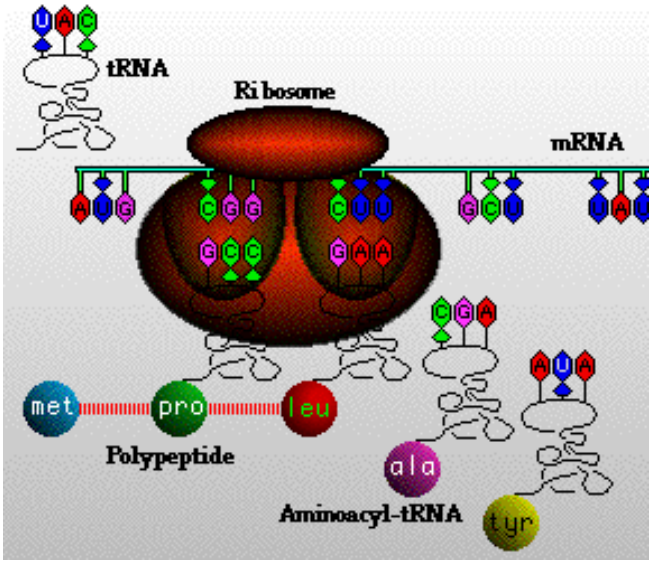

Fig. 2-4 Protein synthesis on a ribosome (taken from http://tidepool.st.usm.edu/pix/protsynth.gif)

2.2.2 Methionine Metabolism and N-end Rule

Methionine is the most "expensive" amino acid to synthesize[28] and plays a key role among the 20 amino acids which are incorporated into proteins because of its involvement in the initiation of translation. Thus, it serves as a signal measuring the general health of a cell and couples the translation to the metabolism and the chemical environment of a cell. This role appears to be ubiquitous[29]. Methionine metabolism is also an important aspect of cellular physiology and methionine is involved in oxidative stress, methylation, gene expression and has been linked to cell cycle progression. In *E. coli*, the metabolism of methionine is now well-known and all the important enzymes have been characterized: Methionyl-tRNA synthetase (EC 6.1.1.10) and Methionyl-tRNA formyltransferase (EC 3.5.1.27) are involved in the formation of N-formyl-Met-tRNA, peptide deformylase (EC 3.5.1.27) cleaves the formyl group from nascent formyl-methionine peptides and MetAP (EC 3.4.11.18) removes the N-terminal methionine (see Fig. 2-5).

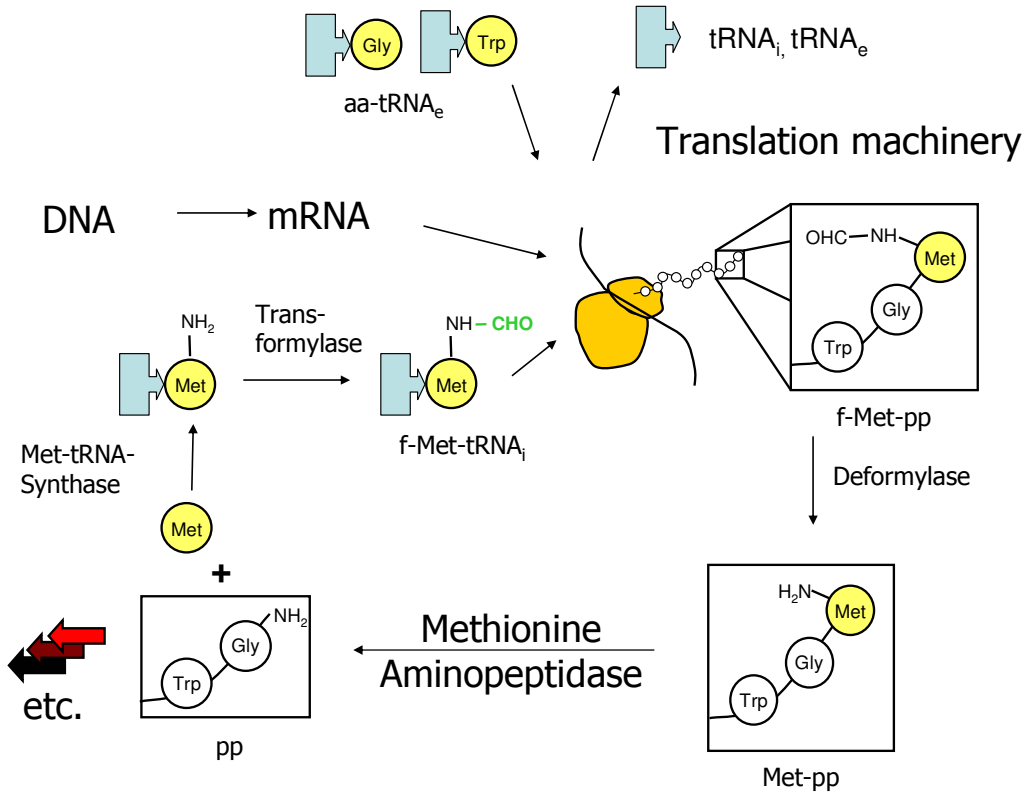

Fig. 2-5 Methionine cycle of eubacteria. pp, polypeptide; aa, amino acyl; $tRNA_i$, initiator tRNA; $tRNA_e$, tRNAs for peptide elongation

For a significant fraction of the intracellular proteins, the amino-terminal methionine is removed enzymatically after the initiation of translation (about 50-60 % in the case of *E. coli*[30]) by the MetAP. This process is mostly dependent on the adjacent residue. The (exposed) N-terminal moiety plays an important role in protein recognition by other enzymes and therefore MetAP activity is a determinating factor for further protein processing (such as acetylation and myristoylation), protein stability and intracellular protein localization. Cotranslational removal of the initiator methionine occurs when the nascent chain is still quite short (20-40 residues) and presumably in conjunction with N_α-acetylation[31] but after deformylation[32]. The absence of the N-terminal domains in the eubacterial and archaeal isoforms (type-Ia and -IIa) is consistent with the view that the removal of methionine in these organisms is largely a post-translational event.

Statistical analysis of N-terminal methionine removal in both pro- and eukaryotic cytosolic proteins demonstrated that the penultimate residue determinates the fate of the methionine and that some amino acids inhibit and some others cause its removal[33]. The same removal-specificity for the N-terminal methionine has also been predicted from mutant cytochrome sequences (altered iso-1-cytochromes *c* from yeast) by Sherman *et al.*[34]. In addition, it has been demonstrated that the half-lives of ßgal proteins in *Saccharomyces cerevisiae* are strikingly different, depending on the nature of the amino acid at the amino-terminus[35]. These findings led to the formulation of the N-end rule:

Stabilizing and destabilizing residues can be distinguished at the N-terminus of a protein. Methionine is considered a stabilizing residue and thus the retention of the initiator methionine acts as a protectant that prevents premature or inappropriate protein degradation. When a newly formed protein is proteolytically processed *in vivo* and exposes one of the destabilizing residues Ile, Glu, His, Tyr, Gln, Asp, Asn, Phe, Leu, Trp, Lys or Arg, this protein is then subsequently targeted for multiple ubiquitination and selective degradation[36]. As a consequence, destabilizing amino acids are generally absent on the N-terminus of relatively long-lived, noncompartmentalized proteins.

This degradative pathway, where amino-terminal recognition of proteolytic substrates is involved, is called the N-end rule pathway, distinguishing it from other proteolytic pathways and ubiquitin-dependent processes. Interestingly, the N-end rule inversely matches the

substrate specificity of MetAPs: N-terminal residues containing a destabilizing amino acid are non-MetAP substrates (see 2.3.1 Substrate Specificity). Thus, any protein that has its N-terminal methionine removed by MetAP will retain a stabilizing N-terminal residue.

2.2.3 Physiological Relevance of MetAP Activity

Methionine is removed from the majority of proteins. This is essential for the further processing such as acetylation or myristoylation and thus MetAPs play a key role in the functional regulation of proteins. Myristoylation has been shown to be required for the proper functioning of several signaling proteins and in targeting towards membranes[37]. The removal of the starter methionine is in some cases also required for biological activity when N-terminal residues have a role in catalysis as for example cysteine in yeast glutamine-fructose-6-phosphate amidotransferase (GFA1)[38].

Taken together, methionine removal is important for proper subcellular localization of proteins, for degradation, protein turnover and for the targeting of proteins to cellular membranes[29, 39]. MetAPs have also been shown to be involved in gene regulation of genes connected with methionine synthesis and to be susceptible to the intracellular methionine concentration[40]. MetAPs and methionine metabolism are linked in several ways, including recycling of methionine, product inhibition, and gene regulation.

The physiological importance of MetAP activity is underscored by the lethality of organisms where all MetAP genes have been deleted or all MetAP gene products are inhibited. This has been shown for *E. coli*, *S. typhimurium* and *S. cerevisiae*[41-43]. Whether this will also be the case in higher eukaryotes cannot be answered yet, but it is likely given the lethality of the yeast double null mutant. As there are only specific inhibitors for MetAP-II available up to now, specific inhibitors of the type-I isoenzyme, potent dual inhibitors or transgenic or knock-out animals will be required to prove this assumption.

2.3 Properties of MetAPs

2.3.1 Substrate Specificity

As yeast null mutants lacking only one type of MetAP can survive[42, 44], the two MetAP types might have largely similar (perhaps redundant) functions. This is supported by the fact that all MetAPs have a similar substrate specificity. The MetAP activity is strictly methionine specific and it is dependent on the radius of gyration of the penultimate residue: The methionine residue is generally removed from proteins where the adjacent amino acid is small and uncharged (glycine, alanine, serine, threonine, cysteine, proline and valine). This has been shown *in vitro* using different substrates but also *in vivo* (see Fig. 2-6):

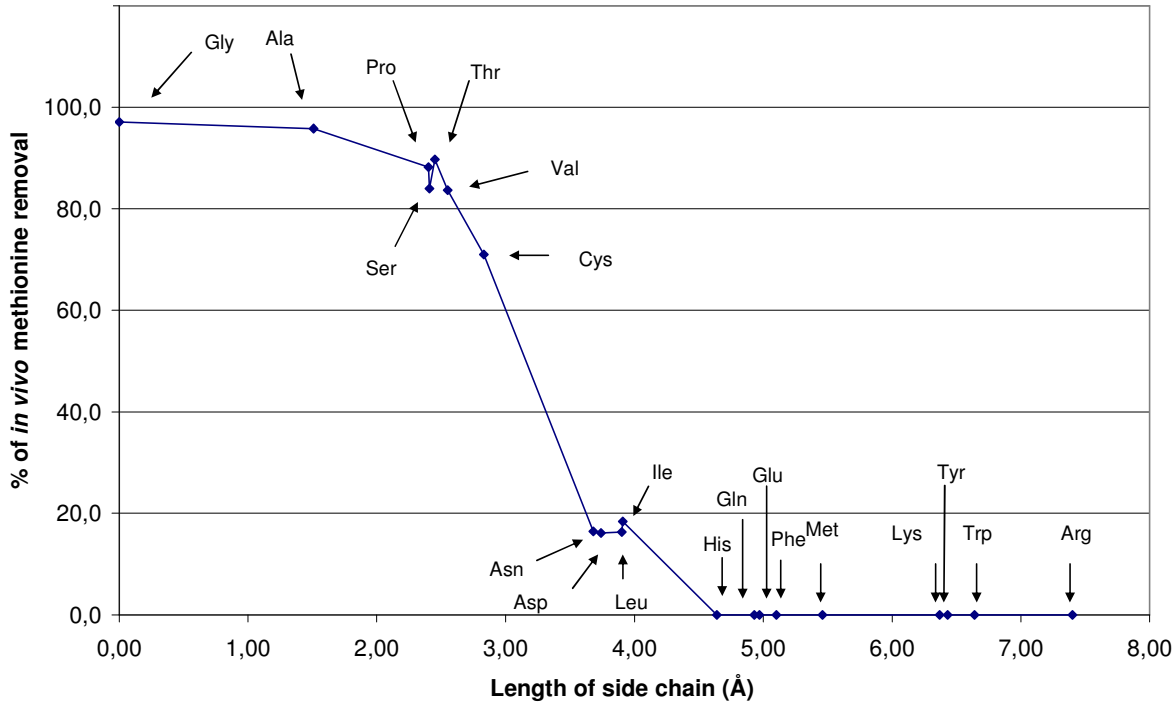

Fig. 2-6 Extent of methionine processing for *E. coli* determined *in vivo* for a protein with a N-terminal sequence (Met)-Xaa-Gln-Val-Ala- with 20 different amino acids for Xaa[45], Length of side chain: Maximal distance between the α-carbon and the most distal non-hydrogen atom of the side chain

In most instances, an adjacent residue with a side chain size (radius of gyration) smaller than 0.129 nm is preferred. For side chain sizes that are larger than 0.143 nm, MetAP is unable to remove the methionine. Thus, only proteins with a stabilizing amino acid (according to the N-end rule) in the penultimate position are substrates of the MetAPs.

It has also been reported that the amino acid in the antepenultimate position has an influence on the MetAP activity. For example, proline is at least partially inhibitory[2, 45], and significant variations occur in MetAP activity among substrates that have identical residues at the first two positions[4]. In a similar fashion, processes like acetylation and myristoylation are also mostly determined by specific (exposed) amino acids but seem to be affected by other effects such as peptide length or downstream residues[46, 47].

E. coli MetAP utilizes only tripeptides or larger substrates and has an absolute specificity for a methionine residue at the amino terminus[4]. However, the third residue (as seen in X-ray structures with bound substrate-like inhibitors) is completely solvent accessible and makes no direct contact with the enzyme[48].

2.3.2 Metal Dependency

MetAPs are metal-dependent enzymes. They have been claimed to be binuclear Co(II) dependent enzymes, but the identity and number of the *in vivo* metal ion is still under debate and is discussed in 4.2.3.5 (Metal Specificity). In short, Co(II), Zn(II), Mn(II), Ni(II) and Fe(II) are possibly relevant *in vivo*. It is not entirely clear whether MetAPs function as mono- or binuclear enzymes. However, it can be stated that Co(II) activates all MetAPs known so far, and that two metal ions are present in all existing MetAP X-ray structures.

2.3.3 Structure of the EcMetAP

The *E. coli* gene encoding this enzyme consists of 264 codons and encodes a monomeric enzyme with a molecular mass of 29,333 daltons[4]. The *E. coli* MetAP (EcMetAP) is a soluble, globular protein.

2.3.3.1 Tertiary Structure

A limited number of folding motifs can be used to describe the three-dimensional architecture of globular proteins. One of these is the pita-bread fold of, for example, the *E. coli* MetAP, a protein scaffold that can support a diverse set of catalytic functions[14]. This structure displays internal pseudo-2-fold symmetry as can be seen in Fig. 2-7.

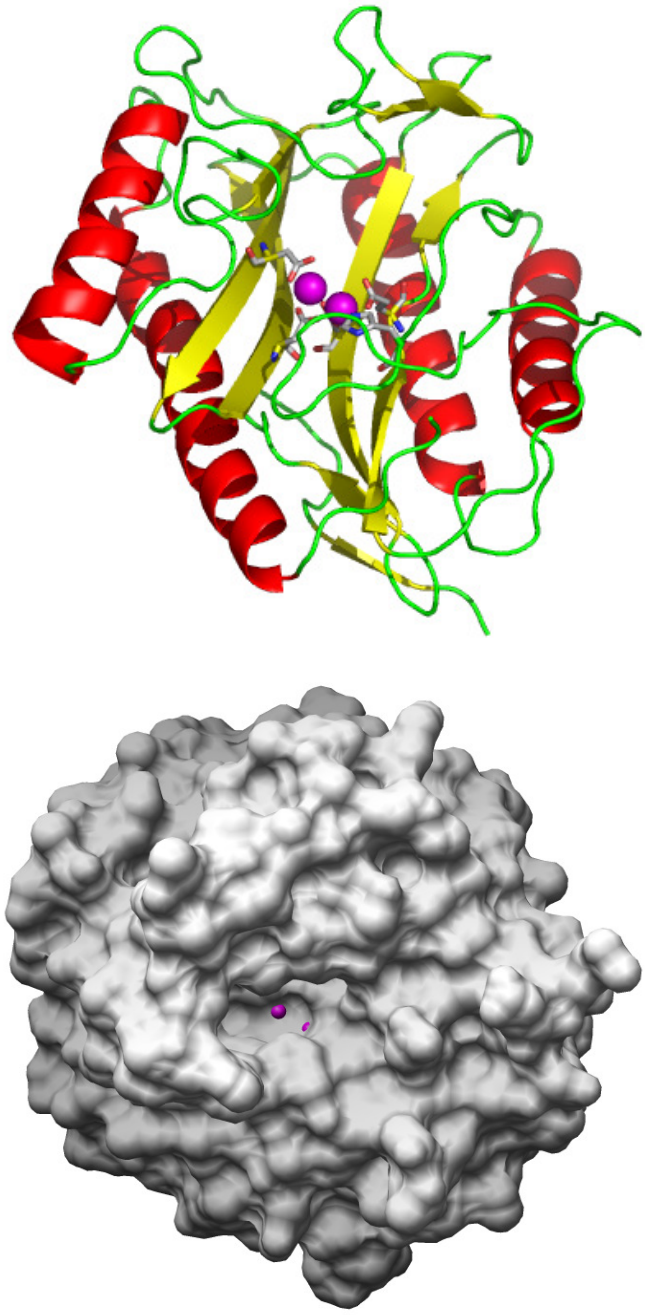

Fig. 2-7 *E. coli* MetAP, above: tertiary structure of the EcMetAP, the central ß-sheet is depicted in yellow, the alpha helices in red and the loops in green, the cobalt ions are shown in magenta, surrounded by the five conserved active site residues; below: molecular surface of the EcMetAP (created with the program CHIMERA[49]), the cobalt ions are shown in magenta

Structurally, both halves of the polypeptide chain are arranged around a pair of cobalt ions. A central antiparallel ß-sheet is covered on one side by two pairs of α-helices and by a C-terminal loop and on the other side forms the active site together with some irregular loops and two metal ions.

Protein data base searches using both sequence- and structure-based profiles identified several other proteins with the pita-bread fold including creatinase, aminopeptidase P, proline dipeptidase and p67[13].

2.3.3.2 Metal Binding Site

The EcMetAP active site is composed of a catalytically essential binuclear metal center generated by five strictly amino acids which are conserved in all MetAPs known so far: Asp97, Asp108, Glu204, Glu235 and His171. These ligands interact with the two metal ions in a monodentate (His171 and Glu204) or a bidentate manner (Asp97, Asp108 and Glu235) and lead to a trigonal bipyrimidal coordination for one cobalt ion (Co_1) and an approximately octahedral coordination for the second one (Co_2). In addition, several solvent molecules are present in the crystal structure of the apo-enzyme (2MAT). Two of them are directly coordinated to the metal centre: One of those bridges between the two cobalt ions, while a second one is terminally ligated to Co_2. Individual mutation of the five metal-binding amino acids residues resulted in complete loss of enzymatic activity and ability to bind Co(II)[50].

The only other invariant amino acids (among all MetAPs known so far) in the active site are His79 and His178, located on opposite sides of the cavity and slightly above the metal center[14, 51] as can be seen in Fig. 2-8. The mutation of these two histidines results in a dramatic loss of activity. Seven cysteines are present but none of these form disulfide bridges.[51]

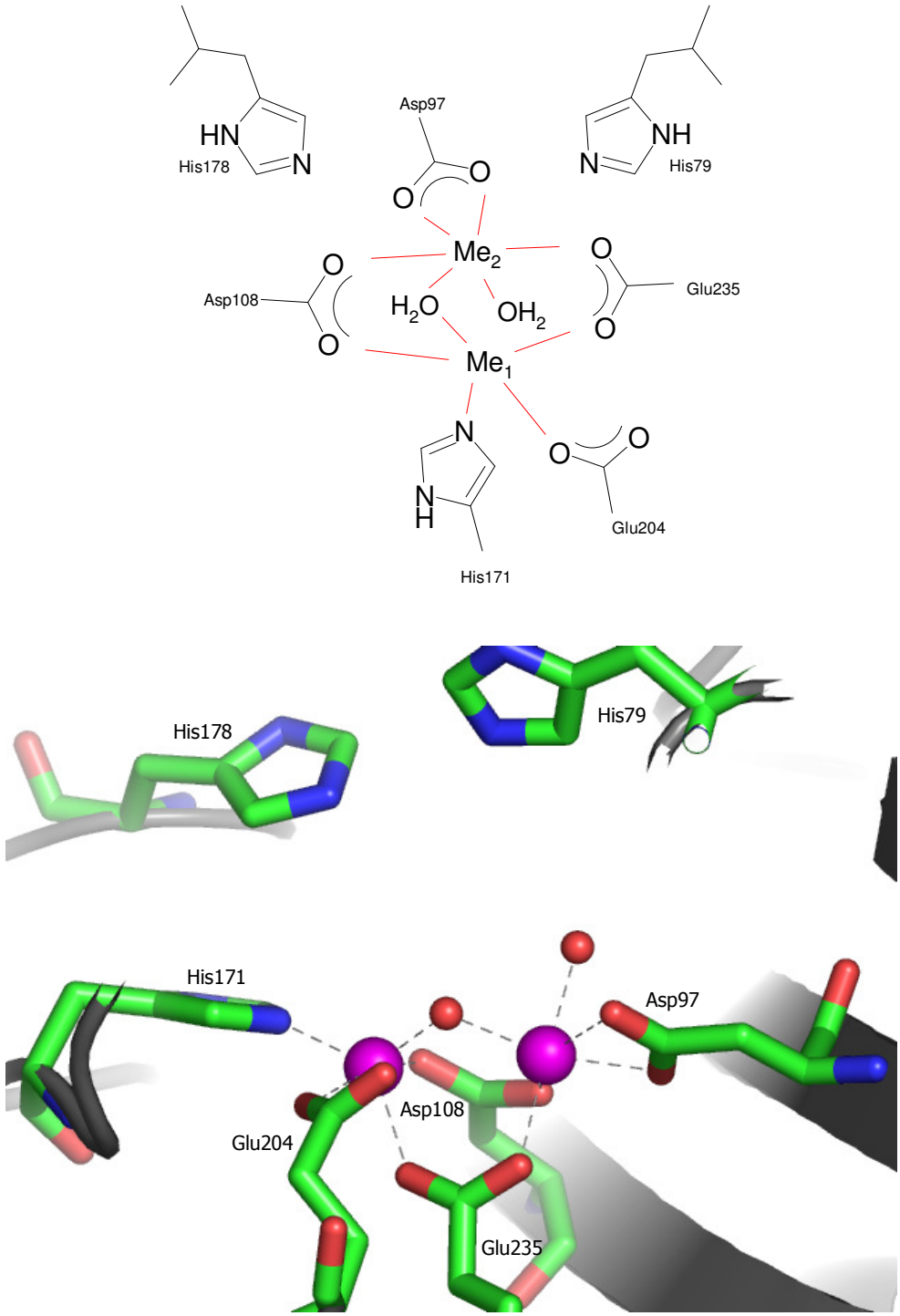

Fig. 2-8 Metal binding site of the EcMetAP, above: schematic drawing, below: picture based on the X-ray structure 2MAT

In addition to the cobalt ions, a sodium ion can be seen in 90% of the published crystal structures. This Na^+-ion is positioned near Val76 and about 15 Å away from the metal binding site and might mediate an interaction between the subdomains of the folded protein, thus stabilizing the metal center and/or positioning the solvent accessible loop that contains His79[52].

2.3.3.3 Substrate Recognition Site

Near the metal binding site, a hydrophobic cavity is lined by the side chains of a set of amino acids (see Table 2-1) that form the binding site for the amino-terminal methionine side chain, required for substrate recognition.

Table 2-1 Comparison of the metal binding and substrate recognition sites of type-I and type-II MetAPs; a) for HsMetAP-II, b) according to sequence alignments with 8 different type-II MetAPs

	S1-subsite (recognizes Met)	Metal binding Site	S1'-subsite
EcMetAP(-I)	Cys59, Tyr62, Tyr65, Cys70, His79, Phe177, Trp221[51, 53]	Asp97, Asp108, His171, Glu204, Glu235	Tyr168, Cys169, Gly170, His185, Glu204, Pro205, Met206, Gln233[54]
Type-II MetAPs	Pro, Gly, Ile, His, Met, Tyr[a][55]	Asp, Asp, His, Glu, Glu[a][56]	Leu, Gly, Glu, Phe, Glu[b][54]

Whereas the active site residues are strictly conserved, variations do occur among the putative substrate-binding residues. Type-I and type-II MetAPs use different sets of amino acid residues. This explains the (slight) differences in substrate binding and enzyme activities of the different types of MetAPs.

Alignment studies revealed that Cys70 and Trp221 are conserved among type-I, but not type-II MetAPs[50]. In addition, extensive mutagenesis studies of the S1-site of EcMetAP[55] and of other residues[50] have been performed. The residues Tyr65 and Trp221 are essential for the proper functioning of the enzyme. Cys70 also seems to play a crucial role in substrate catalysis. Mutation of Cys70 opened up the binding pocket and changed substrate specificity[55, 57].

A picture of the EcMetAP substrate recognition site with bound methionine is shown in Fig. 2-9.

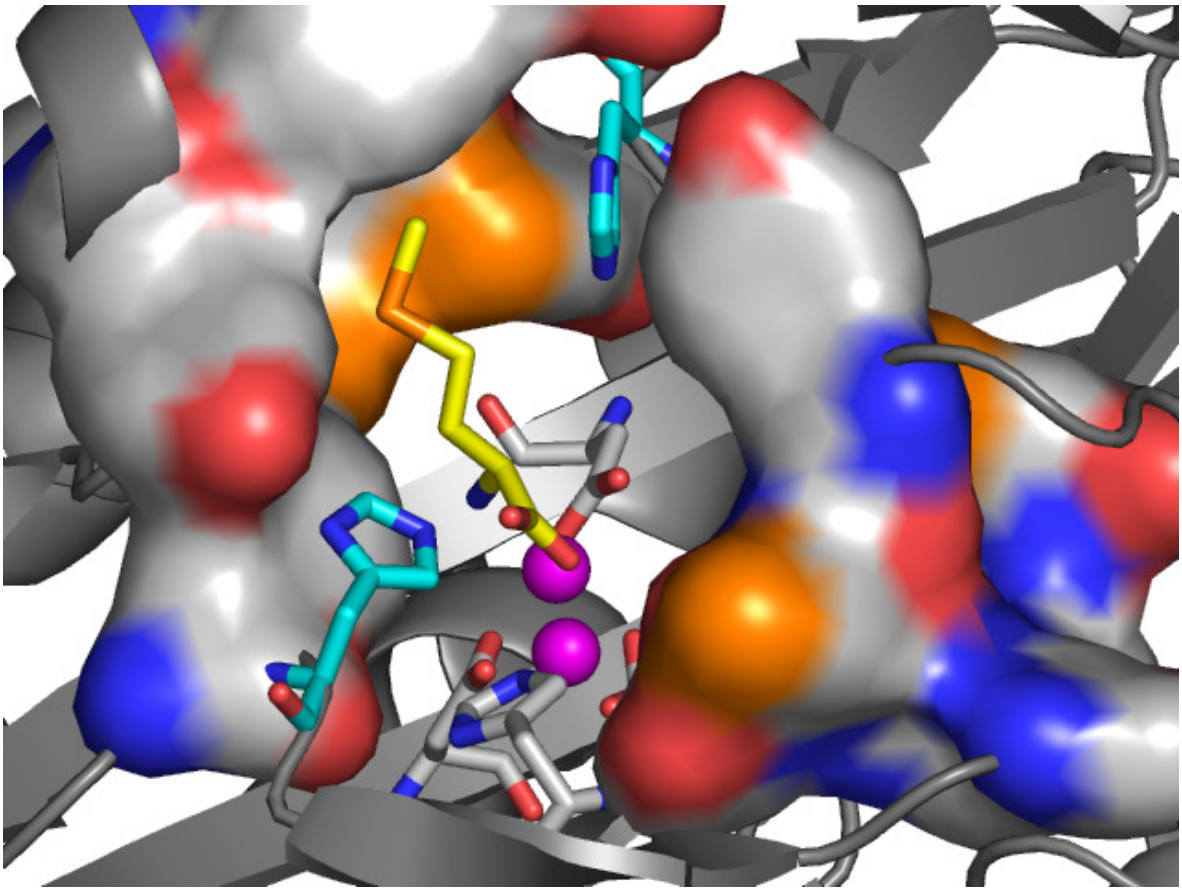

Fig. 2-9 Structure of the EcMetAP with bound methionine (1C21). The metal binding site is depicted with sticks, the Co(II) ions are shown in magenta, the flanking histidines (His79 and His178) in light blue, methionine in yellow. The surface of the S1-subsite that recognizes methionine can be seen on the left side, the surface of the S1'-subsite can be seen opposite on the right.

2.3.4 Reaction Mechanism

Based on X-ray structures of EcMetAP with bound substrates and substrate-like inhibitors, on mutational studies and on comparison with enzymes with a similar active site, the following reaction mechanism has been proposed (Fig. 2-10):

Binding of the substrate, which includes direct interactions with both metals, leads to an expansion of the coordination sphere of Co_1 from five to six. This alternation in the electronic character of the binuclear center may activate the μ-hydroxide for nucleophilic attack and facilitate proton transfer to Glu204. The idea that the bridging water molecule is deprotonated is confirmed by computational and experimental results discussed in 4.3.3 (Protonation States of MetAP). Recent theoretical work on the reaction mechanisms of other enzymes indicate that the nucleophilic attack on the substrate might also originate from a "terminally" bound

and not a bridging hydroxide ion as its nucleophilicity is higher. The location of the carbonyl oxygen atom of the substrate upon binding also is under debate.

The resulting tetrahedral intermediate is stabilized by chelation to Co_1 and by hydrogen-bonding interactions with His178 and His79. Proton transfer from Glu204 to the nitrogen atom of the scissile bond may facilitate breakdown of the intermediate to products. His79 may interact directly with the nitrogen of the scissile peptide bond, playing a critical role in substrate recognition and being a key residue[48]. A movement of that residue towards the metal center can be seen upon binding of a bestatin based inhibitor[53].

Due to the possibility that several MetAPs may use only one metal ion and the proximity of His79 to Co_1, this residue could function as a proton donor to the leaving amino group as proposed for His141 of arginase[58]. The Co_2-substrate interaction could be replaced by the acidic Co_2 ligands and other residues in the vicinity. In these cases, the charged form of the N-terminus is most likely bound and the addition of the second metal ion may be inhibitory or utilized in the *in vivo* regulation of activity[58].

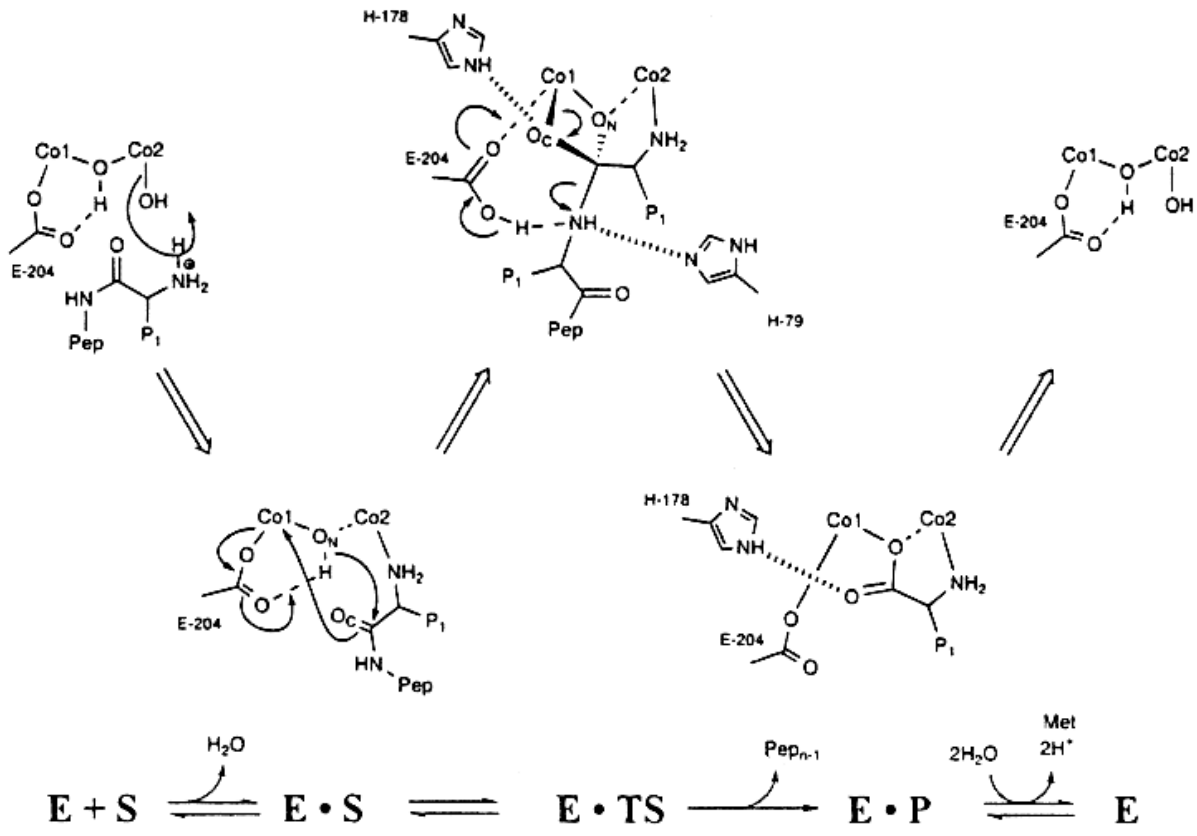

Fig. 2-10 Proposed reaction mechanism[48]

2.3.5 MetAPs of Different Species

The *E. coli* MetAP (EcMetAP) was for the first time isolated and partly characterised by Ben-Bassat[4], the *Salmonella typhimurium* MetAP (termed peptidase M) by Miller[3] and Wingfield[59]. The pepM gene of *S. typhimurium* has been cloned and the nucleotide sequence determined[60]. Additionally, the MetAPs of yeast[44, 61], of porcine liver[9] and human MetAPs have been overexpressed and characterized[62, 63]. The gene sequences of MetAPs have been determined in several clinically important pathogens such as *Mycobacterium tuberculosis* in tuberculosis, *Enterococcus faecalis* in urinary tract infection and endocarditis, *Streptococcus pneumoniae* in pneumonia, *Haemophilus influenzae* in respiratory tract infections and *Helicobacter pylori* in ulcers. MetAP genes have also been identified in *Pyrococcus furiosus*, *Methanococcus jannaschi*, *Bacillus subtilis* and in the cyanobacterium *Synechocystis*[62] among many other organisms.

2.3.5.1 *Pyrococcus furiosus* MetAP (PfMetAP)

PfMetAP has been cloned, overexpressed and characterized[64]. It seems to be evolutionary located at the eukarya-bacteria boundary[6], because on the one hand, there is a high degree of sequence homology in the stretches surrounding the five preserved cobalt-binding residues and it is lacking the N-terminal extension but on the other hand it has a long insert of about 60 amino acid residues in the C-terminal domain as can be seen in type-II MetAPs.

PfMetAP is thermostable and exhibits maximum activity at 90 °C. DSC (Differential scanning calorimetry) revealed that the heat stability is likely a result of electrostatic stabilization due to extra ion pairs compared to EcMetAP and a stable (globule-like) conformation[65]. The crystal structure supports these findings and contributes the heat stability to a unusually high number of internal hydrogen bonds and ion-pairs and the overall fold[66].

2.3.5.2 Yeast MetAPs

Due to the easy handling of yeast cultures and the possibility of genetic manipulations, *S. cerevisiae* has been used (apart from *E. coli*) for extensive studies of MetAPs. Both type-I and type-II MetAP can be found in *S. cerevisiae*. Apart from single amino acid mutations, null mutants lacking, for example, only one type of MetAP provide insight into the similarities and differences between the two types *in vivo*:

Cloning of the yeast MetAP-I enzyme revealed a considerable degree of sequence identity (about 40 %) between its C-terminal domain (~30 kDa) and the complete prokaryotic sequences[16]; however, the N-terminal domain (~12 kDa) is unique. Yeast MetAP-I (42 kDa) is 22 % homologous to yeast MetAP-II and about 40 % homologous to bacterial MetAPs. Yeast MetAP-II encodes a protein that shows 55 % homology with rat p67[42]. Both types are associated to ribosomes[47].

Unlike in the case of the prokaryotic gene, the deletion of the yeast MetAP-I gene is not lethal, although the mutant strain has a drastic change in its doubling time and decreased colony size[44]. The MetAP-II null strain, like the MetAP-I null strain, is also viable but with a slower growth rate compared to the wild type (but faster than the MetAP-I null strain, suggesting that MetAP-I plays a larger role than MetAP-II in promoting cell growth). The MetAP-I, MetAP-II double-null strains are nonviable[42].

The deletion of the N-terminal domain of yMetAP-I has no effect on its catalytic activity *in vitro*, but it does compromise the ability of the enzyme to complement the slow growth phenotype of a MetAP-I null yeast strain[16]. In addition, point mutations in the zinc finger region that almost completely abolish complementation ability result in dissociation of the enzyme from the ribosome[67]. Thus, the zinc finger region is important for ribosome association and for MetAP function *in vivo*. This result has been confirmed by coexpression experiments of truncated and wild type MetAP-II[68].

The two types of MetAPs seem to exhibit a different substrate cleavage pattern *in vivo*[47]. In addition, type-II MetAP seems to be more susceptible to product inhibition by methionine than type-I[40] and is therefore more sensitive to the intracellular methionine concentration.

In conclusion, the removal of N-terminal methionine is an essential function in yeast, as in prokaryotes, but yeast requires two MetAPs to provide the essential function which can only be partially provided by MetAP-I or MetAP-II alone.

2.3.5.3 Human MetAPs (HsMetAP)

As in the case of yMetAP, the N-terminus is not required for activity or stability of HsMetAP-II[69]. In spite of the similarities and the conserved active site residues, HsMetAP-II has different substrate specificity as it can also cleave substrates smaller than a dipeptide, such as Met-AMC and Met-pNA[69].

HsMetAP-II has become a target protein for drug development because this enzyme seems to be involved in the process of angiogenesis. Thus, specific inhibitors might be used as anti-cancer drugs. A connection with tumor promotion can be suggested due to the upregulation of MetAP-II-levels by carcinogenic phorbolesters. MetAP-II expression correlates with cell growth and nondividing tissue culture cells lack immunodectectable levels of MetAP-II[20]. For further information about the physiological role of the human MetAP-II cfr. 4.3.2.2 (Covalent Inhibitors, Mode of Action on the Molecular Basis).

3 Aims of this Work

The Methionine Aminopeptidase plays a central role in the cellular protein metabolism of both eukaryotic and prokaryotic cells. The main aim of this work was the development and characterization of inhibitors of the *E. coli* methionine aminopeptidase as potential antibacterial, antifungal or antiparasitic drugs. As the human enzyme is involved in tumor progression and angiogenesis, a deeper understanding of this type of enzyme, the underlying mechanisms and the binding modes of inhibitors might also prove useful for the development of anticancer drugs.

Expression and purification of the enzyme was the first essential step towards this aim. A stock of transformed BL21(DE3) cells was kindly provided by Prof. Brian Matthews (University of Oregon). After isolation of the plasmid and a new transformation of competent *E. coli* cells, the protein should be overexpressed and purified by affinity chromatography according to published procedures.

For the screening of inhibitor, a cheap and easy to handle assay system was required. After an extensive literature research, a published assay procedure should be modified to an end-point method and optimized.

After these initial steps, the enzyme should be characterized with respect to biochemical properties. This includes parameters such as pH-optimum and metal dependency but also the binding of an epoxide-containing inhibitor (fumagillin), a known covalent inhibitor of MetAPs. Besides, other small molecules with an epoxide group were to be synthesized and tested.

For the discovery of new leading structures, computational screening methods and molecular modeling also performed in our working group should be combined with the screening of different classes of compounds. A series of derivatives should be synthesized to improve *in vitro* affinity and to gain insight into structure-activity relationships. Finally, the most promising compounds should be tested for their antibacterial potency and X-ray studies should be used to clarify the binding mode of the best compounds and of other inhibitors described in the literature.

These results might prove useful for the further development of drugs. They hopefully will provide additional facts that can be used for the interpretation of certain phenomena that cannot be explained so far, for example the lack of correlation between the (high) *in vitro* and

(low) *in vivo* potency of known inhibitors. Furthermore, they are likely to have an impact on the proposed reaction mechanism of this enzyme and might lead to a better understanding of the demands of potential drugs.

4 Results and Discussion

4.1 Expression and Purification of EcMetAP

EcMetAP was overexpressed using the BL21(DE3) strain transformed with a modified pET(28b)-vector encoding for a His-tagged EcMetAP that was kindly provided by Prof. Matthews and Dr. Lowther[70]. As freshly transformed cells normally give much higher yields, the plasmid was isolated with commercially available kits and the *E. coli* strain re-transformed. Plasmid isolation was checked with gel electrophoresis (see Fig. 4-1). The sequence encoding for EcMetAP is inserted in the cloning site between the NcoI and the XhoI-site and consists of about 1100 bp. The modified plasmid has a size of about 6.3 kb. Digestion with SmaI (4300) and NcoI (296) results in the two expected fragments of 2.3 kb and 4 kb.

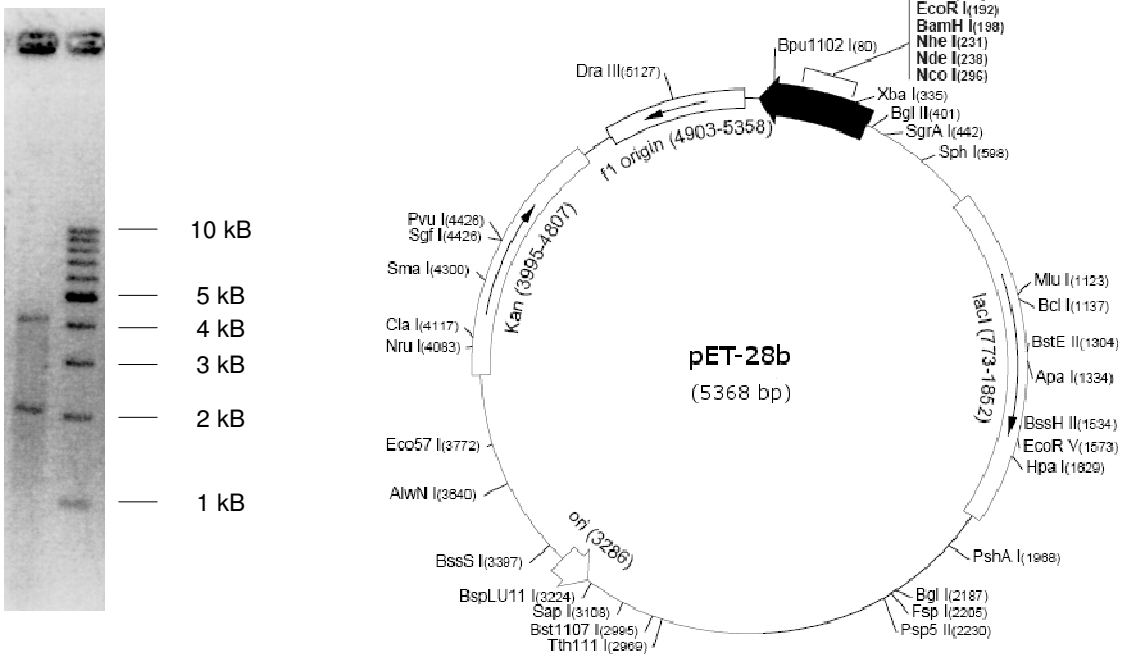

Fig. 4-1 Left: Agarose gel after digestion of the isolated plasmid with SmaI and NcoI; right: pET-28b vector (Novagen) with restriction sites

The EcMetAP was then overexpressed and isolated according to literature procedures[70]. Affinity chromatography using a Ni(II)-loaded NTA-agarose-column was used for the purification of the overexpressed His-tagged enzyme. The tag was then cleaved off with biotinylated thrombin and the thrombin was removed with streptavidin agarose. After removal of the His-Tag by a second NTA-column, the MetAP was then further purified by size-exclusion chromatography using a Superdex column (cf. Fig. 4-2).

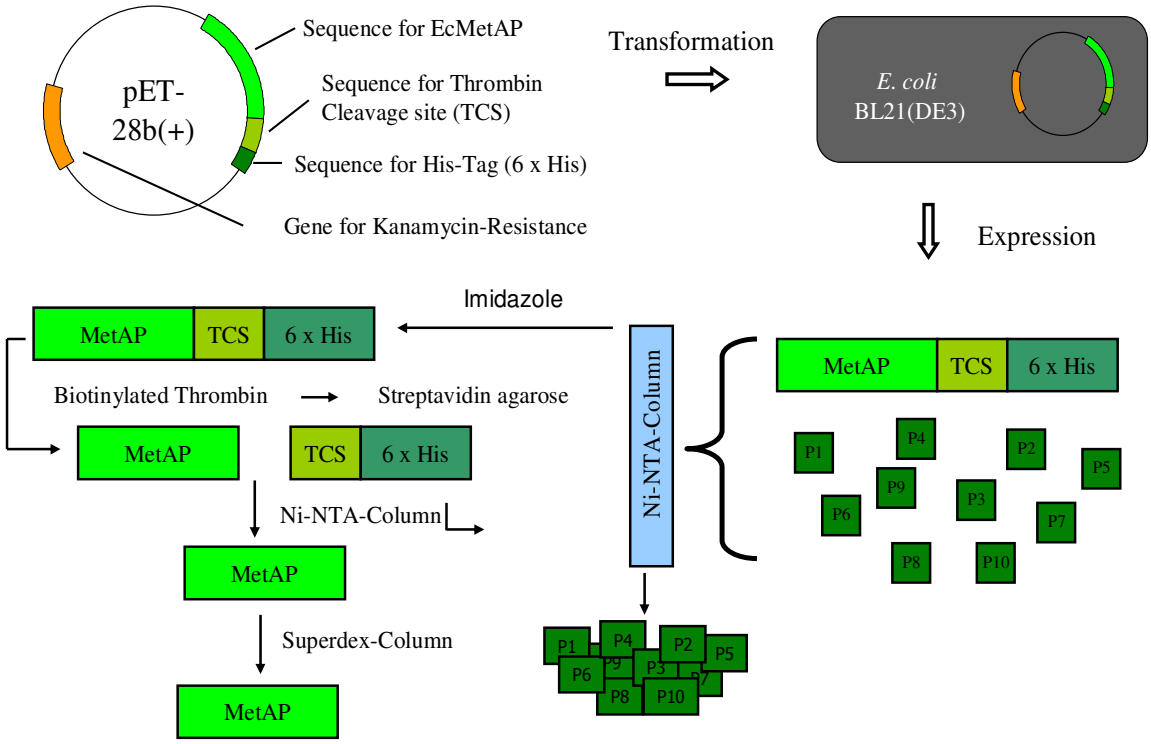

Fig. 4-2 Schematic drawing of the expression and purification procedure for EcMetAP

The purity of the enzyme was checked with SDS-PAGE (cf. Fig. 4-3), and the removal of the His-tag was further followed with ESI-MS-MS and MALDI-TOF-MS (cf. Fig. 4-4).

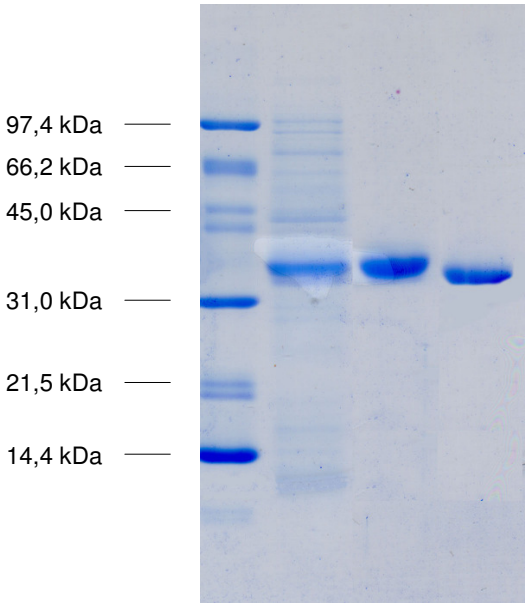

Fig. 4-3 SDS-PAGE of: induced *E. coli* cells (left), His-tagged EcMetAP after purification by a Ni-NTA-column (middle) and EcMetAP after removal of the His-tag with thrombin and purification by a Superdex-column (right); 7 µl of a 0.5 mg/ml enzyme solution were applied.

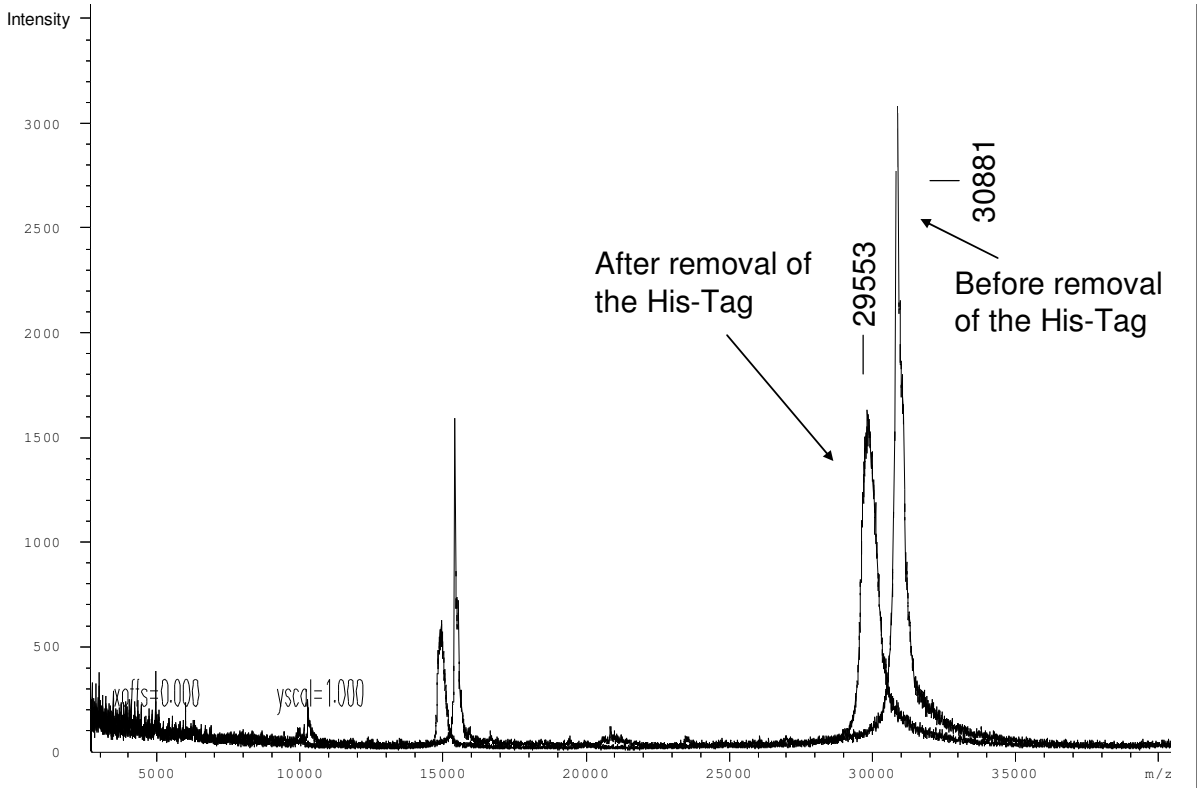

Fig. 4-4 left: MALDI-TOF-MS measurements of EcMetAP before and after removal of the His-tag

The detected masses for the His-tagged and the "free" enzyme were as follows:

	His-tagged	after His-tag-removal	Δ (MW His-Tag)
MALDI-TOF-MS	30881 Da	29553 Da	1243
ESI-MS-MS	30857 Da	29641 Da	1216
calculated (MetAP-LVPR-|-GSLEHHHHHH)[a]	31,0 kDa	29,8 kDa	1,2 kDa

[a] http://www.sciencegateway.org/tools/proteinmw.htm

4.2 Assay Development and Characterization of EcMetAP

4.2.1 Overview: MetAP Assays

Several assays have been described in the literature for the testing of MetAP activity. Most of them are discontinuous assays where the reaction of the MetAP is separated from the detection of its activity. Frequently, a small peptide with an N-terminal starter methionine is used as substrate and cleavage of this methionine is performed in a buffer at neutral pH and 37 °C. Usually, cobalt is used to activate the MetAP. There are some differences in how the reaction is stopped and the released methionine is detected: In general, EDTA is used to inactivate MetAP at the end-point but also denaturation of the enzyme by heat or TFA are common. Yeast MetAP for example is readily inactivated by "generic" metalloprotease inhibitors (such as EDTA or o-phenanthroline), sulfhydryl-modifying reagents ($HgCl_2$ and pHMB) or by zinc ions[61].

Most differences exist in the detection part. Two general principals can be distinguished: Either a chromatographic method is applied where the released methionine is separated from the shortened substrate[71, 72] (this method can be used in the presence of methionine or chromophores) or the released methionine is chemically modified resulting in a compound that allows photometric measurement. Of course, combinations of the two principles may be used (with precolumn derivatization procedures). For example, AQC (6-aminoquinolyl-N-

hydroxysuccinimidyl carbamate) reacts with amino acids to form stable asymmetric urea derivatives which can be analyzed by reversed-phase HPLC[73, 74]. Other assays use either a chromogenic or a fluorogenic tag for derivatization and the resulting derivatives are also analyzed by HPLC or capillary electrophoresis.

Although being very sensitive, these methods are often time-consuming and inconvenient, especially if a large number of tests should be performed, for example for the screening of inhibitors. Additionally, the colorimetric detection of single amino acids or the chemical derivatization of the peptides followed by chromatographic analysis require the removal of the methionine prior to the assay and are subject to interference by other chromophores[71].

An easy to handle continuous assay using thioesters as a substrate has been reported by Zhuo and coworkers[75]. A free thiol group is generated upon enzymatic removal of the methionine and quantitated with Ellman's reagent (DTNB). However, this method seems inconvenient as DTNB also reacts with the thiol groups of MetAP-cysteines. It has been shown that DTNB inactivates MetAP due to the modification of a cysteine residue near the active site[71]. Additionally, initial tests performed in our group revealed that the thioester substrates are not very stable and generate problems with background noise depending on pH and (nucleophilic) solvent, thus decreasing sensitivity.

Zhuo and coworkers also reported another continuous assay using Met-Pro-pNA coupled to a prolyl-aminopeptidase[75]. However, Met-Pro-pNA is not a good substrate for EcMetAP which prefers tripeptides or larger peptides and the prolyl aminopeptidase used is no longer commercially available. Besides, this enzyme is closely related to MetAP: It is also metal dependent and predicted to share the same pita-bread fold. All five conserved active site residues of the EcMetAP are also conserved in three different prolyl aminopeptidases[14]. Therefore, the probability of an interference (of for example inhibitors) with the detection enzyme is relatively high and metal-specific tests are difficult.

Besides the detection of methionine with the ninhydrine reaction after TLC, a photometric method is very common that monitors the release of methionine using the highly toxic and carcinogenic o-dianisidine (3,3'-dimethoxybenzidine) together with an amino acid oxidase (AAO) and a peroxidase from horseradish (HRP)[4, 6, 50, 59]. Oxidation of the released methionine by AAO generates H_2O_2 that is used as a substrate by HRP to oxidize

o-dianisidine as a cosubstrate. The resulting product can be measured by absorption at 450 nm (cfr. Fig. 4-5).

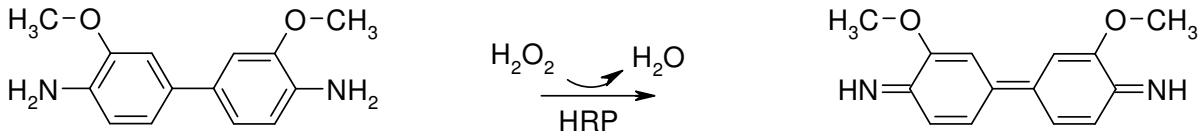

Fig. 4-5 Reaction scheme for the photometric detection of o-dianisidine with horseradish peroxidase (HRP)

Based on this procedure, an improved fluorogenic assay has been reported by Yang and coworkers[69]. This method uses the substance "Amplex Red" instead of o-dianisidine and the oxidation product can be measured fluorometrically. It is a cheap, easy to handle and sensitive assay, and it can be performed in 96 well plates. As there was a Wallac Victor multiplate reader available to us, it was decided to establish this fluorimetric assay. The complete reaction scheme is outlined in Fig. 4-6:

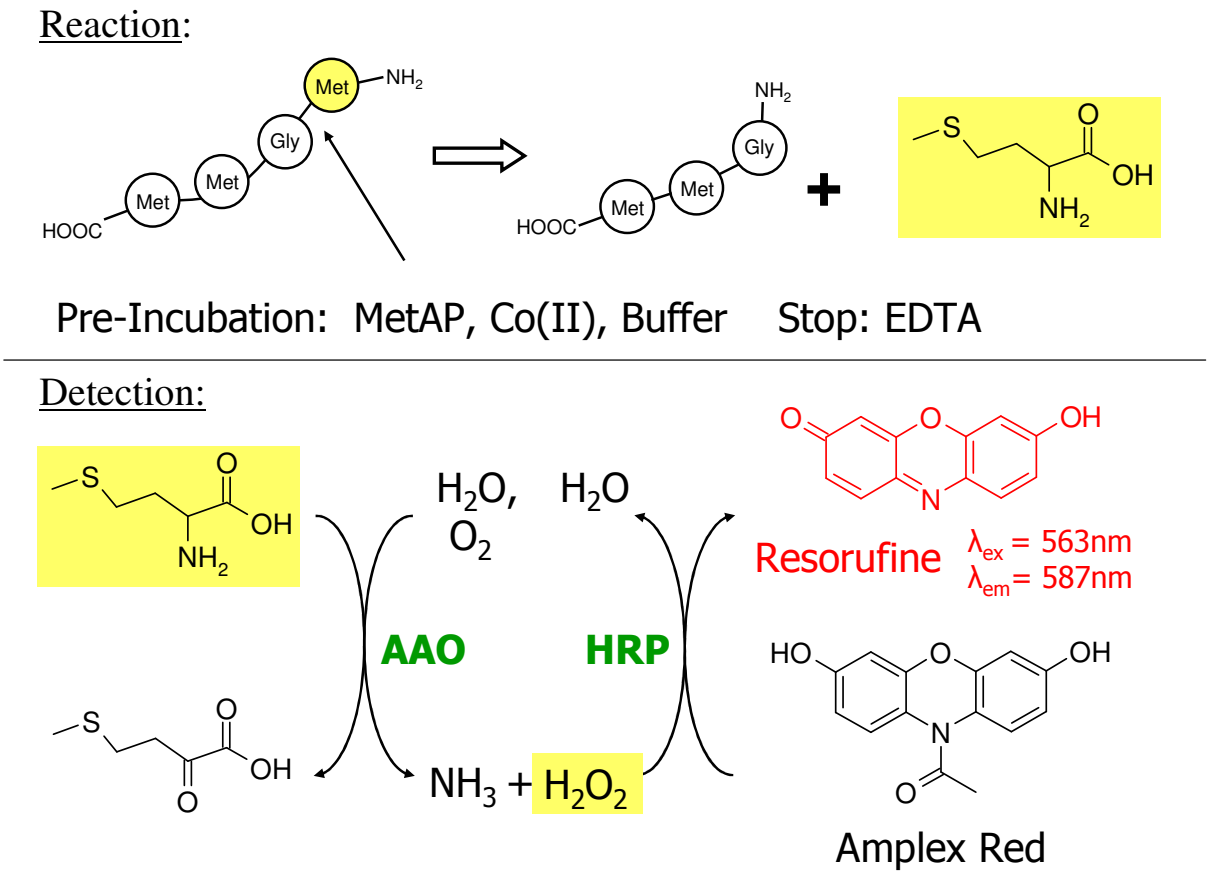

Fig. 4-6 Reaction mechanisms of the Amplex Red Assay for the quantification of MetAP-activity, AAO: L-Amino acid oxidase, HRP: Horseradish peroxidase

However, the drawbacks of this assay should not be withheld. Besides being time-consuming as the detection reactions need 30-60 minutes to reach completion, any remaining MetAP activity (due to incomplete inactivation) or contaminating peptidase activity could generate significant background signal. In addition, substances with oxidizing or reducing properties must not be present in larger amounts because they may interfere with the chemistry of the detection part. However, testing of such substances at concentrations smaller than ~1 µM are possible. Taken together, the advantages surpass the disadvantages.

4.2.2 Assay Development and Validation

It was decided to change the continuous assay into an end point assay because of the following reasons:

i) The amount of DMSO during the MetAP reaction should be as low as possible as the enzyme is very susceptible to organic solvents. As it is recommended to store the Amplex Red stock solution in DMSO, the addition after the MetAP reaction seemed advantageous.

ii) The MetAP properties and activity should be influenced as little as possible by other enzymes; therefore the presence of AAO and HRP should be avoided during the substrate hydrolysis reaction.

iii) There are difficulties in the measurement of starting velocities as is normally done in continuous assays when the assay is performed on a 96 well plate with a multiplate reader because of the nature of the instrument (time lag between the reading results of different wells) and because of liquid handling (simultaneous reaction start) which can easily be avoided in a discontinuous assay.

Additionally, the volume was increased from 50 µl to 250 µl in order to reduce the error derived from handling small volumes. Concentrations in the following refer to the reaction part. Exceptions are the concentrations of EDTA, resorufine and Amplex Red that refer to the detection part. The volumes were 200 µl for the reaction part and an overall volume of 250 µl after the addition of the reagents of the detection part unless stated otherwise.

The assay development was started with the detection part. The following factors were important:

i) Detection limit

ii) Concentration of methionine to be detected

iii) Concentration of MGMM during the MetAP reaction and consequently remnant MGMM present during the detection of the released methionine

iv) Concentration of detection enzymes (L-Amino Acid Oxidase, Horseradish Peroxidase)

v) Concentration of EDTA as reaction stopper

vi) Concentration of Amplex Red

4.2.2.1 Detection Limit

Resorufine was used as standard for the evaluation of the detection limit (cf. Fig. 4-7).

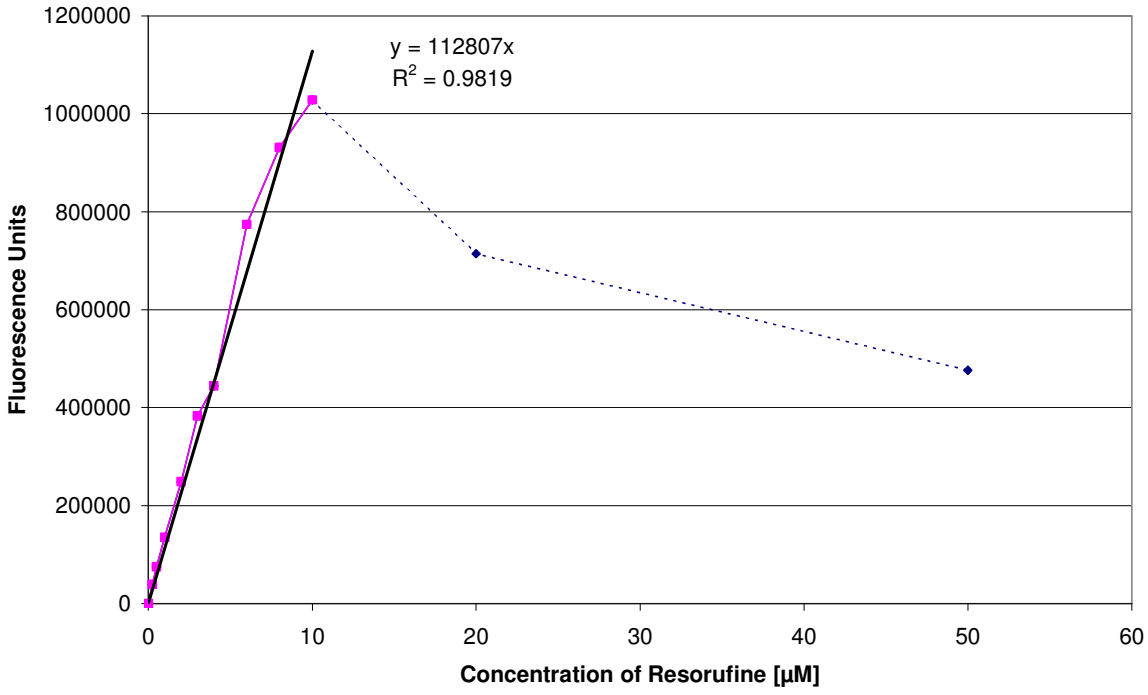

Fig. 4-7 Detection range using resorufine as a reference (volume 250 µl)

A linear correlation between the concentration of resorufine and the fluorescence units measured is given in the range from zero up to 10 µM resorufine. The detection range was then checked with different concentrations of H_2O_2 in the presence of Amplex Red and finally with different concentrations of methionine in combination with the detection enzymes for the conversion of Amplex Red to resorufine. The fluorescence values obtained were slightly lower but comparable to those obtained with resorufine.

4.2.2.2 Concentration of Detection Enzymes

As there are two enzymes involved in the detection of methionine, it is important that the first reaction, the generation of H_2O_2, is the rate-limiting step. For this reason, the ratio of the detection enzymes was kept as published with a much higher concentration of HRP compared to AAO. Unfortunately, Amplex Red is converted to resorufine in the presence of the substrate MGMM even if no methionine is present (resp. released by the MetAP). In order to investigate if this oxidation of Amplex Red is unspecific or dependent on the detection enzymes, different concentrations of HRP/AAO were tested (cfr. Fig. 4-8).

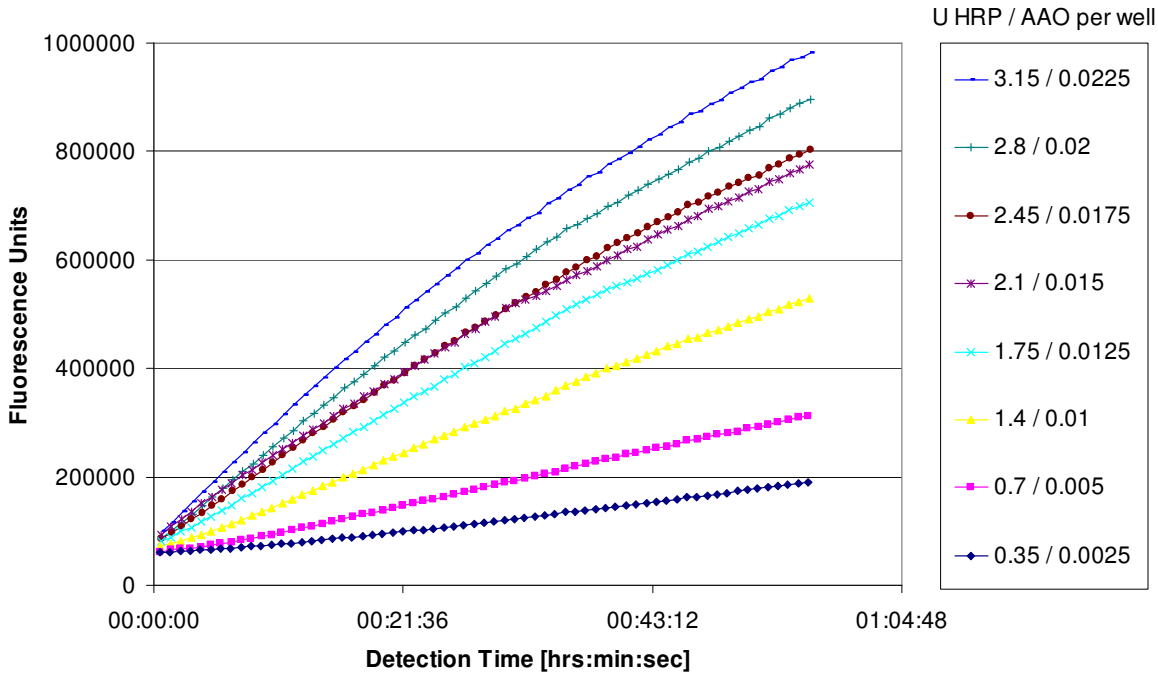

Fig. 4-8 Dependency of the amount of detection enzymes and the increase of the blank in the presence of 180 µM MGMM in the reaction part (100 µl, final concentration 72 µM), 40 µM Amplex Red and 9 mM EDTA (final volume 250 µl)

This increase of the zero-value correlates with the concentration of detection enzymes present. Possibly, AAO is (to a small percentage) able to oxidize MGMM, which is confirmed by tests with different amounts of MGMM (see 4.2.2.3, Concentration of MGMM Present During the Detection).

4.2.2.3 Concentration of MGMM Present During the Detection

It should be tested if the increase of the blank is based on the oxidation of Amplex Red by H_2O_2 that is generated by the side reaction of AAO with the substrate. An alternative explanation would be a direct unspecific oxidation. This could happen either by the contact with oxygen or by a cross reaction with one of the detection enzymes. Thus, several concentrations of MGMM were incubated with the detection enzymes and Amplex Red (cf. Fig. 4-9).

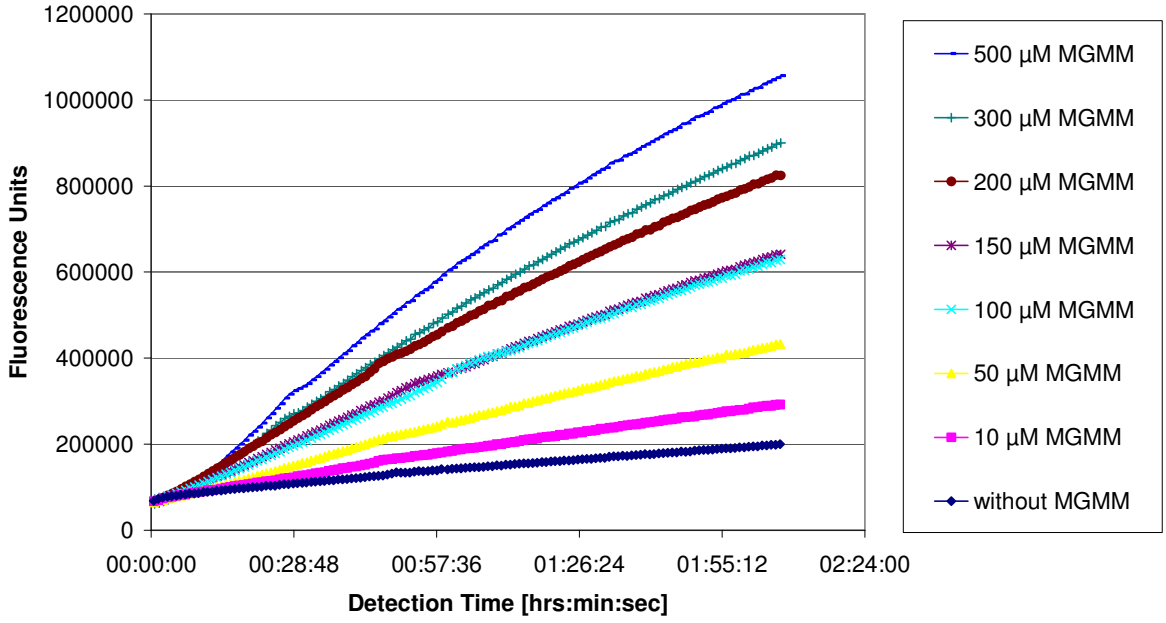

Fig. 4-9 Dependency of the MGMM concentration (in the reaction part, 100 µl) and the increase of the zero value in the presence of 1.4 U/well HRP, 0.01 U/well AAO, 40 µM Amplex Red and 9 mM EDTA (final volume 250 µl)

The increase of fluorescence correlates with the concentration of MGMM. In the case where no MGMM (and no methionine) is present, a slight increase can be observed that can possibly be attributed to the oxidation of Amplex Red on contact with air.

For calibration curves and other measurements, the difference of the measured fluorescence F_P and the blank F_Z was determined. The resulting curve(s) reached a plateau after 40-60 min that remained stable for about 30 min. In summary, it has been shown that

i) the increase of the blank is dependent on the amount of detection enzymes used (Fig. 4-8) as well as on the MGMM concentration (Fig. 4-9)

ii) the concentration of EDTA used does not influence the increase of the blank (data not shown)

iii) the concentration of detection enzymes does have an impact on the detection time but does not influence the resulting fluorescence difference between F_P and F_Z (MAX (ΔF_P-ΔF_Z), data not shown).

The absolute fluorescence values increase with the amount of detection enzymes. Thus, the detection limit is reached faster with higher concentrations of detection enzymes. The same applies for higher concentrations of MGMM, which decreases the sensitivity of the assay. Therefore, all of these concentrations should be as low as possible.

On the other hand, a reduced amount of detection enzymes leads to a very long detection time and a reduced concentration of MGMM also brings up some problems: The amount of released methionine (from MetAP activity) depends within certain limits on the amount of substrate. Thus, less MGMM decreases the sensitivity of the assay as more MetAP is needed for the same amount of released methionine (or a longer reaction time is required).

As there is a detection limit and for the assay results the difference between the measured fluorescence F_P and the blank (zero value F_Z) is determined, it is important to find a compromise between the concentration of MGMM and the detection enzymes. On the one hand, the MGMM concentration has to be high enough to allow the enzyme to work under saturated conditions during the whole reaction time, and the concentration of the detection enzymes also should be as high as possible in order to shorten the duration of the detection part. On the other hand, both the MGMM and the detection enzyme concentration should be as low as possible in order to avoid a strong increase of the blank. The reaction time should not be too long to minimize unspecific hydrolysis of MGMM although MGMM was shown to be stable even when incubated for 45 min at 37 °C (data not shown).

200 µM MGMM, 1.05 U/well HRP, 0.0075 U/well AAO and 9 mM EDTA proved to be suitable conditions and were used for further tests.

4.2.2.4 Calibration Curves

In Fig. 4-10, the calibration curve for 0-8.75 µM methionine in the presence of 200 µM MGMM is depicted.

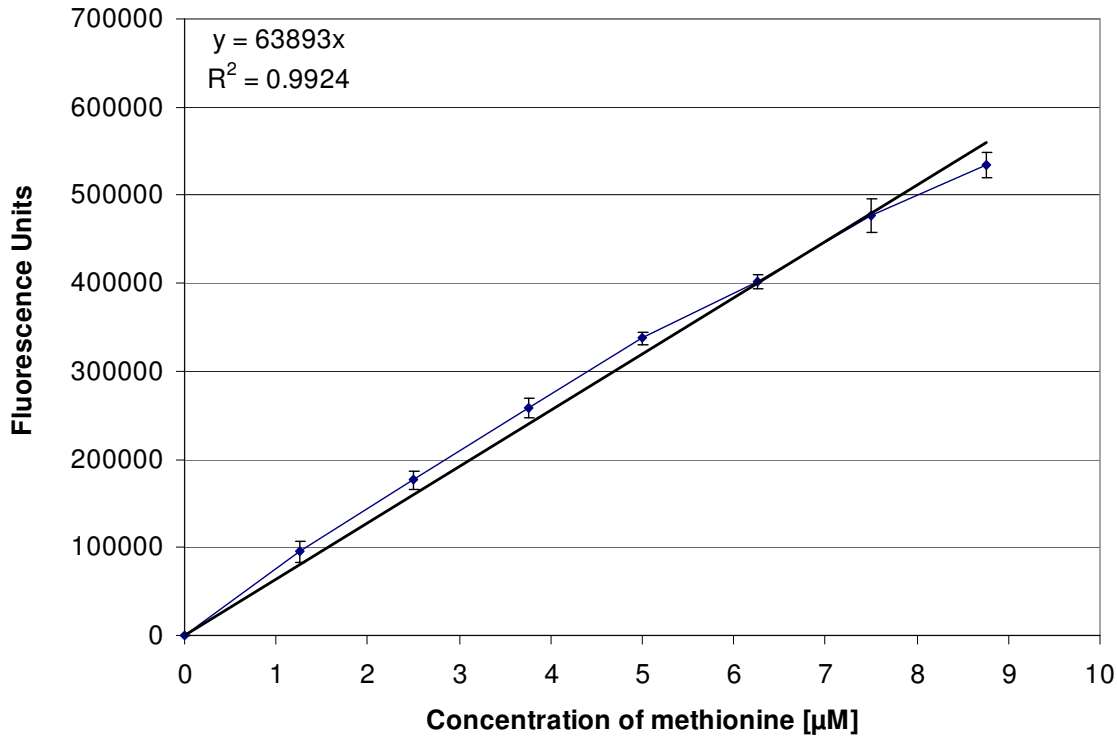

Fig. 4-10 Calibration curve in the presence of 200 µM MGMM in the reaction part (200 µl, final concentration 160 µM), 1.05 U/well HRP, 0.0075 U/well AAO, 9 mM EDTA, 10 µM Amplex Red (final volume 250 µl)

The results of other calibration experiments are summarized in Table 4-1.

In general, 200 µM MGMM was used. The calibration curves with MGMM concentrations other than 200 µM were needed for the determination of the K_M-value. The correlation coefficient R^2 was always 0.99 or higher.

It should be noted that – although always linear and in good correlation with the concentration of methionine – the absolute fluorescence values measured are dependent on factors such as age and state of used HRP, AAO and Amplex Red stock solution. Parameters of the Multiplate Reader such as intensity of the lamp also influence these values.

Table 4-1 Calibration curves for different MGMM concentrations present during detection

Concentration of MGMM [µM]	Calibration curve
100	F = 65282*[µM Met]
150	F = 64337*[µM Met]
200	F = 63893*[µM Met]
400	F = 61802*[µM Met]
800	F = 60588*[µM Met]
1200	F = 60188*[µM Met]
2000	F = 55638*[µM Met]
3000	F = 51562*[µM Met]

4.2.2.5 Assay Optimization

In the described continuous assay, 50 µM Amplex Red were used. It has been shown that up to 10 µM of released methionine can be detected and that 10 µM Amplex Red is sufficient and gives the same results as 20, 30 and 40 µM (data not shown), reducing the costs of the assay as well as the amount of DMSO present during detection.

EcMetAP is highly interfering with plastic. For example, vortexing of the MetAP solution in Eppendorf vials diminishes the activity to 5 %. Even pipetting of MetAP solution into eight wells one well after the other reduces the activity to 20 %. In order to limit the inactivation of MetAP by minimizing the adsorption of the protein on plastic, several substances have been tested as additives such as detergents (for example Tween 20), glycerole or BSA. Although 0.1 % BSA slightly reduces (and Tween 20 increases) the fluorescence values maintained, this does not affect linearity. Only BSA proved to be an effective additive reaching its maximum effect at concentrations from 0.05 to 0.1 %. Therefore, the MetAP dilutions used in the assay were made with 0.1 % BSA in buffer. 0.1 % BSA during the assay decreases the amount of required enzyme by a factor of 10 and was used for further assays.

It should be noted that although substances with oxidizing or reducing properties interfere with the detection part, DTT is tolerated in small amounts (tested up to 3 µM) but reduces the linear detection range (data not shown). However, it is not possible to use GSH in the concentrations mentioned in the literature (5 mM) because it forms a precipitate with Co(II).

4.2.2.6 Assay Validation

In order to optimize the reaction time and to adjust the concentrations of enzyme and substrate used, the turnover rate of the MetAP for different conditions should be investigated.

It has been shown that

i) the turnover of MGMM after a given reaction time is proportional to the amount of MetAP used (Fig. 4-11)

ii) the turnover of MGMM with a constant amount of MetAP is proportional to the reaction time up to about 20 min (Fig. 4-12).

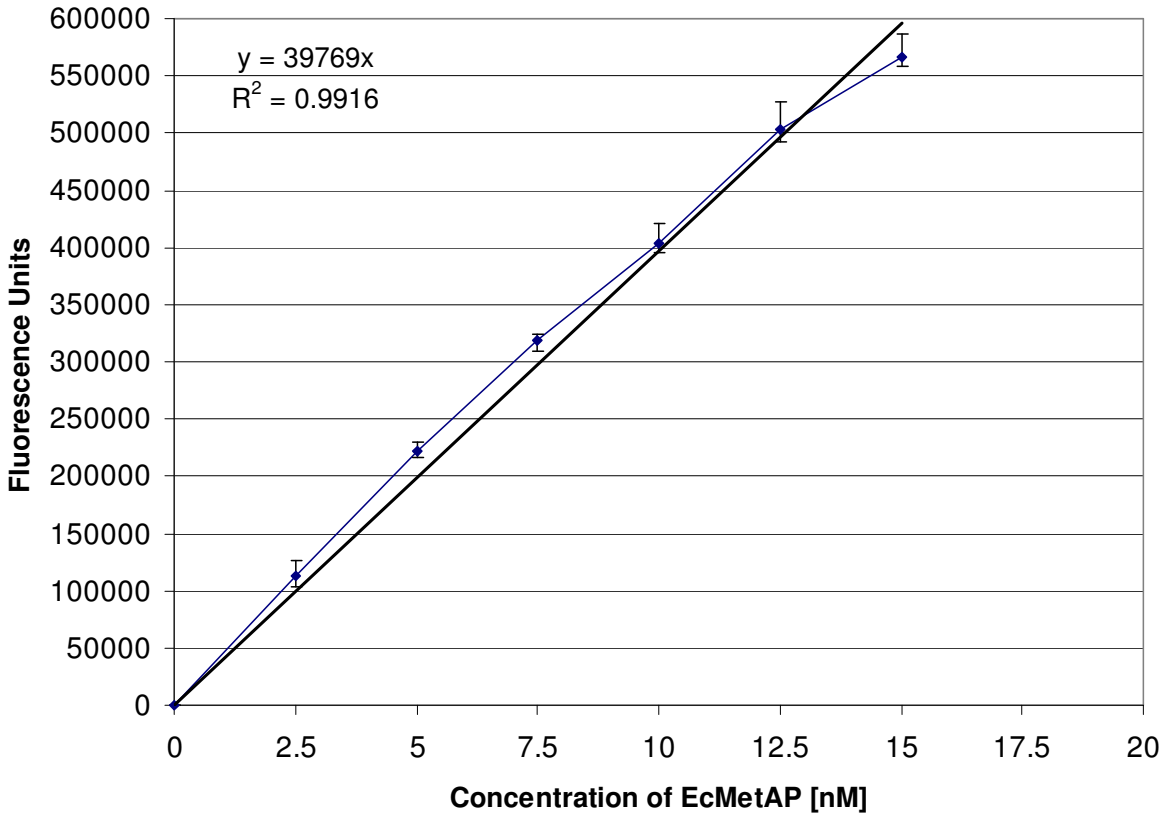

Fig. 4-11 Correlation between the concentration of EcMetAP and substrate turnover (15 min reaction time), 200 µM MGMM, 1.05 U/well HRP, 0.0075 U/well AAO, 9 mM EDTA, 10 µM Amplex Red (final volume 250 µl)

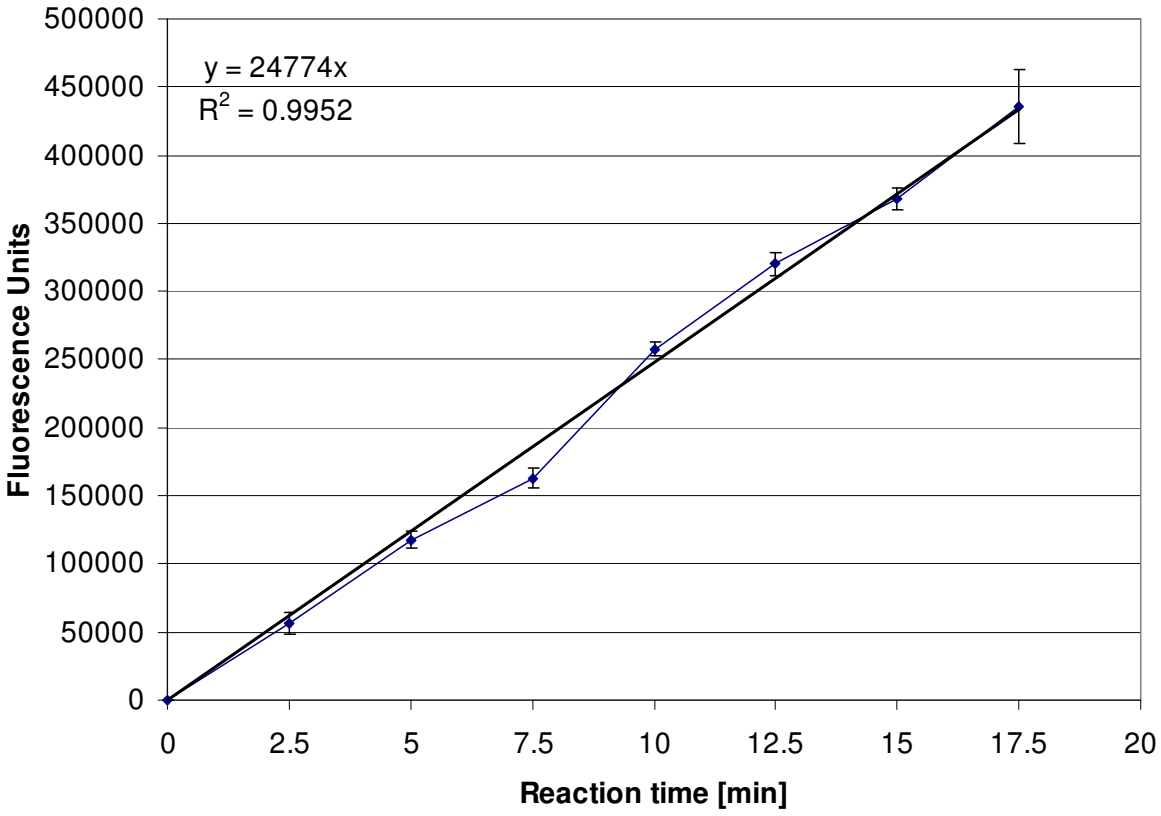

Fig. 4-12 Correlation between the reaction time and substrate turnover (10 nM MetAP), 200 µM MGMM, 1.05 U/well HRP, 0.0075 U/well AAO, 9 mM EDTA, 10 µM Amplex Red (final volume 250 µl)

The reaction time was set to 15 min with 10 nM MetAP and 200 µM MGMM used during the reaction part.

After these successful experiments, the assay was used for the subsequent characterization of the EcMetAP and for further tests.

4.2.3 Characterization of the EcMetAP

4.2.3.1 Determination of the K_M-value

The K_M-value (substrate concentration with the semi-maximal conversion-rate) was determined by incubation of the enzyme with eight different substrate concentrations. The conversion rate(s) and the parameters mentioned in Table 4-2 were calculated from the calibration curves (Table 4-1) and analyzed using the Lee and Wilson modified Lineweaver-Burk-equation[76].

Table 4-2 Substrate- and product-concentrations after 15 min reaction and resulting conversion rates

Initial MGMM conc. µM	Fluoresc. value meas.	Conversion factor (Fluoresc. for 1 µM Met)	Released Met µM	Final substrate-conc. µM	Medium substrate-conc. s* µM	1/s* µM-1	Reaction-rate v* µmol/(l*15 min)	1/v* l*15 min/µM
100	41305	65282	0.633	99.367	99.684	0.010	0.633	1.580
150	58469	64337	0.909	149.091	149.546	0.007	0.909	1.100
200	63690	63893	0.997	199.003	199.502	0.005	0.997	1.003
400	101329	61802	1.640	398.360	399.180	0.003	1.640	0.610
800	157792	60588	2.604	797.396	798.698	0.001	2.604	0.384
1200	201657	60188	3.350	1196.650	1198.325	0.001	3.350	0.298
2000	211828	55638	3.807	1996.193	1998.096	0.001	3.807	0.263
3000	227404	51562	4.410	2995.590	2997.795	0.000	4.410	0.227

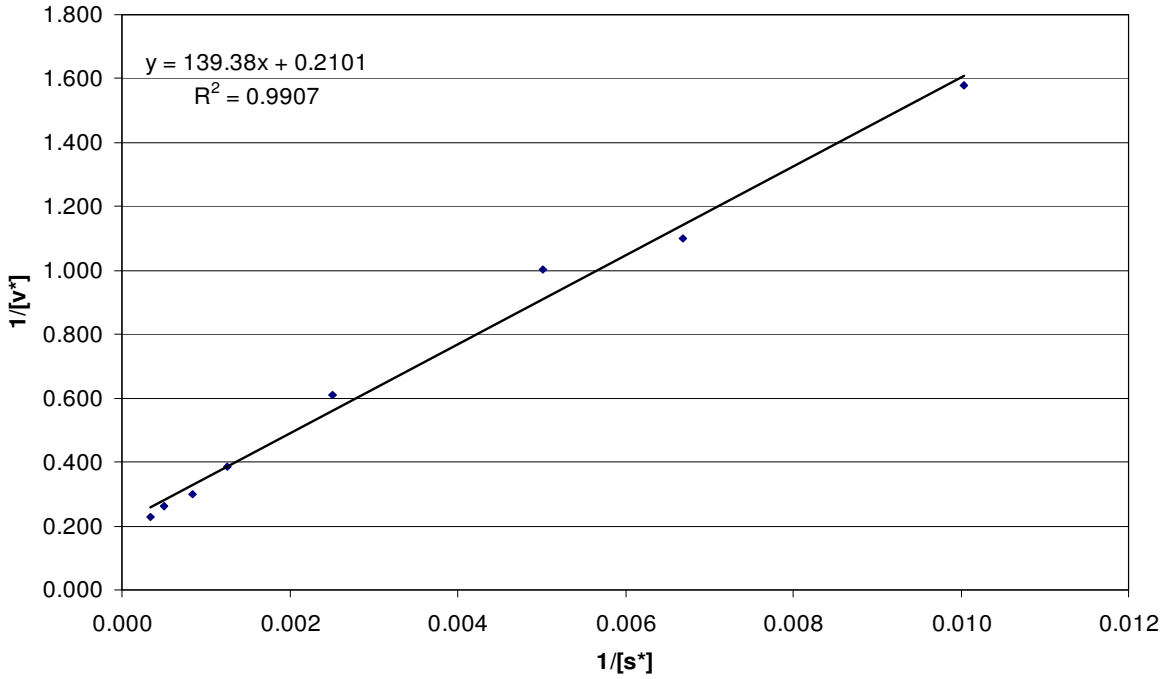

Fig. 4-13 Graphical portrayal of 1/s* against 1/v* after Lee-Wilson for the determination of the K_M-value

The K_M-value was determined in three independent measurements as the reciprocal of the negative x-axis-intercept of the graphical portrayal of 1/s* against 1/v* (see Fig. 4-13)**.** After solving the equation

$$y = mx + n \;\Leftrightarrow\; x = -\frac{n}{m}$$

the K_M was determined to be 804 µM (± 105 µM).

Normally, the substrate concentration within an assay should be in the range of the K_M-value and up to 20% of the substrate should be cleaved within an assay. It was clear from Fig. 4-7 that only up to 10 µM Met could be detected. Therefore, 200 µM MGMM were judged to be sufficient for the enzyme to work under saturated conditions (with a turnover of max. 10 µM or 5 %) and this substrate concentration was used for the further testing.

4.2.3.2 Stability of the EcMetAP Kept on Ice

Unlike HsMetAP-II that can be stored at 4 °C for several months without a significant loss of activity[69], EcMetAP is very susceptible to oxidation. In the literature, it is described that in the presence of 15 mM Met at 4 °C it takes 14 days for EcMetAP to lose 90 % of its activity and that in the absence of Met, the rate of activity loss increases 10-fold. Addition of fresh Met does not restore activity[71].

The MetAP is immediately inactivated by bubbling molecular oxygen through the solution and inactive MetAP is not reactivated by fresh Co(II). This can be explained considering the redox potential of Co(II)/Co(III). This potential is 1.18 V, much higher than the potential of Fe(II)/Fe(III) with 0.77 V that is readily oxidized on contact with air. Thus, simple oxidation of the metal is not the likely route of inactivation. A likely target of oxidation is one or more of the seven cysteine residues in the molecule as cysteine modification with iodoacetamide leads to inactivation[59]. The sulfur atoms in Cys59 and Cys70 are close enough to form a disulfide bond which would partially close the opening to the active site or induce conformational change. This is supported by the fact that TCEP, a reagent specifically reducing disulfide bonds, can reactivate oxidized MetAP; and untreated MetAP was more active than MetAP treated with DTNB, a substance specifically reacting with cysteine RSH groups[71].

For these reasons, the activity of EcMetAP-aliquots kept on ice was determined after different storage times:

The amount of released Met drops by about 80 % when the solution is kept on ice for about 8 hrs (Table 4-3). This is mainly due to the aging of the (diluted) MetAP solution.

The findings above support the facts described in the literature as methionine or another antioxidant was absent in the stock solution of EcMetAP and during the assay. In addition, BSA was also absent, therefore much higher MetAP-concentrations were needed and adsorption to plastic surfaces might also partly explain the drop in activity.

Table 4-3 Dependency between the age of MetAP solutions kept on ice and MetAP activity for 400 nM MetAP, without BSA

Storage Time [hrs]	Activity [%]
0	100
4	84.2
8	27.1

4.2.3.3 Influence of DMSO and EtOH

As many of the inhibitors described in the literature are only sparingly soluble in water, stock solutions of DMSO or EtOH are often necessary for the testing of compounds. Therefore, the impact of different concentrations of DMSO and EtOH on the activity of EcMetAP was examined (Fig. 4-14).

It has been shown that the turnover rate of MGMM is strongly decreased by the presence of DMSO or EtOH (Fig. 4-14). Even small amounts (1 %) result in a drop of activity of about 30 % for EtOH and even 60 % for DMSO. As a consequence, more EcMetAP would be needed for testing. Thus, the amount of these solvents (derived from inhibitor solutions) should be minimized in order to retain the high sensitivity of the assay. For further tests, a maximum concentration of 0.1 % DMSO or EtOH was used.

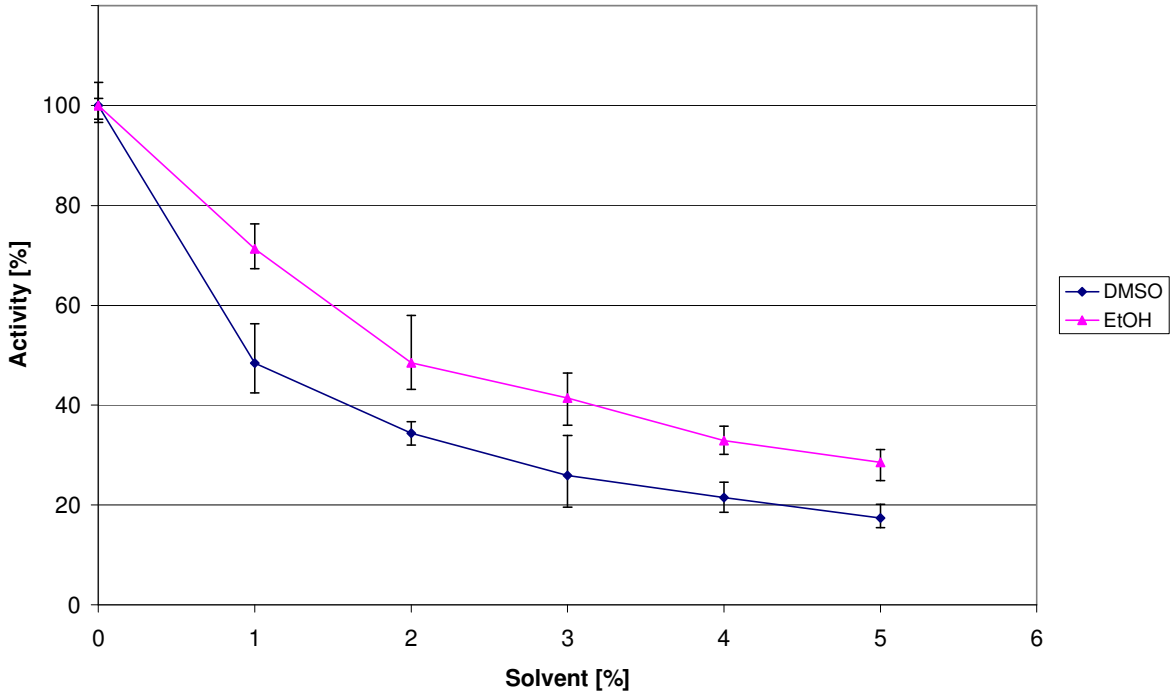

Fig. 4-14 Influence of EtOH and DMSO on MetAP activity (10 nM MetAP, 200 µM $CoCl_2$, 200 µM MGMM, 1.05 U/well HRP, 0.0075 U/well AAO, 9 mM EDTA, 10 µM Amplex Red, final volume 250 µl)

4.2.3.4 pH-Profile of MetAP Activity

The activity of EcMetAP over a broad pH-range was examined (cfr. Fig. 4-15) and the region with the highest activity was again measured in detail (cfr. Fig. 4-16).

The pH-optimum was determined to be 7.5. This is in accordance with the value from literature. Several tests demonstrate that MetAP has a pH optimum near neutrality: 7.5 was reported for EcMetAP[75, 77] and 7.0 for ScMetAP[44, 61].

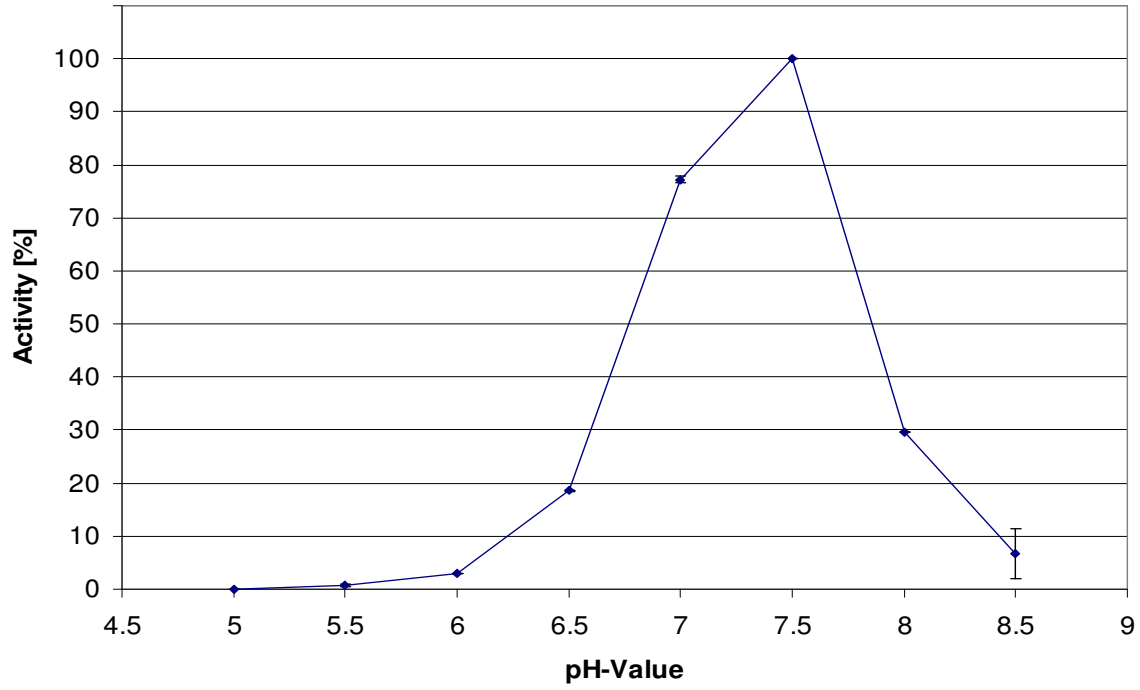

Fig. 4-15 Dependency between MetAP activity and pH-value, range 5 - 8.5 (10 nM MetAP, 200 µM $CoCl_2$, 200 µM MGMM, 1.05 U/well HRP, 0.0075 U/well AAO, 9 mM EDTA, 10 µM Amplex Red, final volume 250 µl)

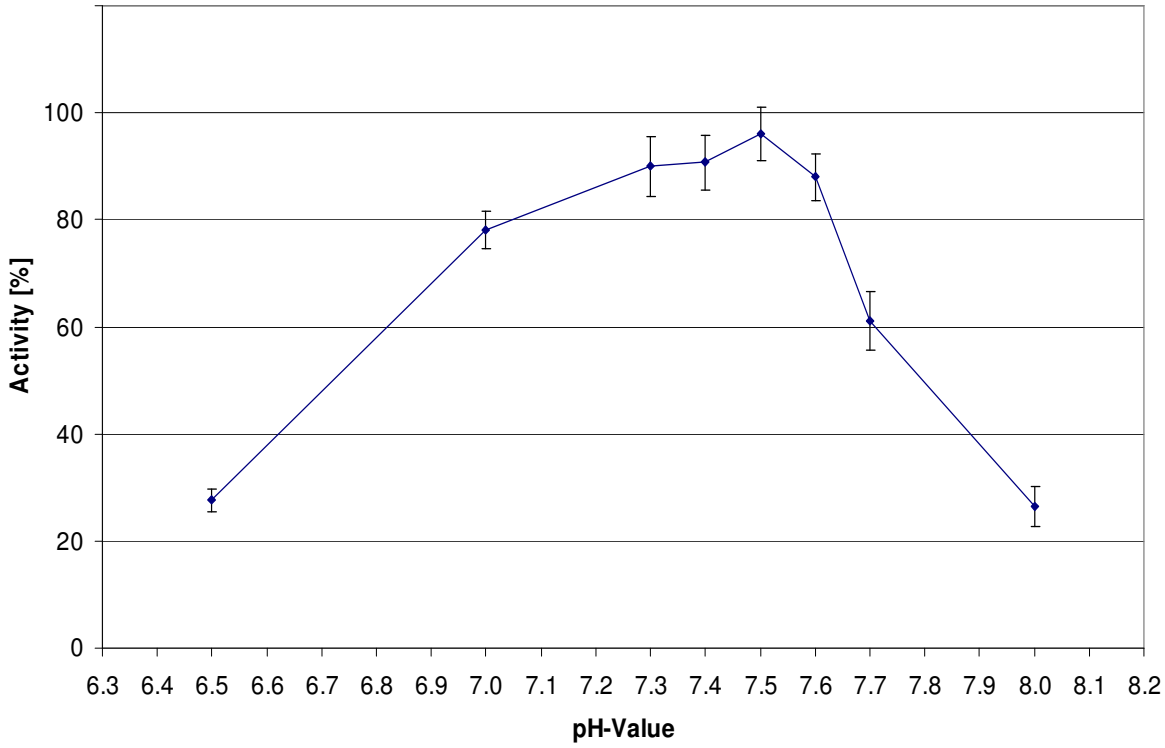

Fig. 4-16 Dependency between MetAP activity and pH-value, range 6.5 – 8 (10 nM MetAP, 200 µM $CoCl_2$, 200 µM MGMM, 1.05 U/well HRP, 0.0075 U/well AAO, 9 mM EDTA, 10 µM Amplex Red, final volume 250 µl)

4.2.3.5 Metal Specificity

4.2.3.5.1 Overview

The identity of the metal ion bound *in vivo* has not been firmly established. All types of MetAPs are known to be stimulated by Co(II) and inactivated by EDTA, therefore it has been assumed that MetAPs are Co(II)-dependent enzymes. Activity has also been observed with other metal ions, depending on the type and origin of MetAP, assay conditions and substrate used. These results are summarized in Table 4-4.

Table 4-4 Metal dependency of different MetAPs

MetAP of	activated by	inactive with	Other observations	Ref.
Synechocystis	Co(II), Mn(II), Zn(II), Mg(II)		*Synechocystis* expresses three different MetAPs-I differing in substrate specificity, divalent metal ion requirement, pH and temperature optima	[62]
S. typhimurium	Co(II)		The metal is loosely associated and lost during purification	[59]
S. aureus	Co(II), Mn(II), Zn(II)		Ni(II) activates the enzyme at low concentrations and strongly inhibits the Co(II)-activated enzyme at higher concentration; an activation by Fe(II) was not reproducible	[78]
E. coli	Co(II)		The metal is loosely associated and lost during purification	[59]
E. coli	Co(II)	Mn(II), Cu(II), Zn(II), Mg(II)	The enzyme is inactive in the presence of EDTA and its activity is Na^+/K^+-dependent	[4]
E. coli	anaerobically: Co(II), Fe(II), Mn(II), Zn(II), Co(II)+GSH, Fe(II)+GSH, Zn(II)+GSH		Fe(II) is proposed as the relevant metal ion, this is underlined by ICP analysis. Whole cell analysis showed that the Fe(II)-, Mn(II)- and Zn(II)-levels increase upon MetAP-expression with the largest increase for Fe(II). Excess metal ions are inhibitory. The addition of Co(II) and Fe(II) resulted in the highest activity even in the presence of glutathione. Zn(II) and GSH resulted in a slightly active enzyme, Mn(II) and GSH were not tested.	[79]
E. coli	anaerobically: Co(II), Fe(II)		Only one metal ion seems to be relevant for activity and is tightly bound, this is underlined by ICP analysis, EPR spectra and ^{1}H-NMR spectra. The second ion is loosely associated and there is a weak binding site for a third metal ion. K_D = 200 nM for the first and 2.5 mM for the second binding site.	[80]
E. coli	aerobically: Fe(II)			[78]
E. coli	Co(II), Zn(II)		Activity with Zn(II) is observed when MetAP is prior treated with EDTA, MetAP is inactivated by higher Zn(II)-concentrations.	[52]
E. coli	Mn(II)		Maximum activity was observed with one equivalent of metal, K_D = 3-6 µM for the first binding site	[81]

MetAP of	activated by	inactive with	Other observations	Ref.
E. coli	Co(II), Mn(II), Zn(II), Ni(II)		The activation by Ni(II) and Zn(II) is substrate dependent: Ni(II) activates the enzyme only with Met-AMC, Zn(II) not with Met-AMC but with Met-S-Gly-Phe	[82]
P. furiosus	Co(II)			[66]
P. furiosus	Fe(II), Co(II)	Zn(II)	Maximum activity was observed with one equivalent of metal, K_D = 20-50 nM for the first, 350 µM for the second binding site	[83]
P. furiosus	Co(II), Mg(II)	Zn(II), Mn(II)		[6]
P. furiosus	Mn(II)		Maximum activity was observed with one equivalent of metal, K_D = 1 µM for the first binding site	[81]
S. cerevisiae I	Co(II), Zn(II), Mn(II), Ni(II), Zn(II)+GSH, Mn(II)+GSH	Ca(II), Cu(II), Fe(II), Mg(II), Co(II)+GSH, Ni(II)+GSH	Zn(II) is proposed as the relevant metal ion	[84]
S. cerevisiae I	Co(II), Zn(II), Mn(II)	Ni(II), Mg(II), Ca(II), Cd(II), Cu(II)	Met-S-Gly-Phe was used as a substrate	[85]
S. cerevisiae II	Co(II)	Mg(II), Mn(II), Cu(II), Fe(II), Zn(II)	MetAP is inactivated by EDTA, o-phenanthroline and by Zn(II)	[61]
S. cerevisiae II	Co(II)			[44]
Human MetAP I	Co(II), Mn(II), Zn(II)+GSH, Co(II)+GSH, Fe(II)+GSH			[86]
Human MetAP I	Co(II), Zn(II)			[87]
Human MetAP II	Mn(II), Co(II), Mn(II)+GSH, Co(II)+GSH		The importance of Mn(II) is underlined by *in vivo* inhibition tests with metal selective inhibitors, Zn(II)+GSH and Ca(II)+GSH resulted in a slightly active enzyme	[86]
Human MetAP II	Co(II)	Zn(II)	Zn(II) and excess Co(II) are inhibitory, Zn(II) was excluded as relevant	[69]

Apart from Co(II), also Zn(II), Mn(II), Ni(II) and Fe(II) have been claimed to be the relevant metal ion.

The idea of Fe(II) being the *in vivo* metal ion is supported by the analysis of the metal content changes of whole *E. coli* cells by inductively coupled plasma emission analysis. Nevertheless, Fe(II) activates EcMetAP only under anaerobic conditions.

Activation by Zn(II) is generally observed under special assay conditions such as the presence of 5 mM GSH. However, anaerobic analysis of EcMetAP suggested that Zn(II) is not the relevant ion[52, 80, 88].

Only few results concerning metal-specificity have been obtained under *in vivo* conditions. In 1987, the influence of different metal ions that had been added to the growth medium on the

Met-cleavage of TNF in *E. coli* has been analyzed. A linear correlation was observed with Mn(II) (see Fig. 4-17) and there is clear indication that N-terminal excision is strongly stimulated by the addition of external manganese to the growth medium[89]. Additionally, the pH value has an influence: Met cleavage is promoted at a pH above neutral[89]. The second *in vivo* result also favours Mn(II) as the *in vivo* relevant metal ion[86], albeit for HsMetAP-II. Here, metal-selective inhibitors with Mn(II)-specificity correlate with growth inhibition whereas an inhibitor without Mn(II)-specificity does not inhibit growth (although the compound accumulates in the cytosol). In addition, several Mn(II)-specific inhibitors tested and crystallized with human MetAP-II are active *in vivo*[90]. Recently, Wilce *et al.* reported the crystal structure of proline aminopeptidase from *E. coli*, which contains two manganese ions per subunit and shows similarity to the *E. coli* MetAP in sequence and structure[91].

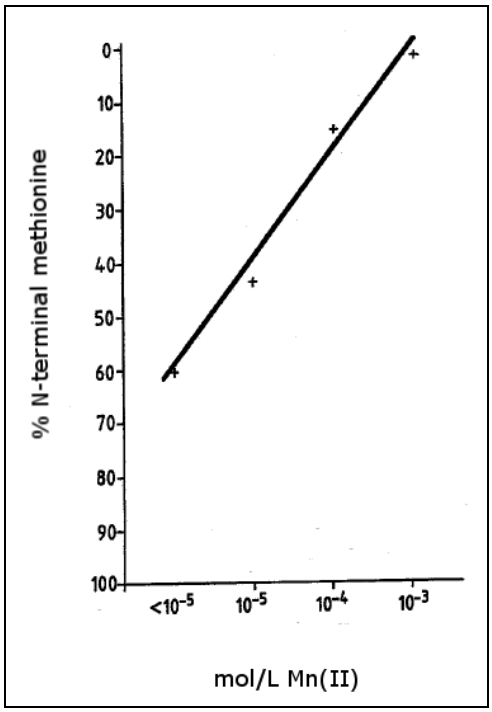

Fig. 4-17 Dependency of Mn(II) addition and N-terminal methionine of TNF, according to [89]

However, the activation of MetAPs by different metal ions is dependent on the assay conditions and factors such as type and origin of the MetAP or substrate used and varies with aerobic or anaerobic conditions. For the screening of inhibitors, Co(II) is generally used as it reliably activates all MetAPs. Thus, the question of the relevant metal ion still is contentious.

4.2.3.5.2 Concentration of Co(II)

First, the concentration of Co(II) was varied over a broad range (1-10000 equivalents, cfr. Fig. 4-18) and the area with the highest activity was studied in detail (cfr. Fig. 4-19).

The highest activity was observed with 50-300 µM $CoCl_2$. This amount is in the lower range of metal concentrations used by other groups. Concentrations of 100 µM[75] up to even 1.5 mM Co(II)[92] are used. The drop of activity at higher metal concentration has been observed before, for example in Co(II)-loaded yMetAP and in the zinc dependent enzyme carboxypeptidase[93]. In the case of MetAP, excess cobalt may be binding to the bridging hydroxide ligand which is crucial for catalytic activity.

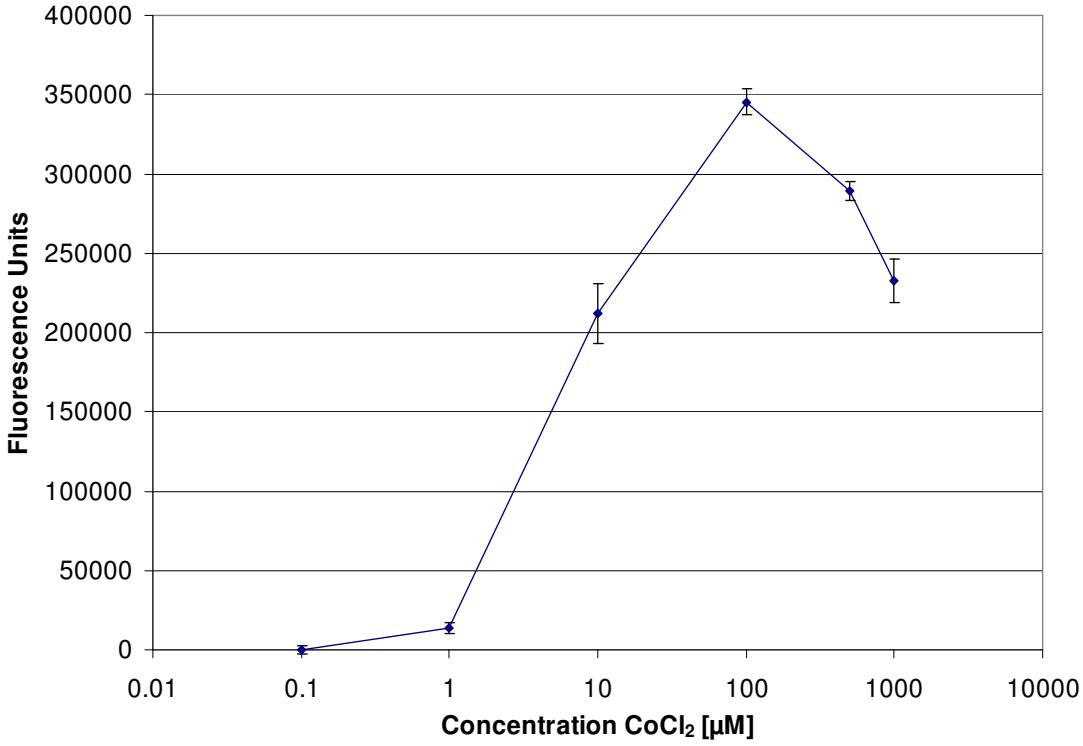

Fig. 4-18 Dependency of MetAP activity from Co(II) concentration; range 0.1-1000 µM (10 nM MetAP, 200 µM MGMM, 1.05 U/well HRP, 0.0075 U/well AAO, 9 mM EDTA, 10 µM Amplex Red, final volume 250 µl)

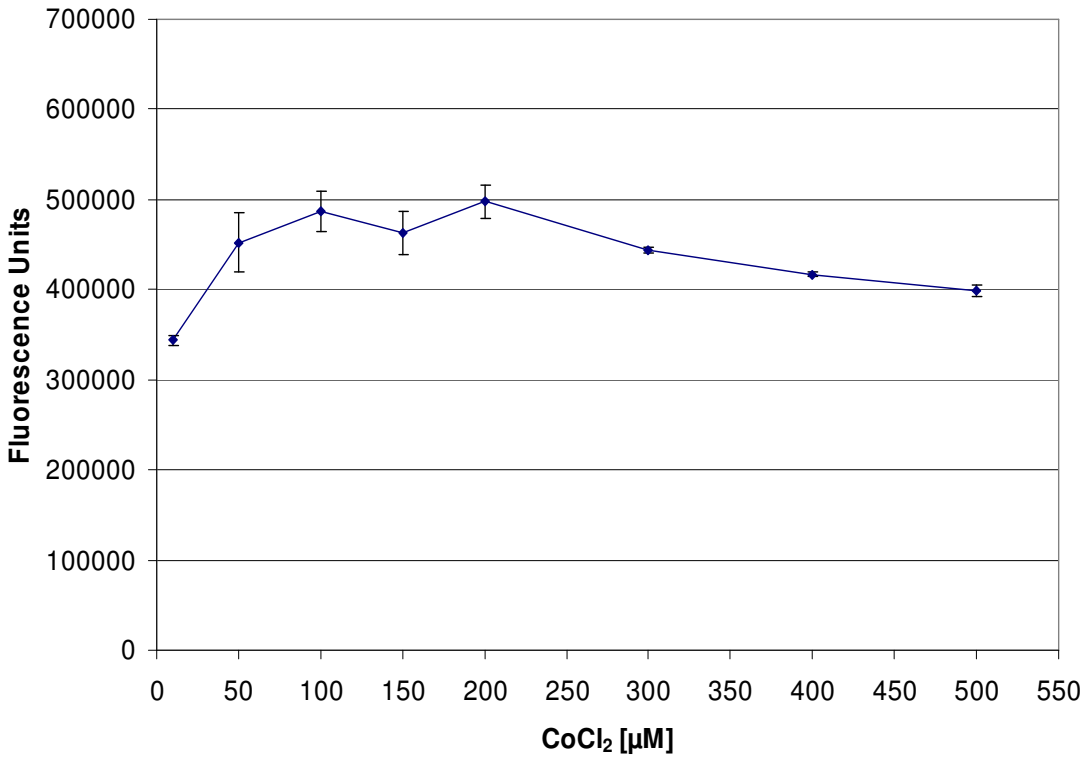

Fig. 4-19 Dependency of MetAP activity from Co(II) concentration; range 10-500 µM (10 nM MetAP, 200 µM MGMM, 1.05 U/well HRP, 0.0075 U/well AAO, 9 mM EDTA, 10 µM Amplex Red, final volume 250 µl)

4.2.3.5.3 Metal Specificity

The following divalent metal ions were tested for their ability to activate the isolated apo-enzyme: Zn(II), Mn(II), Mg(II), Ni(II), Ca(II), Cu(II), Fe(II) and Fe(III). Co(II) was used as a reference.

Apart from Co(II), only Mn(II) was able to activate the apo-enzyme, albeit higher concentrations were needed and the maximum turnover rate was only about 30 % when compared to the maximum activation of the Co(II)-loaded form. Contrary to Co(II), no optimal concentration could be determined for Mn(II) up to a concentration of 1 mM and the activity of the Mn(II)-loaded MetAP seems to reach a plateau.

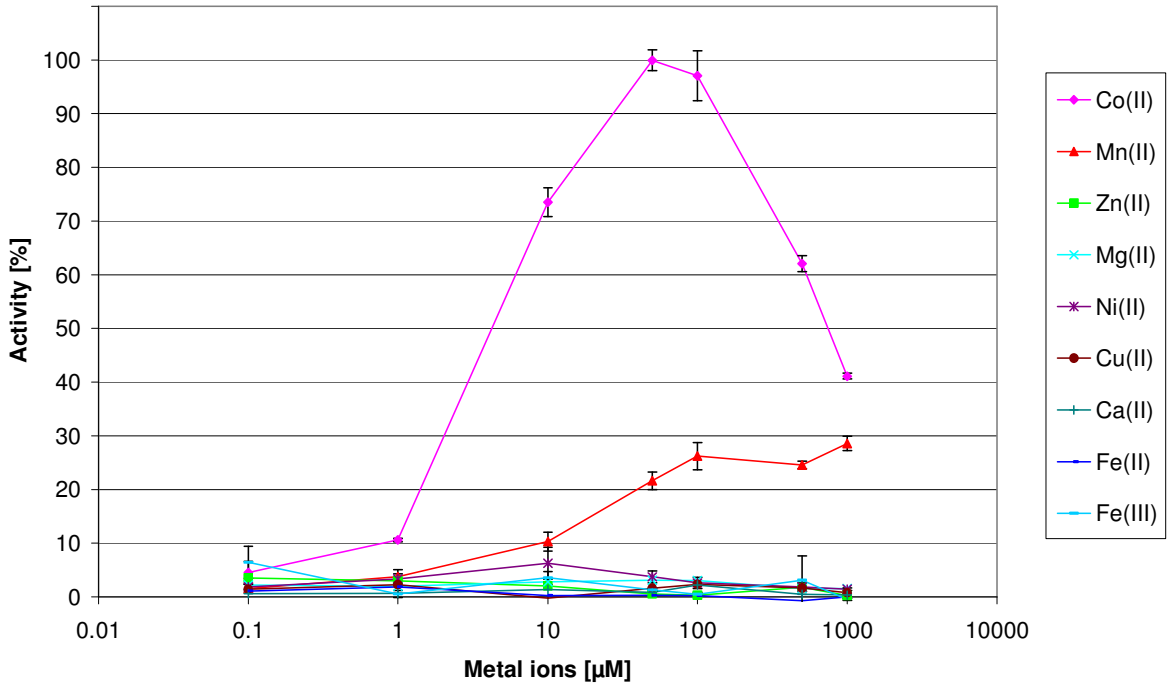

Fig. 4-20 Metal specificity of EcMetAP (10 nM MetAP, 200 µM MGMM, 1.05 U/well HRP, 0.0075 U/well AAO, 9 mM EDTA, 10 µM Amplex Red, final volume 250 µl)

When competing the above mentioned metal ions individually against 200 µM Co(II), all ions acted as inhibitors and decreased MetAP activity. Cu(II) and Zn(II) are most effective inhibitors of the Co(II)-activated EcMetAP and have an IC_{50}-value between 1 and 10 µM, Mn(II), Fe(II) and Mg(II) have an IC_{50}-value of 100 µM whereas Mg(II), Ca(II) and Fe(III) had no (dose dependent) effect on MetAP activity. The results are summarized in Table 4-5.

Table 4-5 Metal competition tests with 200 µM $CoCl_2$ and various concentrations of different metal ions. Shown is the residual activity [%] compared to 200 µM $CoCl_2$ without any other metal ion added (100 %)

[µM]/Me	Zn(II)	Cu(II)	Ni(II)	Fe(II)	Mn(II)	Mg(II)	Fe(III)	Ca(II)
0.01	97.3	100	100	100	100	100	100	100
0.1	94.8	100	100	100	100	100	100	100
1	90.1	96.4	100	100	100	91.6	100	100
10	22.9	3.7	100	91.0	100	96.4	100	100
100	0	0	39.5	45.1	63.5	95.5	100	100
200	0	0	14	9.1	51.2	98.1	100	100
400	0	0	2.9	4.5	41.2	88.3	100	100

The inactivation by other divalent metal ions may not be due to an interference with the active site but can also stem from an influence on the protein fold or an interaction with other metal-binding residues such as cysteines or histidines. Therefore, these results do not shed light on the question of the relevant metal ion. However, these findings at least seem to rule out Ca(II), Mg(II) and Fe(III) as relevant cations as they seem to be unable to compete with Co(II) and do not disturb the activity of a Co(II)-loaded enzyme.

In summary, the results from the metal specificity-tests together with the findings described in the literature clearly favour Co(II) and Mn(II) as candidates for the *in vivo* metal ion of the EcMetAP.

4.3 Covalent Inhibitors

4.3.1 Angiogenesis

In 1974, Folkman[94] suggested that many cells capable of forming tumors appear in the body at a certain frequency but the vast majority never develop into detectable tumors. The growth of these silent “microtumors” is limited due to the lack of an adequate blood supply needed to provide the nutrients and oxygen to rapidly dividing cells. These tumors never increase in size as the cells continue to divide but simply replace the cells lost due to lack of nutrients. However, at an unknown critical stage in tumor progression, a small percentage of these size-restricted “microtumors” gain the ability to induce new blood vessel formation (neovascularization) in the surrounding tissue. An increase in newly formed, highly permeable blood vessels serves to provide oxygen and essential nutrients as well as to increase the potential for tumor cells to be released into circulation. Recent experimental evidence confirms a major role for angiogenesis in the metastasis by providing conduits through which invasive tumor cells can disseminate.

Because angiogenesis contributes significantly to both the growth of tumors and their metastasis (tumor progression) and has also been established as an important step for the pathogenesis of a number of human diseases including diabetic retinopathy and rheumatoid arthritis, inhibitors of this process have significant clinical potential. In comparison with conventional chemotherapy, it is hoped that anti-angiogenic therapy will have a number of clinical advantages, including low toxicity, lack of drug resistance, and easy access of the drugs to the targeted endothelial cells.

4.3.2 Fumagillin and Analogs

4.3.2.1 Overview

The fungal metabolite fumagillin and some derivatives (i.e. Ovalicin and TNP-470, cfr. Fig. 4-21) suppress the formation of new blood vessels and tumor growth.

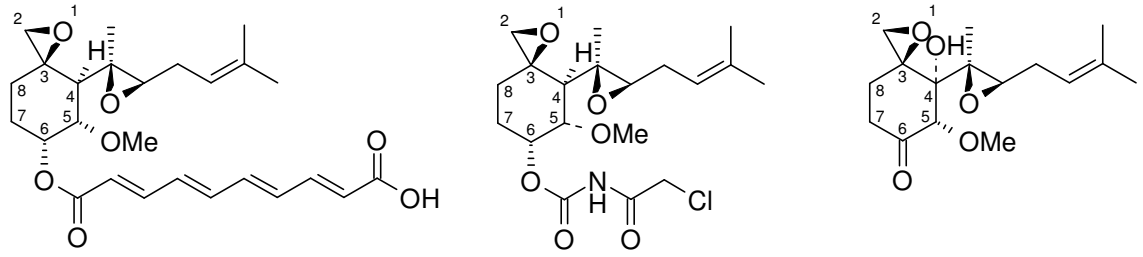

Fig. 4-21 Fumagillin and analogs

Fumagillin was originally identified as an antibacteriophagic[95] and amebicidal agent[96, 97] but fell into oblivion afterwards. Its rediscovery reminds of the story of penicillin: In 1990, a group working with cell cultures noticed a fungal contamination that selectively inhibited endothelial cell proliferation[98]. The fungus was classified as *Aspergillus fumigatus fresenius* and cultivated. Then, the active compound was isolated and identified as fumagillin.

Subsequently, many attempts have been made to improve the activity of fumagillin. TNP-470 is a semisynthetic analogue and entered human clinical trials for the treatment of AIDS-related Kaposi's sarcoma, metastatic breast cancer, androgen-independent prostate cancer, brain cancer, pediatric solid tumors, lymphomas, acute leukemias, advanced squamous cell cancer of the cervix, and metastatic renal carcinoma[99-102]. Another TNP-470 based MetAP-II inhibitor has been reported useful for the treatment of rheumatoid arthritis[103]. These compounds are also potent against *P. falciparum* and other parasites and might be useful for the treatment of malaria or leishmaniasis[104].

However, there are also known side effects of these drugs: Prolonged administration of fumagillin or TNP-470 leads to severe weight loss. TNP-470 has a short serum half-life (2-6 min in human) and dose-limiting side effects such as a (reversible) characteristic neuropsychiatric symptom complex (anaesthesia, disturbance of equilibrium and agitation)[105]. Chemical derivatives are still being synthesized in order to improve the poor pharmacokinetic behaviour and dose-limiting toxicity of TNP-470 that can at least in part be attributed to the presence of two epoxides and a chloroacetyl group[106]. Replacement of the fatty-acid residue in Fumagillin by a trans-cinnamic acid ester with a tri-methyoxy phenyl moiety gave a 1000 times more potent substance (CKD-731) than TNP-470[107].

In spite of the side effects, these inhibitors have been reported to be useful in combination with traditional chemotherapeutic agents and may be utilized to potentiate conventional

chemotherapy[108, 109]. Drug resistance in tumor cells or endothelial cells does not appear to occur during angiogenesis inhibition. In addition, these drugs might be tolerated for chronic use.

Epoxides are normally considered to be highly reactive chemical species. In the absence of general acid or Lewis acid catalysis however, reactions with physiological nucleophiles that open the epoxide ring can be expected to be extremely slow. Furthermore, additional structural elements of the inhibitor including chirality have a strong effect on reactivity. Examples of inhibitors that exploit electrophilic functionality besides fumagillin are, for example, the clinically used drug fosfomycin and inhibitors for HIV protease or cysteine proteases[88]. These and other (natural) compounds are able to alkylate or acylate their protein targets with incredible specificity in spite of their chemical potential for reactivity.

4.3.2.2 Mode of Action on the Molecular Basis

The underlying molecular mechanism of the effects observed by fumagillin and its derivatives was unknown until a fumagillin-binding protein, the human MetAP-II was identified independently by two groups[110, 111].

First, fumagillin was thought to inhibit only the human MetAP-II. It has been demonstrated that wild type yeast treated with fumagillin continues to grow; yeast only lacking MetAP-II is also resistant to its addition and growth of a MetAP-I deletion strain is strikingly inhibited[110]. Thus, the action of this epoxide is selective and highly specific for MetAP-II *in vivo*. Later it has been shown that both yMetAP-I and EcMetAP(-I) can also be inhibited by using higher concentrations and longer incubation times[70]. Fumagillin also binds to the Mn(II)-loaded EcMetAP[112]. A computational approach supports the hypothesis that the parasitic MetAPs are also the targets of fumagillin[113].

Fumagillin was found to form an irreversible adduct with one of the conserved histidine residues in the active site, His79 of EcMetAP and the corresponding His231 of HsMetAP-II. With *E. coli*, this has been shown by Lowther and coworkers[70], for the human enzyme this was demonstrated by Griffith and coworkers[92]. The crystal structure of HsMetAP-II with bound fumagillin is available[56] (cfr. Fig. 4-22).

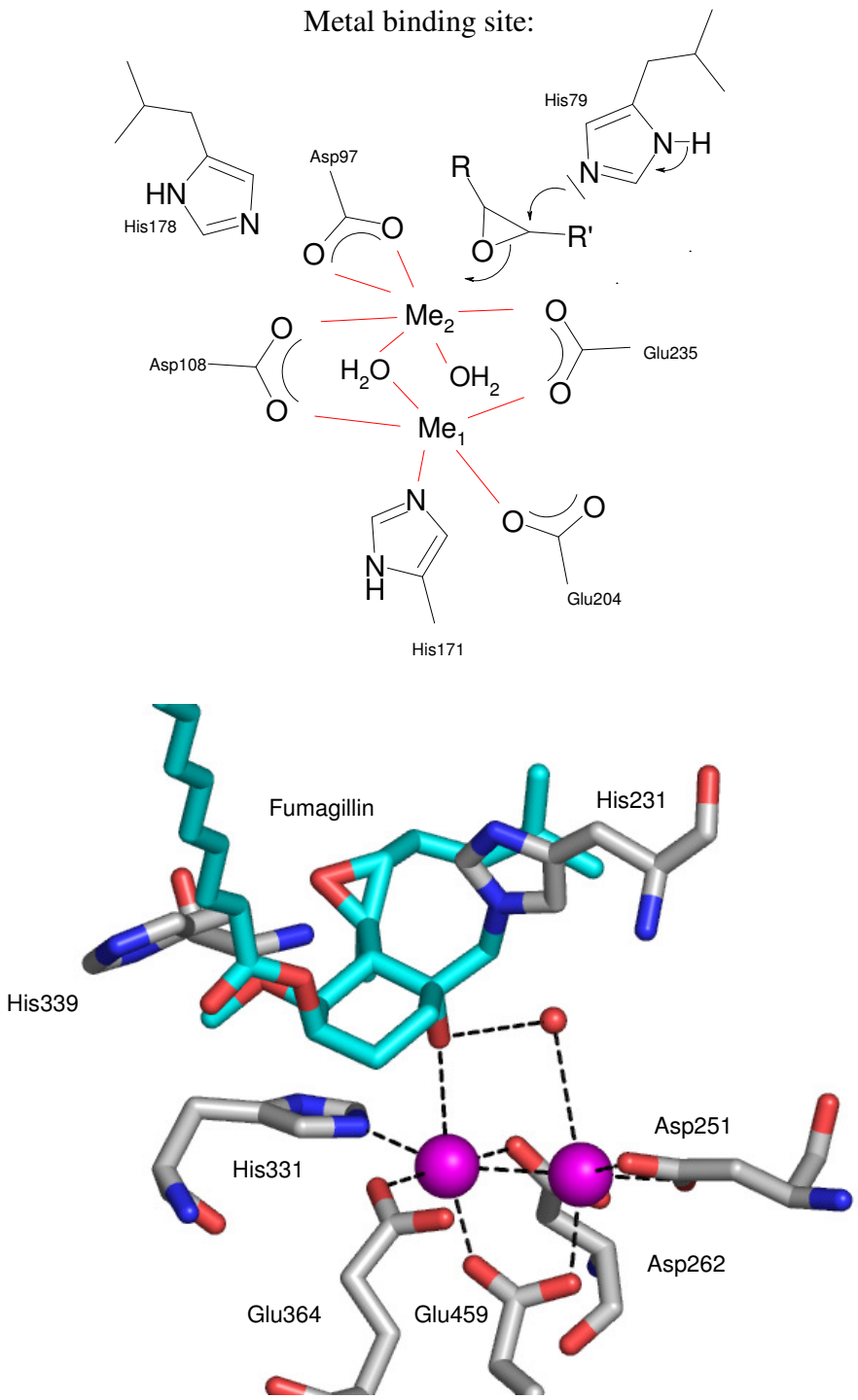

Fig. 4-22 above: schematic drawing of the fumagillin binding, numbering is forEcMetAP; below: picture of HsMetAP-II with bound fumagillin, generated from 1BOA[56]. The nitrogen from His231 binds to the carbon of the spirocyclic epoxide and the oxygen liberated from the epoxide is coordinated to a cobalt ion and hydrogen bonded to a water molecule.

Some precedent can be found in which an active-site histidine is specifically alkylated by inhibitors such as the inhibition of chymotrypsin by tos-L-phenylchloromethylketone[114].

Only the epoxide at C_3 of fumagillin confers to binding and anti-angiogenic activity[111]. Changes in the substituent at the C_6 position influence potency and bioavailability and also may cause different side effects[98, 111].

The question arises why fumagillin inhibition is specific for MetAP-II over MetAP-I because the two enzymes have very similar active sites. Several explanations seem possible: Considering MetAP-I, the binding histidine (His-79) might be too far away from the epoxide group and moving either fumagillin towards the histidine or *vice versa* would lead to sterical clashes[56]. In addition, an increased side chain flexibility of the histidine that is covalently modified by fumagillin can be observed in the HsMetAP-I enzyme in computational studies[115]. Recent results show that a single amino acid residue is responsible for the specificity exhibited by the class of anti-angiogenic agents for MetAP-II over MetAP-I and for ovalicin-resistance[116]. Alanine in the position 362 of the HsMetAP-II is substituted by a threonine in the type-I enzyme. Mutation of this residue to alanine conferred ovalicin-sensitivity to MetAP-I, but it is not clear how these mutations affect the movement of amino acids in the binding pocket in response to the binding of the inhibitor.

4.3.2.3 Mode of Action on the Physiological Basis and Role of MetAP-II

Fumagillin or TNP-470 arrest endothelial cells in the late G1 phase of the cell cycle at low nanomolar concentrations[117]. The correlation between the antiproliferative activity of fumagillin with the ability to inhibit MetAP-II activity *in vitro*[111, 118] and *in vivo*[119] suggests that MetAP-II is the physiologically relevant target.

Many groups have tried to clarify the relation between MetAP-inhibition and endothelial cell cycle arrest. Although MetAP-II expression correlates with cell growth and MetAP-II is found at higher concentrations in tumors[120, 121], it has been ruled out that differential expression of MetAPs in different types of cells[122, 123] is the reason for selective inhibition of endothelial cell proliferation. Upregulation of MetAP-II by exposure to fumagillin can be observed both in endothelial and in non-endothelial cells.

As fumagillin-based inhibitors only interfere with the catalytic moiety of the enzyme, a different substrate spectrum has been postulated to be the reason for the physiological effects. MetAP-I and MetAP-II can widely compensate for each other, but MetAP-II specific cellular substrates with MetAP-II being 1000-fold more efficient than MetAP-I have been identified,

for example glyceraldehyde-3-phosphate dehydrogenase (GAPDH), cyclophilin A[119] and 14-3-3γ. 14-3-3 proteins are ubiquitous cytosolic adaptor proteins involved in cell cycle control, apoptosis and transcriptional control. Retention of the amino-terminal methionine even only in a small subset uf cellular proteins might further lead to dysfunction of proteins, to changes in protein stability or to mislocalization of proteins within cells due to prevention of N-terminal myristoylation[124].

An impact on kinases and the activation of the so-called "p53-pathway" could also be the answer for cell cycle arrest upon MetAP-II inhibition. Activation of p53, a protein acting as a transcriptional activator of genes, leads to the inhibition of Cyclin dependent kinases (CDKs). CDKs drive cell cycle progression and are in turn regulated at cell cycle checkpoints by CDK inhibitors such as $p21^{CIP/WAF}$ or $p16^{INK4a}$. CDK inhibition consequently leads to cell cycle arrest at the G1 to S transition[125, 126]. This is called the "p53-pathway". TNP-470 induces expression of $p21^{CIP/WAF}$ only in endothelial cells but not in embryonic or adult fibroblasts and thus potently inhibits the activation of CDKs. Moreover, primary endothelial cells isolated from $p53^{-/-}$ and $p21^{CIP/WAF-/-}$ mice are resistant to the cytostatic activity of TNP-470[123]. This $p21^{WAF1/CIP1}$ accumulation and concentration dependent induction of apoptosis has also been observed with other MetAP-II inhibitors[127].

However, a variety of other observations has been mentioned in the literature such as the inhibition of thymidine uptake that would suggest specific inhibition of DNA synthesis[128, 129]. Fumagillin can also induce apoptosis owing to early mitochondrial damage in malignant cells[129]. The anti-angiogenic effect of fumagillin has also been attributed to the inhibition of Ets-1 transcription factor expression[130] and down-regulation of the anti-apoptotic gene bcl-2 and of telomerase activity[131] whereas bcl-2 overexpression counteracted the effect of MetAP-II inhibition[129].

The crucial role of MetAP-II in cell cycle progression is strengthened by a report that proliferation of human endothelial cells can be blocked by human MetAP-antisense oligonucleotides[129, 132]. Another group, however, found that depletion of MetAP-II by siRNA did not inhibit endothelial cell growth and MetAP-II-depleted endothelial cells remained responsive to inhibition by fumagillin[133]. Furthermore, a bengamide analogue can selectively inhibit MetAP-II without inhibiting endothelial cell proliferation. These results indicate that MetAP-II is not required for endothelial cell proliferation and are strengthened by tests with Cytochalasin E, an epoxide-containing metabolite of *Aspergillus clavatus* resembling TNP-470. Cytochalasin E is a potent and selective inhibitor of endothelial cell growth *in vitro* and

inhibits angiogenesis and tumor growth *in vivo*, but does not inactivate MetAP-II even at high concentrations[134].

In summary, the link between MetAP-inhibition and cell cycle arrest still remains unknown. One possibility for an explanation might be the existence of another MetAP-family in humans: MetAP-III[135]. MetAP-III and MetAP-I/MetAP-II might exhibit different expression and tissue distribution profiles, suggesting additional or different roles for MetAP-III in cellular metabolism and in an organism as a whole. Unfortunately, this enzyme has not been characterized and its physiological role is not yet clear. Further studies are clearly needed.

4.3.3 Protonation States of MetAPs

4.3.3.1 Computational Studies

The aim of this study was to clarify the native protonation state of the enzyme, which is needed for the development of novel inhibitors. When using molecular modeling techniques for the screening of compound-databases, not only the tertiary structure of the target protein but also the distribution of charges is crucial for the result of the docking process. Especially the metal-binding site and the cavity for substrate binding are important as these areas represent the expected binding site of potent novel inhibitors. Protons cannot be “seen” in electron density maps with normal X-ray experiments. Thus, it is not clear whether an oxygen atom represents a water molecule or a hydroxide ion. As a first step toward an understanding of the catalytic and inhibitor-binding mechanisms of MetAPs, we have performed a computational study of different protomeric states of the methionine aminopeptidase active site using a combined quantum-mechanical/molecular mechanical simulation approach[136] in our group.

Due to the uncertainty of the Co spin system and the multiplicity of the bi-cobalt system, Zn was used for the simulations. Before, it was checked that there were no major geometric or dynamic differences to a bi-zinc system, confirming another previously performed theroretical analysis[137].

In the 1.9-Å resolution X-ray structure of EcMetAP (pdb code 2MAT), one water molecule (or hydroxide ion) is bridging the two cobalt ions and another water molecule is bound to the cobalt ion that is not coordinated to the histidine. Three different protomeric states were examined (cfr. Fig. 4-23), one with two bound water molecules (A), one with a bridging hydroxide ion and a water molecule (B), and one with two hydroxide ions(C). As the bridging water molecule is more activated by the metal ions than the terminally bound water molecule, a protomeric state with a bridging water molecule and a bound hydroxide ion seems unlikely.

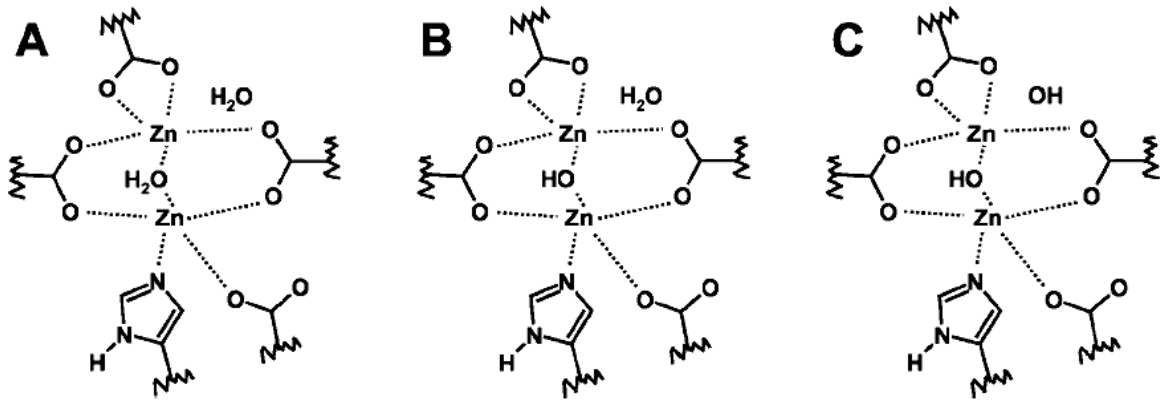

Fig. 4-23 Three different protomeric states of EcMetAP for which CPMD simulations were performed

The results of this study indicated that two protonation states are possible, namely A and B. They are intrinsically stable and quite similar to the 2MAT X-ray structure. The main changes are as follows:

i) The bridging water leaves the position between the two metals in the bi-water simulation (A) and remains bound to one of the cobalt ions, resulting in a stable system.

ii) In the water-hydroxide simulation (B), the bridging hydroxide remains in place and one of the metal-coordinating carboxylic acid groups twists to a position that is perpendicular to the X-ray structure. Nevertheless, this residue remains a binding partner for one of the metal ions and the system remains stable.

iii) Large deviations from the crystal structure were observed in the bi-hydroxide system (C). This system proved to be unstable.

These results are confirmed by X-ray structure analysis as in a structure determined at a more acidic pH no bridging water molecule is present between the two metals (pdb code 1BN5) contrary to the structure determined at a pH larger than 7 (2MAT).

4.3.3.2 pH-Dependency of Fumagillin Binding

The binding of fumagillin is expected to be favoured at more acidic pH as it requires protonation of the epoxide oxygen, whereas a more basic pH would be required for catalysis. To experimentally verify the theoretical results, the substrate hydrolysis and inhibitor binding reaction at different pH values were studied (cfr. Fig. 4-24). Covalent modification experiments can also help to clarify the active site residues if not known, their protonation state and to give an insight into the apparent pK_a values of reactive groups[138].

Whereas the pH-optimum of the substrate hydrolysis is at pH 7.4-7.5 (see Fig. 4-15), the binding of fumagillin becomes increasingly favoured at lower pH. This becomes even more apparent when looking at the %-inhibition values (cfr. Fig. 4-25). A shift of one pH-unit to a more acidic pH increases the inhibition of the enzyme by a factor of about 2-3.

Apart from the different binding capacity of fumagillin at different pH-values, another interesting observation was made: Preincubation of the MetAP at a more acidic pH (for 15 min prior to the reaction at pH 7.4) increased the activity of the enzyme compared to the preincubation at pH 7.4. It can only be speculated that (maybe) in the pH range from pH 6-7 the enzyme is better protected from oxidation whereas an even more acidic pH (< 6) or more basic pH (>8) inactivates the enzyme by an irreversible denaturation. Another possible explanation for this phenomenon might be a reduced interference with plastic at a more acidic pH.

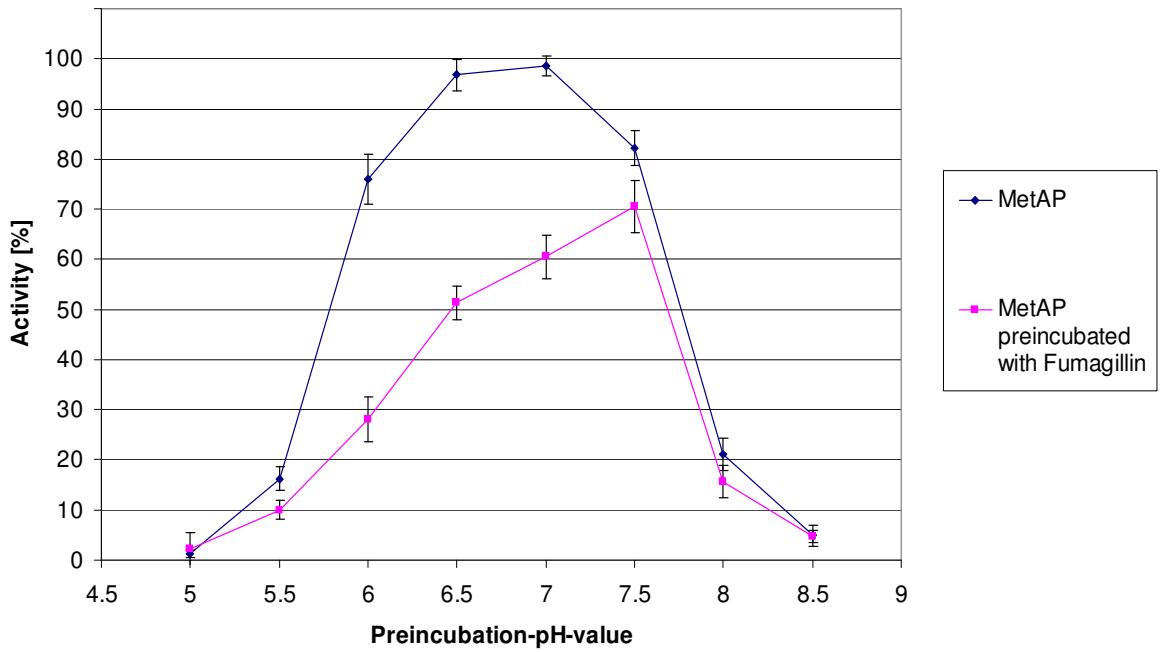

Fig. 4-24 Dependency of the fumagillin-binding on EcMetAP and the preincubation pH-value

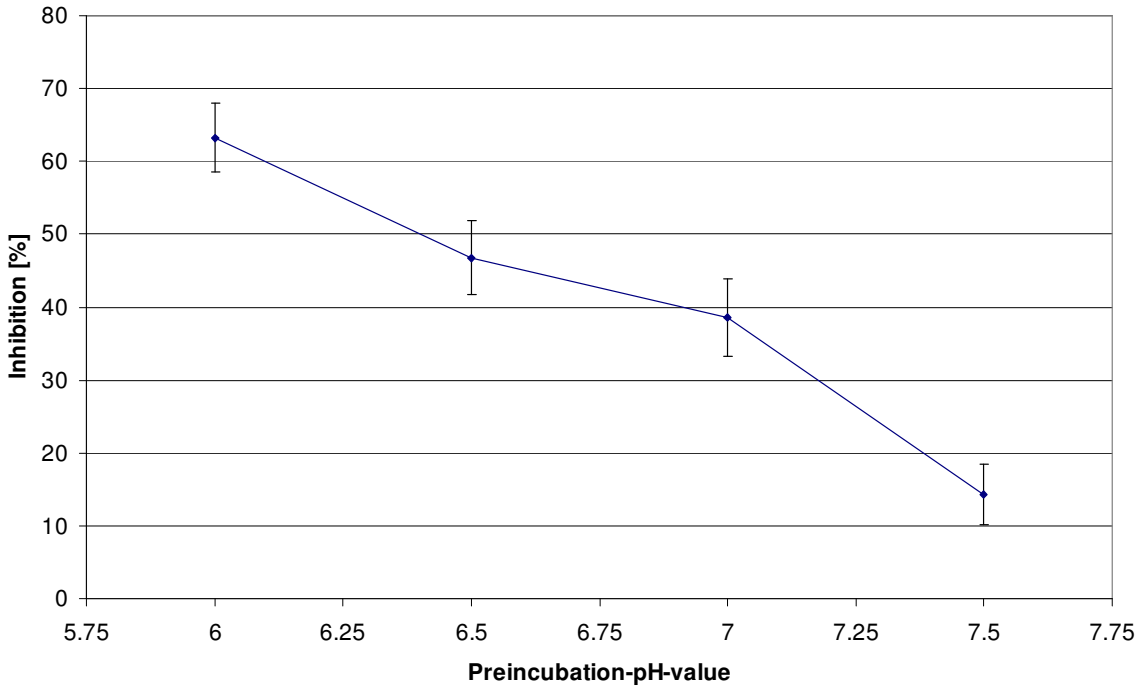

Fig. 4-25 Dependency of the inactivation of EcMetAP upon fumagillin-binding and the preincubation pH-value

4.3.3.3 Conclusions

The results indicate that two protonation states are possible without disrupting the active site geometry: At a more basic pH, one water molecule is deprotonated and bridging the two metal ions. This protonation state (B, cfr. Fig. 4-23) is expected to be relevant for the catalytic process of substrate hydrolysis. The other protomeric state (A) with two water molecules present in the active site at more acidic pH, each one coordinating a different metal ion, is relevant for the covalent binding of fumagillin to MetAP. This process requires protonation of the epoxide oxygen. Proton donation from an active site group, in particular from one of the active site water molecules, is more likely in the protonation state with two water molecules (i.e. at more acidic pH).

However, the increased binding capability of fumagillin at a more acidic pH-value might surprise at first as it may be argued that an active site residue is more likely protonated than the metal-coordinating water/hydroxide ion that induces the binding of fumagillin. Only the histidines His79 and His178 site are likely to be protonated but as

i) the literature values for the histidine side chain pK_a are about 6.2 and the histidines therefore are less basic than the hydroxide ion with an apparent pK_a value of about 7 and

ii) a protonated and therefore positively charged His79 is less prone to act as a nucleophile on fumagillin

it can be assumed that both His79 and His178 remain neutral.

These findings have implications for the development of covalent inhibitors of the MetAP and add a new perspective to the pharmacological properties of the anti-angiogenic drug fumagillin. The fact that the extracellular pH in tumors is more acidic than in normal tissues and assuming that the endothelial cells of vessels in tumors are under the influence of the acidic extracellular tumor pH, the pH profile of the fumagillin-MetAP binding reaction might lead to selectivity (or targeting) of the fumagillin effect to tumor vessels.

Irreversible inhibitors different from fumagillin should preferably be compounds that are activated by a nucleophilic attack (coming from the hydroxide ion) or by deprotonation. Such inhibitors would be much more active at physiological pH than fumagillin.

Furthermore, the results presented above allow the following conclusions:

i) In the X-ray structure of *E. coli* MetAP (2MAT), the bridging water molecule is most probably deprotonated. However, an active site with two (fully protonated) water molecules coordinated to the metal ions is also stable, albeit with a different coordination geometry.

ii) The active site of binuclear EcMetAP is therefore characterized by the presence of a water molecule with a pK_a-value of ~ 7. This value is lower than the apparent pK_a-value of 8.1 obtained by kinetic and spectroscopic methods[77]. This value is also at the lower border of the pK_a values reported for waters coordinating to zinc ions in organic complexes[139].

iii) The substrate hydrolysis reaction starts with the attack of the metal-bound hydroxide ion to the carbonyl carbon of the scissile peptide bond. This mechanism differs slightly from the one that is given in the recent literature[58] where the deprotonation of the metal-bridging water occurs after the substrate has been bound in the active site.

Recent theoretical work on the reaction mechanism of imipenem binding to the di-nuclear zinc-ß-lactamase[140] and the substrate hydrolysis mechanism of the di-nuclear bovine lens leucine aminopeptidase[141] indicate that the nucleophilic attack on the substrate originates from a “terminally” bound and not a bridging hydroxide ion. The nucleophilicity of a hydroxide ion that is complexed to one metal ion is higher than that of a bridging hydroxide. Considering these results, we suggest a mechanism in which a bridging hydroxide (as in the crystal structure) is found in the resting state of the enzyme and the binding of the substrate causes a rearrangement of the complexation pattern. Subsequently, the amide carbonyl carbon is attacked by the terminally bound hydroxide ion, which has an increased nucleophilicity as compared to the bridging hydroxide ion in the resting state.

4.3.4 Testing

4.3.4.1 Fumagillin Analogs

A series of fumagillin analogs was kindly provided by Prof. Giannis (University of Leipzig) and was tested for inhibitory activity. The results are summarized in Table 4-6.

Although some compounds resemble fumagillin and TNP-470 very much and would be expected to have some potency against EcMetAP, none of the compounds showed any remarkable inhibitory activity. This is probably due to the fact that these compounds were made available as stock solutions in DMSO (10 and 100 mM). In analogy to our own observations with fumagillin, these substances may be susceptible to oxidation or hydrolysis of the epoxide moieties and thus to inactivation. The IC_{50}-value of fumagillin decreases to 50-80 µM upon storage compared to 9 µM of freshly isolated substance. This is the case if it is dissolved in DMSO and stored at -20° but even if it is stored as a solid at room temperature. However, the increase in inhibition-potency at a lower preincubation-pH seen with fumagillin can also be observed with these substances but was not sufficient for the determination of IC_{50}-values.

Table 4-6 Inhibition tests of fumagillin analogs; preincubated 15 min at pH 7.5 (resp. pH 6.5)

Cpd.	Formula	IC_{50} [µM]	% inhibition (at a certain concentration)
Fumagillin	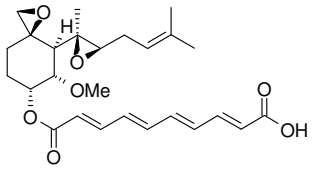	9.2 [a]	---
MAZ152	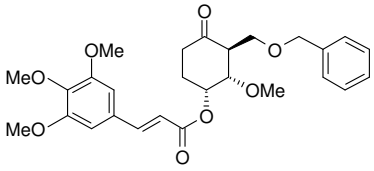	> 10	0 % inhibition at 10 µM
MAZ173	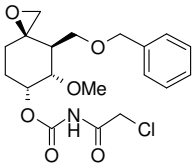	> 300	23 % inhibition at 100 µM 28 % inhibition at 200 µM 31 % inhibition at 300 µM 18 % inhibition at 50 µM (preincubated at pH 6.5)
MAZ281	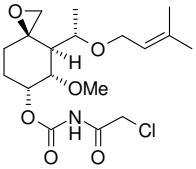	> 10	1 % inhibition at 10 µM
MAZ283	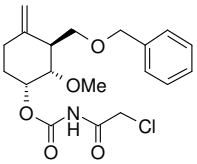	> 300	18 % inhibition at 100 µM 26 % inhibition at 200 µM 33 % inhibition at 300 µM 23 % inhibition at 50 µM (preincubated at pH 6.5)
MAZ289	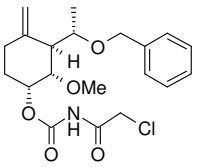	> 300	17 % inhibition at 100 µM 19 % inhibition at 200 µM 29 % inhibition at 300 µM 15 % inhibition at 50 µM (preincubated at pH 6.5)
MAZ234	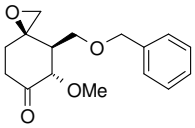	> 300	2 % inhibition at 100 µM 9 % inhibition at 200 µM 7 % inhibition at 300 µM 14 % inhibition at 50 µM (preincubated at pH 6.5)
MAZ290	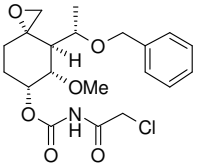	> 300	15 % inhibition at 100 µM 23 % inhibition at 200 µM 31 % inhibition at 300 µM 19 % inhibition at 50 µM (preincubated at pH 6.5)
MAZ293	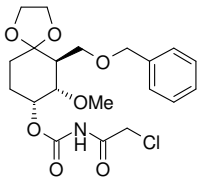	> 300	10 % inhibition at 100 µM 18 % inhibition at 200 µM 24 % inhibition at 300 µM 13 % inhibition at 50 µM (preincubated at pH 6.5)

Cpd.	Formula	IC_{50} [µM]	% inhibition (at a certain concentration)
MAZ294	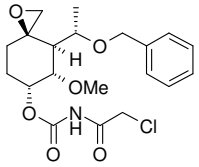	> 10	2 % inhibition at 10 µM
MAZ295	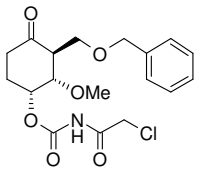	> 10	11 % inhibition at 10 µM
H344.1	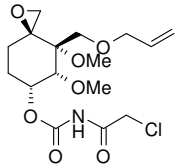	> 300	2 % inhibition at 100 µM 7 % inhibition at 200 µM 6 % inhibition at 300 µM
H352.1	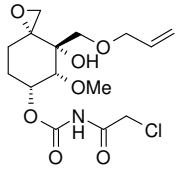	> 10	8 % inhibition at 10 µM
H353.1	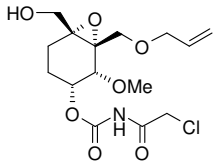	> 10	9 % inhibition at 10 µM
NSP113	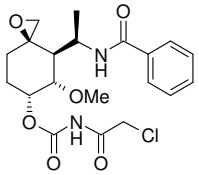	> 300	16 % inhibition at 100 µM 22 % inhibition at 200 µM 28 % inhibition at 300 µM

a) preincubated 30 min at pH 7.5

4.3.4.2 Peptide-based Reactive Inhibitors

The following compounds were kindly provided by Prof. Schirmeister (Würzburg University, Germany). Many of them are peptide-based and contain a reactive moiety, such as an aziridine-ring or and epoxide-group (cfr. Table 4-7).

Table 4-7 Peptide-based reactive inhibitors, preincubated 30 min at pH 7.5

Cpd.		IC_{50} [µM]	% inhibition (at a certain concentration)
SCH1	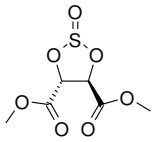	< 100	69 % inhibition at 100 µM 95 % inhibition at 300 µM
SCH2	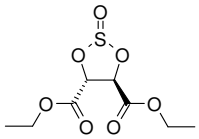	< 100	68 % inhibition at 100 µM 80 % inhibition at 300 µM
SCH3	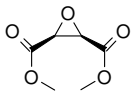	> 300	7 % inhibition at 300 µM
SCH4	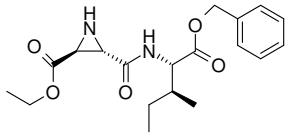	> 300	16 % inhibition at 300 µM
SCH5	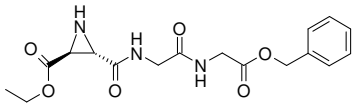	< 100	81 % inhibition at 100 µM 90 % inhibition at 300 µM
SCH6	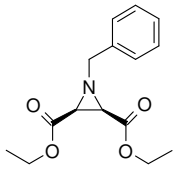	> 300	27 % inhibition at 300 µM
SCH7	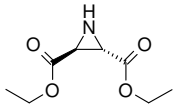	> 300	35 % inhibition at 300 µM
SCH8	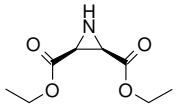	> 300	22 % inhibition at 300 µM
SCH9	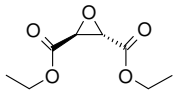	100-300	24 % inhibition at 100 µM 66 % inhibition at 300 µM
SCH10	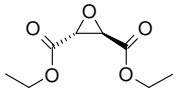	< 100	52 % inhibition at 100 µM 82 % inhibition at 300 µM
SCH11	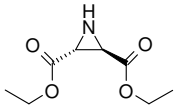	> 300	24 % inhibition at 300 µM
SCH12	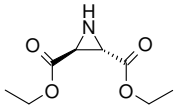	> 300	21 % inhibition at 300 µM
SCH13	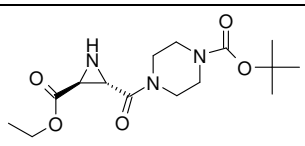	> 300	27 % inhibition at 300 µM

Cpd.		IC_{50} [µM]	% inhibition (at a certain concentration)
SCH14	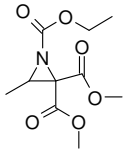	< 100	28 % inhibition at 100 µM 58 % inhibition at 300 µM
SCH15	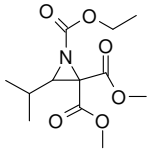	< 100	69 % inhibition at 100 µM 80 % inhibition at 300 µM
SCH16	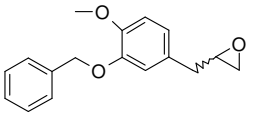	100-300	52 % inhibition at 300 µM
SCH17	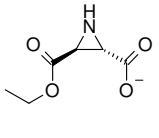	> 300	4 % inhibition at 300 µM
SCH18	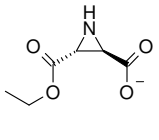	> 300	10 % inhibition at 300 µM
SCH19	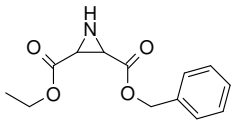	> 300	16 % inhibition at 300 µM
SCH20	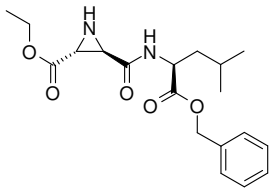	> 300	39 % inhibition at 300 µM
SCH21	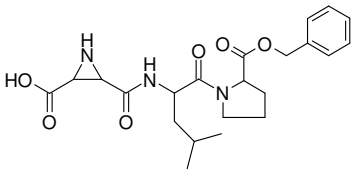	> 300	43 % inhibition at 300 µM
SCH22	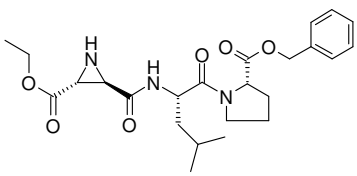	> 300	27 % inhibition at 300 µM
SCH23	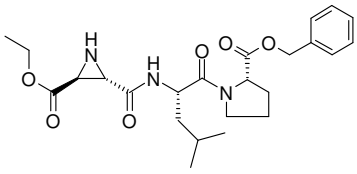	100-300	46 % inhibition at 100 µM 84 % inhibition at 300 µM

In contrast to the inactive fumagillin analogs, some potent inhibitors could be identified among the peptide-based compounds, such as SCH1, SCH2 and SCH5. Whether these substances are competitive or non-competitive inhibitors of the EcMetAP remains to be established. When comparing SCH4 and SCH5, the finding that replacing glycine at the penultimate residue of the active compound SCH5 by isoleucine in SCH4 diminishes activity reminds of the substrate specificity of EcMetAP which prefers small residues adjacent to methionine. Another fact that becomes clear is that the stereochemistry is an important factor. This can be seen when comparing a corresponding pair of compounds such as SCH22 and SCH23 or SCH9 and SCH10.

4.3.4.3 Substituted Epoxides and Other Covalent Inhibitors

Based on the inhibition of EcMetAP by fumagillin, a series of small epoxides was synthesized. The idea was that groups with different electronical effects could have an impact on the reactivity of the epoxide-moiety and thus influence the activity. The results are summarized in Table 4-8.

Most of the epoxides were readily available by starting either from the corresponding styrenes or aldehydes (Fig. 4-26).

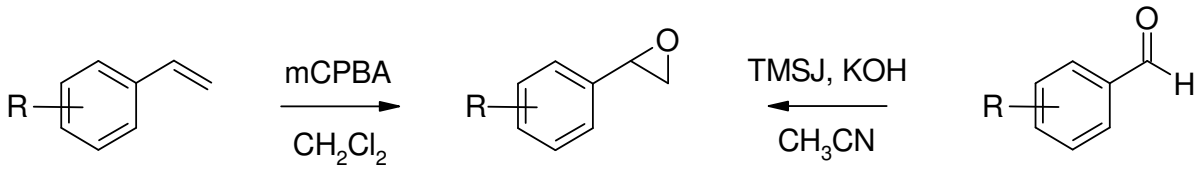

Fig. 4-26 General procedures for the synthesis of epoxides

In addition, several styrenes and aldehydes were tested, among these the starting materials for the synthesis of the epoxides (cfr. 8 Appendix, Table 8-1 and Table 8-2).

The effect of an enhanced potency at a more acidic pH could also be observed for these small molecules, comparable to the fumagillin analogs. Thus, an inhibitor exerts the same inhibitory

effect when preincubated at a more acidic pH with a reduced preincubation time compared to the original assay conditions.

Table 4-8 Testing of small phenyloxiranes preincubated for 30 min at pH 7.5 unless stated otherwise (see footnote)

Compound		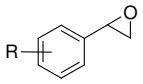	IC_{50} [µM]	% inhibition (at a certain concentration)
Fumagillin		see above	9.2	
R/S-Phenyloxirane		R = H	> 300	20 % inhibition at 100 µM (preinc. at pH 6.5)[a] 19 % inhibition at 100 µM 30 % inhibition at 300 µM
R-Phenyloxirane		R = H	> 300	4 % at 100 µM[a] 6 % inhibition at 100 µM (preinc. at pH 6.5)[a] 9 % inhibition at 100 µM 17 % inhibition at 300 µM
S-Phenyloxirane		R = H	> 300	18 % at 100 µM[a] 23 % inhibition at 100 µM (preinc. at pH 6.5)[a] 31 % inhibition at 100 µM 38 % inhibition at 300 µM
RS 1	2-(2-Chloro-phenyl)-oxirane	2-Cl	> 300	9 % inhibition at 100 µM (preinc. at pH 6.5)[a] 6 % inhibition at 100 µM 14 % inhibition at 300 µM
RS 2	2-(3-Chloro-phenyl)-oxirane	3-Cl	> 300	15 % inhibition at 100 µM (preinc. at pH 6.5)[a] 23 % inhibition at 100 µM 40 % inhibition at 300 µM
RS 3	2-(4-Chloro-phenyl)-oxirane	4-Cl	100-300	25 % inhibition at 100 µM (preinc. at pH 6.5)[a] 42 % inhibition at 100 µM 56 % inhibition at 300 µM
RS 4	2-o-Tolyl-oxirane	2-Me	> 300	17 % inhibition at 300 µM
RS 5	2-m-Tolyl-oxirane	3-Me	> 300	45 % inhibition at 300 µM
RS 6	2-p-Tolyl-oxirane	4-Me	> 300	30 % inhibition at 100 µM 59 % inhibition at 300 µM
RS 7	2-(2-Methoxy-phenyl)-oxirane	2-OMe	> 300	46 % inhibition at 300 µM
RS 8	2-(3-Methoxy-phenyl)-oxirane	3-OMe	> 300	40 % inhibition at 300 µM
RS 9	2-(4-Methoxy-phenyl)-oxirane	4-OMe	> 300	42 % inhibition at 300 µM
RS 10	2-(2-Nitro-phenyl)-oxirane	2-NO_2	> 300	9 % inhibition at 300 µM
RS 11	2-(3-Nitro-phenyl)-oxirane	3- NO_2	> 300	27 % inhibition at 300 µM
RS 12	2-(4-Nitro-phenyl)-oxirane	4- NO_2	> 300	0 % inhibition at 300 µM

a) 15 min preincubation

Table 4-9 Testing of small epoxides preincubated 30 min at pH 7.5

Compound			IC_{50} [µM]	% inhibition (at a certain concentration)
Fosfomycin		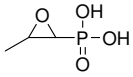	> 500	0 % inhibition at 500 µM
7-Oxa-bicyclo[4.1.0]heptane			> 300	7 % inhibition at 300 µM
RS 13	3-Phenyl-oxirane-2-carboxylic acid-methyl ester	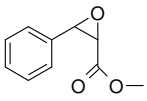	> 300	25 % inhibition at 300 µM
TH7		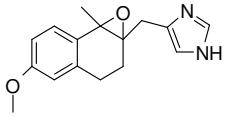	> 300	12 % inhibition at 300 µM
RS 14	3-Phenyloxiran-2-carbonitrile	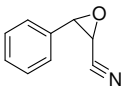	100-300	39 % inhibition at 100 µM 53 % inhibition at 300 µM
RS 15	1-Oxa-spiro[2.5]octane -2-carbonitrile	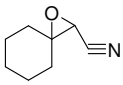	> 300	13 % inhibition at 100 µM
RS 16	4-((E)-1-Methyl-propenyl)-1-oxa-spiro[2.5]octane	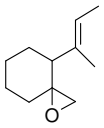	> 100	7 % inhibition at 100 µM[a] 6 % inhibition at 300 µM

a) 15 min preincubation

None of the small epoxides was able to significantly inhibit EcMetAP, possibly because of the lack of the required stereochemical properties and because of the small size of these compounds. Both these factors are very important for affinity. In addition, no pattern relating to activity with either the position of a substituent or its inductive and mesomeric effect could be observed. Although there are differences in activity (even simple molecules such as R- and S-phenyloxirane differ by a factor of two), this can have many reasons as the binding site of these compounds is not known and relatively high concentrations are needed to observe any effects.

The same applies for the styrenes and aldehydes tested. Interestingly, the aldehydes were generally better inhibitors than the epoxides. The best compound tested was 2-hydroxy-benzaldehyde with an IC_{50}-value of about 6 µM, thus better than fumagillin under otherwise identical conditions. If the aldehydes also act as covalent inhibitors is not clear. They could react with one of the seven cysteine residues of EcMetAP in an aldol-like reaction. In the case of 2-hydroxy-benzaldehyde, interaction with the metal ions and thus a competitive mode of

action also seems possible. However, inactivation of the enzyme by any of these compounds seems to be unspecific.

In summary, no promising lead structure for new, covalent inhibitor could be identified and we focused on competitive inhibitors.

4.4 Competitive Inhibitors

4.4.1 Overview

The interest in MetAP-inhibitors is mainly focused on fumagillin and over covalent inhibitors of MetAP-II due to its role in angiogenesis. There are only a few inhibitors reported for type-I MetAPs, although it is a unique and essential enzyme in bacteria. Since the metal ions are part of the catalytic site, the design of metal chelators has been a popular approach for developing MetAP inhibitors both for type-I and type-II. Competitive MetAP-inhibitors can be divided into different classes.

One class contains compounds that mimic peptide substrates and coordinate to the metal ions. These inhibitors use for example an α-hydroxy-β-aminoacyl (bestatin) group[142] or an internal hydroxamic acid as a structural group to chelate the metal ions[143]. The bengamides (a marine natural product isolated from sponges) and synthetic analogs thereof[124] share a similar binding mode.

A second class contains a triazole or a pyrazole group as the metal complexing or coordinating ligand. 1,2,4-triazoles represent a novel class of potent non-peptidic inhibitors for the MetAPs[78, 86, 144]. Structural moieties such as carboxylic acids or thiazole-2-oxalamides[145] or thiazole-2-ylamides[146] are present in some other potent inhibitors.

A third class of competitive inhibitors consisting of α-keto heterocycles and aminoketones bind as transition-state analogs.

Recently, a series of furan-carboxylic acids has been reported as competitive inhibitors of Mn(II)-loaded EcMetAP and the crystal structure of the enzyme-inhibitor-complex has been determined (pdb code 1XNZ). An overview of the reported inhibitors together with their metal selectivity, their *in vitro* and *in vivo* activity is given in Table 4-10.

Table 4-10 Competitive inhibitors of MetAPs, the summary describes the type of MetAP/species a class of inhibitors is active against, the metal ions it was tested with, its *in vivo* activity and whether a crystal structure with bound inhibitor exists or not

Ref.	Class of compounds described	Summary:
[146]	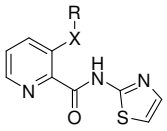 X=NH, O	EcMetAP / ScMetAP: Co(II) *in vivo* inactive no crystal structure available
[86]	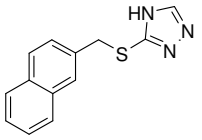	HsMetAP-II: Zn(II), Ni(II), Co(II), Fe(II) *in vivo* inactive no crystal structure available
[86]	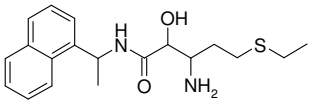	HsMetAP-II: **Mn(II)**, Zn(II), Ni(II), Co(II), Fe(II) *in vivo* **active** no crystal structure available
[147]	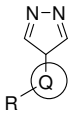 Q=aryl or heteroaryl group	HsMetAP-II: Co(II) (other metals not tested) *in vivo* **active** no crystal structure available
[148]	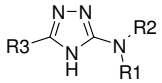	HsMetAP-II: Co(II) (other metals not tested) *in vivo* **active** no crystal structure available
[82]	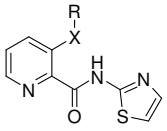 X=NH, O 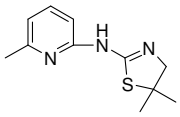	EcMetAP: Co(II), Ni(II), inactive with Mn(II) and Zn(II) no crystal structure available
[82]	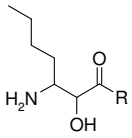 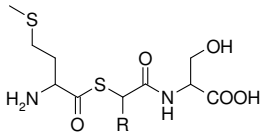	EcMetAP: Co(II), Ni(II), Mn(II), Zn(II) no crystal structure available
[143]	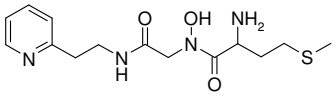	EcMetAP (Factor 25/50 worse against HsMetAP-I/II): Co(II) no crystal structure available
[124]	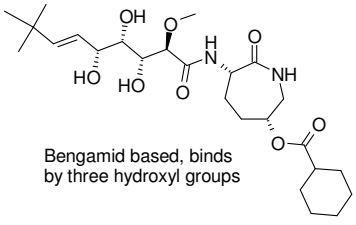 Bengamid based, binds by three hydroxyl groups	HsMetAP-I/II: Co(II) (other metals not tested) *in vivo* **active** crystal structure available[a]

Ref.	Class of compounds described	Summary:
[78]	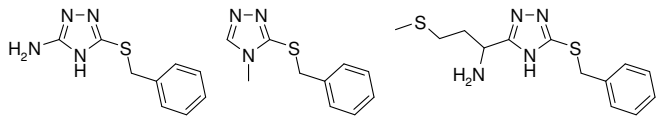 N_1 and N_2 coordinate to the active site	SaMetAP: Co(II), Zn (II) (other metals not tested, right: *in vitro* inactive) *in vivo* inactive crystal structure available[a]
[118]	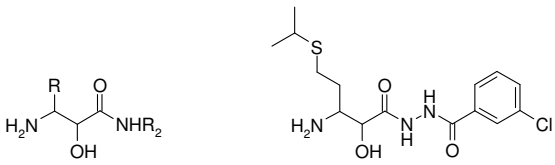	HsMetAP-II (weak against type-I): **Mn(II)** (other metals not tested) *in vivo* **active** crystal structure available[a]
[90]	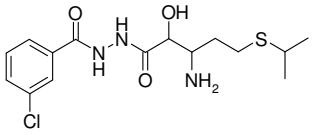	HsMetAP-II (weak against type-I): **Mn(II)** (other metals not tested) *in vivo* **active** crystal structure available (1R58)
[149]	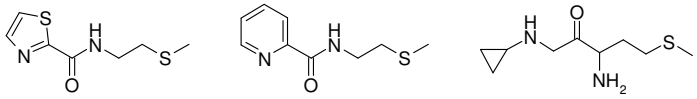	SaMetAP: Co(II) crystal structures available (1QXW, 1QXY, 1QXZ)
[85]	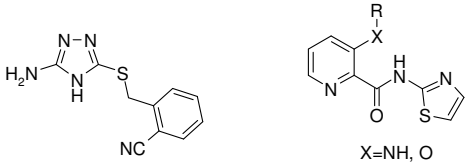 X=NH, O	ScMetAP: Co(II) (other metals not tested) *in vivo* inactive no crystal structure available
[87]	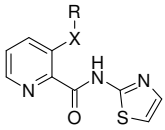 X=NH, O	EcMetAP (weak against HsMetAP-I) Co(II) (other metals not tested) no crystal structure available
[145]	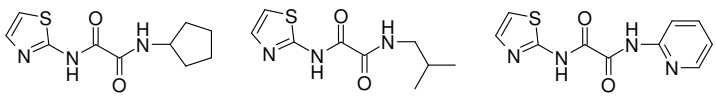	EcMetAP: Co(II)-selective no crystal structure available
[145]	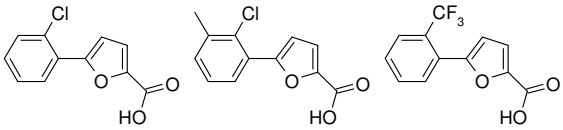	EcMetAP: Mn(II)-selective crystal structure available (1XNZ)
[144]	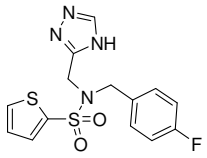	HsMetAP-II: Co(II)-selective, Factor 40 worse with Mn(II), cell-permeable *in vivo* inactive no crystal structure available

a) not deposited in the PDB

4.4.1.1 Mode of Action on the Molecular Basis

Up to now, X-ray structures are available for the characterization of the inhibitory mechanism of the bestatin based inhibitors, of the transition-state analogs, of the carboxylic acid derivatives and of the triazoles: All of these compounds interact with the active site metal ions and are able to replace the bridging water molecule. For the bestatin-like inhibitors, generally three vicinal chelating groups are present for the complexation of the metal ions. The binding mode of the bestatin-based inhibitors is depicted in Fig. 4-27.

Fig. 4-27 left: Bestatin; right: Binding mode of a bestatin based inhibitor, picture generated from pdb code 3MAT

In the case of the triazole-based inhibitors, each of the triazole nitrogen atoms in positions 1 and 2 interacts with one of the two cobalt ions in the di-nuclear cobalt-binding site such that their N-N-bond is nearly parallel to the Co-Co-axis of the metal binding site[78]. The carboxylic acid derivatives that inhibit the Mn(II)-loaded EcMetAP (1XNZ) use the carboxylic acid moiety to replace the bridging water molecule and to coordinate to the metal ions.

Despite the common mode of action of these substances, selectivities can be observed depending on the kind and origin of MetAPs and on the metal ions used.

4.4.1.2 Mode of Action on the Physiological Basis: Biological Activity

Although the triazoles are a potent class of inhibitors described for the MetAP-I, they do not show antibacterial activity when tested against various organisms. The lack of correlation between *in vitro* potency and *in vivo* activity has also been observed for other *in vitro* highly

active compounds (normally tested against Co(II)- loaded MetAPs) such as the pyridine-2-carboxylic acid-thiazole-2-ylamides. Other *in vitro* potent inhibitors against HsMetAP-II found by screening with a Co(II)-loaded enzyme failed to inhibit endothelial cell proliferation in a cellular assay[144]. There are various possible explanations for these phenomena, including permeability, efflux, *in vivo* affinity or kind and number of the relevant *in vivo* metal ion. It might also be possible that certain inhibitors need the presence of two divalent metal ions to be able to bind to the metal binding site. Whether metal-selective inhibitors against the Mn(II)-loaded form of EcMetAP are active *in vivo* is not yet clear.

4.4.2 Derivatives of a Published Inhibitor

Compound RS 17 was reported as a potent EcMetAP inhibitor[146]. The compound was synthesized (cfr. Fig. 4-28) and tested as a reference. It has an IC_{50}-value in the lower nanomolar range.

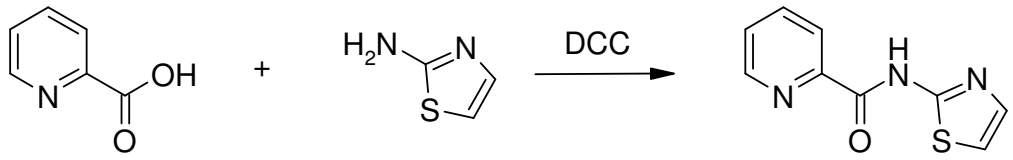

Fig. 4-28 Synthesis of RS 17

Several derivatives of this substance were synthesized in order to

i) improve the activity and
ii) gain insight into structure activity relationships

Structural modifications (RS 18 - RS 25) of the lead compound RS 17, however, had no beneficial effect. Replacement of the thiazole ring by an isoxazole ring or changing the carboxamide into a sulfonamide decreased the potency whereas the sulfonamide group had a stronger effect. Furthermore, the picolinic-acid moiety was kept as a structural key element and several cyanoalkyl-esters and –amides were synthesized and tested. These structural

elements were added (RS 21 - RS 24) to change the competitive inhibitor to a covalent inhibitor as explained for RS 26 and RS 27 below in Fig. 4-29. However, the idea to add reactive groups to the picolinic acid moiety did not increase the activity. The results are summarized in Table 4-11.

Table 4-11 Testing of pyridine-2-carboxylic-acid derivatives

Compound			IC_{50} [µM]	% inhibition (at a certain concentration)
RS 17	Pyridine-2-carboxylic acid thiazol-2-ylamide	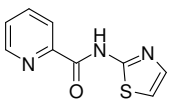	0.063 ± 0.011	
RS 18	Pyridine-2-carboxylic acid (5-methyl-isoxazol-3-yl)-amide	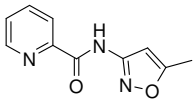	2.84	
RS 19	Pyridine-2-sulfonic acid thiazol-2-ylamide	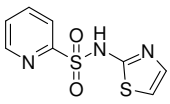	98.5	
RS 20	Pyridine-2-sulfonic acid (5-methyl-isoxazol-3-yl)-amide	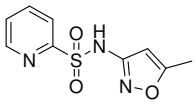	120.1	
RS 21	Pyridine-2-carboxylic acid cyanomethyl-amide	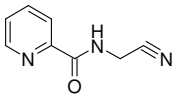	109.5	
RS 22	Pyridine-2-carboxylic acid cyanomethyl-ester	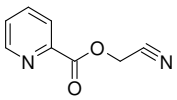	79.9	
RS 23	Pyridine-2-carboxylic acid 2-cyano-ethyl ester	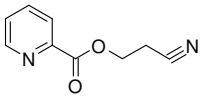	>> 100	0 % inhibition at 50 µM 17 % inhibition at 100 µM
RS 24	Pyridine-2-carboxylic acid 3-cyano-propyl ester	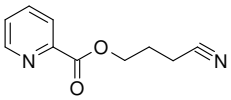	> 100	12 % inhibition at 1 µM 45 % inhibition at 100 µM
RS 25	4-Nitro-N-thiazol-2-yl-benzamide	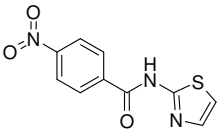	> 100	21 % inhibition at 100 µM

4.4.3 Screening

As structural modifications of the potent substance RS 17 yielded no promising results, a new leading structure should be identified. Based on docking runs and virtual screening results, several substances were tested for activity against the EcMetAP.

Among these were drugs, drug-like compounds, compounds from our own in house-library but also intermediates from synthetic procedures of the synthesis of the epoxides (cfr. 4.3.4.3). In addition, several other compounds were synthesized and tested. The most interesting compounds are listed below (cfr. Table 4-12) and a complete summary of the residual results is given in chapter 8 (Appendix).

RS 26 and RS 27 were synthesized to use methionine as a recognition element for the substrate binding site and the cyanoethylester moiety as a binding group for nucleophiles. The deprotonation of the cyanoethylester causes cleavage of the ester bond and subsequent formation of acrylonitrile, which can then bind (as a “Michaelis-like” electrophile) to one of the cysteine residues near the MetAP active site. The sequence of reactions is depicted in Fig. 4-29 and would be based on a “basic activation” and not on an acidic activation as with fumagillin.

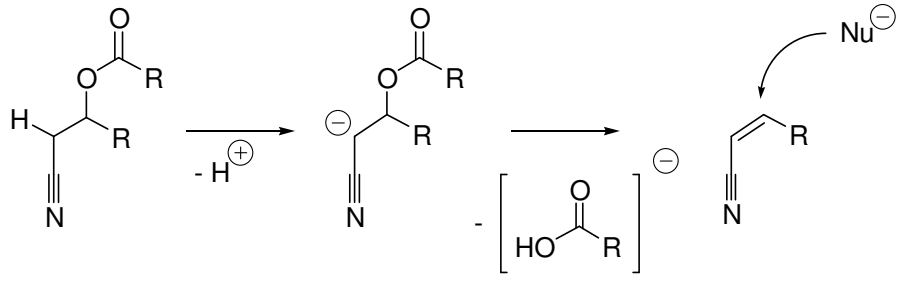

Fig. 4-29 Basic activation and subsequent possible binding mode of a cyanoethylester

The same idea was applied for the synthesis of the compounds RS 21 - RS 24. However, none of the compounds with a cyanoalkyl moiety showed any significant inhibition.

Table 4-12 Screening of inhibitors against Co(II)-loaded EcMetAP

Compound		Formula	IC_{50} [µM]	% inhibition (at a certain concentration)
Pyridine-2-carboxylic acid		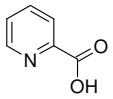	20.3	
Nicotinic acid		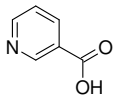	> 300	0 % inhibition at 300 µM
Ethacridine lactate		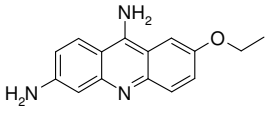	96.2	
Chlorpromazine-HCl		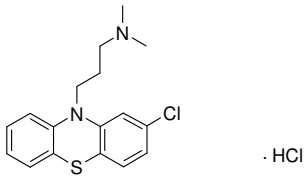	32.9	
Anthrone		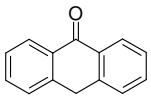	~10	19 % inhibition at 1 µM 49 % inhibition at 10 µM 95 % inhibition at 25 µM
Phenothiazine		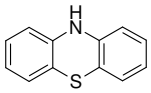	1-10	13 % inhibition at 1 µM 65 % inhibition at 10 µM 80 % inhibition at 25 µM
RS 26	Methionyl-cyanoethylester	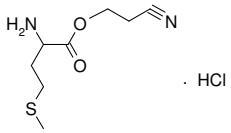	>> 100	0 % inhibition at 100 µM
RS 27	Boc-Methionyl-cyanoethylester	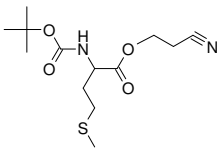	>> 50	0 % inhibition at 50 µM
Thiabendazole		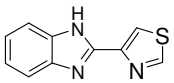	0.472	
Quinolin-8-ol		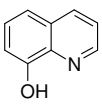	0.772	
Phenanthroline		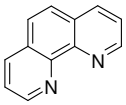	0.489	

As expected from the virtual screening, planar substances that fit nicely in the active site showed moderate to good IC_{50}-values. Of all the compounds tested, the metal-complexing substances such as thiabendazole, phenanthroline and quinolin-8-ol showed the best activity.

4.4.4 Quinoline-Derivatives

As quinolin-8-ol had an IC_{50}-value in the lower micromolar range, the substance itself and some corresponding derivatives like quinolin-2-ol or quinolin-8-amine are commercially available (at a low price) and can easily be modified, a small series of quinoline-derivatives was prepared and tested. The results are summarized in Table 4-13.

Table 4-13 Testing of quinoline-derivatives

Compound			IC_{50} [µM]	% inhibition (at a certain concentration)
Quinolin-8-ol		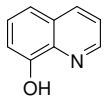	0.772 ± 0.017	
Quinolin-2-ol		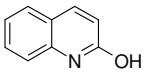	>> 1	5,2 % inhibition at 1 µM
Quinolin-8-ylamine		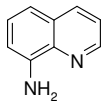	> 10	37,4 % inhibition at 10 µM
RS 28	Benzoic acid quinolin-8-yl ester	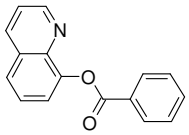	> 10	23,2 % inhibition at 10 µM
RS 29	N-Quinolin-8-yl-benzamide	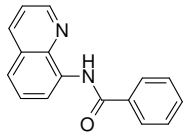	> 10	0 % inhibition at 10 µM
RS 30	N-Quinolin-8-yl-benzenesulfonamide	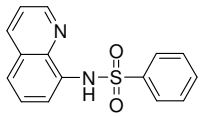	> 10	46,8 % inhibition at 10 µM
RS 31	Benzenesulfonic acid quinolin-8-yl ester	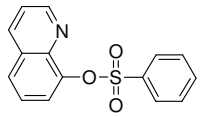	>> 1	5,7 % inhibition at 1 µM
RS 32	Toluene-4-sulfonic acid quinolin-8-yl ester	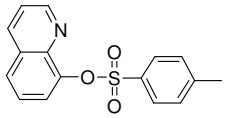	>> 1	1,0 % inhibition at 1 µM
RS 33	Pyridine-2-sulfonic acid quinolin-8-yl ester	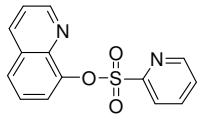	> 10	1,8 % inhibition at 1 µM 37,4 % inhibition at 10 µM

Disruption of the metal binding moiety led to an almost complete loss of activity in all cases. Esterification with either a carboxylic acid or a sulfonic acid led to the non-active compounds RS 28 and RS 31-RS 32. The idea to strengthen the metal-chelating properties by the use of a 2-pyridine ring (RS 33) had no beneficial effect.

As the starting materials for the preparation of other (substituted) quinoline-derivatives are quite expensive and structurally distinct derivatives are not easy to synthesized, we focused on the preparation and testing of the more easily accessible benzimidazoles. Besides, thiabendazole and many other benzimidazole anthelminthics are well-known drugs in clinical practice, and therefore thiabendazole congeners can be expected to have acceptable pharmacokinetic properties and less side effects than the unspecific metal chelator quinolin-8-ol.

4.4.5 Benzimidazoles

4.4.5.1 Overview

Benzimidazole derivatives such as thiabendazole, mebendazole or carbendazim are used as broad-spectrum anthelmitic and/or antifungal drugs. Helminths infect 25% of the world's population[150]. Certain benzimidazoles such as albendazole, a thiabendazole analogue, have been reported to be effective in treating AIDS-associated microsporidian infection, and other benzimidazoles showed *in vitro* potency against AIDS-associated fungal infections[151]. There is biochemical, genetic and cytological evidence that benzimidazoles prevent microtubule formation by binding to ß-tubulin.[152-154]. Additional effects, e.g. inhibition of fumarate reductase[155, 156], inhibition of superoxide dismutase[157], an influence on the energy balance of parasitic worms[158] or on the glucose/glycogen levels[159] have been observed. Interference with the terminal electron transport system[160] and with the vitamin B12 metabolism (due to competition with 5,6-dimethylbenzimidazole in the formation of the coenzyme)[161] have also been proposed. However, these mechanisms do not seem to be valid generally and the relevance of these additional effects is difficult to assess, since they have usually been observed either at comparably high and probably unphysiological concentrations of the

benzimidazole drugs or only in specific organisms. Resistance to benzimidazoles is based on a mutation in ß-tubulin genes[154] and often linked to a single amino acid change.

4.4.5.2 Thiabendazole

Thiabendazole was the first anthelmintic drug of the benzimidazole group and discovered in 1964[150]. Thiabendazole was originally described as an anthelmintic[162] and later on as fungicidal[163]. As other benzimidazoles, for example mebendazole and carbendazim, were reported to interfere with microtubule formation, a similar mode of action has been assumed for the antifungal activity of thiabendazole because:

i) thiabendazole has a similar spectrum of activity against fungi compared to carbendazim

ii) acquired resistance to carbendazim implies resistance to thiabendazole and *vice versa*

This assumption has been proven in 1978 by Davidse[152]. Thiabendazole completely inhibits mitosis in hyphae of *Aspergillus nidulans* based on interference with microtubule assembly by tubulin interaction with a K_i-value of 35 µM[152]. Thiabendazole causes cell elongation in *E. coli* and in cyanobacteria, possibly by acting in a similar manner on FtsZ, a structural analogue of tubulin and a bacterial cell division protein[164].

Despite side effects like frequent anorexia and nausea, occasionally dizziness and vomiting[165], thiabendazole is still in use for the treatment of strongyloidiasis[166, 167], a parasitic infection widely distributed in tropical and subtropical areas. Serious clinical problems with complications and refractory strongyloidiasis are observed especially in immunocompromised patients[150] such as those infected with human T cell leukaemia virus Type 1 (HTLV-1), HIV or corticosteroid-treated patients. Thiabendazole is nowadays mostly used for postharvest fruit treatment and in veterinary medicine, especially for the treatment of dermatoses[168].

4.4.5.3 Determination of the K_i-value of Thiabendazole

The K_M'-value was determined as described in 4.2.3.1 by incubation of EcMetAP with eight different substrate concentrations and 500 nM Thiabendazole. The K_M'-value was determined in three independent measurements as the reciprocal of the negative X-axis-intercept of the graphical portrayal of 1/s* against 1/v* to be 1904 ± 195 µM. The K_M'-value allows the calculation of the K_i-value (a). The K_i-value can alternatively be determined from the IC_{50}-value and the substrate concentration (b):

a) $K_i = [I]/((K_M'/K_M)-1)$

b) $K_i = IC_{50}/(1+([S]/K_M))$

The results are summarized in Table 4-14. Thus, the K_i-value derived from the IC_{50}-value (according to the Cheng and Prusoff equation for competitive inhibitors[169]) is 0.378 µM and is in excellent agreement the K_i-value determined according to the Lee and Wilson modified Lineweaver-Burk equation[170] of 0.366 µM.

Table 4-14 Constants for EcMetAP

K_M [µM]	K_M' [µM]	K_i [µM] (Method a)	K_i [µM] (Method b)
907 ± 176	1904 ± 195	0.366	0.378

Compared to the K_i-values of 34 µM resp. 68 µM for the binding of thiabendazole to fungal tubulin from two *Penicillium expansum* strains (competed against [^{14}C]carbendazim)[152], the K_i-value of 0.4 µM for the *E. coli* MetAP shows the high potential of this compound and might offer a new explanation for the mechanism of action not of the benzimidazoles generally but at least of thiabendazole. Therefore, thiabendazole might serve as a new lead compound for the development of anti-cancer but also anti-bacterial and anti-fungal substances that act by inhibiting the methionine aminopeptidase.

4.4.5.4 Procedures for the Synthesis of Thiabendazole Analogs

A variety of benzimidazoles is readily available by several procedures. Generally, a (substituted) diamine is heated with an appropriate carboxylic acid in the presence of polyphosphoric acid or with an amidine in the presence of sodium acetate to yield the desired benzimidazole (Fig. 4-30).

Method B is more preferable due to its shorter reaction time (10 min compared to 2-4 hrs). In addition, it seems to work for all kinds of amidines whereas there can be problems with method B depending on the used carboxylic acids. Method B normally requires prior steps for the preparation of the amidine salt. However, the amidine salts are generally readily available from the corresponding nitriles.

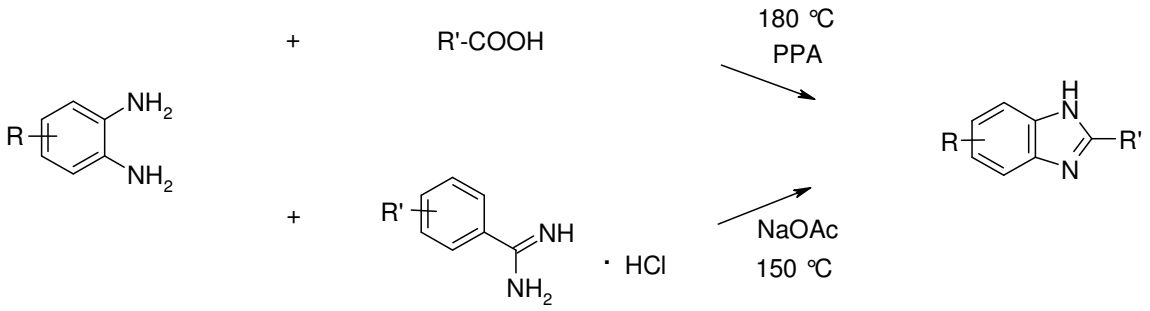

Fig. 4-30 Procedures for the synthesis of substituted benzimidazoles; PPA = Polyphosphoric acid

As thiazole-4-carboxylic acid is rather expensive, a synthetic procedure was established that was also suitable for large scale production. Therefore, thioformamide is generated from formamide and P_4S_{10} and reacted *in situ* with 3-bromopyruvic acid that is readily available from pyruvic acid (cfr. Fig. 4-31).

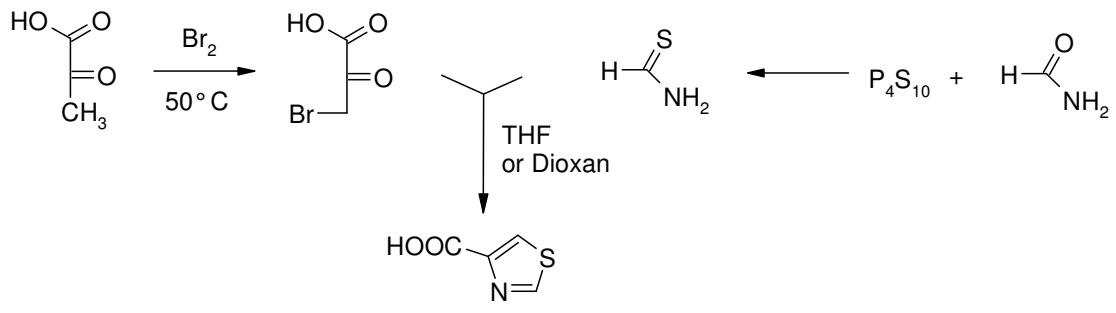

Fig. 4-31 Procedure for the synthesis of thiazole-4-carboxylic acid

The resulting product precipitates as a hydrobromide and can be filtered off. The salt can then be dissolved in water/NaOH and the carboxylic acid precipitates at pH 2-3.

Thus, a series of substituted benzimidazoles and thiabendazole analogs was synthesized and tested.

4.4.5.5 Testing of Thiabendazole Analogs

In order to gain insight into structure-activity relationships, several strategies should be embarked on:

1. changes of the heterocycle
2. alkylation of the benzimidazole moiety
3. substitutions in the 5-/6-position(s)
4. changes in the benzimidazole skeletal structure

As different heteroaryl carboxylic acids as well as o-phenylenediamine are commercially available, a considerable number of thiabendazole analogs can easily be synthesized in a short time. Thus, the thiazole ring of thiabendazole was substituted by other heterocycles. Commercially available thiabendazole analogs like mebendazole or albendazole normally have a carbamic ester substitution in this position and were also tested.

As the the nitrogen in position one of the benzimidazole moiety can be deprotonated, it is accessible to electrophilic substitutions. Alkylation of this nitrogen with alkylhalogenides should be used to introduce substituents that might reach a binding pocket near the metal binding site. This idea was derived from our docking results with manual positioning of thiabendazole into the active site.

Several 5-/6- substituted diamines can either be purchased or are readily available. Thus, the benzimidazole moiety was substituted in the positions 5 and/or 6.

Finally, the benzimidazole-moiety was changed by introducing one or more nitrogens, thus changing the benzimidazole for example to a purine.

The results are summarized below (cfr. Table 4-15 to Table 4-18).

Table 4-15 IC_{50}-values of 2-substituted benzimidazoles with Co(II)-loaded EcMetAP

Cpd.: Nr (Name)	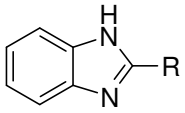 R	**IC50 [µM] (% inhibition at 10 µM)**
Thiabendazole	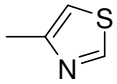	0.472 ± 0.060
Carbendazim	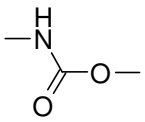	> 10 (17.6 ± 2.9)
RS 34	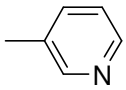	> 10 (4.2 ± 2.7)
RS 35	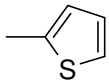	> 10 (5.4 ± 5.0)
RS 36 Fuberidazole	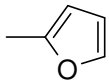	> 10 (10.4 ± 3.7)
RS 37	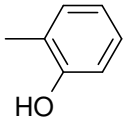	> 10 (30.4 ± 6.3)
RS 38	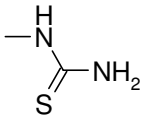	8.956 ± 1.319
RS 39	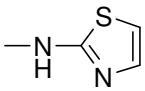	0.540 ± 0.028
RS 40	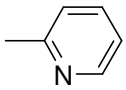	0.574 ± 0.082
RS 41	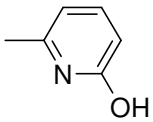	1.343 ± 0.274
RS 42	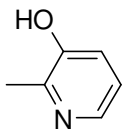	0.777 ± 0.033
RS 43	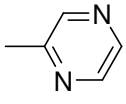	4.591 ± 0.389

Table 4-16 IC_{50}-values of N-alkylated benzimidazoles with Co(II)-loaded EcMetAP

Cpd.	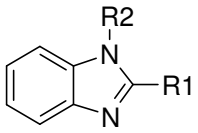		**IC_{50} [µM] (% inhibition at 10 µM)**
	R1	R2	
RS 44	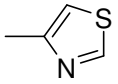	—CH_3	0.497 ± 0.007
RS 45	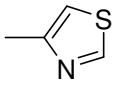	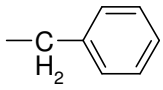	0.461 ± 0.013
RS 46	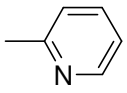	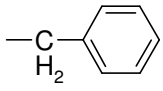	0.992 ± 0.130

Table 4-17 IC_{50}-values of 5- and/or 6-substituted benzimidazoles with Co(II)-loaded EcMetAP

Cpd.	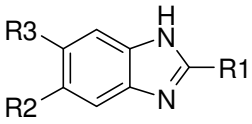			**IC_{50} [µM] (% inhibition at 10 µM)**
	R1	R2	R3	
RS 47	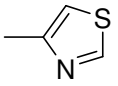	—CH_3	H	7.157 ± 0.065
RS 48	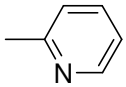	—CH_3	H	2.086 ± 0.286
RS 49	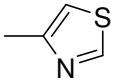	—CH_3	—CH_3	> 10 (47.8 ± 3.5)
RS 50	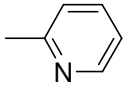	—CH_3	—CH_3	2.433 ± 0.284
RS 51	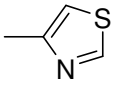	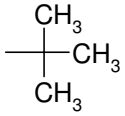	H	3.906 ± 0.582
RS 52	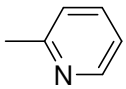	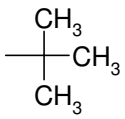	H	2,598 ± 0.376
RS 53	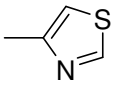	—NO_2	H	1.218 ± 0.128

Cpd.	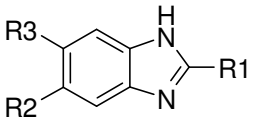			**IC_{50} [µM] (% inhibition at 10 µM)**
	R1	R2	R3	
RS 54	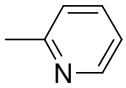	—NO_2	H	0.162 ± 0.019
RS 55	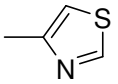	—NH_2	H	3.390 ± 0.242
RS 56	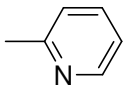	—NH_2	H	0.967 ± 0.024
RS 57	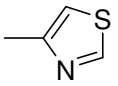	—F	H	4.307 ± 0.635
RS 58	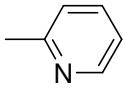	—F	H	1.511 ± 0.192
RS 59	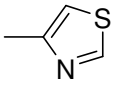	—Cl	H	5.153 ± 1.023
RS 60	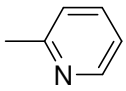	—Cl	H	1.695 ± 0.147
RS 61	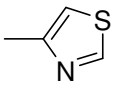	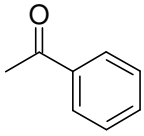	H	2.397 ± 0.470
RS 62	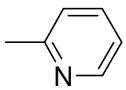	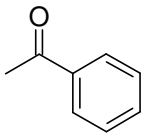	H	0.403 ± 0.045
RS 63	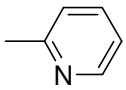	—CN	H	0.431 ± 0.018
Mebendazole	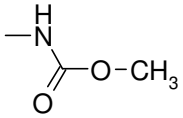	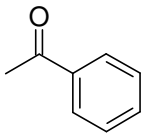	H	> 10 (29.0 ± 6.3)
Albendazole	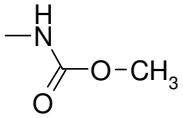	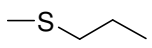	H	> 10 (15.5 ± 7.2)
Fenbendazole	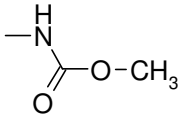	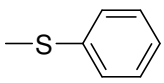	H	> 10 (6.1 ± 4.5)

Table 4-18 IC_{50}-values of different 2-substituted heterocycles derived from benzimidazole with Co(II)-loaded EcMetAP

Cpd.	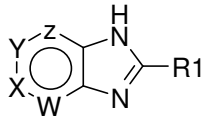					**IC_{50} [µM] (% inhibition at 10 µM)**
	R1	W	X	Y	Z	
RS 64	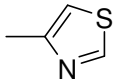	N	H	H	H	0.078 ± 0.007
RS 65	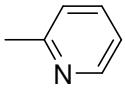	N	H	H	H	0.105 ±0.001
RS 66	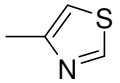	H	N	H	H	1.724 ± 0.158
RS 67	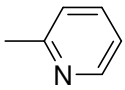	H	N	H	H	0.550 ± 0.081
RS 68	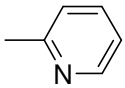	N	H	N	H	0.376 ± 0.023
RS 69	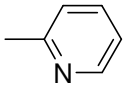	N	H	H	N	0.240 ± 0.041

4.4.5.6 Structure-Activity Relationships

At first, the thiazole-ring of thiabendazole should be substituted by different aromatic heterocycles. Only the substitution by a 1,3-thiazole-2-yl-amine moiety (RS 39) or by 2-pyridine (RS 40) gave active compounds. Other substituents such as 3-pyridine, 2-thiophene, 2-furane or 2-phenol resulted in almost complete loss of activity as was the case for the commercially available thiabendazole derivatives mebendazole, albendazole, carbendazim and fenbendazole with the carbamic ester residue in the 2-position of the benzimidazole system. This indicates that the binding of thiabendazole and the active congeners is based on interaction with metal ion(s) as it is known that both thiabendazole and the compound with a (2-)pyridine ring replacing the thiazole ring (RS 40) are metal-chelating agents: For both these compounds metal complexes with different divalent metal ions have been characterized; for thiabendazole even Co(II)-complexes have been synthesized and analysed. Efforts to improve

the activity of RS 40 by adding a hydroxy-group in 3- or 6-position of the pyridine were unsuccessful and slightly decreased the potency in both cases.

Using compound RS 40 as secondary lead compound, the benzimidazole-nitrogen was methylated or benzylated. The alkylation of this nitrogen from thiabendazole had no effect but the benzylated compound RS 40 (RS 46) was slightly less active than the parent compound. These results support the idea that N-3 of the benzimidazole is involved in metal binding and that changing the N-1 substituent has no effect on the binding motif. However, the original aim to reach a substrate binding pocket and to improve the potency by introducing a large substituent at N-1 was not achieved. Next, the effects of small substituents in the 5- and the 6-position of the benzimidazole moiety have been explored. Changes in these positions (with some exceptions) led to a decline in potency. Most derivatives were less active than the parent compound by a factor from two to five, regardless of which substituent was chosen (halogen, amino, methyl or dimethyl). Derivatives of the lead compound RS 40 tolerated substitutions in the 5- and the 6- position better than the corresponding derivatives of thiabendazole. The compounds RS 61 and RS 62 suggest that even larger substituents might be accepted. This observation would rule out any sterical reasons for the loss of potency observed but implies the assumption of an identical binding mode. The nitrile-derivative and the 5-nitro derivative of RS 40 were more active than the parent compound. In contrast, the corresponding 5-nitro-thiabendazole was less active than thiabendazole.

The hint that a polar substituent in position 5 can improve the potency in some cases led to changes in the benzimidazole scaffold: Introducing a nitrogen in position 5 of the benzimidazole had no effect on the pyridine-derivative but decreased the activity of the thiabendazole-derivative. When shifting the position of the nitrogen from 5 to 4, the affinity increased independently of the nature of the heterocycle in position 2: Both modified lead compounds (RS 64 and RS 65) had an IC_{50} in the nanomolar range (80-100 nM). Other variations of the pyridine derivative yielded no further improvement: Introducing another nitrogen in position 7 and thus changing the benzimidazole into a pyrazine decreased the potency to an IC_{50}-value of 240 nM and changing it into a purine resulted in a further decline of the IC_{50}-value to 376 nM.

In summary, substitutions of the thiazole-ring were only tolerated if the metal-binding motive was not disrupted. Further substitutions had either no effect (for example N-alkylation) or led to a decrease in potency (with some exceptions). However, the pyridine-derivative is less sensitive to changes in the 5- and 6-position. Changing the benzimidazole-scaffold to 1H-imidazo[4,5-b]pyridine resulted in two compounds with improved potency with an IC_{50}-value close to compound RS 17.

Thus, three compounds were available for further tests that showed a high *in vitro*-activity – the compound RS 17 described in the literature and the two modified parent compounds RS 64 and RS 65. All of them have IC_{50}-values between 50-100 nM against Co(II)-loaded MetAP). However, none of all the compounds mentioned was able to inhibit the EcMetAP when tested with Mn(II) up to 10 µM. Nonetheless, these compounds together with the parent compounds were chosen for further testing on their antibacterial activity.

4.5 Crystal Structures

The most promising compounds were tested for their antibacterial activity. However, activity could only be observed at rather high concentrations (cfr. 4.6 Determination of MIC-values) and there was no correlation between *in vitro* and *in vivo* potency. This lack of correlation has been observed by other groups before. These findings, together with an unsatisfying docking pose, the disappointing results of compounds such as RS 45 or RS 46 that were synthesized because of ideas based on the manual positioning of thiabendazole into the metal binding site during molecular modeling, and the goal to continue this work with a rational inhibitor design brought us to clarify the binding mode of thiabendazole by resolving the crystal structure.

4.5.1 Published X-ray Structures

The first crystal structure of the *E. coli* MetAP was published in 1992 with a resolution of 2.4 Å. The resolution of this structure could later be improved to 1.9 Å and permitted visualization of the coordination geometry and solvent structure of the active-site bi-nuclear metal center[52] (see Fig. 2-8). Up to now, 32 structures of MetAPs are deposited in the PDB. A summary is given in Table 4-19.

Table 4-19 Crystal structures of MetAPs deposited in the PDB (www.pdb.org)

Year	Code	Res. [Å]	Species	Me(II)	Complex
1992	1MAT	2.40	*E. coli*	Co(II)	without bound inhibitor
1997	1XGM	2.80	*P. furiosus*	Co(II)	without bound inhibitor
1997	1XGN	2.90	*P. furiosus*	Co(II)	without bound inhibitor
1997	1XGO	3.50	*P. furiosus*	---	without bound inhibitor
1997	1XGS	1.75	*P. furiosus*	Co(II)	without bound inhibitor
1998	1BN5	1.80	*Human-II*	Co(II)	without bound inhibitor
1998	1BOA	1.80	*Human-II*	Co(II)	in complex with fumagillin
1999	1B59	1.80	*Human-II*	Co(II)	in complex with ovalicin
1999	1B6A	1.60	*Human-II*	Co(II)	in complex with TNP-470
1999	1C21	1.80	*E. coli*	Co(II)	in complex with methionine
1999	1C22	1.75	*E. coli*	Co(II)	in complex with trifluoromethionine

Year	Code	Res. [Å]	Species	Me(II)	Complex
1999	1C23	2.00	*E. coli*	Co(II)	in complex with methionine phosphonate
1999	1C24	1.70	*E. coli*	Co(II)	in complex with methionine phosphinate
1999	1C27	1.95	*E. coli*	Co(II)	in complex with norleucine phosphonate
1999	1QQ9	1.53	*S. griseus*	Zn(II)	in complex with methionine
1999	2MAT	1.90	*E. coli*	Co(II)	without bound inhibitor
1999	3MAT	2.00	*E. coli*	Co(II)	transition-state complex with aminohydroxyheptanoic acid
1999	4MAT	2.00	*E. coli*	---	His79Ala mutant
2002	1KQ0	2.00	*Human-II*	Zn(II)	in complex with D-methionine
2002	1KQ9	1.90	*Human-II*	Zn(II)	in complex with L-methionine
2002	1O0X	1.90	*T. maritima*	---	without bound inhibitor
2003	1QXW	1.67	*S. aureus*	Co(II)	in complex with an aminoketone inhibitor 54135
2003	1QXY	1.04	*S. aureus*	Co(II)	in complex with a ketoheterocycle inhibitor 618
2003	1QXZ	1.68	*S. aureus*	Co(II)	in complex with a ketoheterocycle Inhibitor 119
2003	1QZY	1.60	*Human-II*	Co(II)	in complex with a bengamide inhibitor Laf153
2003	1R58	1.90	*Human-II*	Mn(II)	in complex with A357300
2003	1R5G	2.00	*Human-II*	Mn(II)	in complex with A311263
2003	1R5H	2.40	*Human-II*	Mn(II)	in complex with A320282
2004	1TKJ	1.15	*S. griseus*	Zn(II)	in complex with D-methionine
2004	1WKM	2.30	*P. furiosus*	Mn(II)	in complex with methionine
2004	1XNZ	1.52	*E. coli*	Mn(II)	in complex with 5-(2-chlorophenyl)furan-2-carboxylic acid
2004	1Y1N	1.51	*M. tuberculosis*	---	without bound inhibitor

4.5.2 Inhibitor Binding Modes

A few structures with bound competitive inhibitors are known, for example EcMetAP with bound transition state analogs, bestatin based inhibitors or triazole based inhibitors (pdb codes 1C21, 1C22, 1C23, 1C27, 3MAT, cfr. Table 4-10 and Table 4-19). All these inhibitors somehow coordinate to the metal ion(s) in the active site. Recently, the crystal structure of a Mn(II)-form of the *E. coli* MetAP complexed with a Mn(II) specific inhibitor has been described[145], pdb code 1XNZ. The active site aligns very well with those of the di-Co(II)-form, indicating no major changes in geometry upon the replacement of Co(II) by Mn(II)[145]:

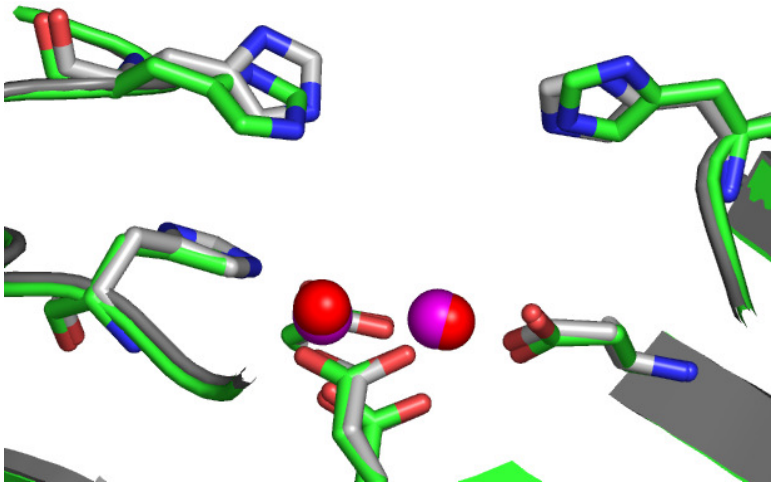

Fig. 4-32 Alignment of Mn(II)- and Co(II)-loaded EcMetAP (1XNZ and 2MAT). Co(II) ions are shown in magenta and the corresponding MetAP in silver/blue, Mn(II)-ions are shown in red and the corresponding MetAP in green/blue

The inhibitor coordinates to the active site metal ion. Additionally, high-resolution crystal structures of *S. aureus* MetAP-I in complex with various keto heterocycles and aminoketones were determined that also coordinate to the active site and form an uncleavable tetrahedral intermediate upon binding[149]. In two of these cases, the formation of the tetrahedral intermediate results in a favourable metal binding environment that allows trapping of a cobalt ion that in turn helps in the stabilization[149]. However, the stabilization by a third metal ion under *in vivo* conditions was questioned because 10 mM $CoCl_2$ were present during crystallization[149]. Thus, neither the binding mode nor the use of a different metal ion can explain the discrepancy between *in vitro* and *in vivo* activity of some compounds.

Therefore, it was tried to clarify the binding mode of thiabendazole by X-ray structure determination.

4.5.3 Crystal Structure Determination

Crystallization screens and crystallization trials based on literature procedures were performed in cooperation with Prof. Klebe, Marburg University (Germany). For transportation, the protein was shock-frozen on dry-ice/ethanol at about 20 mg/ml. About 400 different conditions were tested but these initial screenings yielded no results. Thus, the concentration of the enzyme solution was varied (13 mg/ml, 23 mg/ml and 33 mg/ml) and screenings were performed with and without the addition of octanoylsucrose as an additive. Then, different protein charges were used for crystallization screens, the salt composition of the buffer of the protein stock solution was changed and the same tests as mentioned were performed again. In addition, these tests were also performed with the His-tagged protein obtained during the purification of the protein and with Co(II)-loaded- and apo-MetAP. As there were still no crystals, a new batch of protein was prepared and several crystallization trials were performed in Saarbrücken before freezing the protein. Thus, many small crystals of apo-EcMetAP were obtained (cfr. Fig. 4-33) after 24 hrs using conditions described in the literature[52]. The size of a single crystal was about 0.25 x 0.25 mm.

It can be stated that only freshly prepared protein is suitable for crystallization. Therefore, the protein was concentrated and kept at 4 °C for the following procedures. However, it was possible to obtain crystals after freezing a small sample of the solution at very high concentration (about 60 mg/ml) and storage for 2 days at -80 °C. If crystallization is possible after a longer storage period remains to be established. Crystals were also obtained with freshly prepared EcMetAP isolated from a frozen cell pellet. When kept at 4 °C, the concentrated protein solution can be used for about 10 days for crystallization trials, although the quality of the crystals declines. The addition of TCEP, a compound that reduces disulfide bonds and can reactivate oxidized EcMetAP might be used to prolong this time period.

It should also be noted that even with the use of freshly and not frozen protein, no crystals were obtained with any of the screening conditions of the applied screening sets (cfr. 7.3.2). In addition, Co(II) could not be substituted by Mn(II) under the successful conditions.

The slightly different conditions mentioned by Roderick and coworkers [51, 171] are also suitable for crystallisation. However, more protein is needed here.

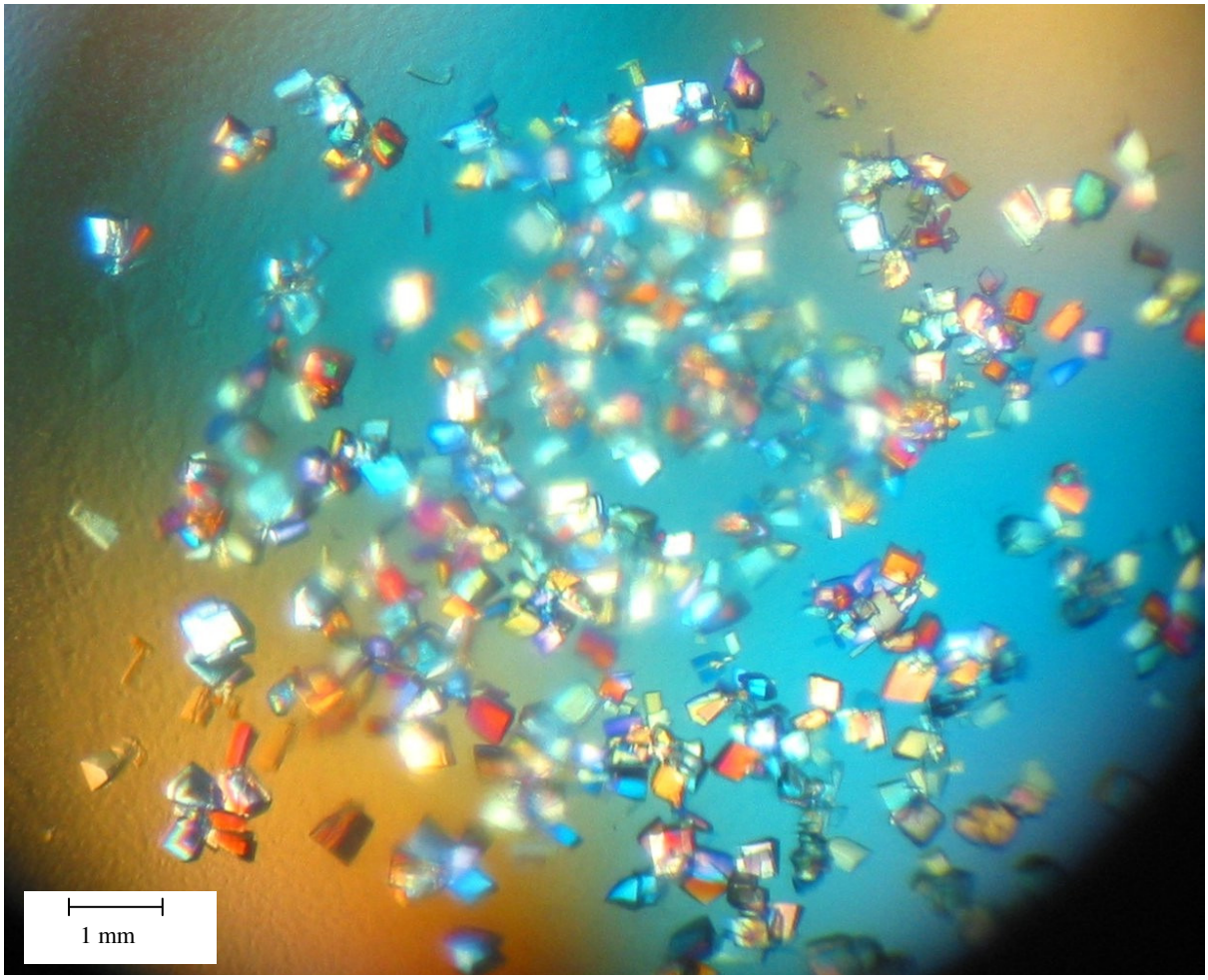

Fig. 4-33 Crystals of EcMetAP without an inhibitor

Cocrystallization of the EcMetAP with thiabendazole yielded fewer but slightly larger crystals (cfr. Fig. 4-34).

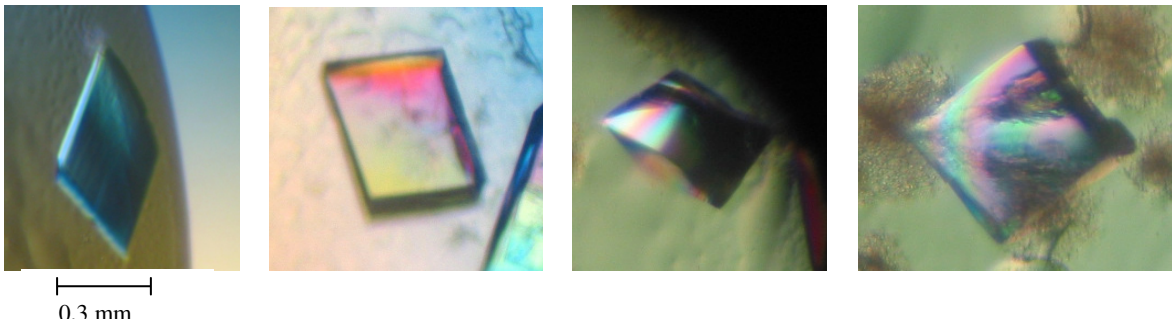

Fig. 4-34 Crystals of EcMetAP cocrystallized with thiabendazole

The same procedure was applied for three different inhibitors: Thiabendazole (I), RS 40 (II) and RS 17 (III). A suitable crystal was measured for each inhibitor and the determination of the structure revealed surprising results:

In all cases, the inhibitor does not coordinate towards the metal ions of the active site as could be expected but binds with an auxiliary third metal ion to His79. This metal complex is connected to the water molecule bridging the two Co(II) ions in the metal binding site. A schematic drawing can be seen in Fig. 4-35 and images generated from the crystal structures in Fig. 4-36.

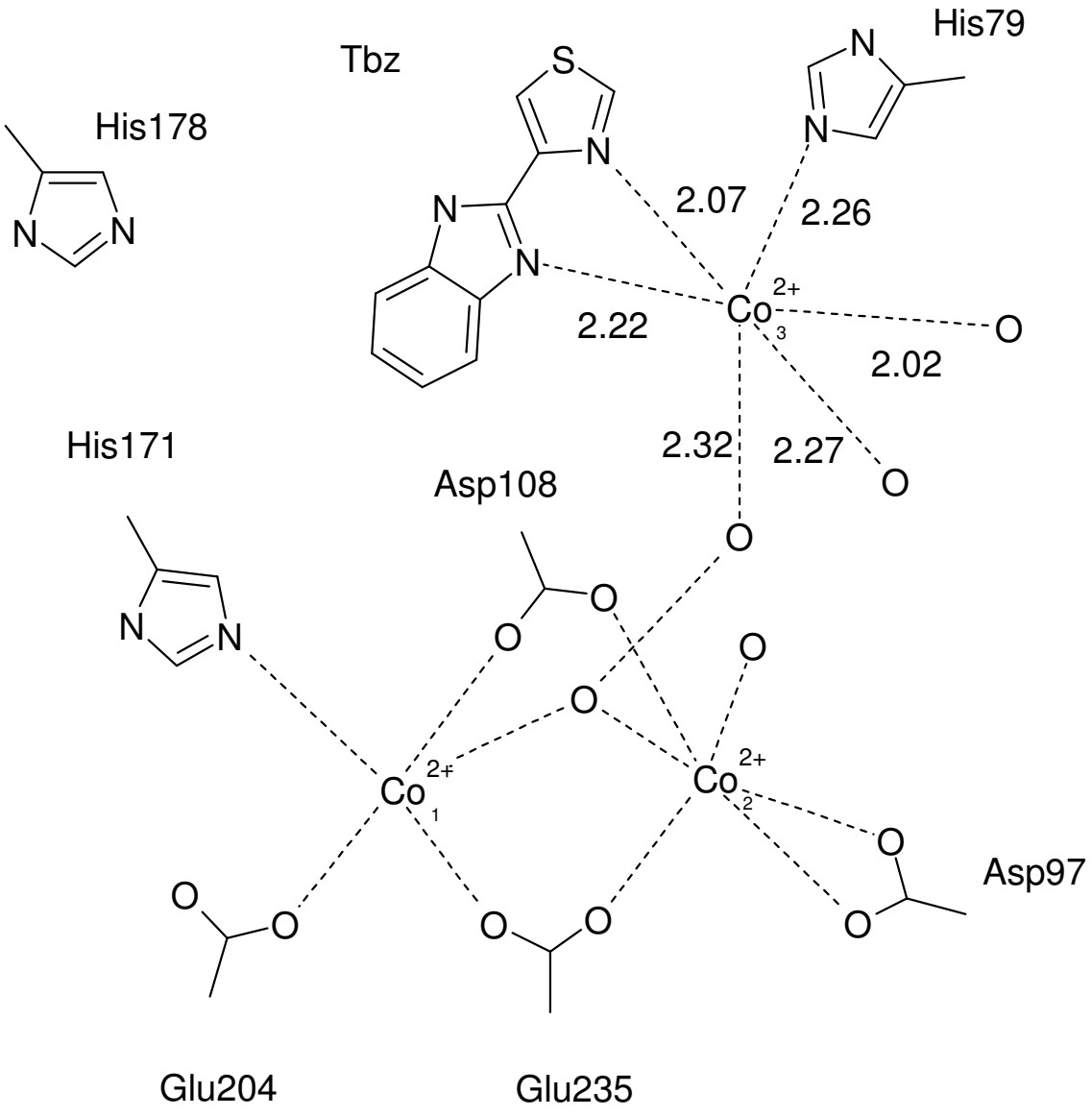

Fig. 4-35 Schematical drawing for the binding mode of thiabendazole (Tbz) to EcMetAP

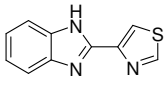

I

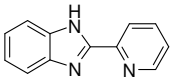

II

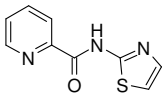

III

I

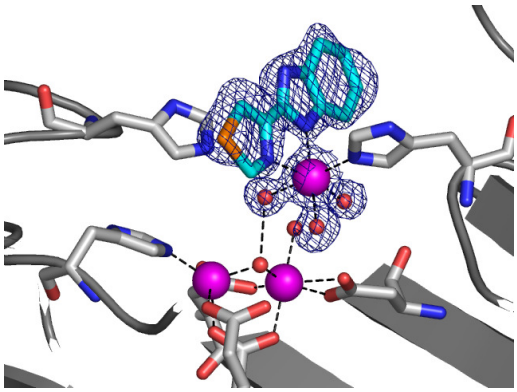

II

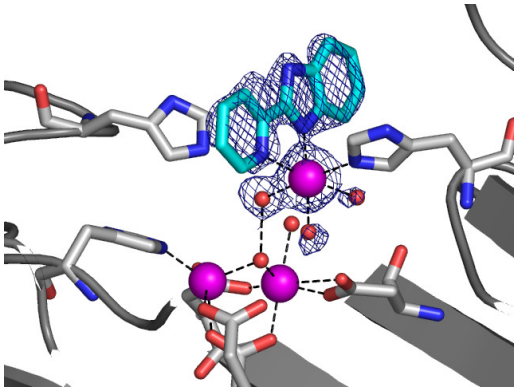

III

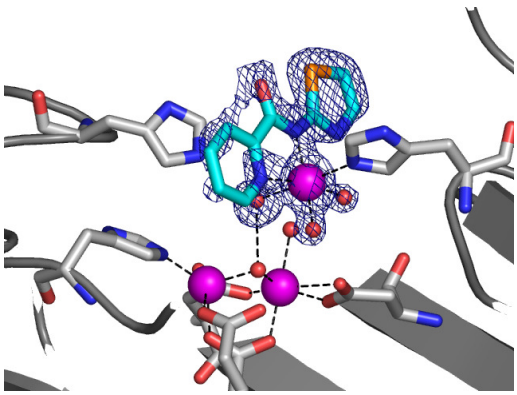

Cpnd.	HOH	Bave	Bsdv	Bmin	Bmax
I	270	35.66	9.66	14.90	63.24
II	239	37.75	13.10	13.74	87.18
III	292	35.36	11.25	11.66	71.59

Cpnd.	Lig	Bave	Bsdv	Bmin	Bmax
I	14	29.37	4.17	20.34	40.16
II	15	54.21	11.23	40.17	72.43
III	14	37.38	7.65	24.10	47.08

Cpnd.	Protein	Bave	Bsdv	Bmin	Bmax
I	2064	24.86	10.75	11.64	101.18
	1063 main c.	22.18	7.34	11.64	72.88
	1001 side c.	27.72	12.86	12.48	101.18
II	2033	23.38	11.08	8.13	111.21
	1063 main c.	20.55	6.26	8.13	67.42
	1001 side c.	26.40	13.92	8.3	111.21
III	2033	21.97	10.95	7.09	96.96
	1063 main c.	18.89	6.82	7.09	66.90
	1001 side c.	25.24	13.31	7.80	96.96

Cpnd.	Bave			
	2 Co(II) act. site	1 bound Co(II)	1 add. Co(II)	1 add. Na(I)
I	17.36	25.09	54.86	22.46
II	17.61	35.22	not refined	18.11
III	13.67	30.50	41.37	22.18

Fig. 4-36 Electron density of thiabendazole (above), of 2-pyridine-2-yl-1H-benzimidazole (middle) and of pyridine-2-carboxylic acid thiazole-2-ylamid (below) near the active site. The 2Fo - Fc electron density is contoured at 1σ in blue and shown within a radius of 1.5 Å around the inhibitor, the auxiliary cobalt ion and the complexing water molecules.

Table 4-20 Data Collection and Refinement Statistics for the MetAP-inhibitor complexes. [a] Values in brackets are statistics for the highest resolution shell; [b] R_{sym} =[$\Sigma_h\Sigma_i|Ii(h) - \langle I(h)\rangle|/\Sigma_h\Sigma_i\ Ii(h)$] x 100, where $\langle I(h)\rangle$ is the mean of the I(h) observation of reflection h. [c] Rcryst = Σhkl\|Fo - Fc\|/Σhkl\|Fo\|. [d] Rfree is calculated in the same manner as Rcryst but from 5 % of the data that were not used for refinement. [e] From Procheck[172]. [f] The residue Asn77 is in a disallowed region. This residue is characteristic of all MetAPs and is the second residue contained within a distorted type II' ß-turn (residues 76-79), observed in all structures thus far studied. The distortion is most likely induced by a putative sodium ion coordinated to the carboxyl oxygens of Asn77, Cys234 and Glu79[173].

ligand:	I	II	III
space group	$P2_1$	$P2_1$	$P2_1$
unit cell parameters (Å, deg for β)	a = 38.9 , b = 66.1, c = 48.5, β=111.2	a = 38.9 , b = 64.7, c = 48.8, β=111.5	a = 38.7 , b = 65.0, c = 48.6, β=111.5
data statistics			
resolution range (Å)	30-1.6	20-1.7	30-1.6
highest resolution shell (Å)	1.63-1.6	1.73-1.7	1.63-1.6
no. of observations	101657	47499	68688
no. of unique reflections	29881	23646	27964
completeness (%)	98.2 [75.8][a]	95.0 [91.9]	94.5 [72.6]
mean I/σ	14.8 [2.9]	10.7 [2.3]	17.3 [3.6]
R_{sym} (%)[b]	8.6 [41.8]	7.0 [37.4]	4.4 [21.3]
Refinement statistics and RMS deviations:			
refined residues	262	262	262
refined inhibitor atoms	14	15	14
refined Co/Na atoms	4/1	3/1	4/1
refined water molecules	270	239	292
R_{cryst} (Fo > 4σ Fo; Fo)[c]	16.0, 16.8	16.5, 17.7	16.3, 16.8
R_{free} (Fo > 4σ Fo; Fo)[d]	22.2, 23.3	25.4, 26.7	22.1, 22.9
bond lengths (Å)	0.009	0.006	0.009
bond angles (deg)	2.3	2.0	2.3
Average B values			
protein atoms (Å^2)	24.9	23.4	22.0
main chain (Å^2)	22.2	20.6	18.9
side chain (Å^2)	27.7	26.4	25.2
Co_1, Co_2 (active site, Å^2)	17.4	17.6	13.7
Co_3 (inhibitor, Å^2)	25.1	35.2	30.5
inhibitor atoms (Å^2)	29.4	54.2	37.4
waters (Å^2)	35.7	37.8	35.4
B values Na^+ / Co_4 (Å^2)	22.5 / 54.9	18.1/---	22.2 / 41.4
Ramachandran plot[e]			
most favoured (%)	91.7	91.2	91.2
additionally allowed (%)	7.9	8.4	8.4
generously allowed (%)	0.0	0.0	0.0
disallowed (%)[f]	0.4	0.4	0.4

This way, these inhibitors block the entrance of the active site without interfering with the active site itself as can be seen in Fig. 4-37 for thiabendazole:

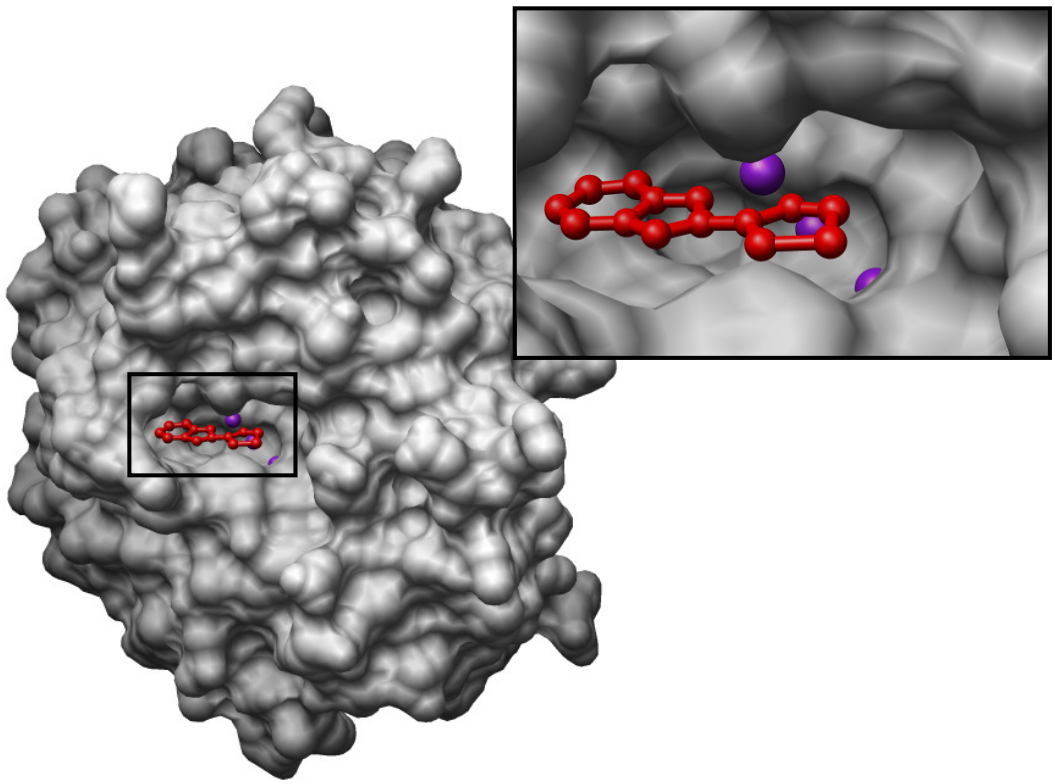

Fig. 4-37 *E. coli* MetAP with bound thiabendazole (red), the cobalt ions are shown in magenta

The structure with thiabendazole as a ligand was deposited in the PDB (pdb-code 1YVM). The two other structures were not deposited because different binding modes cannot be ruled out. For III, the density was only partly visible and for II, the B-values are very high. Nevertheless, clear density for the third Co(II)-ion could be observed in all cases. It was checked that this Co(II) ion is not present under otherwise identical conditions.

This binding mode offers an explanation for the *in vivo*-inactivity: These inhibitors are in need of Co(II) ions to exhibit their inhibitory ability as they bind as metal complexes. Possibly, the *in vivo* Co(II)-concentration is too low to allow the formation of this complex and Co(II) can probably not be substituted by another metal ion. Katz *et al*. were the first to describe serine protease inhibitors that are zinc-mediated and thus use metal ions for their binding capability[174], similar to the binding of thiabendazole. Other substances are likely to

share the same binding mode, as many of the EcMetAP inhibitors described possess structural elements with metal complexing properties such as hydroxamic acids or heterocycles flanked by an amine group. *In vitro* screening results of metal dependent enzymes should therefore be considered with caution and should be accompanied by either a screening with different metal ions (when the cofactor can be substituted) or by *in vivo* screening assays.

The binding mode of thiabendazole might also give the explanation why excess cobalt is inhibitory for EcMetAP. Comparing the ratios of Co(II) and EcMetAP during the assay procedure and during crystallization, it becomes clear that the ratio is much higher during *in vitro* tests (200 µM metal ions:10 nM enzyme compared to 1 mM metal ions:0.4 mM protein). Therefore, it may well be possible that at very high Co(II)-concentrations within an assay, a Co(II)-ion binds even without the presence of an inhibitor to His79 (or perhaps His178) and not to the bridging hydroxide ligand which was suggested by other authors[93] (cfr. 4.2.3.5.2, Concentration of Co(II)). This would block the entrance to the active site in the same way as an inhibitor-cobalt-complex.

4.6 Determination of MIC-values

Some of the thiabendazole-derivatives, for example RS 48, RS 60 and RS 54 have been described to be active against *E. coli* and other bacteria, with MIC-values of 10-100 µg/ml[175]. Thus, the even (*in vitro*) more active derivatives were expected to be promising candidates for antibacterial drugs. Consequently, the three compounds with the lowest IC_{50}-values (Compounds RS 17, RS 64 and RS 65) together with the parent compounds thiabendazole and RS 40 were tested for their antibacterial activity, using the *E. coli* strain BL21(DE3) as the test organism and ciprofloxacine as a reference. The results are shown in Fig. 4-38.

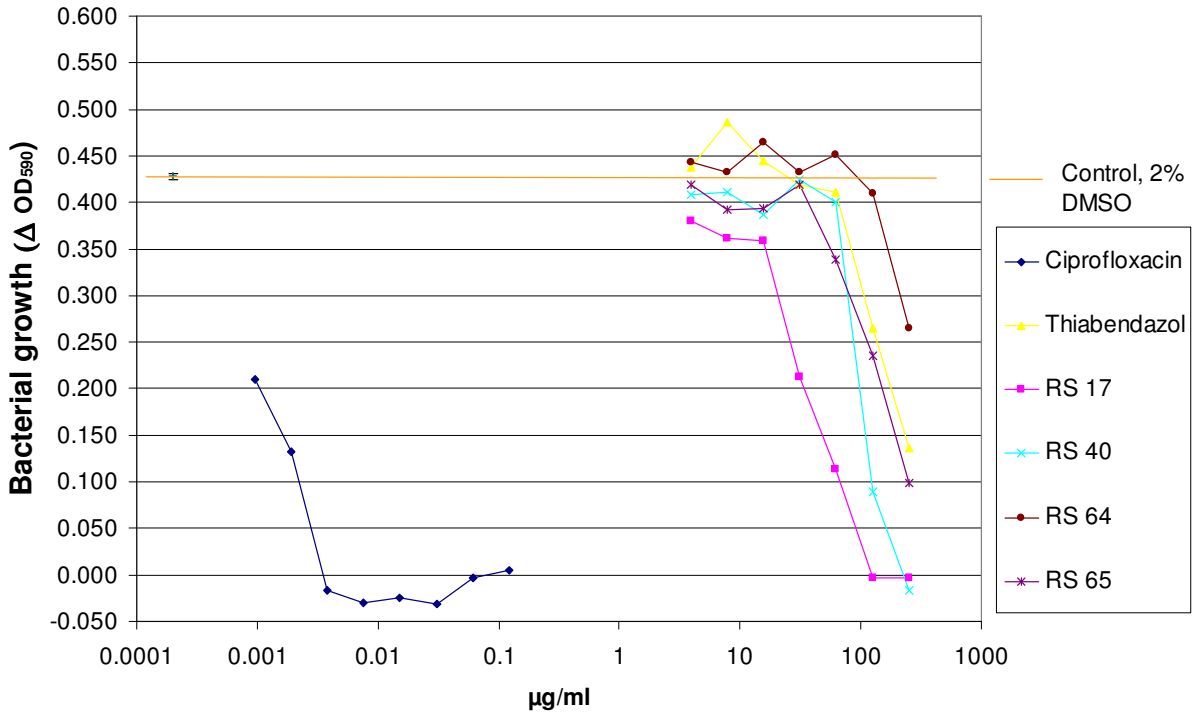

Fig. 4-38 MIC-value determination of different benzimidazoles with *E. coli*, 48 hrs incubation

None of the thiabendazole derivatives significantly inhibited the growth at concentrations up to 100 µg/ml in spite of the good *in vitro* activity against EcMetAP. The substance with the lowest IC_{50}-value, RS 17, also showed the best *in vivo* activity. However, RS 64 and RS 65 with similar IC_{50}-values *in vitro* were not as active as RS 17. Among the thiabendazole derivatives, RS 40 was the most active compound. As only high concentrations of these substances led to observable effects (125 and 250 µg/ml) and other aspects such as

pharmacokinetic properties and a possible metabolism have to be taken into account, it is difficult to obtain a proper correlation between the *in vitro* IC_{50}-values and the MIC-values.

Given the fact that Co(II) is needed for the binding of thiabendazole and its derivatives, the following hypothesis should be tested: Thiabendazole and its congeners should have (in theory) a higher *in vivo*-potency when applied as a Co(II)-complex. The pharmacokinetic properties of these complexes are not known, just like the stability constants of the complexes. These factors could counteract the expected improvement. Nevertheless, an increase in intracellular Co(II)-levels is very probable if Co(II) is added externally. Even without proper permeation of the Co(II)-complexes through the cell membrane these substances should be more effective *in vivo*. This can be supposed assuming "normal" cell permeation of the substances and subsequent formation of a Co(II)-complex within the cells. This process and the corresponding binding capacity to the target protein should correlate with (increasing) Co(II)-levels.

In addition, antimicrobial activity of several thiabendazole-metal complexes has been observed[176] and the preparation of complexes of thiabendazole with transition metals has been described in the literature[177].

After initial tests with different amounts of Co(II)-ions added to the growth medium, RS 17 (as the compound with the best MIC-value) and thiabendazole (as the lead compound for the synthesized library) were chosen as test compounds and the following results were obtained.

4.6.1 Comparison of MIC-values with and without Co(II)

First, three different Co(II)-concentrations were tested: 0.0122 mM, 0.122 mM and 1.22 mM $CoCl_2$. Whereas the addition of 0.0122 mM $CoCl_2$ had almost no effect on either bacterial growth or the MIC-values of the compounds, the addition of 1.22 mM $CoCl_2$ was lethal for the *E. coli* strain BL21(DE3) and inhibitors could not be tested. The addition of 0.122 mM $CoCl_2$ proved advantageous and was used for the further testing as it offered the possibility to observe effects combined with only a minor decline in bacterial growth without inhibitors.

For compound RS 17, the following curves were determined (cfr. Fig. 4-39). A clear left-shift of the curve could be observed, confirming the expected influence of Co(II)-addition.

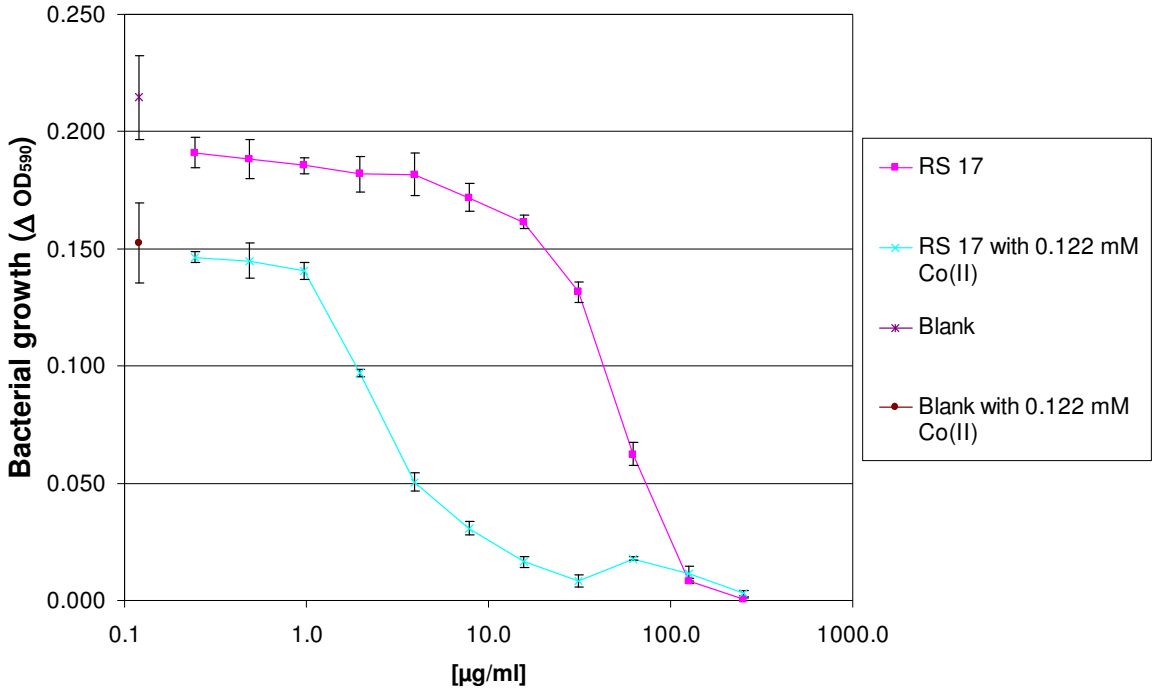

Fig. 4-39 MIC-value determination with compound RS 17 and 0.122 mM $CoCl_2$ added to the growth medium, 16 hrs incubation, values with inhibitors were determined in duplicate, blank values in quadruplicate

For thiabendazole, this effect was also visible but only became apparent at high concentrations and a longer incubation time. The results for both RS 17 and thiabendazole are shown in Table 4-21.

In summary, the addition of Co(II) improved the MIC-values of both compounds tested. The effect was more pronounced with compound RS 17 compared to thiabendazole. This could be based on the higher stability of its Co(II)-complex and the correlating lower IC_{50}-value compared to the thiabendazole-Co(II)-complex but could also be the result of differing pharmacokinetic properties. Defining the MIC-value as the concentration that inhibits bacterial growth by more than 90 %, the potency of RS 17 was improved by a factor of about 6-8 and a complete inhibition of bacterial growth could be reached by 125 µg/ml - 250 µg/ml thiabendazole. This result could not be achieved when no Co(II) was present.

Table 4-21 Inhibition of bacterial growth of compound RS 17 and thiabendazole with and without the addition of 0.122 mM $CoCl_2$. Inhibition rates smaller than 15 % are titled "---". Incubation times were 16 hrs for Compound RS 17 and 45 hrs for thiabendazole; values with inhibitors were determined in duplicate, blank values in quadruplicate

Compound RS 17			Thiabendazole		
Concentration [µg/ml]	% inhibition without Co(II)	% inhibition with Co(II)	Concentration [µg/ml]	% inhibition without Co(II)	% inhibition with Co(II)
250.0000	99.8 ± 0.3	98.1 ± 0.8	250.0000	57.8 ± 3.3	99.2 ± 2.1
125.0000	96.1 ± 0.5	92.7 ± 2.0	125.0000	44.1 ± 8.1	76.8 ± 0.3
62.5000	70.9 ± 2.3	88.3 ± 0.5	62.5000	23.3 ± 1.6	44.1 ± 7.0
31.2500	38.7 ± 2.2	94.7 ± 1.7	31.2500	---	---
15.6250	24.7 ± 1.4	89.2 ± 1.6	15.6250	---	---
7.8125	19.9 ± 2.8	79.8 ± 2.0	7.8125	---	---
3.9063	15.4 ± 4.2	66.9 ± 1.5	3.9063	---	---
1.9531	15.2 ± 3.6	36.3 ± 1.0	1.9531	---	---

5 Summary and Conclusion

After the successful expression and purification of the *E. coli* methionine aminopeptidase, a cheap and easy to handle assay system was developed for the screening of inhibitors and for the characterisation of the enzyme. Experiments with fumagillin, a covalent inhibitor that inhibits angiogenesis, confirmed computational studies trying to calculate the protonation state of the active site of the EcMetAP. This enzyme is metal dependent, although the identity of the metal ion is not yet entirely clear. Co(II) activates all MetAPs known so far but also Mn(II) seems a promising candidate. The active site consists of five conserved residues surrounding two metal ions that are "connected" by a bridging water molecule. The protonation state of this water molecule, however, is not entirely clear. Both the computational studies and the experiments investigating the pH-dependency of the binding of fumagillin indicated that two protonation states are possible: One (at a lower pH) is relevant for the binding of fumagillin, an epoxide that is more easily bound when it is protonated prior to the nucleophilic attack of a histidine near the active site. A more basic pH is relevant for the cleavage of substrates. The pK_a-value of the bridging water molecule can be estimated to be about 7. Based upon these results, a modified reaction mechanism could be proposed. Additionally, these differences in enzymatic behaviour might be exploited for the further design and development of anticancer agents.

After this initial characterisation of the enzyme, a screening of inhibitors was performed. Small epoxides were synthesized and tested in addition to fumagillin analogs, peptidomimetics, known drugs and substances from our in-house library. In summary, several hundred substances were tested. With the aid of molecular modeling and virtual screening it was possible to find an *in vitro* active substance: Thiabendazole, a known antifungal and antiparasitic drug has an IC_{50}-value of about 500 nM. Subsequently, a series of thiabendazole-analogs was synthesized and tested. It became clear that only substances with a functional metal-binding motif are able to inhibit Co(II)-loaded EcMetAP. However, it was difficult to gain further insight into structure-activity relationships even with the assistance of molecular modeling methods. In addition, all of the substances proved inactive against the Mn(II)-loaded EcMetAP. They were also unable to inhibit the growth of *E. coli* in concentrations up to 100 µg/ml in spite of supposedly acceptable pharmacokinetic properties and a high *in vitro*-potency with Co(II) present. These findings, together with a questionable docking-pose, the

desire to continue this work with a rational drug design and the need to use high concentrations of *in vitro* highly active substances to observe an effect on bacterial growth brought us to resolve crystal structures of the EcMetAP with bound inhibitor. A new and surprising binding mode was the result: Thiabendazole exerts no direct interactions with the active site metal ions as could be expected by X-ray structures of other competitive inhibitors, docking results and of the molecular properties of thiabendazole. In contrast to other competitive inhibitors, thiabendazole binds via a third "auxiliary" metal ion (thus as a metal-complex) to a conserved histidine near the active site and blocks the entrance to the catalytic site. Further X-ray structures of a thiabendazole analogue and of a competitive inhibitor described in the literature (of a different class) revealed an identical mode of action, indicating a possible generalisation of this binding mode for at least to classes of compounds: Properties and *in vivo*-results of other structurally distinct classes of competitive inhibitors give cause for the assumption that this binding mode might be even more widespread.

The unexpected binding mode explains the inactivity of many compounds when tested for antibacterial or anti-angiogenic activity, as the screening for inhibitors is normally done with (unphysiologically high concentrations of) Co(II) as the cofactor. Other divalent metal ions – although able to substitute for the Co(II) in the active site needed for enzymatic activity – seem to be unable to act as a binding-mediator. However, the Co(II)-complexes derived from these substances should have a higher inhibitory *in vivo*-potency than the "free substances". The last step after the clarification of the binding mode was therefore the proof of principle. In consequence, two of the compounds with the proven binding mode were used as model substances and their antibacterial effect against *E. coli* was tested again, but this time additional Co(II) was added to the growth medium of the bacteria. This action increases the potency of both thiabendazole and of the compound taken from the literature, thus confirming the expected effect and underlying the binding mode clarified by crystallization experiments.

The pharmacokinetic properties of these metal-complexes are probably unfavourable. Therefore, it remains questionable if these substances should be used as lead compounds for the future drug development and the design of inhibitors using other physiologically more common ions such as Ca(II) or Mg(II) will be a challenging task. Even if the aim to get new, potent antibacterial drugs was only partly achieved, the *in vitro* results of the thiabendazole analogs together with the crystallization experiments could be used to develop a new scoring function for predicting the binding affinities of compounds to a binding site with metal ions.

With this scoring function, it is possible to distinguish between the active and the inactive substances which was not possible with commonly available functions such as ChemScore or with the scoring functions of GOLD. Thus, it will be possible to get reliable docking poses and affinity predictions in the future not only for virtual screening procedures with the EcMetAP but also with other target (metallo-) proteins where the crystal structure is available.

In conclusion, *in vitro* screening results should always be considered very carefully to avoid unneeded expenditure of human labour, especially when working with metal-dependent enzymes. The binding mode of inhibitors should be confirmed by crystal structure determination, even if this is often difficult if the crystallization conditions are unknown or when working with membrane bound proteins.

During this work, it was possible to combine experimental procedures, molecular modeling techniques and crystallization experiments to gain a deeper understanding of the target protein. Hopefully, the results presented here will be useful for the future design and development of anticancer, antibacterial, antifungal and antiparasitic drugs.

6 Zusammenfassung

Nach der erfolgreichen Überexpression und Aufreinigung der *E. coli* Methionin-Aminopeptidase ist es gelungen, ein günstiges und einfach durchzuführendes Testverfahren zu etablieren. Dieses Testverfahren kann in 96-Well-Platten durchgeführt werden und ist daher sowohl zur Charakterisierung des Enzyms geeignet als auch für Screening-Versuche um neue, potentielle Hemmstoffe zu identifizieren.

Der erste Teil der Arbeit befasst sich mit dem Protonierungszustand des aktiven Zentrums, der z.B. wichtig ist für die Aufklärung der bei der Umsetzung von Substraten ablaufenden Reaktionen. Bei der Methionin-Aminopeptidase handelt es sich um eine Metalloprotease. Allerdings ist noch nicht klar, welches Metall als Cofaktor *in vivo* fungiert. Auf jeden Fall aktiviert Co(II) alle bisher bekannten Methionin-Aminopeptidasen, unabhängig von Spezies und Subtyp. Daneben gilt aber auch u.a. Mn(II) als möglicher Cofaktor. Das aktive Zentrum besteht aus fünf bei allen Methionin-Aminopeptidase-Arten identischen Aminosäuren, die zwei Metallionen umgeben; die beiden Metallionen wiederum werden durch ein Wassermolekül überbrückt. Der Protonierungszustand dieses Wassermoleküls ist nicht bekannt und spielt neben dem Reaktionsmechanismus auch eine Rolle bei der Bindung von bestimmten Hemmstoffen. Fumagillin ist solch ein kovalent bindender Hemmstoff der Methionin-Aminopeptidase und ist gilt als potentielles Krebstherapeutikum, da Fumagillin die Angiogenese verhindert. Um nun den Protonierungszustand des aktiven Zentrums aufzuklären wurden zunächst einige Computersimulationen mit diversen theoretisch denkbaren bzw. möglichen Protonierungszuständen durchgeführt. Parallel wurde experimentell die pH-Abhängigkeit der Fumagillin-Bindung untersucht. Die Computersimulationen wurden durch die experimentellen Daten bestätigt und beide Lösungsansätze kommen zu folgendem Ergebnis: Prinzipiell scheinen zwei Protonierungszustände möglich zu sein: Das überbrückende Wassermolekül lässt sich durch einen pKs-Wert von ca. 7 charakterisieren und kann unter physiologischen Bedingungen entweder als koordinierendes Wassermolekül oder als überbrückendes Hydroxid-Ion vorliegen. Der Zustand bei einem niedrigeren pH-Wert ist relevant für die Bindung von Fumagillin. Dieses Epoxid wird leichter gebunden, wenn es vor dem nucleophilen Angriff eines sich in der Nähe des aktiven Zentrums befindlichen Histidins protoniert wird. Für die Spaltung von Substraten allerdings scheinen basischere Bedingungen günstiger zu sein. Aufgrund dieser Ergebnisse konnte ein modifizierter Reaktionsmechanismus vorgeschlagen werden. Zusätzlich bieten diese Ergebnisse wichtige

Hinweise für das zukünftige Design kovalent bindender Hemmstoffe und für die weitere Entwicklung von Krebstherapeutika.

Der zweite Teil der Arbeit befasst sich mit der Entwicklung neuer Hemmstoffe der *E. coli* Methionin Aminopeptidase. Nach der oben erwähnten ersten Charakterisierung des Enzyms sollte ein Screening durchgeführt werden. Zu diesem Zweck wurden kleine Moleküle mit einer Epoxid-Gruppe synthetisiert und neben diversen Fumagillin-Analoga, Peptidomimetika, bekannten Arzneimitteln, Derivaten von bekannten Hemmstoffen und anderen Substanzen aus dem Arbeitskreis getestet. Es wurden ca. 35 Substanzen synthetisiert und mehrere Hundert Substanzen wurden insgesamt untersucht. Mit der zsätzlichen Hilfe von virtuellen Screening-Methoden konnte schließlich eine *in vitro* sehr aktive Substanz identifiziert werden: Thiabendazol, ein bekanntes Fungizid und in der Behandlung von Parasiten eingesetztes Arzneimittel. Der IC_{50}-Wert von Thiabendazol liegt bei ca. 500 nM. Eine Reihe von Thiabendazol-Analoga wurde synthetisiert und getested. Es wurde klar, dass nur Substanzen mit einer potentiellen Metallbindungsstelle die Co(II)-aktivierte *E. coli* Methionin Aminopeptidase hemmen konnten. Es war allerdings schwierig, weitere Struktur-Wirkungs-Beziehungen zu erkennen. Auch der Einsatz von Molecular-Modeling Methoden brachte keine weiteren Erkenntnisse. Zudem waren alle Substanzen unwirksam gegen das Mn(II)-aktivierte Enzym und konnten das Wachstum von *E. coli* Bakterien erst in einer Konzentration von über 100 µg/ml hemmen, obwohl sie an dem freien Enzym teilweise IC_{50}-Werte von unter 100 nM aufweisen und aufgrund der Verwendung von Thiabendazol als Arzneimittel wahrscheinlich auch akzeptable pharmakokinetische Eigenschaften besitzen.

Aufgrund dieser Ergebnisse, einer fragwürdigen Docking-Position von Thiabendazol beim virtuellen Screening und dem Wunsch, diese Arbeit mit einem rationalen Wirkstoffdesign fortzuführen brachten uns dazu, die Kristallstruktur der *E. coli* Methionin-Aminopeptidase mit gebundenem Hemmstoff aufzuklären. Das Ergebnis war ein neuer und überaschender Bindungsmodus: Thiabendazol übt keinerlei direkte Wechselwirkungen mit den Metallionen des aktiven Zentrums aus, wie aufgrund von Röntgenstrukturen der Methionin-Aminopeptidase mit anderen kompetitiven Hemmstoffen oder auch aufgrund unserer eigenen Docking-Versuche erwartet wurde. Stattdessen bindet Thiabendazol mit Hilfe eines dritten Metallions, also als Metallkomplex, an ein im Laufe der Evolution erhalten gebliebenes Histidin in der Nähe des aktiven Zentrums und blockiert so dessen Eingang. Weiterführende Röntgenstrukturuntersuchungen mit einem Thiabendazol-Analogon und einer in der Literatur beschriebenen Verbindung einer anderen Klasse lassen den gleichen Bindungsmodus erkennen. Diese Ergebnisse und die Tatsache, dass auch andere Verbindungsklassen ein

unterschiedliches *in vitro*- und *in vivo*-Verhalten zeigen, legen die Vermutung nahe, dass dieser Bindungsmodus noch weiter verbreitet sein könnte. Dieser unerwartete Bindungsmodus erklärt die antibakterielle oder auch antiangiogenetische Unwirksamkeit vieler Substanzen – schließlich wird das Screening für neue Hemmstoffe normalerweise mit (unphysiologisch) hohen Co(II)-Konzentrationen durchgeführt.

Andere zweiwertige Metallionen können nicht als „Bindungsvermittler“ fungieren, auch wenn sie anscheinend die Co(II)-Ionen im aktiven Zentrum ersetzen können. Die Co(II)-Komplexe dieser Verbindungen sollten bei vorausgesetzter Stabilität zumindest theoretisch eine höhere *in vivo*-Potenz besitzen als die „freien“ Substanzen. Der letzte Schritt in dieser Arbeit nach der Aufklärung des Bindungsmodus war schließlich der Beweis des Bindungsprinzips: Zwei der Substanzen, die ihre *in vitro*-Hemmaktivität als Co(II)-Komplexe ausüben, wurden als Modellsubstanzen ein weiteres Mal auf ihre antibaktielle Aktivität untersucht, allerdings wurde diesmal Co(II) zum Wachstumsmedium der Bakterien gegeben. Dadurch konnte in beiden Fällen eine signifikante Verstärkung der Hemmwirkung beider Substanzen festgestellt werden. Da die Metallkomplexe wahrscheinlich ungünstige pharmakokinetische Eigenschaften haben, bleibt die Frage offen, ob diese Verbindungen als Leitsubstanzen für die weitere Hemmstoffentwicklung dienen sollten. Auch dürfte es sehr schwierig werden, die Substanzen so zu modifizieren, dass das Co(II) durch andere physiologische Metallionen wie Ca(II) oder Mg(II) ersetzt werden kann.

Auch wenn das Ziel neue, potente antibakteriell wirksame Stoffe zu finden nur zum Teil erreicht wurde, war es möglich, anhand der Kristallisationsexperimente in Kombination mit den *in vitro*-Ergebnissen eine neue Scoring-Funktion namens Turboscore für das virtuelle Screening von Substanzen zu entwickeln. Diese Funktion besitzt spezielle Parameter um Bindungsaffinitäten zwischen Heteroatomen und Metallionen zu bewerten. Mit Turboscore ist es möglich, zwischen aktiven und inaktiven Substanzen zu unterscheiden, was mit kommerziell erhältlichen Funktionen und Programmen wie GOLD oder ChemScore nicht gelungen war. Mit dieser Scoring-Funktion wird es möglich sein, für virtuelle Screening Versuche nicht nur mit der *E. coli* Methionin Aminopeptidase sondern auch mit anderen metallabhängigen Proteinen in der Zukunft zuverlässige Docking-Positionen zu erhalten.

Zusammenfassend lässt sich sagen, dass *in vitro* Versuche immer vorsichtig bewertet werden sollten. Ganz besonders aber dann, wenn es sich um metallabhängige Enzyme handelt. Wenn es irgendwie möglich ist, sollte der Bindungsmodus eines Hemmstoffs mittels

Röntgenstruktur überprüft werden, auch wenn dies bei unbekannten Kristallisationsbedingungen oder bei membrangebundenen Enzymen oft schwierig ist.

Bei dieser Arbeit ist es gelungen, durch eine Kombination von experimentellen Verfahren, computerunterstützten Modeling-Versuchen und Röntgenkristallstrukturuntersuchungen ein tieferes Verständnis der *E. coli* Methionin-Aminopeptidase und deren Hemmstoffen zu erhalten. Hoffentlich werden die hier präsentierten Ergebnisse nützlich sein für die weitere Hemmstoffentwicklung von zukünftigen antibakteriellen, fungiziden, antiparasitären Wirkstoffen bzw. Krebstherapeutika.

7 Materials and Methods

All chemicals and reagents were of the highest quality available and were obtained from Acros (Neuss, Germany), Aldrich (Steinheim, Germany), Bachem (Weil am Rhein, Germany), Fluka (Neu-Ulm, Germany), Lancaster (Mülheim am Main, Germany), Merck (Darmstadt, Germany), Macherey-Nagel (Düren, Germany), Molecular Probes/Invitrogen (Karlsruhe, Germany), Roche (Mannheim, Germany), Roth (Karlsruhe, Germany), Serva (Heidelberg, Germany), Sigma-Aldrich (Deisenhofen, Germany). Chemicals and solvents were normally used without further purification. The constitution of buffers and media used within this work are described in the respective (bio-) chemical sections. The most important chemicals and reagents are listed below, laboratory equipment, material and other instruments are listed in each section.

Enzymes

Horseradish Peroxidase	Sigma-Aldrich (Deisenhofen, Germany)
Amino acid oxidase (from *Crotalus adamanteus*, Type I)	Sigma-Aldrich (Deisenhofen, Germany)
Ribonuklease A (RNAse A)	Roth (Karlsruhe, Germany)
Desoxyribonuklease I (DNAse I)	Roche (Mannheim, Germany)
Restriction enzymes	New England Biolabs (Frankfurt, Germany) or Takara (Otsu, Japan)

Chemicals

Amplex Red	Molecular Probes/Invitrogen (Karlsruhe, Germany)
MGMM	Bachem (Weil am Rhein, Germany)
N-Octanoylsucrose	Calbiochem (San Diego, USA)

7.1 Chemistry

7.1.1 General Information

7.1.1.1 ^{1}H-NMR-Spectroscopy

^{1}H-NMR spectra were recorded on a Bruker (Karlsruhe, Germany) DRX-500 spectrometer (500 MHZ). Chemical shifts are reported as values (ppm) relative to either internal tetramethylsilane (0 ppm) or the solvent peak. The abbreviations of the signals are: s (singulet), d (doublet), dd (double doublet), t (triplet), q (quartet), m (multiplet). Coupling constants (J) are given in Hz.

7.1.1.2 Elemental Analyses

Elemental analyses were performed in the group of Prof. Huber, Department of Analytical Chemistry, University of the Saarland.

7.1.1.3 IR-Spectroscopy

IR spectra were measured with a Vector 33, Bruker (Karlsruhe, Germany); with a Zn/Se-ATR-Unit (ATR Harrick MVP, Software OPUS Version 4.0).

7.1.1.4 Melting Points

Melting points were measured with a Stuart Melting Point Apparatus SMP3, Bibby Sterlin (Essex, United Kingdom). The heating rate was 6 °C / min.

7.1.1.5 Laboratory Equipment/Other Instruments

Vacuum distillations of solvents during purification of compounds were done with a Rotavapor R, Büchi (Uster, Swiss) and a membrane vacuum pump CVC-2, Vacuumbrand (Wertheim, Germany). For the temperature regulation of the water bath the thermostat E51 from Haake (Erlangen, Germany) was used. Fluorescent lamp was a Minuvis from Desaga (Heidelberg, Germany). Magnetic stirrers (model RTC basic) were from IKA (Staufen, Germany).

7.1.2 Synthetic Procedures and Characterization of Compounds

Some of the compounds were synthesized for the first time. Although some of the other compounds are mentioned in the literature, they are often not characterized or no detailed procedure is given. The nomenclature of the compounds is according to the IUPAC.

7.1.2.1 List of Compounds

Cpd.	Proc.	Cpd.	Proc.	Cpd.	Proc.	Cpd.	Proc.
RS 1	A	RS 73	F-5	RS 33	H	RS 52	O
RS 2	A	RS 74	G	RS 34	O	RS 53	T
RS 3	A	RS 75	H	RS 35	O	RS 54	T
RS 4	A	RS 26	I	RS 36	O	RS 55	U
RS 5	A	RS 27	I	RS 37	O	RS 56	U
RS 6	A	RS 17	J	RS 38	P	RS 57	O
RS 7	B	RS 18	J	RS 39	Q	RS 58	O
RS 8	B	RS 19	K	RS 40	O	RS 59	O
RS 9	B	RS 20	L	RS 41	O	RS 60	O
RS 10	B	RS 21	M	RS 42	O	RS 61	O
RS 11	C	RS 22	N	RS 43	R	RS 62	R
RS 12	C	RS 23	I	RS 44	S	RS 63	V
RS 13	D	RS 24	I	RS 45	S	RS 64	O
RS 14	E	RS 25	N	RS 46	S	RS 65	O
RS 15	E	RS 28	H	RS 47	O	RS 66	O
RS 16	F-1	RS 29	H	RS 48	O	RS 67	O
RS 70	F-2	RS 30	H	RS 49	O	RS 68	R
RS 71	F-3	RS 31	H	RS 50	O	RS 69	R
RS 72	F-4	RS 32	H	RS 51	O		

7.1.2.2 Preparation of Starting Materials

7.1.2.2.1 Starting Materials for the Preparation of Derivatives of RS 17

For the preparation of derivatives of pyridine-2-carboxylic acid, pyridine-2-sulfonylchloride and pyridine-2-carbonyl chloride were needed as starting materials and prepared according to the following procedures:

Pyridine-2-sulfonyl chloride[178-181]:

2-Mercaptopyridine (20 g, 0.18 mol) was dissolved in concentrated HCl (250 ml), and chlorine gas was bubbled through at 0 °C for 2 h. The mixture was poured into ice-water (500 ml) and extracted three times with dichloromethane. The combined organic fractions were washed with brine and dried with Na_2SO_4. After filtering, concentration under reduced pressure yielded a clear oil that solidified in the freezer. The yield was 88 % (Lit. 55-97 %) and the product was used without further purification.

Pyridine-2-carbonyl chloride[182, 183]:

To a stirred solution of thionyl chloride (15 ml) was added picolinic acid (2.47 g, 20 mmol) with heating at 85 °C for 1 h. The reaction mixture was evaporated to afford crude picolinic chloride as a dark purple solid. The yield was 100 % and the product was used without further purification.

7.1.2.2.2 Starting Materials for the Preparation of Derivatives of Thiabendazole

Pyridine-2-carboxamidine hydrochloride and Pyrazine-2-carboxamidine hydrochloride[184]:

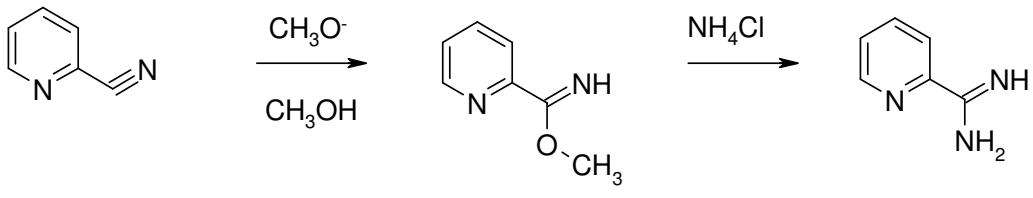

Fig. 7-1 Reaction scheme for the preparation of pyridine-2-carboxamidine (or other amidines)

A solution of 26.0 g (0.25 mol) of 2-cyanopyridine (or 2-cyanopyrazine) and 1.35 g (0.025 mol) of sodium methoxide in 25 ml of methanol was allowed to stand overnight at room temperature. The amidine salt has then been prepared *in situ* from the imidate with an amount of ammonium chloride equivalent to the total base present. The reaction mixture was merely stirred for a few hours until the salt dissolved. The reaction time varied from 1-24 hrs. The solvent methanol was evaporated to recover the amidine salt that was used without further purification. The yield was 96 % (m. p. 146-148 °C) for Pyridine-2-carboxamidine hydrochloride (Lit. 149-151 °C) and 63 % (m.p. 217-220 °C, decomp.) for Pyrazine-2-carboxamidine hydrochloride (Lit. 215-218 °C).

Thiazole-4-carboxylic acid:

The reaction scheme is depicted in Fig. 4-31. At first, bromopyruvic acid was prepared according to Ref.[185]:

1 mol of pyruvic acid was heated to 50 °C in a 3-neck flask equipped with ground glass joints, and 1 mol of bromine, previously dried by shaking with concentrated H_2SO_4, was added dropwise with stirring and exclusion of moisture. The heat of the reaction was usually sufficient to keep the temperature at 50 °C; external temperature control was resorted to when necessary. The thick fuming syrup was immediately poured into a large crystallizing dish, the flask washed with a small amount of hot benzene, and the washing added to the main product. Sometimes the material set in the flask to a fuming crystal mass which was dissolved in a small amount of hot benzene. The mixture was placed in a vacuum desiccator over moist NaOH pellets, and the solvent removed by suction. On the next day the material was ground to a fine powder and kept *in vacuo* over NaOH pellets for 48 to 72 hrs with frequent renewal of the alkali, until no more fumes of HBr were given off. The yield was 97 %, m.p. 55-57 °C (Lit: 70-98 %, 55-74 °C).

The thiazole-4-carboxylic acid was then prepared using a modification of the procedure described in Ref [186, 187].

To a stirred solution of 7.75 g (172 mmol) of formamide in 250 ml of THF (or 200 ml dioxan), which was cooled to 0 °C, was added all at once 13.2 g (30 mmol) of solid P_4S_{10}. After this addition, the ice bath was removed and the reaction was stirred at 30 °C (refluxed) for 3 hrs. The resultant mixture was cooled to room temperature, filtered and added to a solution of 2.7 g (16.2 mmol) of 3-brompyruvic acid in some THF (or dioxane). The mixture

was then heated to 40-50 °C (50-60 °C) for 3 hrs and a precipitate started to appear. After cooling, the precipitate was filtered off, dissolved in some water with concentrated H_2SO_4 and the pH adjusted to pH 2-3 with NH_4OH, and the product precipitated as a white solid in the refrigerator. Yields were normally about 22 % (up to 56 %), m.p. 193-195 °C (Lit: 27 %, m.p. 195-197°). ^{1}H-NMR (500 Mhz, d_6-DMSO, ppm): 8.53 (1H, s), 9.17 (1H, s).

Pyrazine-2,3-diamine[188-190].

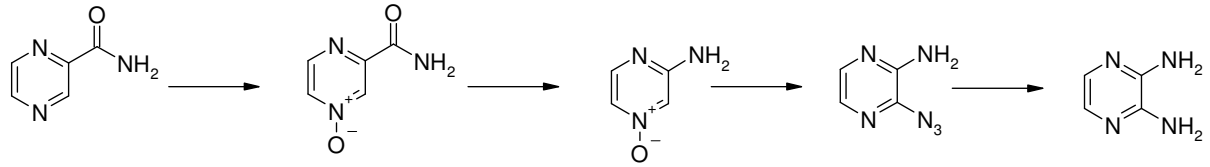

Fig. 7-2 Reaction scheme for the preparation of Pyrazine-2,3-diamine

A solution of pyrazinecarboxamide (24.6 g, 0.20 mol) in 90 % formic acid (100 ml) and 30 % hydrogen peroxide (62.5 ml) was stirred and heated. The temperature was kept between 40-50 °C for 4 hrs and then at 40 °C for 1 hr. A colourless solid started to separate from the solution after heating for approximately 10 minutes. The mixture was refrigerated overnight, then filtered, washed with water and dried to give 59 %, m.p. 303-306 °C (Lit: 66 %, m.p. 303-306 °C) of the N-oxide. This material was used directly in successive transformation without further purification.

Sodium hypochlorite solution (4.0 mmol/ml available chlorine) was added dropwise to a stirred solution of sodium hydroxide (8.08 g, 0.20 mmoles) in water (125 ml) at room temperature. The amide (6.956 g, 0.050 mmol) was added in one portion to the above solution, and the resulting mixture was heated at 70 °C with stirring for 1 hour. During this period, the amide dissolved. After cooling below 20 °C, the solution was acidified to pH 0 with concentrated hydrochloric acid and then again basified at pH 9-10 with 2 N NaOH. The mixture was evaporated to dryness *in vacuo*, and the residue was powdered and extracted with chloroform by a Soxhlet extractor for 24 hrs to give 70 %, m.p. 175-177 °C (Lit: 78 %, m.p. 177-178 °C) of 3-aminopyrazine-1-oxide.

To 1 mmol of the oxide, which was stirred under nitrogen, MeCN (8 cm^3), trimethylsilyl azide (0.17 cm^3, 1.2 mmol) and finally diethylcarbamoylchloride (0.16 cm^3, 1.2 mmol) were added *via* syringe. The mixture was stirring under reflux for 18 hrs and then evaporated under

reduced pressure. The residue was subjected to chromatography on silica gel eluting with hexane-EtOAc (10:1 to 3:1) and gave 92 %, m.p. 228 °C (decomp) (Lit: 99 %, m.p. 225 °C (decomp)) of 2-amino-3-azidopyrazine.

A mixture of the azidopyrazine (1 mmol) and tin(II) chloride dihydrate (1.128 g, 5 mmol) in 12 N HCl (3.0 ml) and MeOH (3.0 ml) was stirred and heated at 60 °C until the starting material was completely consumed. After cooling to room temperature., the solution was basified with solid Na_2CO_3 to pH 8-9 and then evaporated to dryness *in vacuo*. The residue was extracted with EtOAc while hot, or by Soxhlet apparatus, and the extract was dried ($MgSO_4$). Evaporation and chromatography on silica gel gave 2,3-diaminopyrazine, 14 %, m.p. 191-193 °C (Lit: 87 %, m.p. 207-209 °C). The low yield in the last step can be explained by a prolonged allowed reaction time or a higher reaction temperature what can lead to the forming of 3-amino-2(1H)-pyrazinone. The diamine was used without further purification.

7.1.2.3 General Procedures and Analytical Data

Procedure A: Preparation of chloro- and methyl-substitued phenyloxiranes[191, 192] **RS 1, RS 2, RS 3, RS 4, RS 5, RS 6:**

3-Chloroperbenzoic acid (3.71 g of 57 % mCPBA, 9.8 mmol) was added portionwise over a 15-min period to a cold (ice bath) stirring solution of a suitable substituted styrene (1.5 g, 8.2 mmol) in CH_2Cl_2 (50 ml). The reaction mixture was gradually warmed to room temperature and allowed to stir for 1 h, at which time it was diluted with CCl_4 (50 ml), and the precipitated 3-chlorobenzoic acid was removed by suction filtration. The filtrate was washed with a 1:1 mixture of 5 % aqueous $NaHCO_3$ and 5 % aqueous $NaHSO_3$ (3x25 ml). the aqueous layer was subsequently extracted with CCl_4 (2x100 ml), the combined organic extracts were dried over anhydrous Na_2SO_4 and concentrated under reduced pressure to yield the epoxide as a colorless liquid.

RS 1**: Procedure A**

2-(2-Chloro-phenyl)-oxirane: yield 64 %, 86 °C (13 mbar) (Lit 41 °C (0.2 torr). C_8H_7ClO (154.60). ^{1}H-NMR (500 Mhz, $CDCl_3$, ppm): 2.66 (1H, dd, J=5.4, 2.5 Hz), 3.18 (1H, dd, J=5.7, 4.1 Hz), 4.21 (1H, dd, J=4.1, 2.5 Hz), 7.20-7.26 (3H, m), 7.33-7.36 (1H, m)

RS 2**: Procedure A**

2-(3-Chloro-phenyl)-oxirane: yield 60 %, 96 °C (13 mbar). C_8H_7ClO (154.60). ^{1}H-NMR (500 Mhz, $CDCl_3$, ppm): 2.75 (1H, dd, J=5.4, 2.6 Hz), 3.14 (1H, dd, J=5.3, 4.1 Hz), 3.83 (1H, dd, J=4.1, 2.6 Hz), 7.15-7.19 (1H, m), 7.25-7.28 (3H, m)

RS 3**: Procedure A**

2-(4-Chloro-phenyl)-oxirane: yield 66 %, 97 °C (13 mbar). C_8H_7ClO (154.60). ^{1}H-NMR (500 Mhz, $CDCl_3$, ppm): 2.74 (1H, dd, J=5.4, 2.5 Hz), 3.13 (1H, dd, J=5.4, 4.1 Hz), 3.82 (1H, dd, J=3.8, 2.8 Hz), 7.19-7.21 (2H, m), 7.29-7.32 (2H, m)

RS 4**: Procedure A**

2-o-Tolyl-oxirane: yield 65 %, 80 °C (13 mbar). $C_9H_{10}O$ (134.18). ^{1}H-NMR (500 Mhz, $CDCl_3$, ppm): 2.41 (3H, s), 2.68 (1H, dd, J=5.7, 2.8 Hz), 3.14 (1H, dd, J=5.7, 4.1 Hz), 3.99 (1H, dd, J=4.1, 2.5 Hz), 7.13-7.21 (4H, m)

RS 5**: Procedure A**

2-m-Tolyl-oxirane: yield 68 %, 81 °C (13 mbar). $C_9H_{10}O$ (134.18). ^{1}H-NMR (500 Mhz, $CDCl_3$, ppm): 2.34 (3H, s), 2.68 (1H, dd, J=5.7, 2.8 Hz), 3.12 (1H, dd, J=5.7, 4.4 Hz), 3.82 (1H, dd, J=4.1, 2.8 Hz), 7.07-7.12 (3H, m), 7.21-7.24 (1H, m)

RS 6**: Procedure A**

2-p-Tolyl-oxirane: yield 39 %, 83 °C (13 mbar). $C_9H_{10}O$ (134.18). ^{1}H-NMR (500 Mhz, $CDCl_3$, ppm): 2.33 (3H, s), 2.78 (1H, dd, J=5.7, 2.8 Hz), 3.11 (1H, dd, J=5.7, 4.1 Hz), 3.81 (1H, dd, J=4.1, 2.8 Hz), 7.07-7.12 (3H, m), 7.08-7.27 (4H, m)

Procedure B: Preparation of methoxy- and nitro-substitued phenyloxiranes[193-198], **RS 7**, **RS 8**, **RS 9**, **RS 10**:

The literature procedures differ in the reaction conditions such as time, temperature and ratio of reactants. After trying several different conditions, the following procedure was used: In a three-neck flask with reflux condenser and under nitrogen 10 mmol Trimethylsulfoniumjodide (TMSJ), 20 mmol KOH, 2.5 mmol water and 10 ml acetonitril were heated for 30 min at 60 °C and stirred vigorously. Then 10 mmol aldehyd dissolved in 10 ml acetonitril were added dropwise and heating was continued for an additional 3 hrs. After cooling the solid phase (KI, KOH) was separated and the solution was narrowed *in vacuo*. The residue was diluted with absolute ether and more KI precipitated. This procedure was repeated until no more KI precipitated. The filtrate was then dried over sodium sulfate and the solvent evaporated. The residue was distilled (or recrystallized). It is crucial that the KOH is powdered; the reaction did not work with pastilles as for example described in Ref.[198].

RS 7**: Procedure B**

2-(2-Methoxy-phenyl)-oxirane: yield 47 %, 102 °C (18 mbar). $C_9H_{10}O_2$ (150.18). ^{1}H-NMR (500 Mhz, $CDCl_3$, ppm): 2.70 (1H, dd, J=5.7, 2.5 Hz), 3.13 (1H, dd, J=5.7, 4.1 Hz), 3.86 (3H, s), 4.20 (1H, dd, J=4.1, 2.8 Hz), 6.86-6.95 (2H, m), 7.13-7.15 (1H, m), 7.23-7.27 (1H, m)

RS 8**: Procedure B**

2-(3-Methoxy-phenyl)-oxirane: yield 36 %, 112 °C (13 mbar). $C_9H_{10}O_2$ (150.18). ^{1}H-NMR (500 Mhz, $CDCl_3$, ppm): 2.76 (1H, dd, J=5.4, 2.5 Hz), 3.11 (1H, dd, J=5.4, 4.1 Hz), 3.79 (3H, s), 3.83 (1H, dd, J=4.1, 2.5 Hz), 6.80-6.89 (3H, m), 7.25 (1H, t, J=7.9 Hz)

RS 9**: Procedure B**

2-(4-Methoxy-phenyl)-oxirane: yield 29 %, 112 °C (13 mbar). $C_9H_{10}O_2$ (150.18). ^{1}H-NMR (500 Mhz, $CDCl_3$, ppm): 2.80 (1H, dd, J=5.4, 2.5 Hz), 3.11 (1H, dd, J=5.4, 4.1 Hz), 3.80 (3H, s), 3.81 (1H, dd, J=4.1, 2.5 Hz), 6.86-6.89 (2H, m), 7.18-7.21 (2H, m)

RS 10**: Procedure B**

2-(2-Nitro-phenyl)-oxirane: yield 77 %, m.p. 65 °C. $C_8H_7NO_3$ (165.15). ^{1}H-NMR (500 Mhz, $CDCl_3$, ppm): 2.67 (1H, dd, J=5.7, 2.5 Hz), 3.30 (1H, dd, J=5.4, 4.4 Hz), 4.48 (1H, dd, J=4.4, 2.8 Hz), 7.46-7.50 (1H, m), 7.60-7.68 (2H, m), 8.14-8.16 (1H, dd, J=8.2, 0.9 Hz)

Procedure C: Preparation[199-202] of **RS 11** and **RS 12**:

To a solution of 50 mmol aldehyde in 250 ml CH_2Cl_2 were added 0.4 mmol TBAJ, 80 mmol TMSJ and 50 ml of 50 % NaOH. The mixture was heated under reflux for 24 hrs and after cooling added to 1 l of ice-water. The organic phase was separated, the water phase extracted with CH_2Cl_2 and the combined organic extracts were dried over sodium sulfate and the solvent evaporated. The product was then purified over silica gel (Ether-petrolether 1:1 for 2-(3-Nitro-phenyl)-oxirane) or recrystallized from MeOH (for 2-(4-Nitro-phenyl)-oxirane).

RS 11**: Procedure C**

2-(3-Nitro-phenyl)-oxirane: yield 74 %, oil. $C_8H_7NO_3$ (165.15). ^{1}H-NMR (500 Mhz, $CDCl_3$, ppm): 2.81 (1H, dd, J=5.4, 2.5 Hz), 3.23 (1H, dd, J=5.4, 4.1 Hz), 3.98 (1H, dd, J=4.1, 2.5 Hz), 7.52-7.54 (2H, m), 8.13-8.17 (2H, m)

RS 12**: Procedure C**

2-(4-Nitro-phenyl)-oxirane: yield 57 %, m.p. 84 °C (Lit. 67 %, 84-85 °C). $C_8H_7NO_3$ (165.15). ^{1}H-NMR (500 Mhz, $CDCl_3$, ppm): 2.78 (1H, dd, J=5.7, 2.5 Hz), 3.23 (1H, dd, J=5.7, 4.1 Hz), 3.97 (1H, dd, J=4.1, 2.5 Hz), 7.44-7.47 (2H, m), 8.19-8.22 (2H, m)

Procedure D: Preparation[203] of **RS 13**:

In a three-neck flask with reflux condenser, $CaCl_2$-tube, dropping funnel and stirrer, 300 ml of absolute ethanol and 6.99 g of natrium were given. After complete solution of the natrium, a mixture of each 0.3 mol of dry starting materials was added dropwise while cooling with ice. For the synthesis of glycid esters, a mixture of 0.2 mol benzaldehyde and 0.3 mol of chloro acetic acid ethyl ester was used at -10 °C. The mixture was left overnight at room temperature and then neutralized with acetic acid and added to 1 l of ice water. The mixture was extracted with ether several times and the combined organic extracts were washed well with water and dried over sodium sulfate. After evaporation of the solvent, the residue was purified by distillation.

RS 13**: Procedure D**

3-Phenyloxirane-2-carboxylic acid-methyl ester: yield 85 %, 130 °C (7 mbar) (Lit. 90 %, 130 °C (7 mbar)). $C_{10}H_{10}O_3$ (178.19). ^{1}H-NMR (500 Mhz, d_6-DMSO, ppm): 3.51 (1H, d, J=1.9 Hz), 3.82 (3H, s), 4.1 (1H, d, J=1.6 Hz), 7.26-7.41 (5H, m)

Procedure E: Preparation of the oxirane-carbonitriles[204, 205], **RS 14** and **RS 15**:

15.1 g of chloro acetonitrile (0.2 mol) were added slowly to a vigorously stirred mixture of an aldehyde or a ketone (23.3 g benzaldehyde, 0.22 mol), 40 ml of a 50 % NaOH, 50 ml dichloromethane and 1 g of triethylbenzylammoniumchloride at 15-20 °C. Stirring was continued for another 40 min at this temperature. Then, the mixture was diluted with 30 ml of water and the organic phase was separated. It was washed two times with water, dried over sodium sulfate and distilled. When using ketones it is better to leave out the dichloromethane and add 80 ml of ether instead after the reaction.

RS 14**: Procedure E**

3-Phenyl-oxirane-2-carbonitrile: yield 51 %, 100-104 °C (13 mbar) (Lit. 50 %, 104-108 °C (19 mbar) and 79 %, 87 ° (5 mm)). C_9H_7NO (145.16). ^{1}H-NMR (500 Mhz, $CDCl_3$, ppm): 3.95 (1H, d, J=1.89 Hz), 3.76 (1H, d, J=3.47 Hz), 4.23 (1H, d, J=3.78 Hz), 4.27 (1H, d, J=1.89 Hz), 7.24-7.27 (1H, m), 7.37-7.44 (4H, m)

RS 15**: Procedure E**

1-Oxa-spiro-[2.5]octane-2-carbonitrile: yield 59 %, 128-134 °C (13 mbar) (Lit. 45 %, 130-135 °C (19 mbar) and 75 %, 120 °C (6 mm)). $C_8H_{11}NO$ (137.18). ^{1}H-NMR (500 Mhz, $CDCl_3$, ppm): 1.48-1.85 (10 H, m), 3.22 (1H, s)

Procedure F: Preparation of **RS 16**

The epoxide RS 16 was synthesized according to the following sequence starting with cyclohexanone via the intermediates RS 70 to RS 73.

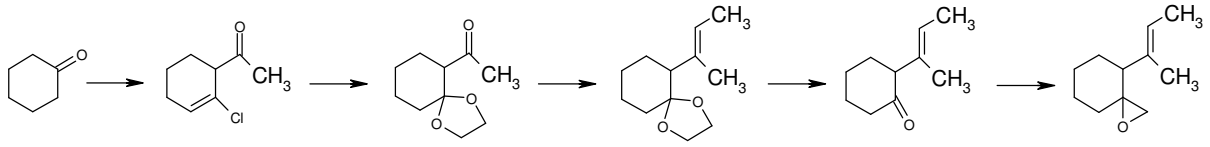

RS 70 RS 71 RS 72 RS 73 **RS 16**

Fig. 7-3 Reaction scheme for the preparation of RS 16

Procedure F-1: 1-(2-Chloro-cyclohex-2-enyl)-ethanone[206], RS 70:

Into a three-neck flask provided with a stirrer, a reflux codenser protected from atmospheric moisture, and a dropping funnel, 120 g of aluminium chloride and 150 ml of dry dichloroethane were put. A mixture of 36.5 g of cyclohexanone and 86 g of acetyl chloride was added with vigorous stirring and cooling by water at room temperature; the mixture was stirred for 18 hours and then decomposed with ice to which 15 ml of concentrated HCl had been added. The organic layer was separated, and the water layer was extracted three times with dichloroethane. The combined extracts were washed with water and dried over calcium chloride. The solvent was driven off in a slight vacuum and the residue distilled, the fraction with b.p. 105-120 °C (20 mm) being collected. After redistillation there was obtained 49.5 g (82 %) of a substance with b.p. 124-129 (30 mm). A third distillation yielded the product.

Procedure F-2: 1-(1,4-Dioxa-spiro[4.5]dec-6-yl)-ethanone[206], RS 71:

Into a three-neck flask provided with a stirrer, a dropping funnel, and a reflux condenser with a tube containing soda-lime, a solution of 7.2 g potassium hydroxide in 50 ml of glycole was put. 60 ml of dioxane was added and the mixture heated to boiling. Then 19.7 g of acetyl-2-chloro-cyclohexene-2 was added dropwise with vigorous stirring, and the mixture was boiled and stirred for 5 hrs. The cooled reaction mixture was poured into water and extracted four times with ether, the extracts dried with magnesium sulfate, and the solvent distilled off. Fractionation of the residue *in vacuo* and redistillation yielded the product.

Procedure F-3: 6-((E)-1-Methyl-propenyl)-1,4-dioxa-spiro[4.5]decane[207], RS 72

Ethyltriphenylphosphoniumbromid (74.2) g in dry DMSO (150 ml) was added to a solution of methylsulfinylmethanide [from NaH (4.8 g) and anhydrous DMSO (40 ml)] and to the

resulting red solution the ketone (6-acetyl-1,4-dioxaspiro[4,5]decane (18.4 g; 100 mmol)) in dry DMSO/THF (1:1, 25 ml) was added over 0.5 hr. The mixture was stirred at 50 °C overnight, diluted with water (500 ml) and extracted with hexane (3x300 ml). The combined extracts were washed with water, dried and evaporated o give a residue which on distillation yielded the alkene as a colourless liquid.

Procedure F-4: 2-((E)-1-Methyl-propenyl)-cyclohexanone[207], RS 73:

The cyclic acetal RS 72 (14.5 g) in acetone (60 ml) was stirred with toluene-4-sulfonic acid (0.5 g) and water (2ml) for 5 hrs, after which time the product was isolated. Distillation gave the ketone as a colourless liquid.

Procedure F-5: 4-((E)-1-Methyl-propenyl)-1-oxa-spiro[2.5]octane[207], **RS 16**:

A solution of the ketone RS 73 (10.0 g) in dry DMSO/THF (1:1, 40 ml) was added to dimethylsulfoxonium methanide [from NaH (1.68 g), TMSI (15.4 g) and anhydrous DMSO (40 ml] during 10 min. After stirring at 50 °C for an additional 1.5 hrs the product was isolated. Fractionation of the crude extract on a 25-cm spinning-band column gave starting material and the spiro epoxide as a colourless liquid.

RS 16**: Procedure F-1**

4-((E)-1-Methyl-propenyl)-1-oxa-spiro[2.5]octane: yield 61%, b.p. 80 °C (12 mbar), n_D^{20} 1.4790 (Lit. 85 %, n_D^{20} 1.4801). $C_{11}H_{18}O$ (166.27). ^{1}H-NMR (500 Mhz, $CDCl_3$, ppm): 1.60 (3H, d, J=6.0 Hz), 1.67 (3H, s), 2.34, 2.43, 2.6 and 2.9 (2H, q, J=5.5 Hz), 5.45 (3H, q, J=6.0 Hz)

RS 70**: Procedure F-2**

1-(2-Chloro-cyclohex-2-enyl)-ethanone: yield 78 % resp. 69%, b.p. 105 °C (27 mbar), n_D^{20} 1.4960 resp. 1.4969 (Lit. 82 %, b.p. 108-109° (15 mm), nD_{20} 1.4985; other Lit. data (Patent): b.p. 93-98° (9 mm), n_D^{20}=1.4952). $C_8H_{11}ClO$ (158.63).

RS 71**: Procedure F-3**

1-(1,4-Dioxa-spiro[4.5]dec-6-yl)-ethanone: yield 68 %, b.p. 121-123 °C (13 mbar), n_D^{20} 1.4788 (Lit. 61 %, b.p. 121-122 °C (10 mm), n_D^{20} 1.4781). $C_{10}H_{16}O_3$ (158.63).

RS 72**: Procedure F-4**

6-((E)-1-Methyl-propenyl)-1,4-dioxa-spiro[4.5]decane: yield 54 %, b.p. 101 °C (12 mbar), n_D^{20} 1.4827 (Lit. 77 %, b.p. 96-98 °C (7.5 mm), n_D^{20} 1.4805). $C_{12}H_{10}O_2$ (196.29). ^{1}H-NMR (500 Mhz, $CDCl_3$, ppm): 1.59 (3H, d, J=5.5 Hz), 1.69 (3H, s), 2.66 (1H, dd, J=12.5, 4.0 Hz), 3.81 (4H, s), 5.25 (1H, q, J=5.5 Hz)

RS 73**: Procedure F-5**

2-((E)-1-Methyl-propenyl)-cyclohexanone: yield 87 %, b.p. 90 °C (11 mbar), n_D^{20} 1.4840 (Lit. 89 %, b.p. 59-60 °C (1.25 mm), n_D^{20} 1.4805). $C_{10}H_{16}O$ (152.24). ^{1}H-NMR (500 Mhz, $CDCl_3$, ppm): 1.62 (3H, d, J=6.0 Hz), 1.68 (3H, s), 3.34 (1H, m), 5.38 (1H, q, J=6.0 Hz)

Procedure G: Procedure[208] for the synthesis of **RS 74**:

To a solution of benzoyl chloride (7.73 g, 55 mmol) in ether (50 ml) were added successively an appropriate allylic alcohol (50 mmol) and triethylamine (55 mmol) at 0 °C under N_2. After stirring at 0 °C for 2 hrs and then at room temperature overnight, the mixture was diluted with EtOAc and washed successively with 2 HCl (2x10 ml), saturated $NaHCO_3$ and brine. The organic layer was dried ($MgSO_4$) and concentrated, and the residue was distilled under reduced pressure.

RS 74**: Procedure G**

Benzoic acid 3-methyl-but-2-enylester: yield 81 %, b.p. 123-126 °C (13 mbar) (Lit: 84 %, 82 °C (0.01 mm Hg)). $C_{12}H_{14}O_2$ (190.24). ^{1}H-NMR (500 Mhz, $CDCl_3$, ppm): 1.78 (6H, d, J=7.9 Hz), 4.82 (2H, d, J=7.3 Hz), 5.45-5.49 (1H, m), 7.42 (2H, t, J=7.9 Hz), 7.53 (1H, t, J=7.6 Hz), 8.04 (2H, dd, J=8.5, 1.3 Hz)

Procedure H: General procedure for the preparation of -ester and –amide-derivatives[209] of quinoline, **RS 28** - **RS 33** and compound **RS 75**:

25 mmol of an appropriate amine or alcohol, pyridine (44 mmol) and an appropriate carboxylic acid chloride or sulfonic acid chloride (26 mmol) were heated on a steam-bath for 2 hrs, then poured into water and the product was collected and recrystallized or purified by chromatography over silica gel.

RS 75**: Procedure H**

4-Methyl-N-pyridin-3-yl-benzenesulfonamide: yield 82 %, m.p. 190 °C, recrystallized from EtOH (Lit. 191-192 °C). $C_{12}H_{12}N_2O_2S$ (248.31). ^{1}H-NMR (500 Mhz, d_6-DMSO, ppm): 2.33 (3H, s), 7.27 (1H, ddd, J=8.2, 4.7, 2.6 Hz), 7.35 (2H, d, J=7.9 Hz), 7.49 (1H, ddd, J=8.5, 2.8, 1.6 Hz), 7.65 (2H, d, J=8.2 Hz), 8.24 (1H, d, J=4.7, 1.6 Hz), 8.27 (1H, d, J=2.8 Hz), 10.48 (1H, br. s)

RS 28**: Procedure H**

Benzoic acid-quinolin-8-yl-ester: yield 89 %, m.p. 121-123 °C, recrystallized from EtOH (Lit. 118-126 °C). $C_{16}H_{11}NO_2$ (249.27). ^{1}H-NMR (500 Mhz, $CDCl_3$, ppm): 7.46 (1H, dd, J=8.5, 4.4 Hz), 7.55 (2H, t, J=7.9 Hz), 7.59-7.62 (2H, m), 7.66 (1H, tt, J=7.6, 1.3 Hz), 7.76-7.80 (1H, m), 8.25 (1H, dd, J=8.2, 1.6 Hz), 8.37 (2H, dd, J=8.5, 1.3 Hz), 8.93 (1H, dd, J=4.4, 1.6 Hz)

RS 29**: Procedure H**

N-Quinolin-8-yl-benzamide: yield 71 %, m.p. 91-92 °C, purified over silica gel (EtOAc-Hexan 1+2) (Lit. 90-93 °C). $C_{16}H_{11}N_2O$ (248.29). ^{1}H-NMR (500 Mhz, $CDCl_3$, ppm): 7.48 (1H, dd, J=8.2, 4.1 Hz), 7.53-7.62 (5H, m), 8.10 (2H, dd, J=7.9, 1.3 Hz), 8.20 (1H, d, J=8.2 Hz), 8.85 (1H, dd, J=4.1, 1.3 Hz), 8.95 (1H, dd, J=7.6, 1.3 Hz), 10.75 (1H, br. s)

RS 30**: Procedure H**

N-Quinolin-8-yl-benzenesulfonamide: yield 77 %, m.p. 128-132 °C (Lit 133-135 °C), recrystallized from ethanol. $C_{15}H_{12}N_2O_2S$ (284.34).^{1}H-NMR (500 Mhz, $CDCl_3$, ppm): 7.36 (2H, t, J=7.9 Hz), 7.41-7.49 (4H, m), 7.86 (1H, dd, J=6.6, 1.9 Hz), 7.90-7.93 (2H, m), 8.13 (1H, dd, J=8.2, 1.6 Hz), 8.76 (1H, dd, J=4.1, 1.6 Hz), 9.33 (1H, br. s)

RS 31**: Procedure H**

Benzenesulfonic acid quinolin-8-yl ester: yield 94 %, m.p. 111-112 °C, recrystallized from EtOH (Lit. 111 °C). $C_{15}H_{11}NO_3S$ (285.32).^{1}H-NMR (500 Mhz, $CDCl_3$, ppm): 7.43-7.49 (3H, m), 7.55 (1H, t, J=7.9 Hz), 7.60 (1H, td, J=7.5, 1.3 Hz), 7.68 (1H, d, J=7.6 Hz), 7.78 (1H, d, J=8.2 Hz), 8.03 (2H, d, J=8.2 Hz), 8.21 (1H, d, J=8.5 Hz),8.86 (1H, t, J=1.9 Hz)

RS 32**: Procedure H**

Toluene-4-sulfonic acid quinolin-8-yl ester: yield 80 %, m.p. 117-118 °C (Lit 115-117 °C), recrystallized from EtOH. $C_{16}H_{13}NO_3S$ (299.35). ^{1}H-NMR (500 Mhz, d_6-DMSO, ppm): 2.38 (3H, s), 7.40 (2H, d, J=8.2 Hz), 7.49 (1H, dd, J=7.6, 1.3 Hz), 7.55-7.63 (2H, m), 7.81 (2H, d, J=8.5 Hz), 7.95 (1H, dd, J=8.5, 1.3 Hz), 8.40 (1H, dd, J=8.2, 1.6 Hz), 8.83 (1H, dd, J=4.1, 1.9 Hz)

RS 33**: Procedure H**

Pyridine-2-sulfonic acid quinolin-8-yl ester: yield 26 %, m.p. 112-115 °C, purified over silica gel (EtOAc-Hexan 1+1,5). $C_{14}H_{10}N_2O_3S$ (286.31). ^{1}H-NMR (500 Mhz, d_6-DMSO, ppm): 7.55-7.57 (2H, m), 7.62 (1H, t, J=7.9 Hz), 7.79-7.81 (1H, m), 7.98 (1H, dd, J=8.2, 0.9 Hz), 8.09 (1H, dt, J=7.6, 1.3 Hz), 8.14 (1H, td, J=7.9, 1.9 Hz), 8.42 (1H, dd, J=8.2, 1.6 Hz), 8.71 (1H, dd, J=4.1, 1.9 Hz), 8.75 (1H, ddd, J=4.7, 1.6, 0.9 Hz)

Procedure I: Procedure[210] for the preparation of **RS 26** and **RS 27**:

A solution of a suitably protected amino acid (1 mmol) in methylene chloride/DMF (10 ml) was stirred with cyanoethanol (2 mmol) in the presence of a catalytic amount of DMAP. A solution of DCC (1.1 mmol) in methylene chloride was added dropwise. The reaction was

stirred at room temperature overnight. At the end of the reaction, after filtering DCU, the solvent was removed under reduced pressure. The residual mass was dissolved in EtOAc and succesively washed with 5 % aq. $NaHCO_3$, water, 5 % citric acid and brine. The organic layer was dried over Na_2SO_4 and concentrated. The crude product was purified by flash chromatography (EtOAc-Hexan 1+3.5 to EtOAc-Hexan 2+1 to EtOAc to MeOH).

To 1.0 g (3.3 mmol) of a Boc-protected amino acid (derivative), for example **RS 26**, 25 ml 1 M HCl in ether (25 mmol) were added. After 1 h, another 25 ml of absolute ether were added and the mixture put in the freezer over night. Then, the solvent was evaporated and the residue was recrystallized from THF-ether.

RS 26**: Procedure I**

2-Amino-4-methylsulfanyl-butyric acid 2-cyano-ethyl ester hydrochloride: yield 12 %, m.p. 125-127 °C. $C_8H_{14}N_2O_2S \cdot HCl$ (202.28·36.46). ^{1}H-NMR (500 Mhz, d_6-DMSO, ppm): 2.06 (3H, s), 2.07-2.13 (2H, m), 2.56-2.70 (2H, s), 2.97 (2H, t, J=6.0 Hz), 4.16 (1H, t, J=6.3 Hz), 4.30-4.34 (1H, m), 4.39-4.43 (1H, m), 8.66 (3H, br. s). MS: 202.96 m/z $(M+H)^+$. IR (ZnSe-ATR-FTIR): ν = 3211, 2817 (br), 2593, 2263, 1745, 1492, 1231, 1193, 1076, 1029, 992 cm^{-1}.

RS 27**: Procedure I**

2-tert-Butoxycarbonylamino-4-methylsulfanyl-butyric acid 2-cyano-ethyl ester: yield 49 %, m.p. 56-58 °C (Lit 92 %, m.p. 57-59 °C). $C_{13}H_{22}N_2O_4S$ (302.40). ^{1}H-NMR (500 Mhz, $CDCl_3$, ppm): 1.49 (9H, s), 1.93-2.01 (1H, m), 2.11 (3H, s), 2.17 (1H, s), 2.55-2.62 (2H, m), 2.75 (2H, t, J=6.3 Hz), 4.32-4.41 (2H, m), 4.46 (1H, br. s), 5.13 (1H, br. s)

Procedure J: General procedure for the preparation of carboxylic acid amides[146]:

To a mixture of a suitable carboxylic acid (for example pyridine-2-carboxylic acid (1.23 g, 10 mmol)), thiazol-2-ylamine (1.01 g, 10 mmol) or another suitable amine and HOBT (1.45 g, 10.75 mmol) in dry DMF (10 ml) was added DCC (2.16 g, 10.05 mmol). The reaction mixture was stirred at room temperature for 24 hrs. The reaction mixture was then diluted with 50 ml of EtOAc and 20 ml of H_2O. The aqueous phase was extracted with EtOAc and the combined organic phases were then washed with 10 % HCl (and/or $NaHCO_3$ if needed), water and brine. The organic phases were dried over sodium sulfate, filtered and the solvent evaporated *in vacuo*. The residue was then chromatographed (3:1 petrolether-EtOAc) to yield the product.

RS 17**: Procedure J**

Pyridine-2-carboxylic acid thiazol-2-ylamide[146]: yield 47 %, m.p. 146-148 °C. $C_9H_7N_3OS$ (205.24). ^{1}H-NMR (500 Mhz, d_6-DMSO, ppm): 7.36 (1H, d, J=3.5 Hz), 7.58 (1H, d, J=3.5 Hz), 7.72-7.75 (1H, m), 8.11 (1H, td, J=7.9, 1.9 Hz), 8.19 (1H, dt, J=7.9, 1.2 Hz), 8.76-8.78 (1H, m), 11.98 (1H, br. s). MS: 205.91 m/z $(M+H)^+$

RS 18**: Procedure J**

Pyridine-2-carboxylic acid (5-methyl-isoxazol-3-yl)-amide: yield 69 %, m.p. 125-128 °C. $C_{10}H_9N_3O_2$ (203.20). ^{1}H-NMR (500 Mhz, d_6-DMSO, ppm): 2.42 (3H, s), 6.75 (1H, s), 7.70 (1H, ddd, J=7.5, 4.7, 1.3 Hz), 8.07 (1H, td, J=7.7, 1.9 Hz), 8.14 (1H, dt, J=7.9, 0.9 Hz), 8.73 (1H, ddd, J=4.7, 1.5, 0.9 Hz), 11.0 (1H, s); MS: 204.6 m/z $(M+H)^+$. IR (ZnSe-ATR-FTIR): ν = 3206, 2927, 1730, 1688, 1606, 1523, 1466, 1441, 1416, 1266, 1016, 891, 797, 738, 698, 683, 618 cm^{-1}.

RS 23**: Procedure J**

Pyridine-2-carboxylic acid 2-cyano-ethyl ester: yield 4 %, oil, purified twice over silica gel (gradient from hexane-ethylacetate 2:1 to ethylacetate to methanol). $C_9H_8N_2O_2$ (176.18). ^{1}H-NMR (500 Mhz, d_6-DMSO, ppm): 2.92 (2H, q, J=6.6 Hz), 4.64 (2H, t, J=6.6 Hz), 7.54-7.56 (1H, m), 7.91 (1H, td, J=7.6, 1.9 Hz), 8.17 (1H, dt, J=7.9, 1.2 Hz), 8.79-8.81 (1H, m). MS: 177.6 m/z $(M+H)^+$. IR (ZnSe-ATR-FTIR): ν = 2968, 2254, 1725, 1585, 1438, 1305, 1244, 1127, 1089, 1046, 993, 822, 747, 705, 620 cm^{-1}.

RS 25**: Procedure J**

4-Nitro-N-thiazol-2-yl-benzamide: yield 11 %, m.p. 287-290 °C, recrystallized from methanol (Lit. 278-297 °C). $C_{10}H_7N_3O_3S$ (249.25). ^{1}H-NMR (500 Mhz, d6-DMSO, ppm): 7.32 (1H, d, J=3.5), 7.59 (1H, d, J=3.8 Hz), 8.29-8.38 (4H, m), 13.02 (1H, br. s). MS: 249.94 m/z $(M+H)^+$

Procedure K: Preparation[211] of **RS 19**:

A solution of 4 mmol amine and 4.8 mmol of pyridine-2-sulfonyl chloride (0.853 g) in a 1:1 mixture of ether (8ml) and 4 M K_2CO_3 (8ml) was stirred vigorously for 1-6 hrs at 0 °C. The aqueous phase was extracted with dichloromethane (2x20 ml), dried (Na_2SO_4), and evaporated to dryness. The residue was then dissolved in aqueous NaOH and precipitated again with HCl.

RS 19 **: Procedure K**

Pyridine-2-sulfonic acid thiazol-2-ylamide yield 22 %, m.p. 183-185 °C (decomp.). $C_8H_7N_3O_2S_2$ (241.29). ^{1}H-NMR (500 Mhz, d_6-DMSO, ppm): 6.87 (1H, d, J=4.7 Hz), 7.27 (1H, d, J=4.9 Hz), 7.60 (1H, ddd, J=7.6, 4.7, 1.3 Hz), 7.93 (1H, dt, J=7.9, 0.9 Hz), 8.03 (1H, td, J=7.9, 1.9 Hz), 8.64 (1H, ddd, J=4.7, 1.9, 0.9 Hz), 12.87 (1H, br. s). MS: 242.5 m/z $(M+H)^+$. IR (ZnSe-ATR-FTIR): ν = 2792 (br), 1572, 1523, 1426, 1300, 1163, 1113, 1083, 1003, 935, 856, 772, 738, 650, 612, 592, 554 cm^{-1}.

Procedure L: Preparation[212] of **RS 20**:

In a 10 ml-flask, isoxazol-2-ylamine (1.0 g, 10.2 mmol) was dissolved in 4 g of anhydrous pyridine and 2-Pyridine-sulfonic acid chloride (3.0 g, 16.8 mmol) was added with stirring. Solution takes place with evolution of heat and the reaction was completed by warming at 60 °C for one-half to one hour. The crude derivative obtained by pouring the dark solution into ice-water was dissolved in one equivalent of aqueous sodium hydroxide, decolorized, and reprecipitated by addition of hydrochloric acid. The product can be recrystallized from hexane/EtOAc.

RS 20**: Procedure L**

Pyridine-2-sulfonic acid (5-methyl-isoxazol-3-yl)-amide: yield 91 %, m.p. 155-158 °C. $C_9H_9N_3O_3S$ (239.25). ^{1}H-NMR (500 Mhz, d_6-DMSO, ppm): 2.29 (3H, d, J=0.9 Hz), 6.12 (1H, s), 7.69 (1H, ddd, J=7.6, 4.4, 0.9 Hz), 8.04 (1H, dt, J=7.9, 0.9 Hz), 8.12 (1H, td, J=7.9, 1.6 Hz), 8.72 (1H, ddd, J=4.7, 1.6, 0.9 Hz), 11.67 (1H, br. s). MS: 240.5 m/z $(M+H)^+$. IR (ZnSe-ATR-FTIR): ν = 2789 (br), 1620, 1586, 1499, 1431, 1339, 1254, 1179, 1122, 1088, 1034, 1005, 927, 892, 781, 737, 692, 590, 558 cm^{-1}.

Procedure M: Preparation[213] of **RS 21**:

Amino alcohol (1 mmol) and triethylamine (2 mmol) were stirred in CH_2Cl_2 (25 ml) and cooled to 0 °C. The appropriate acid chloride (1 mmol) was added dropwise to the solution, and the mixture was stirred for 18 hrs at room temperature. Water was added, and the layers were separated. The organic layer was washed with saturated $NaHCO_3$ solution, dried, filtered, and evaporated to give the crude amide, which were purified by recrystallization from hexane/EtOAc.

RS 21**: Procedure M**

Pyridine-2-carboxylic acid cyanomethyl-amide: yield 50 %, m.p. 165-168 °C, purified twice over silica gel (EtOAc-Hexan 1:2 and 1:3) and recrystallized from EtOAc-Hexan 1:1. $C_8H_7N_3O$ (161.16). ^{1}H-NMR (500 Mhz, d_6-DMSO, ppm): 4.31 (2H, d, J=6.0 Hz), 7.65 (1H, ddd, J=7.6, 5.0, 1.6 Hz), 8.03 (1H, td, J=7.6, 1.6 Hz), 8.07 (1H, dt, J=7.9, 1.3 Hz), 8.68 (1H, d, J=4.7 Hz), 9.46 (1H, t, J=5.4 Hz). MS: 162.08 m/z $(M+H)^+$. IR (ZnSe-ATR-FTIR): ν = 3329, 2362 (w), 1666, 1507, 1467, 1431, 1291, 1160, 1002, 899, 818, 752, 661, 622, 596 cm^{-1}.

Procedure N: Preparation of pyridine-2-carboxylic acid cyano alkyl esters[214], **RS 22**, **RS 24**:

To a stirred suspension of picolinic acid (12.4 g, 100 mmol) in dry triethylamine (20 ml, 200 mmol), chloro acetonitril (15 g, 200 mmol) was slowly added with stirring. The mixture warmed up to 60 °C and solidified after some time because of separation of triethylamine-hydrochloride. Heating was continued for 1 h. Then, the solvent was evaporated and the dark solid was taken up with $CHCl_3$/water (1:1), treated with charcoal and filtered. After that, the phases could easily be separated. The water phase was saturated with K_2CO_3 and extracted with $CHCl_3$ (3x50 ml). The combined organic fractions were dried over K_2CO_3 with addition of charcoal and distillation of the brown oily residue after evaporation of the solvent yielded the product. The product was further purified by chromatography on silica gel (EtOAc).

RS 22**: Procedure N**

Pyridin-2-carboxylic acid-cyanomethyl ester: yield 57 %, light yellow oil, purified over silica gel (EtOAc) after distillation, 120 °C (0.3 mbar) (Lit 133-137 °C (0.1 torr), m. p. 42-43 °C). $C_8H_6N_2O_2$ (162.15). ^{1}H-NMR (500 Mhz, d_6-DMSO, ppm): 5.27 (2H, s), 7.70 (1H, dd, J=7.6, 4.7 Hz), 8.04 (1H, t, J=7.9 Hz), 8.11 (1H, dd, J=7.9, 0.9 Hz), 8.76 (1H, td, 4.7, 0.9 Hz). MS: 162.96 m/z $(M+H)^+$. IR (ZnSe-ATR-FTIR): ν = 3211, 2817, 2593, 1745, 1604, 1492, 1231, 1193, 1076, 1029, 992 cm^{-1}.

RS 24**: Procedure N**

Pyridin-2-carbonsäure-cyanopropyl ester: yield 76 %, oil, purified over silica gel (EtOAc) after removal of residual chlorobutyronitrile by distillation. $C_{10}H_{10}N_2O_2$ (190.20). ^{1}H-NMR (500 Mhz, d_6-DMSO, ppm): 2.05 (2H, q, J=6.6 Hz), 2.67 (2H, q, J=7.2 Hz), 4.35 (2H, t, J=6.2 Hz), 7.63-7.66 (1H, m), 8.00 (1H, td, J=7.6, 1.9 Hz), 8.11 (1H, dt, J=7.9, 1.2 Hz), 8.72-8.74 (1H, m). MS: 191.6 m/z $(M+H)^+$. IR (ZnSe-ATR-FTIR): ν = 2959, 2247, 1737, 1720, 1584, 1438, 1305, 1281, 1244, 1131, 1088, 1045, 955, 821, 747, 706, 620 cm^{-1}.

Procedure O: General Procedure for the preparation of substituted heteroaryl-benzimidazoles[215] for the compounds **RS 34**, **RS 35**, **RS 36**, **RS 37**, **RS 40**, **RS 41**, **RS 42**, **RS 47**, **RS 48**, **RS 49**, **RS 50**, **RS 51**, **RS 52**, **RS 57**, **RS 58**, **RS 59**, **RS 60**, **RS 61**, **RS 64**, **RS 65**, **RS 66** and **RS 67**:

A mixture of an appropriate derivative of o-phenylendiamine, the corresponding carboxylic acid and 5-20 equivalents of polyphoshoric acid was stirred in an oil bath at 180 °C for 2 hrs. The solution was cooled and poured in a thin stream into rapidly stirred water. The pH was adjusted to 9 with 26 % ammonium hydroxide. The solid was collected by filtration, dissolved

in hot ethanol and treated with charcoal. The ethanol was evaporated again and the residue was recrystallized unless stated otherwise.

RS 34**: Procedure O**

2-Pyridin-3-yl-1H-benzoimidazole: light purple solid, yield: 93 %, m.p. 245 °C, recrystallized twice from ethanol. $C_{12}H_9N_3$ (195.23). ^{1}H-NMR (500 Mhz, d_6-DMSO, ppm): 7.23-7.25 (2H, m), 7.59 (1H, dd, J=8.2, 4.7 Hz), 7.64 (2H, br. s), 8.50 (1H, dt, J=7.9, 1.9 Hz), 8.7 (1H, dd, J=5.0, 1.6 Hz), 9.36 (1H, d, J=2.2 Hz), 12.94 (1H, br. s). MS: 196.15 m/z $(M+H)^+$. IR (ZnSe-ATR-FTIR): ν = 3042-2795 (br), 2359, 1488, 1447, 1429, 1316, 1108, 961, 882, 769, 753, 742, 711, 699, 634, 534 cm^{-1}.

RS 35 **: Procedure O**

2-Thiophen-2-yl-1H-benzoimidazole: light brown solid, yield: 80 %, m.p. 344 °C, recrystallized from ethanol. $C_{11}H_8N_2S$ (200.26). ^{1}H-NMR (500 Mhz, d_6-DMSO, ppm): 7.17-7.21 (2H, m), 7.23 (1H, dd, J=5.0, 3.5 Hz), 7.56 (2H, s), 7.72 (1H, dd, J=5.0, 1.1 Hz), 7.84 (1H, dd, J=3.8, 1.3 Hz), 12.94 (1H, s). MS: 201.11 m/z $(M+H)^+$. IR (ZnSe-ATR-FTIR): ν = 2642 (br), 1571, 1451, 1423, 1314, 1276, 1235, 1095, 1074, 945, 852, 742, 704 cm^{-1}.

RS 36**: Procedure O**

2-Furan-2-yl-1H-benzoimidazole: light yellow needles, yield: 40 %, m.p. 286 °C, purified by column chromatography (EtOAc-Hexan 1+1,5) and recrystallized from ethanol. $C_{11}H_8N_2O$ (184.20). ^{1}H-NMR (500 Mhz, d_6-DMSO, ppm): 6.73 (1H, m), 7.18 (2H, d, J= 0.95 Hz), 7.19 (1H, d, J=0.63 Hz), 7.49 (1H, br. s), 7.61 (1H, br. s), 7.94 (1H, dd, J=1.9, 0.6 Hz), 12.90 (1H, s). MS: 185.23 m/z $(M+H)^+$. IR (ZnSe-ATR-FTIR): ν = 2661 (br), 1631, 1525, 1443, 1416, 1364, 1319, 1279, 1235, 1011, 979, 906, 884, 732, 589 cm^{-1}.

RS 37**: Procedure O**

2-(1H-Benzoimidazol-2-yl)-phenol: light grey-green solid, yield: 40 %, m.p. 242 °C, recrystallized from ethanol. $C_{13}H_{10}N_2O$ (210.24). ^{1}H-NMR (500 Mhz, d_6-DMSO, ppm): 3.57 (1H, br. s), 7.02-7.07 (2H, m), 7.28-7.32 (2H, m), 7.37-7.41 (1H, m), 7.69 (2H, dd, J=5.7, 3.5 Hz), 8.08 (1H, dd, J=7.9, 1.6 Hz), 13.21 (1H, br. s). MS: 211.15 m/z $(M+H)^+$. IR (ZnSe-ATR-FTIR): ν = 3324, 1632, 1590, 1491, 1453, 1420, 1396, 1321, 1282, 1262, 1238, 1134, 839, 799, 724, 560 cm^{-1}.

RS 40**: Procedure O**

2-Pyridin-2-yl-1H-benzoimidazole: white solid, yield: 93 %, m.p. 224 °C, recrystallized from ethanol and washed with hexane. $C_{12}H_9N_3$ (195.23). ^{1}H-NMR (500 Mhz, d_6-DMSO, ppm): 7.19-7.26 (2H, m), 7.50-7.52 (1H, m), 7.53-7.55 (1H, m), 7.70 (1H, d, J=7.9 Hz), 8.00 (1H, td, J=7.9, 1.9 Hz), 8.33 (1H, d, J=7.9 Hz), 8.72-8.74 (1H, m), 13.09 (1H, s). MS: 196.15 m/z $(M+H)^+$. IR (ZnSe-ATR-FTIR): ν = 2923 (br), 1442, 1400, 1315, 1280, 1122, 742, 702, 543 cm^{-1}.

RS 41**: Procedure O**

6-(1H-Benzoimidazol-2-yl)-pyridin-2-ol: white solid, yield 46 %, m.p. 284-285 °C washed with some hot ethanol. $C_{12}H_9N_3O$ (211.23). ^{1}H-NMR (500 Mhz, d_6-DMSO, ppm): 3.0-4.0 (1H, br. s (weak)), 6.66 (1H, d, J=8.5 Hz,), 7.24 (2H, m), 7.45 (1H, d, J=5.8 Hz), 7.63 (2H, s), 7.72 (1H, t, J=7.9 Hz), 12.8 (1H, br. s (weak)). MS: 212.15 m/z $(M+H)^+$. IR (ZnSe-ATR-FTIR): ν = 3241, 2922 (br), 1658, 1617, 1547, 1523, 1463, 1156, 1019, 907, 805, 740, 721, 657, 582, 545 cm^{-1}.

RS 42**: Procedure O**

2-(1H-Benzoimidazol-2-yl)-pyridin-3-ol: light-grey solid, yield 98 %, m.p. 189 °C, purification not necessary. $C_{12}H_9N_3O$ (211.23). ^{1}H-NMR (500 Mhz, d_6-DMSO, ppm): 3.0-4.0 (1H, br. s (weak)), 7.31 (2H, d, J=3.5 Hz), 7.45 (1H, dd, J=8.5, 4.4 Hz), 7.51 (1H, dd, J=8.5, 1.5 Hz), 7.61 (1H, br. s,), 7.76 (1H, br. s,), 8.28 (1H, dd, J=4.4, 1.3 Hz), 13.15 (1H, br. s). MS: 212.15 m/z $(M+H)^+$. IR (ZnSe-ATR-FTIR): ν = 2979 (br), 1464, 1382, 1279, 1249, 797, 741, 535 cm^{-1}.

RS 47 **: Procedure O**

5-Methyl-2-thiazol-4-yl-1H-benzoimidazole: brown solid, yield 52 %, m.p. 240-241 °C, recrystallized from aqueous EtOH. $C_{11}H_9N_3S$ (215.28). ^{1}H-NMR (500 Mhz, d_6-DMSO-5 % TFA, ppm): 7.40 (1H, ddd, J=8.5, 1.6, 0.6 Hz), 7.6 –7.61 (1H, m), 8.2 (1H, d, J=8.2 Hz), 8.88 (1H, d, J=1.9 Hz), 9.49 (1H, d, J=1.9 Hz). MS: 216.24 m/z $(M+H)^+$. IR (ZnSe-ATR-FTIR): ν = 3094 (br), 2361, 1627, 1579, 1473, 1444, 1395, 1339, 1309, 1281, 1229, 1195, 1092, 984, 902, 873, 837, 804, 724, 660, 599, 532 cm^{-1}.

RS 48 **: Procedure O**

5-Methyl-2-pyridin-2-yl-1H-benzoimidazole: brown solid, yield 77 %, m.p. 164 °C, purification not necessary. $C_{13}H_{11}N_3$ (209.25). ^{1}H-NMR (500 Mhz, d_6-DMSO-5 % TFA, ppm): 2.51 (3H, s), 7.42 (1H, d, J=8.2 Hz), 7.63 (1H, s), 7.72-7.77 (2H, m), 8.22 (1H, td, J=7.9, 1.6 Hz), 8.41 (1H, d, J=7.9 Hz), 8.91 (1H, d, 4.1 Hz). MS: 210.17 m/z $(M+H)^+$. IR (ZnSe-ATR-FTIR): ν = 2941 (br), 1590, 1445, 1403, 1311, 1120, 995, 794, 742, 701, 536 cm^{-1}.

RS 49 **: Procedure O**

5,6-Dimethyl-2-thiazol-4-yl-1H-benzoimidazole: brown solid, yield 74 %, m.p. 247-249 °C, recrystallized from aqueous EtOH. $C_{12}H_{11}N_3S$ (229.31). ^{1}H-NMR (500 Mhz, d_6-DMSO-5 % TFA, ppm): 2.39 (6H, s), 7.58 (2H, s), 8.86 (1H, d, J=1.6 Hz), 9.48 (1H, d, J=1.9 Hz). MS: 230.33 m/z $(M+H)^+$. IR (ZnSe-ATR-FTIR): ν = 2963 (br), 2360, 1580, 1441, 1408, 1316, 1234, 1202, 1164, 1110, 1096, 999, 908, 850, 724 cm^{-1}.

RS 50 **: Procedure O**

5,6-Dimethyl-2-pyridin-2-yl-1H-benzoimidazole: light brown solid, yield 86 %, m.p. 193 °C, purification not necessary. $C_{14}H_{13}N_3$ (223.28). ^{1}H-NMR (500 Mhz, d_6-DMSO, ppm): 2.32 (6H, s, -CH_3), 7.31 (1H, s), 7.46-7.48 (2H, m), 7.96 (1H, dt, J=7.6, 1.6 Hz), 8.29 (1H, d, J=7.9 Hz), 8.69 (1H, d, J=4.4 Hz), 12.85 (1H, s, -NH). MS: 224.19 m/z $(M+H)^+$. IR (ZnSe-ATR-FTIR): ν = 2920 (br), 2333, 1594, 1450, 1399, 1261, 995, 795, 679 (br) cm^{-1}.

RS 51 **: Procedure O**

5-tert-butyl-2-thiazol-4-yl-1H-benzimidazole: grey-brown solid, yield 50 %, m.p. 165-168 °C, recrystallized from aqueous EtOH. $C_{14}H_{15}N_3S$ (257.36). ^{1}H-NMR (500 Mhz, d_6-DMSO-5 % TFA, ppm): 1.37 (9H, s), 7.67-7.76 (3H, m), 8.91 (1H, d, J=1.9 Hz), 9.49 (1H, d, J=1.9 Hz). MS: 258.46 m/z $(M+H)^+$. IR (ZnSe-ATR-FTIR): ν = 2952 (br), 2361, 1477, 1389, 1306, 1091, 902, 814, 721, 655 cm^{-1}.

RS 52 **: Procedure O**

5-tert-Butyl-2-pyridin-2-yl-1H-Benzoimidazole: grey solid, yield 59 %, m.p. 151 °C, recrystallized from aqueous EtOH. $C_{16}H_{17}N_3$ (252.33). ^{1}H-NMR (500 Mhz, d_6-DMSO-5 % TFA, ppm): 1.38 (9H, s), 7.60-7.88 (4H, m), 8.23 (1H, td, J=7.9, 1.6

Hz), 8.41 (1H, d, J=7.9 Hz), 8.91-8.93 (1H, m). MS: 253.65 m/z $(M+H)^+$. IR (ZnSe-ATR-FTIR): ν = 2950 (br), 2359, 1593, 1445, 1391, 1314, 1280, 1149, 995, 865, 798, 743, 696, 656, 510 cm^{-1}.

RS 57 **: Procedure O**

5-Fluoro2-thiazol-4-yl-1H-benzimidazole: brown-red solid, yield 76 %, m.p. 260-261 °C, recrystallized from aqueous EtOH. $C_{10}H_6FN_3S$ (219,24). ^{1}H-NMR (500 Mhz, d_6-DMSO-5 % TFA, ppm): 7,43 (1H, td, J=9.1, 2.2 Hz), 7,67 (1H, dd, J=8.5, 2.2 Hz), 7,84 (1H, dd, J=8.8, 4.4 Hz), 8,90 (1H, d, J=1.9 Hz), 9,49 (1H, d, J=1.9 Hz). MS: 220,19 m/z $(M+H)^+$. IR (ZnSe-ATR-FTIR): ν = 3092 (br), 2362, 1629, 1477, 1448, 1396, 1351, 1310, 1247, 1221, 1143, 1094, 987, 963, 904, 838, 800, 729, 653, 613, 535 cm^{-1}.

RS 58 **: Procedure O**

5-Fluoro-2-pyridin-2-yl-1H-benzoimidazole: dark purple solid, yield 96 %, m.p. 181 °C, purification not necessary. $C_{12}H_8FN_3$ (213.22). ^{1}H-NMR (500 Mhz, d_6-DMSO-5 % TFA, ppm): 7.44 (1H, td, J=9.3, 2.5 Hz), 7.67 (1H, dd, J=8.5, 2.5 Hz), 7.74-7.77 (1H, m), 7.87 (1H, dd, J=9.1, 4.4 Hz), 8.22 (1H, td, J=7.9, 1.6 Hz), 8.41 (1H, dt, J=7.9, 0.9 Hz), 8.90-8.91 (1H, ddd, J=4.7, 1.6, 0.9 Hz). MS: 214.15 m/z $(M+H)^+$. IR (ZnSe-ATR-FTIR): ν = 3142 (br), 1598, 1478, 1447, 1406, 1309, 1252, 1138, 1107, 999, 964, 836, 793, 745, 693, 610 cm^{-1}.

RS 59 **: Procedure O**

5-Chloro-2-thiazol-4-yl-1H-benzimidazole: grey solid, yield 56 %, m.p. 238-240 °C, recrystallized from aqueous EtOH. $C_{10}H_6ClN_3S$ (235.70). ^{1}H-NMR (500 Mhz, d_6-DMSO-5 % TFA, ppm): 7.57 (1H, dd, J=8.5, 1.9 Hz), 7.82 (1H, d, J=8.5 Hz), 7.88 (1H, d, J=1.9 Hz), 8.90 (1H, d, J=1.9 Hz), 9.48 (1H, d, J=1.9 Hz). MS: 236.24 m/z $(M+H)^+$. IR (ZnSe-ATR-FTIR): ν = 3093 (br), 2361, 1620, 1578, 1441, 1389, 1335, 1308, 1278, 1222, 1193, 1093, 1061, 984, 928, 903, 876, 838, 807, 730, 702, 656, 598, 534 cm^{-1}.

RS 60 **: Procedure O**

5-Chloro-2-pyridin-2-yl-1H-benzoimidazole: white solid, yield 49 %, m.p. 141 °C, extracted with hot benzene and treated with charcoal, then purified over silica gel (EtOAc) and recrystallized from benzene. $C_{12}H_8ClN_3$ (229.67). ^{1}H-NMR (500 Mhz, d_6-DMSO-5 % TFA, ppm): 7.55 (1H, d, J=8.8, 1.9 Hz), 7.73-7.76 (1H, m), 7.83 (1H, d, J=8.5 Hz), 7.88 (1H, d, J=1.9 Hz), 8.20 (1H, td, J=7.9, 1.6 Hz), 8.41 (1H, d, J=7.9 Hz), 8.88-8.90 (1H, m). MS: 230,13 m/z $(M+H)^+$. IR (ZnSe-ATR-FTIR): ν = 3054 (br), 2364, 1595, 1445, 1401, 1305, 1218, 1059, 996, 924, 791, 739, 698 cm^{-1}.

RS 61 **: Procedure O**

Phenyl-(2-thiazol-4-yl-1H-benzoimidazol-5-yl)-methanone: light yellow solid, yield 35 %, m.p. 95-98 °C, purified over silica gel (EtOAc-Hexan 1+2.5) and recrystallized from aqueous ethanol. $C_{17}H_{11}N_3OS$ (305.36). ^{1}H-NMR (500 Mhz, d_6-DMSO-5 % TFA, ppm): 7.6 (2H, t, J=7.9 Hz), 7.71 (1H, t, J=7.6 Hz), 7.79 (2H, d, J=7.9 Hz), 7.90-7.96 (2H, m), 8.10 (1H, s), 8.95 (1H, d, J=1.5 Hz), 9.50 (1H, d, J=1.6 Hz). MS: m/z 305.6 $(M+H)^+$. IR (ZnSe-ATR-FTIR): ν = 2930 (br), 1729, 1644, 1618, 1446, 1405, 1352, 1272, 1179, 1121, 1075, 977, 898, 875, 827, 708, 625, 529 cm^{-1}.

RS 64**: Procedure O**

2-Thiazol-4-yl-1H-imidazo[4,5-b]pyridine: purple solid, yield 97 %, m.p. 306 °C, purification not necessary. $C_9H_6N_4S$ (202.24). ^{1}H-NMR (500 Mhz, d_6-DMSO-5 % TFA, ppm): 7.69 (1H, dd, J=8.2, 5.7 Hz), 8.49 (1H, d, J=7.9 Hz), 8.68 (1H, d, H=5.8 Hz), 8.88 (1H, d, J=1.8 Hz), 9.46 (1H, d, J=1.8 Hz). MS: 203.11 m/z $(M+H)^+$. IR (ZnSe-ATR-FTIR): ν = 3064 (br), 1595, 1417, 1398, 1269, 1097, 906, 884, 837, 800, 771, 734, 643, 565 cm^{-1}.

RS 65**: Procedure O**

2-Pyridin-2-yl-1H-imidazo[4,5-b]pyridine: brown solid, yield 46 %, m.p. 242-243 °C, recrystallized from EtOH. $C_{11}H_8N_4$ (196.21). ^{1}H-NMR (500 Mhz, d_6-DMSO-5 % TFA, ppm): 7.69-7.73 (2H, m), 8.15 (1H, td, J=7.6, 1.5 Hz), 8.44 (1H, d, J=7.9 Hz), 8.52 (1H, dd, J=7.9, 0.9 Hz), 8.71 (1H, d, J=5.5 Hz), 8.87 (1H, d, J=4.3 Hz). MS: 197.15 m/z $(M+H)^+$. IR (ZnSe-ATR-FTIR): ν = 2971 (br), 1592, 1444, 1412, 1376, 1267, 797, 766, 742, 702, 564 cm^{-1}.

RS 66**: Procedure O**

2-Thiazol-4-yl-1H-imidazo[4,5-c]pyridine: white solid, yield 98 %, m.p. 273 °C, purification not necessary. $C_9H_6N_4S$ (202.24). ^{1}H-NMR (500 Mhz, d_6-DMSO, ppm): 7.55 (1H, s), 8.31 (1H, d, J=5.7 Hz), 8.58 (1H, d, 1.9 Hz), 8.93 (1H, s), 9.36 (1H, d, J=1.9 Hz), 13.10 (1H, br. s). MS: 203.11 m/z $(M+H)^+$. IR (ZnSe-ATR-FTIR): ν = 2627 (br), 1620, 1586, 1462, 1405, 1301, 1226, 1082, 1027, 964, 901, 886, 844, 804, 730, 633, 605, 536 cm^{-1}.

RS 67**: Procedure O**

2-Pyridin-2-yl-1H-imidazo[4,5-c]pyridine: white solid, yield 78 %, m.p. 232 °C, recrystallized from EtOH. $C_{11}H_8N_4$ (196.21). ^{1}H-NMR (500 Mhz, d_6-DMSO, ppm): 7.57-7.60 (2H, m), 8.04 (1H, td, J=7.9, 1.6 Hz), 8.34 (1H, d, J=5.7 Hz), 8.38 (1H, d, J=7.9 Hz), 8.77 (1H, d, J=4.8 Hz), 9.00 (1H, s), 13.52 (1H, br. s). MS: 197.15 m/z $(M+H)^+$. IR (ZnSe-ATR-FTIR): ν = 2626 (br), 1621, 1463, 1445, 1407, 1283, 1224, 1171, 1116, 1022, 995, 948, 909, 889, 794, 740, 703, 639, 606, 591, 542 cm^{-1}.

Procedure P: Procedure[216] for the preparation of **RS 38**:

O-phenylenediamine (1.94 g, 0.018 mol) and 5-amino-3H-1,2,4-dithiazole-3-thione (3.3g, 0.022 mol, known as isoperthiocyanic acid) in absolute ethanol (30 ml) was refluxed for 22 hrs. The solvent was distilled from the reaction mixture and the residue treated with aqueous sodium hydroxide (1 N, 3x25 ml) and then filtered. The filtrate was carefully neutralized to pH 7 and kept in a refrigerator for 8 hrs. The white precipitate (3.22 g, 96 %) that had formed was collected, washed with water, and dried.

RS 38**: Procedure P**

1H-Benzimidazol-2-yl-thiourea: white solid, yield 92 %, m.p. 196-198 °C, purification not necessary. $C_8H_8N_4S$ (192.24). ^{1}H-NMR (500 Mhz, d_6-DMSO, ppm): 7.09-7.13 (2H, m), 7.43-7.47 (2H, m), 9.08 (1H, br. s.), 10.24 (1H, br. s.), 11.11 (2H, br. s.). MS: 193.25 m/z $(M+H)^+$. IR (ZnSe-ATR-FTIR): ν = 3081 (br), 1578, 1543, 1439, 1264, 1084, 1024, 833, 741 cm^{-1}.

Procedure Q: Procedure[217] for the preparation of **RS 39**:

To a stirred and refluxing suspension of (1H-benzimidazol-2-yl)-thiourea (3.64 mmol) in water (3 ml) was added dropwise 1,2-dichloroethyl ethylether (3.86 mmol). After 2 hrs, the cooled mixture was basified (NaOH). The product was filtered and recrystallized from aqueous EtOH.

RS 39**: Procedure Q**

(1H-Benzimidazol-2-yl)-thiazol-2-yl-amine: white solid, yield 85 %, m.p. 252-254 °C, recrystallized from aqueous EtOH. $C_{10}H_8N_4S$ (216.27). ^{1}H-NMR (500 Mhz, d_6-DMSO, ppm): 6.90 (1H, d, J=3.8 Hz), 7.03-7.07 (2H, m), 7.30-7.34 (3H, m), 11.65 (2H, br. s.). MS: 217.28 m/z $(M+H)^+$. IR (ZnSe-ATR-FTIR): ν = 2765 (br), 1632, 1601, 1476, 1435, 1370, 1224, 1133, 1061, 1024, 864, 834, 740, 664, 603, 524 cm^{-1}.

Procedure R: General Procedure for the preparation of substituted benzimidazoles[218] for the compounds **RS 43**, **RS 62**, **RS 68**, **RS 69**:

The appropriate diamine, usually as free base, was thoroughly mixed in a mortar with two equivalents each of anhydrous sodium acetate and the amidine salt. The temperature of the mixture was slowly raised until evolution of ammonia set in, and heating was continued until the melt resolidified. The cake was then treated with 1 N-NaOH and the mixture decolorized with charcoal and filtered. The hot filtrate was neutralized with glacial acetic acid or by addition of solid ammonium chloride. The product was filtered and recrystallized from water.

RS 43**: Procedure R**

2-Pyrazin-2-yl-1H-benzoimidazole: yellow solid, yield 85 %, m.p. 242-244 °C, recrystallized from aqueous EtOH. $C_{11}H_8N_4$ (196.21). ^{1}H-NMR (500 Mhz, d_6-DMSO, ppm): 7.23-7.31 (2H, m), 7.57 (1H, dt, J=7.9, 0.9 Hz), 7.76 (1H, d, J=7.9 Hz), 8.76 (1H, d, J=2.5 Hz), 8.80 (1H, dd, 2.5, 1.6 Hz), 9.50 (1H, d, 1.6 Hz), 13.32 (1H, br. s). MS: 196.21 m/z $(M+H)^+$. IR (ZnSe-ATR-FTIR): ν = 3086 (br), 1433, 1313, 1261, 1106, 1046, 1021, 855, 801, 735, 666, 534 cm^{-1}.

RS 62**: Procedure R**

Phenyl-(2-pyridin-2-yl-3H-benzoimidazol-5-yl)-methanone: light yellow solid, yield 20 %, m.p. 73-76 °C, not soluble in 1 N-NaOH, therefore the cake was dissolved in EtOH and the product was precipitated with water and then recrystallized from aqueous EtOH. $C_{19}H_{13}N_3O$ (299.33). ^{1}H-NMR (500 Mhz, d_6-DMSO-5 % TFA, ppm): 7.9 (2H, t, J=7.9 Hz), 7.69-7.80 (4H, m), 7.88-7.96 (2H, m), 8.11 (1H, s), 8.21 (1H, td, J=7.9, 1.5 Hz), 8.44 (1H, d, J=7.9 Hz), 8.91 (1H, d, J=4.9 Hz). MS: m/z 300.6 $(M+H)^+$. IR (ZnSe-ATR-FTIR): ν = 3243 (br), 1644, 1614, 1595, 1572, 1440, 1353, 1317, 1290, 1233, 1110, 955, 901, 824, 796, 724, 704, 646 cm^{-1}.

RS 68**: Procedure R**

8-Pyridin-2-yl-7(9)H-purine: white solid, yield 62 %, m.p. 289-291 °C, recrystallized from H_2O. $C_{10}H_7N_5$ (197.20). ^{1}H-NMR (500 Mhz, d_6-DMSO, ppm): 7.63-7.66 (1H, m), 8.09 (1H, td, J=7.9, 1.6 Hz), 8.43 (1H, d, J=7.6 Hz), 8.81-8.22 (1H, m), 8.98 (1H, s), 9.17 (1H, s). MS: 198.15 m/z $(M+H)^+$. IR (ZnSe-ATR-FTIR): ν = 2966 (br), 1573, 1536, 1469, 1439, 1412, 1387, 1343, 1226, 954, 921, 867, 833, 798, 743, 703, 614, 589, 570, 556 cm^{-1}.

RS 69**: Procedure R**

2-Pyridin-2-yl-1H-imidazo[4,5-b]pyrazine: light brown solid, yield 69 %, m.p. 306-309 °C, recrystallized from aqueous ethanol. $C_{10}H_7N_5$ (197.20). ^{1}H-NMR (500 Mhz, d_6-DMSO, ppm): 7.62-7.65 (1H, m), 8.06-8.10 (1H, m), 7.72-7.75 (1H, m), 8.40 (1H, br. s), 8.44 (1H, dd, J=7.9, 0.9 Hz), 8.50 (1H, br. s), 14.18 (1H, s). MS: 198.33 m/z $(M+H)^+$. IR (ZnSe-ATR-FTIR): ν = 2972 (br), 1468, 1441, 1394, 1357, 1201, 1095, 993, 947, 837, 811, 752, 706, 594, 580 cm^{-1}.

Procedure S: General Procedure for the preparation of N-alkylated benzimidazoles[219] for the compounds **RS 44**, **RS 45** and **RS 46**:

To a suspension of a suitable benzimidazole (thiabendazole or compound RS 17) in dry dimethylformamide and benzene was added a suspension of sodium hydride in benzene. The solution was warmed under nitrogen for 30 min and then a solution of methyl iodide (or benzyl chloride) in benzene was added dropwise and the mixture was refluxed under nitrogen for 1 h. The cooled mixture was washed with water, dried over sodium sulphate, and evaporated to dryness to yield crude product.

RS 44**: Procedure S**

1-Methyl-2-thiazol-4-yl-1H-benzoimidazol: white solid, yield 79 %, m.p. 150 °C, purified over silica gel (EtOAc) and recrystallized from EtOH. $C_{11}H_9N_3S$ (215,28). ^{1}H-NMR (500 Mhz, d_6-DMSO, ppm): 4,17 (3H, s, N-CH_3), 7,24-7,32 (2H, m), 7,62 (1H, dd, J=7.9, 1.3 Hz), 7,66-7,68 (1H, m), 8,49 (1H, d, J=1.9 Hz), 9,35 (1H, d, J=2.2 Hz). MS: 216,13 m/z $(M+H)^+$. IR (ZnSe-ATR-FTIR): ν = 3095, 3032, 2924, 2854, 1459, 1430, 1404, 1367, 1315, 1258, 1097-1018 (br), 917, 876, 799, 731 cm^{-1}.

RS 45**: Procedure S**

1-Benzyl-2-thiazol-4-yl-1H-benzoimidazole: white solid, yield 35 %, m.p. 146 °C, purified over silica gel (EtOAc-Hexan 1+2). $C_{17}H_{13}N_3S$ (291,38). ^{1}H-NMR (500 Mhz, $CDCl_3$, ppm): 6,15 (2H, s, N-CH_2), 7,15-7,17 (2H, m), 7,22-7,31 (4H, m), 7,34-7,37 (2H, m), 7,89-7,91 (1H, m), 8,74 (1H, s), 8,90 (1H, d, J=1.9 Hz). MS: 292,19 m/z $(M+H)^+$. IR (ZnSe-ATR-FTIR): ν = 3073, 2929 (br), 1730, 1494, 1473, 1459, 1404, 1360, 1332, 1310, 1259, 1159-999 (br), 924, 835, 799, 738, 723, 692 cm^{-1}.

RS 46**: Procedure S**

1-Benzyl-2-pyridin-2-yl-1H-benzoimidazole: white solid, yield 47 %, m.p. 116-118 °C, purified over silica gel with EtOAc-Hexan 1+3. $C_{19}H_{15}N_3$ (285.35). ^{1}H-MR (500 Mhz, d_6-DMSO, ppm): 6.23 (2H, s), 7.12-7.28 (7H, m), 7.49-7.52 (1H, m), 7.55-7.59 (1H, m), 7.74-7.78 (1H, m), 8.00 (1H, td, J=7.9, 1.9 Hz), 8.37 (1H, dt, J=8.2, 0.9 Hz), 8.69-8.70 (1H, m). MS: 286.23 m/z $(M+H)^+$. IR (ZnSe-ATR-FTIR): ν = 2928, 2364, 1733, 1586, 1465, 1441, 1394, 1369, 1330, 1278, 730, 695 cm^{-1}.

Procedure T: General Procedure for the preparation of nitrated benzimidazoles[220] for the compounds **RS 53** and **RS 54**:

To a solution of a suitable benzimidazole (thiabendazole or compound RS 17, 164 mmol) in concentrated H_2SO_4 (75 ml) was added concentrated HNO_3 (12.5 ml) dropwise between 0 °C and 10 °C. The mixture was stirred at room temperature for 2 hrs and then poured into ice-water. Cautious neutralization with 50 % NaOH provided a solid, which was filtered off and crystallized from MeOH to yield the desired product.

RS 53**: Procedure T**

5-Nitro-2-thiazol-4-yl-1H-benzoimidazole: light yellow solid, yield 55 %, m.p. 242 °C, recrystallized from EtOH. $C_{10}H_6N_4O_2S$ (246.25). ^{1}H-NMR (500 Mhz, d_6-DMSO-5 % TFA, ppm): 7.84 (1H, d, J=8.8 Hz), 8.23 (1H, dd, J=8.8, 2.2 Hz), 8.51 (1H, d, J=2.2 Hz), 8.76 (1H, d, J=1.9 Hz), 9.43 (1H, d, J=1.9 Hz). MS: 247.13 m/z $(M+H)^+$. IR (ZnSe-ATR-FTIR): ν = 1439, 1374, 1331, 1274, 1195, 1130, 1069, 910, 881, 810, 737, 618cm^{-1}.

RS 54**: Procedure T**

5-Nitro-2-pyridin-2-yl-1H-benzoimidazole: light yellow solid, yield 43 %, m.p. 213-214 °C, recrystallized from MeOH. $C_{12}H_8N_4O_2$ (240.22). ^{1}H-NMR (500 Mhz, d_6-DMSO-5 % TFA, ppm): 7.62-7.65 (1H, m), 7.82 (1H, dd, J=8.8, 0.6 Hz), 8.09 (1H, td, J=7.9, 1.6 Hz), 8.19 (1H, dd, J=9.1, 2.2 Hz), 8.40 (1H, dt, J=7.9, 0.9 Hz), 8.53 (1H, d, J=2.2 Hz), 8.80-8.82 (1H, m), 13.08 (1H, br. s (weak)). MS: 241.17 m/z $(M+H)^+$. IR (ZnSe-ATR-FTIR): ν = 3106 (br), 2332, 1519, 1446, 1437, 1404, 1339, 1316, 1064, 823, 737, 700 cm^{-1}.

Procedure U: Reduction on Pd/charcoal[221] for the compounds **RS 55** and **RS 56**:

1.0 g of a nitro-derivative was dissolved in 100 ml absolute ethanol, and the solution was reduced catalytically over 0.5 g of 10 % palladium-on-charcoal at normal pressure and room temperature. After the uptake of hydrogen was complete, the catalyst was removed by filtration and the solvent was evaporated *in vacuo*. Upon recrystallization the pure compounds were obtained.

RS 55**: Procedure U**

5-Amino-2-thiazol-4-yl-1H-benzimidazole: light yellow solid, yield 62 %, m.p. 233-235 °C, recrystallized from aqueous ethanol. $C_{10}H_8N_4S$ (216.27). ^{1}H-NMR (500 Mhz, d_6-DMSO-5 % TFA, ppm): 7.32 (1H, dd, J=8.8, 1.9 Hz), 7.58 (1H, d, J=1.9 Hz), 7.79 (1H, d, J=8.5 Hz), 8.85 (1H, d, J=1.9 Hz), 9.47 (1H, d, J=1.9 Hz). MS: 217.29 m/z $(M+H)^+$. IR (ZnSe-ATR-FTIR): ν = 3109 (br), 1631, 1408, 1359, 1309, 904, 804, 715, 645, 620 cm^{-1}.

RS 56**: Procedure U**

2-Pyridin-2-yl-1-benzoimidazol-5-ylamine: light yellow solid, yield 80 %, m.p. 217 °C, recrystallized from EtOH. $C_{12}H_{10}N_4$ (210.24). ^{1}H-NMR (500 Mhz, d_6-DMSO-5 % TFA, ppm): 7.31 (1H, d, J=8.5 Hz), 7.6 (1H, s), 7.68-7.71 (1H, m), 7.80 (1H, d, J=8.8 Hz), 8.16 (1H, td, J=7.9, 1.6 Hz), 8.38 (1H, d, J=7.9 Hz), 8.85-8.87 (1H, m). MS: 211.17 m/z $(M+H)^+$. IR (ZnSe-ATR-FTIR): ν = 2984 (br), 1591, 1494, 1438, 1324, 1167, 880, 794, 742, 692, 617 cm^{-1}.

Procedure V: Procedure[222, 223] for the preparation of **RS 63**:

A stirred solution of pyridine-2-carbaldehyde (85.7 mg, 0.8 mmol) and 3,4-diamino-benzonitrile (100 mg, 0.75 mmol) in 8 ml of nitrobenzene was heated at 145 °C under N_2 overnight. The cooled reaction mixture was treated with 3 % HCl (3x25 ml) and the pH adjusted to 8 with NH_4OH. The voluminous precipitate was filtrated and then purified by column chromatography (EtOAc:hexane 1:1) to give **RS 63**.

RS 63**: Procedure V**

2-Pyridin-2-yl-1H-benzoimidazole-5-carbonitrile: white solid, yield 36 %, m.p. 216-218 °C, purified over silica gel (EtOAc-Hexan 1+1). $C_{13}H_8N_4$ (220.24). ^{1}H-NMR (500 Mhz, d_6-DMSO-5 % TFA, ppm): 7.66 (1H, t, J=6.3 Hz), 7.73 (1H, d, J=8.5 Hz), 7.85 (1H, d, J=8.5 Hz), 8.12 (1H, t, J=7.8 Hz), 8.25 (1H, s), 8.41 (1H, d, J=7.9 Hz), 8.83 (1H, d, J=5.6 Hz). MS: 221.15 m/z $(M+H)^+$. IR (ZnSe-ATR-FTIR): ν = 3143 (br), 2222, 1727, 1602, 1470, 1448, 1414, 1312, 1001, 793, 740, 696, 624, 533 cm^{-1}.

7.1.2.4 Elemental Analyses of Thiabendazole Analogs

Cpd.	Molecular formula	Calculated %	Found %
RS 17	$C_9H_7N_3OS$	C 52.67 H 3.44 N 20.47 O 7.80 S 15.62	C 53.86 H 3.38 N 19.34
RS 34	$C_{12}H_9N_3$	C 73.83 H 4.65 N 21.52	C 71.22 H 5.62 N 23.17
RS 35	$C_{11}H_8N_2S$	C 65.97 H 4.03 N 13.99 S 16.01	C 65.98 H 4.54 N 13.47
RS 36	$C_{11}H_8N_2O$	C 71.73 H 4.38 N 15.21 O 8.69	C 71.72 H 4.60 N 14.99
RS 37	$C_{13}H_{10}N_2O$	C 74.27 H 4.79 N 13.32 O 7.61	C 74.05 H 5.03 N 13.30
RS 38	$C_8H_8N_4S$	C 49.98 H 4.19 N 29.14 S 16.68	C 50.50 H 4.47 N 28.39
RS 39	$C_{10}H_8N_4S$	C 55.54 H 3.73 N 25.91 S 14.83	C 56.09 H 3.82 N 25.27
RS 40	$C_{12}H_9N_3$	C 73.83 H 4.65 N 21.52	C 74.13 H 4.56 N 21.28
RS 41	$C_{12}H_9N_3O$	C 68.24 H 4.29 N 19.89 O 7.57	C 68.58 H 4.16 N 19.68
RS 42	$C_{12}H_9N_3O$	C 68.24 H 4.29 N 19.89 O 7.57	C 67.39 H 4.72 N 20.31
RS 43	$C_{11}H_8N_4$	C 67.34 H 4.11 N 28.55	C 67.71 H 3.76 N 28.52
RS 44	$C_{11}H_9N_3S$	C 61.37 H 4.21 N 19.52 S 14.89	C 61.32 H 4.23 N 18.93
RS 45	$C_{17}H_{13}N_3S$	C 70.08 H 4.50 N 14.42 S 11.00	C 70.40 H 5.14 N 13.46
RS 46	$C_{19}H_{15}N_3$	C 79.98 H 5.30 N 14.73	C 80.30 H 5.22 N 14.49
RS 47	$C_{11}H_9N_3S$	C 61.37 H 4.21 N 19.52 S 14.89	C 61.70 H 4.23 N 19.17
RS 48	$C_{13}H_{11}N_3$	C 74.62 H 5.30 N 20.08	C 74.13 H 5.74 N 20.13
RS 49	$C_{12}H_{11}N_3S$	C 62.86 H 4.84 N 18.32 S 13.98	C 62.76 H 5.08 N 18.18
RS 50	$C_{14}H_{13}N_3$	C 75.31 H 5.87 N 18.82	C 75.06 H 6.20 N 18.74
RS 51	$C_{14}H_{15}N_3S$	C 65.34 H 5.87 N 16.33 S 12.46	C 65.31 H 6.12 N 16.11
RS 52	$C_{16}H_{17}N_3$	C 76.46 H 6.82 N 16.72	C 76.29 H 7.00 N 16.72
RS 53	$C_{10}H_6N_4O_2S$	C 48.78 H 2.46 N 22.75 O 12.99 S 13.02	C 49.17 H 2.40 N 22.42
RS 54	$C_{12}H_8N_4O_2$	C 60.00 H 3.36 N 23.32 O 13.32	C 60.46 H 3.30 N 22.92
RS 55	$C_{10}H_8N_4S$	C 55.54 H 3.73 N 25.91 S 14.83	C 55.77 H 3.79 N 25.27
RS 56	$C_{12}H_{10}N_4$	C 68.56 H 4.79 N 26.65	C 69.05 H 4.90 N 26.05
RS 57	$C_{10}H_6FN_3S$	C 54.78 H 2.76 F 8.67 N 19.17 S 14.62	C 55.05 H 2.76 N 18.90
RS 58	$C_{12}H_8FN_3$	C 67.60 H 3.78 F 8.91 N 19.71	C 67.11 H 3.76 N 20.21
RS 59	$C_{10}H_6ClN_3S$	C 50.96 H 2.57 Cl 15.04 N 17.83 S 13.60	C 51.31 H 2.51 N 17.55
RS 60	$C_{12}H_8ClN_3$	C 62.76 H 3.51 Cl 15.44 N 18.30	C 62.59 H 4.07 N 17.91
RS 61	$C_{17}H_{11}N_3OS$	C 66.87 H 3.63 N 13.76 O 5.24 S 10.50	C 67.17 H 3.92 N 13.18
RS 62	$C_{19}H_{13}N_3O$	C 76.24 H 4.38 N 14.04 O 5.34	C 75.72 H 4.52 N 14.42
RS 63	$C_{13}H_8N_4$	C 70.90 H 3.66 N 25.44	C 72.54 H 4.00 N 23.46
RS 64	$C_9H_6N_4S$	C 53.45 H 2.99 N 27.70 S 15.85	C 53.76 H 2.94 N 27.44
RS 65	$C_{11}H_8N_4$	C 67.34 H 4.11 N 28.55	C 66.79 H 4.15 N 29.05
RS 66	$C_9H_6N_4S$	C 53.45 H 2.99 N 27.70 S 15.85	C 53.70 H 2.87 N 27.57
RS 67	$C_{11}H_8N_4$	C 67.34 H 4.11 N 28.55	C 67.82 H 4.02 N 28.16
RS 68	$C_{10}H_7N_5$	C 60.91 H 3.58 N 35.51	C 61.63 H 3.64 N 34.72
RS 69	$C_{10}H_7N_5$	C 60.91 H 3.58 N 35.51	C 61.96 H 2.96 N 35.08

7.2 Biochemistry

7.2.1 Laboratory Equipment, Materials and Instruments

All assays were done with black Polypropylene 96 well plates (V-bottom) from Greiner (Frickenhausen, Germany, Cat.-Nr. 651209) with pipettes (Model Research) from Eppendorf (Hamburg, Germany) or Gilson (Middleton, USA) and measured with a Wallac Victor^2 1420 Multilabel Counter (PerkinElmer, Boston, USA). For the determination of the MIC-values, transparent 96 well plates (flat bottom, Cat.-Nr. 391H8046) from Merck (Darmstadt, Germany) were used.

Table-top centrifuges	
Universal 32 R, Micro 24-48 R	Hettich, Tuttlingen , Germany
Minifuge	Heraeus, Hanau, Germany.
Centrifuge RC 5B Plus	Sorvall, Newtown, USA
Rotors SS-34, SLA-1500	Sorvall, Newtown, USA
Gel electrophoresis chamber EC120	EC-Apparatus Corp., St.Petersburg, USA
Gel electrophoresis chamber flatbed	LTF, Wasserburg, Germany
Gel electrophoresis chamber 45-1010	PeqLab, Erlangen, Germany
Power-Supply Power Packs P25	Biometra, Göttingen, Germany
Power-Supply Power Packs P300	Bio Rad, Munich, Germany
Incubator Shakers	Infors HT, Bottmingen, Switzerland
Incubators	Heraeus, Hanau, Germany
Cell disruption equipm., One shot model, Unit 3	Constant Systems Ltd, Warwick, UK
Microcooler II	Boeckel, Emersacker, Germany
Ultrasonic bath Sonsorex RK 106 Transistor	Bandelin, Berlin, Germany
Water Bath WBU45	Memmert, Schwalbach, Germany
Photometer Heλios β	Unicam, Cambridge, UK
Thermoblock HB 120 Thermoleader	Uni Equip, Martinsried, Germany
Magnetic Stirrer RCT-Basic	IKA-Labortechnik, Staufen, Germany
pH-Meter 766	Knick, Berlin, Germany
Electroporator EC 100	EC-Apparatus Corp., St. Petersburg, USA
Balance 440-45	Kern, Balingen, Germany
Balance SBC 21	SCALTEC, Heiligenstadt, Germany
RP-Osmosis-plant Milli-Q Plus PF	Millipore, Eschborn, Germany
Vortex-Genie 2	Scientific Industries, Bohemia, N.Y., USA

7.2.2 Expression and Purification of EcMetAP

A C-terminal poly-His-tagged form of *E. coli* MetAP was obtained by overexpression in *E. coli* using an Arg-175-Gln mutant kindly provided by Prof. B. W. Matthews and W. T. Lowther. The expression vector used was constructed with the Novagen pet28b expression vector as described in the literature[70]. In short, it encodes for the *E. coli* MetAP Arg-175-Gln mutation with a C-terminal poly-His-tag flanked by a thrombin-cleavage site. The Arg-175-Gln mutation eliminates a secondary thrombin cleavage site on a surface loop and does not affect activity.

The expression and purification of the EcMetAP was done according to a literature procedure[70]:

Four liter fermentation cultures of BL21(DE3) *E. coli* cells containing the expression plasmid were grown in Luria-Bertani broth with kanamycin (100 mg/liter) at 37 °C and 250 rpm. Expression was induced after cooling to 25 °C by the addition of isopropyl ß-D-thiogalactoside to 1 mM at 0.5-0.6 OD_{600} and the cells allowed to grow for another 3 hrs at 25 °C. The cells were centrifuged at 8500 rpm and 4 °C for 15 min, resuspended in medium and centrifuged again at 4500 rpm and 4 °C for 15 min. The cells were frozen at -80 °C and crashed in a mortar under cooling with nitrogen. The resulting powder wass suspended in 100 ml of an altered +T/G buffer at 4 °C [50 mM Hepes, pH 7.9 / 10 % glycerol / 0.1 % Triton X-100 / 0.5 M KCl / 5 mM imidazole and additionally 40 µg/ml DNase / 1 mM $MgCl_2$ / 15 mM methionine / 1 mM PMSF] and the cells lysed in a french press at 1.0 kbar. The resulting solution was then centrifuged at 40,000 g at 4 °C for 30 min. The supernatant was loaded onto a 10-ml nitrilotriacetic acid-agarose column (Qiagen, Hilden, Germany) equilibrated with +T/G buffer. After washing with +T/G buffer and –T/G buffer (-T/G buffer without glycerol, Triton X-100 and inhibitor cocktail), MetAP was eluted at 4 °C with about 160 ml of –T/G buffer containing 60 mM imidazole directly into 1 ml of 500 mM EDTA, pH 8.0. Additional EDTA was added, if necessary, to give a final concentration of 5 mM. The yield/protein concentrations were determined by absorption at 280 nm with the extinction coefficient of 16350 $M^{-1} \cdot cm^{-1}$ with a conversion factor of 1.89. Typical yields were 100-150 mg/liter of culture. Freshly transformed BL21(DE3) gave significantly higher yields. For stored BL21(DE3) cells, typical yields were about 40-75 mg/L.

After dialysis at 4 °C against 25 mM Hepes buffer, pH 7.9, 150 mM KCl, 15 mM Methionine, MetAP was concentrated to a volume of about 30 ml and stored at -80 °C at about 20 mg/ml.

For dialysis and buffer exchange, ultrafiltration can be used (cfr. 7.2.4.1.3 Buffer Exchange and Concentration of Protein Solutions). The poly-His-tail was removed by incubation of 100 mg of MetAP with 0.1-1 U/mg of thrombin (Novagen/Merck, Darmstadt, Germany) / 2,5 mM $CaCl_2$ at 15 °C in a Microcooler for 18-20 hrs. Passage of the protein through another nitrilotriacetic acid-agarose column equilibrated with –T/G buffer resulted in His-tag free protein. For this step, only a small volume of agarose should be used (0.5 ml-1 ml for a digest of about 100 mg). The resulting protein solution was narrowed to 2-3 ml and the MetAP was subsequently loaded onto a Superdex 75 Hi-load, prep-grade 16/60 gel filtration column (Pharmacia/Pfizer, New York, USA) equilibrated with 25 mM Hepes, pH 7.1, 25 mM K_2SO_4, 100 mM NaCl und further purified. Column cleaning and storage of the NTA-column: The column is washed with 100 ml of 100 mM EDTA, then with 150 ml of water and finally with 150 ml of 20 % ethanol. For storage, the enzyme is concentrated to 20-80 mg/ml and shock frozen on dry ice/ethanol or liquid nitrogen and stored at -80 °C.

7.2.3 Assays

All assays were performed in black 96-well microtiter plates with a V-bottom (Greiner, Frickenhausen, Germany, Cat.-Nr. 651209). Reagents and buffers were prepared in deionized milliQ-filtered water. The Wallac Victor multiplate reader settings were as follows:

Height of the plate	14.1 mm
Offset of the wells	11.2 mm, 14.3 mm
Distance between wells	9.0 mm, 9.0 mm
Measurement height	8.00 mm
Scanning horizontal positions	1
Scanning vertical positions	1
Scanning point displacement	1.00 mm
Scanning mode	Rectangular
Label technology	Prompt fluorometry
CW-lamp filter name	544
Emission filter name	590
Measurement time	1.0 s
Emission aperture	Normal
CW-lamp energy	2001
Emission side	Above

The measurement has to be done at room temperature (20-28 °C) as higher temperatures lead to the formation of small gas bubbles that interfere with the fluorescence measurement. Another important aspect for getting reproducible measurements is the mixing of the assay solutions. Especially after adding the detection enzymes in a relative small volume of 20 µl compared to an overall volume of 250 µl, it is important to mix the solution by extensive pipetting with the 8-way pipette. This step should be done very carefully in order to avoid the formation of air bubbles.

7.2.3.1 pH-Dependency of Fumagillin-Binding

In a typical assay, MetAP (49.33 nM) was incubated with $CoCl_2$ (1.33 mM) and buffer (25 mM tris/maleate, 0.1 % DMSO, pH 5-8.5) with and without fumagillin (66.6 µM) for 15 minutes at 37 °C (total volume 30 µl). For the ensuing Met-Gly-Met-Met hydrolysis and detection, the pH was adjusted to 7.5 by adding a mixture of substrate (MGMM), NaCl, buffer (100 mM tris/maleat pH 7.5) and BSA to a total volume of 200 µl resulting in the following concentrations in the assay: MetAP 7-8 nM, $CoCl_2$ 200 µM, NaCl 100 mM, fumagillin 10 µM, BSA 0.1 % and MGMM 200 µM. The reaction was stopped after 15 minutes at 37 °C with a mixture of EDTA/Amplex Red reagent in buffer (100 mM tris/maleate, pH 7.5). Detection was started with the addition of a mixture of horseradish peroxidase/L-amino acid oxidase resulting in a total volume of 250 µl and the following concentrations: 9 mM EDTA, 10 µM Amplex, 1.05 U HRP and 0.0075 U AAO. The resulting fluorescence was measured using a Wallac Victor^2 multiplate reader (Greiner, filters: λ_{ex}=544 nm, λ_{em}= 590 nm) and corrected by the corresponding blanks. All experiments were performed in triplicate with three independent measurements.

7.2.3.2 pH-Profile of MetAP Activity

In a typical assay, MetAP was preincubated with $CoCl_2$, buffer (100 mM tris/maleate, pH 5-8.5), MGMM, NaCl and BSA resulting in the following concentrations: MetAP 12 nM, $CoCl_2$ 200 µM, NaCl 100 mM, BSA 0.1 % (15 minutes, 37 °C, total volume 80 µl). The reaction was started by the addition of 20 µl substrate resulting in 200 µM MGMM and was stopped after 15 minutes at 37 °C and the pH adjusted to 7.4 by adding a mixture of EDTA/Amplex Red Reagent in buffer (1 M tris/maleate pH 7.4). Detection was started with the addition of a

mixture of horseradish peroxidase/L-amino acid oxidase resulting in a total volume of 250 µl and the following concentrations: 9 mM EDTA, 10 µM Amplex, 1.05 U HRP and 0.0075 U AAO. The resulting fluorescence was measured using a Wallac Victor^2 Multiplate Reader (Greiner, filters: λ_{ex}=544 nm, λ_{em}= 590 nm) and corrected by the corresponding zero values. All experiments were performed in quadruplicate.

7.2.3.3 IC_{50}-Values

The IC_{50} value is defined as the concentration of inhibitor that leads to 50 % inhibition of the enzyme. Normally, it is the result of the procentual inhibition of at least three different concentrations that have to lie in the linear range of the sigmoid IC_{50}-value curve (log (concentration of inhibitor) / % inhibition).

In a typical assay, MetAP (20 µl, 75-150 nM in buffer with 0.1 % BSA) was preincubated with $CoCl_2$ (20 µl, 2 mM), buffer (62 µl, 50 mM tris/maleate, pH 7.5), NaCl (20 µl, 1 M) and BSA (18 µl, 1 %) and with inhibitor (20 µl, different concentrations in 50 mM tris/maleate buffer pH 7.5 containing 1 % DMSO) or without inhibitor (20 µl, 50 mM tris/maleate buffer pH 7.5 containing 1 % DMSO) for 30 minutes at 37 °C. Then, the reaction was started by the addition of MGMM (40 µl, 1 mM) resulting in a total volume of 200 µl with the following concentrations: MetAP 7.5-15 nM, $CoCl_2$ 200 µM, NaCl 100 mM, BSA 0.1 % and MGMM 200 µM. The reaction was stopped after 15 minutes at 37 °C by adding a mixture of EDTA/Amplex Red Reagent (29.5 µl, 76.3 mM EDTA and 0.5 µl Amplex 5 mM). Detection was started with the addition of a mixture of horseradish peroxidase/L-amino acid oxidase (16 µl 0.065625 U/µl HRP and 4 µl, 0.001875 U/µl AAO) resulting in a total volume of 250 µl and the following concentrations: 9 mM EDTA, 10 µM Amplex, 1.05 U/well HRP and 0.0075 U/well AAO. The resulting fluorescence was measured using a Wallac Victor2^{TM} Multiplate Reader (Greiner, filters: λ_{ex}=544 nm, λ_{em}= 590 nm) for 100 min and corrected by the corresponding zero values. The IC_{50} values were obtained by calculating the mean value of three independent measurements with all experiments performed once within one assay-procedure (value with a certain inhibitor concentration and corresponding zero value). For IC_{50}-values larger than 10 µM, the procedure was the same but the IC_{50} values were obtained by calculating the mean value of three values corrected against the corresponding zero value within one measurement. Reagents and buffers were prepared in deionized milliQ-filtered water.

7.2.3.4 K_M-Values

First, a bundle of calibration curves was determined for different MGMM concentrations as described above. Instead of MetAP, buffer was used and methionine was added to give final concentrations of 0-8.75 µM in a volume of 200 µl. The final concentrations of MGMM were 100 µM. 150 µM, 200 µM, 400 µM, 800 µM, 1200 µM, 2000 µM and 3000 µM respectively and detection was started after 15 min preincubation at 37 °C. Each methionine concentration was measured in triplicate and corrected against a blank. The correlation for each curve was 0.98 or better.

After the determination of calibration curves, the K_m/K_M'-value(s) was/were determined as follows:

In a typical assay, MetAP (15-60 µl, 7.5 nM) was preincubated with $CoCl_2$ (20 µl, 2 mM), buffer (26-66.5 µl, 50 mM tris/maleate, pH 7.5), NaCl (20 µl, 1 M) and BSA (14-18,5 µl, 1 %) and with thiabendazole (20 µl, 5 µM in 50 mM tris/maleate buffer pH 7.5 containing 1 % DMSO) or without inhibitor (20 µl, 50 mM tris/maleate buffer pH 7.5 containing 1 % DMSO) for 30 minutes at 37 °C. Then, the reaction was started by the addition of the appropriate MGMM solution (40µl) resulting in a total volume of 200 µl with the following concentrations: MetAP 0.5-2 nM, $CoCl_2$ 200 µM, NaCl 100 mM, BSA 0.1 %, thiabendazole 500 nM and MGMM (100 µM-3 mM). The reaction was stopped after 15 minutes at 37 °C by adding a mixture of EDTA/Amplex Red reagent (29.5 µl, 76,3 mM EDTA and 0.5 µl Amplex 5 mM) and the released methionine was quantified as follows: Detection was started with the addition of a mixture of horseradish peroxidase/L-amino acid oxidase (16 µl 0.065625 U/µl HRP and 4 µl, 0.001875 U/µl AAO) resulting in a total volume of 250 µl and the following concentrations: 9 mM EDTA, 10 µM Amplex, 1.05 U HRP and 0.0075 U AAO. The resulting fluorescence was measured using a Wallac Victor^2 Multiplate Reader (Greiner, filters: λex=544 nm, λem= 590 nm) for 100 min and corrected by the corresponding zero values. The K_M value was obtained by calculating the conversion rate of MGMM v* and the mean substrate concentration s* (mean value of the substrate concentration at the beginning of the reaction minus substrate concentration at the end of the reaction) and by plotting 1/s* against 1/v*. The K_M-value was calculated according to the Lee and Wilson modified Lineweaver-Burk equation as the reciprocal value of the negative X-axis intercept. Normally, eight different substrate concentrations were used and the correlation was 0.98 or better. K_M values are given as the mean value of three independent measurements.

7.2.3.5 MIC-Values

The determination of MIC-values was done in 96-well-plates (Greiner, Frickenhausen, Germany). A starting culture of *E. coli* BL21(DE3) was grown overnight and used for the inoculation of the wells. First, solutions of inhibitors in DMSO (12.5 mg/ml) were diluted 1:47.5 with LB-medium (with and without added $CoCl_2$) to give 263 µg/ml with 2 % DMSO (and possibly $CoCl_2$). The following 1:1 dilutions were done with LB-medium containing 2 % DMSO (and possibly $CoCl_2$). Ciprofloxacin was dissolved in 10 % HOAc to 10 mg/ml and a solution of 3.125 µg/ml was done that was further diluted 1:47.5 with LB-medium containing 2 % DMSO. 190 µl of each solution (containing the desired concentration of inhibitor, 2 % DMSO and possibly $CoCl_2$) was placed in a well and 10 µl of the bacterial culture was added. Thus, the final dilution of inhibitors was 1:50 (250 µg/ml). The starting culture was diluted with LB before in such a way that the resulting increase in OD_{590} in each inoculated well was about 0.02. Starting ODs were in the range of 0.1. The plate was incubated at 37 °C and bacteria growth was followed with the Victor Wallac Multiplate reader. The OD_{590} after different times (16 hrs, 45 hrs) of incubation were measured and used for the determination of the MIC-value by comparison against a control (LB, 2 % DMSO and possibly $CoCl_2$ without an inhibitor).

7.2.4 Other Biochemical Methods

7.2.4.1 Working with Proteins

7.2.4.1.1 SDS-Polyacrylamide Gel Electrophoresis (SDS-PAGE)

Proteins can be separated in an electrical field according to their molecular weights with use of the SDS-PAGE[224]. The addition of sodium-dodecylsulfat (as an anionic detergent) to a sample of proteins has several effects: SDS masks the individual charge of a protein. The binding of SDS is proportional to the mass of a protein (1.4 g SDS / g protein). Thus, all proteins are negatively charged and migrate to the anode. Additionaly, SDS breakes H-bonds and hydrophobic interactions. Secondary structures get lost and the proteins are denaturated. The addition of the reducing agent Dithiothreitol (DTT) cleaves disulfide-bonds and abolishes tertiary- and quartenary structures.

The pore size and the separating characteristics depend on the acrylamide-/bisacrylamide concentration of the gel. Normally, 10 or 12.5 % are used according to the size of the proteins and a constant voltage of 120 – 150 V is applied to vertical flatbed gels (8.0 cm x 5,5 cm x 0.075 cm).

For sample preparation the mixture is incubated with reducing sample buffer at 95 °C for 5 min. A small stacking gel is used for concentration of the sample. The molecular weight can be determined with the help of a reference (marker) that contains proteins with a defined MW. Prestained SDS-PAGE Standards Low Range (Prestained Marker BioRad, Kalifornien, USA) was used.

Acrylamid-Gel-Solution:	Acrylamide 30 % (w/v), Bisacrylamide 0.8 % (w/v)
Stacking buffer (4x) pH 6.8:	Tris-HCl (pH 6.8) 0,5 M, SDS 0.4 % (w/v), TEMED 0.4 % (v/v)
Seperating buffer (4x) pH 8.8:	Tris-HCl (pH 8.8) 1,5 M, SDS 0.4 % (w/v), TEMED 0.4 % (v/v)
Ammoniumperoxodisulfat (APS):	10 % (w/v) in MilliQ-water
Reducing sample buffer (2x):	Tris-HCl (pH 6.8) 0,125 M, SDS 4 % (w/v), Glycerole 20 % (v/v), EDTA 2 mM, Bromphenol blue 0.02 % (w/v), DTT 194 mM
SDS-Running-Buffer (10x):	Tris 0.25 M, Glycine 1.92 M, SDS 1 %

Separating-Gel (10 %) example

3.3 ml Acrylamide-solution

2.5 ml Separating Buffer (4x)

4.1 ml MilliQ

0.1 ml 10 % Ammoniumperoxodisulfat solution

Stacking-Gel example

0.44 ml Acrylamide--solution

0.83 ml Stacking-Gel-Buffer (4x)

2.06 ml MilliQ

0.02 ml 10 % Ammoiumperoxodisulfat solution

Table 7-1 Constitution of stacking gels and of separating gels

	Stacking gel	**Separating gel (10 %)**	**Separating gel (12,5 %)**
Acrylamide-Solution	4 % (w/v)	10 % (w/v)	12.5 % (w/v)
Tris-HCl pH 8.8	-	0.375 M	0.375 M
Tris-HCl pH 6.8	0.125 M	-	-
TEMED	0.1 % (v/v)	0.1 % (v/v)	0.1 % (v/v)
SDS	0.1 % (w/v)	0.1 % (w/v)	0.1 % (w/v)
APS	0.6 % (w/v)	0.1 % (w/v)	0.1 % (w/v)

Table 7-2 Constitution of prestained marker BioRad

Protein	**Molecular weight (Dalton)**
Phosphorylase B	113,000
Bovine serum albumin	92,000
Ovalbumin	52,300
Carbonic anhydrase	35,300
Soybean trypsin inhibitor	28,700
Lysozyme	21,300

7.2.4.1.2 Staining of Protein Gels

Gels were stained with the colloidal-coomassie-method according to Neuhoff. Coomassie Brilliant Blue G-250 is an acidic dye that unspecifically binds to cationic and hydrophobic protein side chains. 10 % acetic acid was used for decolorizing. For documentation the gels were incubated for 30 min in a solution 10 % glycerole in water and then dried between two layers of plastic film (Bringmann, Wendelstein, Germany).

7.2.4.1.3 Buffer Exchange and Concentration of Protein Solutions

For the concentration of the protein solution, ultrafiltration was used. Ultrafiltration is a convective process that uses anisotropic semi-permeable membranes to separate macromolecular species and solvents primarily on the basis of size. It is particularly appropriate for the concentration of macromolecules and can also be used to purify molecular species or for solvent exchange. Ultrafiltration is a gentle, non denaturing method that is more efficient and flexible than alternative processes. In this case, Vivaspin 20 (Cat-Nr. VS2001) and Vivaspin 4 (Cat-Nr. VS0403) were used with a cutoff of 10 kDa and a PES-mebrane.

7.2.4.1.4 MALDI-TOF-MS and ESI-MS-MS-Measurements

For the determination of the molecular weight of EcMetAP before and after the cleavage of the His-tag, a protein solution of about 3 mg/ml in buffer was measured in the positive, linear mode with sinapinic acid as matrix for the MALDI-TOF-MS-measurement. The same solution was measured with the ESI-MS-MS with the addition of 1% HOAc with 100 scans (1 scan defined as the average of 10 scans) between 400 and 1500 Da.

7.2.4.2 Working with *Escherichia coli*

7.2.4.2.1 Handling of Strains

Newly transformed strains were stored at -70 °C to protect them from contamination and from losing their original or newly gained function(s). When needed, they can be freshly cultured. For the storage of a strain, the bacteria of a complete grown plate are gathered with a sterile cotton tip and are then resuspended in 1.8 ml PPM-medium (15 g Proteose Pepton, 5 g NaCl, 1 g starch, 1 g KH_2PO_4, 0.8 g K_2HPO_4, 232.5 ml glycerine 86 %, aqua dest. ad 1000 ml) that is distributed on two vials with glass beads for cryoconservation with ethanol/dry ice.

7.2.4.2.2 Preparation of Competent Cells

Several transformation methods such as electroporation or heat shock can be used to transport foreign DNA material into *E. coli*. Only cells that have been prepared for DNA uptake by pre-treatment can be used, so called competent cells. Different protocols exist depending on the method used for transformation. For the generation of chemical competent cells the cells were treated as described by Inoue et al.[225], for the generation of electrocompetent cells, the protocol of Neumann was applied[226].

7.2.4.2.3 Transformation of Competent Cells

Transformation of competent made cells was done either by the SEM method or by electroporation. The protocols are listed below:

SEM method:

- → competent cells are carefully thawed and kept on ice
- → DNA is added (max. 10 µl per 100 µl cells) and incubated for 30 min
- → a heat shock is applied: 30 sec 42° C, then the cells are directly kept on ice again
- → 0.8 ml SOC medium are added and mixed carefully
- → incubation at 37° C at 200 U/min for 1h
- → plating

Electroporation:

- → competent cells are carefully thawed and kept on ice
- → DNA is added (max. 10 µl per 100 µl cells)
- → the mixture is filled in a special 1mm cuvette for electraporation and an impulse of 1800 V is applied
- → 1.0 ml SOC medium are added and mixed carefully
- → incubation at 37° C at 50 U/min for 2h
- → plating

7.2.4.2.4 Media

Luria-Bertani-Medium (LB-Medium)[227] was used to breed bacteria. The pH was adjusted to 7.3 before autoclaving. The addition of kanamycin allowed the selection of plasmid containing cells. For this reason, 50 or 100 mg kanamycin were added per liter of medium. SOC-Medium is used for the regeneration and for the growth of freshly transformed cells.

Luria-Bertani-Medium (LB-Medium)

Trypton	10.0 g
Yeast extract	5.0 g
NaCl	5.0 g
MilliQ-Waterr	ad 1000.0 ml

SOC Medium

Trypton	20.0 g
Yeast extrakt	5.0 g
NaCl	0.5 g
KCl (250 mM Sol.)	10.0 ml
MilliQ-Water	975 ml

The pH-value is adjusted to 7.0 with NaOH. After autoclaving the following solutions were made sterile by filtration and added:

Glucose (1 M Lsg.)	20.0 ml
$MgCl_2$ (2 M Lsg.)	5.0 ml

7.2.4.2.5 LB Agar-Plates

For the production of agar plates, 16.0 g Agar were used per liter LB-Medium. The pH was adjusted to before autoclaving. Kanamycin was added afterwards at about 60 °C.

7.2.4.3 Working with DNA

7.2.4.3.1 Plasmid Isolation

Kits from diverse companies (GFX Micro Plasmid Prep Kit (Amersham Biosciences), E.Z.N.A.® Plasmid Miniprep Kit I and II, peqlab, Erlangen, Deutschland) were used for the isolation of plasmids. They all share a common principle: The cells are lysed open by an alcalic hydrolisis. The purification of plasmid-DNA is done by anion-exchange chromatography. The backbone of nucleic acids contains phophate groups that are negatively charged at pH-values larger than 2 and thus bind to the anion-exchange column and can be eluted with water or buffer. Instructions are provided with every kit and were used according to the manufacturers' instructions.

7.2.4.3.2 Digestion with Restriction Enzymes

Restriction enzymes recognize specific DNA sequences and cut the DNA in a way that fragments with defined ends and sizes are generated. The applied incubation conditions and concentrations of the used reagents correspond to the manufacturers' instructions.

7.2.4.3.3 Gel Electrophoresis

Agarose gel electrophoresis is used for the separation of DNA fragments and for the determination of their size. Negatively charged nucleic acids move to the anode in an electrical field with small fragments moving faster. Separation is performed with 0.8 % or 1.5 % agarose gels. Agar is dissolved in TA-buffer (40 mM Tris, 10 mM Na-acetate, 1mM EDTA, pH 7.8) with heating. DNA samples are diluted 1:10 with sample buffer (10x, 1 % SDS, 50 % glycerole, 0.05 % Bromphenolblue, Takara, Otsu, Japan). Thus, the density is increased and the samples can be pipetted in the pockets of the gel and sink down. A voltage of about 100 V is applied.

The gel is incubated for at least 30 min in ethidiumbromide (1 µg/ml) for detection. Then it is washed with water and the ethidiumbromid that intercalates in the double-stranded DNA can be detected at 312 nm due to its fluorescing properties and can be documented *via* a camera-system.

The size of the DNA fragments can be determined with the help of a reference (marker). A 100 Bp Ladder (Promega; Madison, USA) and a 1 kBp Ladder (Promega; Madison, USA) or alternatively the Lambda DNA-HindIII Marker (New England Biolabs; Frankfurt, Germany) were used as an internal standard within a gel.

7.3 Structural Biology

7.3.1 Material

All crystallization experiments were done with Cryschem Plates (Sitting Drop Plates, HR3-160), Hampton Research, USA) in cooperation with AG Klebe (Department of Pharmaceutical and Medicinal Chemistry, Marburg University).

7.3.2 Crystallization of apo-EcMetAP

Ten different crystal screens (with 48 conditions each) varying in pH, precipitant(s), buffers and additives were tested with different protein concentrations (9 mg/ml, 13 mg/ml, 18 mg/ml, 24 mg/ml and 32 mg/ml), different protein charges, apo-MetAP and His-tagged MetAP and with and without the addition of N-octanoylsucrose but without success. Only salt-crystals were obtained, possibly because of the presence of K_2SO_4 in the protein buffer. Thus, K_2SO_4 was substituted by KCl.

Crystals were grown using a slight modification of the conditions described before[52]. In brief, **freshly prepared** enzyme was kept in buffer containing 25 mM Hepes, pH 6.8, 25 mM KCl, 100 mM NaCl, 1 mM $CoCl_2$, and 15 mM methionine. Crystals of the Co(II)-substituted enzyme were obtained over night at 22 °C by vapor diffusion in 20 µl sitting drops after mixing the protein solution in buffer (13.5 mg/ml) to which N-octanoylsucrose (Calbiochem-Novabiochem Corp., La Jolla, CA) was added to a concentration of 48.8 mM, 1:1 with well solutions (500 µl) containing 24-33 % PEG 4000, 0.1 M Hepes, pH 7.1 and fresh 2 mM $CoCl_2$.

A typical plate for a screening from 10-45% PEG is depicted in Fig. 7-4

100 µl	50 % PEG	180 µl	50 % PEG	250 µl	50 % PEG	290 µl	50 % PEG	330 µl	50 % PEG	390 µl	50 % PEG
50 µl	Buffer	50 µl	Buffer	50 µl	Buffer	50 µl	Buffer	50 µl	Buffer	50 µl	Buffer
350 µl	Water	270 µl	Water	200 µl	Water	160 µl	Water	120 µl	Water	60 µl	Water
120 µl	50 % PEG	200 µl	50 % PEG	260 µl	50 % PEG	300 µl	50 % PEG	340 µl	50 % PEG	410 µl	50 % PEG
50 µl	Buffer	50 µl	Buffer	50 µl	Buffer	50 µl	Buffer	50 µl	Buffer	50 µl	Buffer
330 µl	Water	250 µl	Water	190 µl	Water	150 µl	Water	110 µl	Water	40 µl	Water
140 µl	50 % PEG	220 µl	50 % PEG	270 µl	50 % PEG	310 µl	50 % PEG	350 µl	50 % PEG	430 µl	50 % PEG
50 µl	Buffer	50 µl	Buffer	50 µl	Buffer	50 µl	Buffer	50 µl	Buffer	50 µl	Buffer
310 µl	Water	230 µl	Water	180 µl	Water	140 µl	Water	50 µl	Water	20 µl	Water
160 µl	50 % PEG	240 µl	50 % PEG	280 µl	50 % PEG	320 µl	50 % PEG	370 µl	50 % PEG	450 µl	50 % PEG
50 µl	Buffer	50 µl	Buffer	50 µl	Buffer	50 µl	Buffer	50 µl	Buffer	50 µl	Buffer
290 µl	Water	210 µl	Water	170 µl	Water	130 µl	Water	80 µl	Water	0 µl	Water

Fig. 7-4 Scheme for the pipetting of mother liquor of a PEG-screening in a typical sitting-drop crystallization plate

7.3.3 Co-Crystallization of Inhibitors with EcMetAP

Crystals of the thiabendazole complex were obtained by incubating the enzyme (13.5 mg/ml, 0.43 mM, 49.8 mM N-octanoylsucrose) at room temperature for 5 min with a solution of thiabendazole dissolved in DMSO at 21.8 mg/ml (109 mM) (122.5 µl protein-solution + 2.5 µl inhibitor solution). The final inhibitor:enzyme ratio was 5:1 (1 % DMSO, 24.4 mM N-octanoylsucrose) after mixing the preformed complex 1:1 with well solution (0.1 M Hepes, pH 7.1, 2 mM $CoCl_2$ and 24-33 % PEG 4000).

For compound RS 17, the inhibitor-enzyme ratio was 2.5 : 1 and the well solution contained 4 mM $CoCl_2$. Only a single crystal was obtained with these conditions.

7.3.4 Data Collection and Refinement

The data set was collected on a Rigaku/MSC rotating anode generator (RU 300) operated at 50 kV, 90 mA equipped with a Raxis 4++ imaging plate detector. 360 frames with $\delta(\varphi) = 0.5°$ at a crystal-to-detector distance of 100 mm were collected at -170 °C with 18 % glycerole in mother liquid as cryoprotectant. For compound RS 17, the data set was collected with a Raxis

4 imaging plate according to the conditions and parameters mentioned and consisted of 240 frames.

Data were processed and scaled with HKL 2000[228]. The MetAP-structure published by Lowther and coworkers[52](PDB code 2MAT) was used without the cobalt atoms or water molecules as a starting model for molecular replacement in PHASER[229] followed by a rigid body refinement in CNS[230]. Initial refinement was continued in CNS using positional and slow-cooling protocols followed by restrained B-value refinement. Refinement was then continued with SHELXL-97[231]. At least 20 cycles of conjugate gradient minimization with restraints on bond distances, angles, and B-values were performed for each refinement step. In the final stages, hydrogen atoms were placed in calculated positions without use of additional parameters. Intermittent cycles of model building were done with the program O[232].

The coordinates have been deposited in the PDB (http://www.rcsb.org/pdb/) with access code 1YVM. All images were created with PYMOL[233].

8 Appendix

Listed below are the results of inhibition tests of various substances against Co(II)-loaded EcMetAP:

Table 8-1 Inhibition tests of aldehydes against Co(II)-loaded EcMetAP

Compound	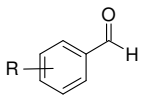	IC_{50} [µM]	% inhibition (at a certain concentration)
Benzaldehyde	R = H	> 300	34 % inhibition at 300 µM
2-Hydroxy-benzaldehyde	2-OH	5.9	
3-Hydroxy-benzaldehyde	3-OH	105.7	
4-Hydroxy-benzaldehyde	4-OH	> 300	6 % inhibition at 100 µM 8 % inhibition at 300 µM
2-Methoxy-benzaldehyde	2-OMe	> 300	36 % inhibition at 300 µM
3-Methoxy-benzaldehyde	3-OMe	100-300	32 % inhibition at 100 µM 61 % inhibition at 300 µM
4-Methoxy-benzaldehyde	4-OMe	> 300	29 % inhibition at 300 µM
2-Nitro-benzaldehyde	2-NO_2	> 300	0 % inhibition at 100 µM 23 % inhibition at 300 µM
3-Nitro-benzaldehyde	3- NO_2	35.0	
4-Nitro-benzaldehyde	4- NO_2	45.2	
Vanilline	4-OH, 3-OMe	> 300	32 % inhibition at 300 µM
2,4-Dichloro-benzaldehyde	2-Cl, 4-Cl	>> 100	0 % inhibition at 100 µM

Table 8-2 Inhibition tests of styrenes against Co(II)-loaded EcMetAP

Compound	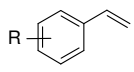	IC_{50} [µM]	% inhibition (at a certain concentration)
Vinyl-benzene	R = H	> 300	4 % inhibition at 300 µM
2-Vinyl-phenole	2-OH	> 300	2 % inhibition at 300 µM
3-Vinyl-phenol	3-OH	> 300	2 % inhibition at 300 µM
4-Vinyl-phenol	4-OH	> 300	4 % inhibition at 300 µM
1-Methyl-2-vinyl-benzene	2-Me	> 300	30 % inhibition at 300 µM
1-Methyl-3-vinyl-benzene	3-Me	> 300	9 % inhibition at 300 µM
1-Methyl-4-vinyl-benzene	4-Me	> 300	2 % inhibition at 300 µM

Table 8-3 Inhibition tests of carboxylic acids against Co(II)-loaded EcMetAP

Compound	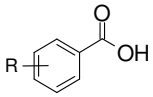	IC_{50} [µM]	% inhibition (at a certain concentration)
2-Hydroxy-benzoic acid	2-OH	> 100	0 % inhibition at 100 µM
3-Amino-benzoic acid	3-NH_2	> 100	0 % inhibition at 100 µM
4-Amino-benzoic acid	4-NH_2	> 100	0 % inhibition at 100 µM
2-Nitro-benzoic acide	2-NO_2	> 100	0 % inhibition at 100 µM
3-Nitro-benzoic acid	3- NO_2	> 100	0 % inhibition at 100 µM
4-Nitro-benzoic acid	4- NO_2	> 100	0 % inhibition at 100 µM
Nicotinic acid	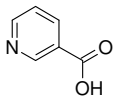	> 300	0 % inhibition at 300 µM
Pyridine-2-carboxylic acid	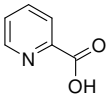	20.3	

Table 8-4 Inhibition tests of sulfonamides against Co(II)-loaded EcMetAP

Compound	IC_{50} [µM]	% inhibition (at a certain concentration)
Sulfamethoxazol	68,0	
Sulfaphenazol	> 300	0 % inhibition at 300 µM
Sulfathiazol	> 300	36 % inhibition at 300 µM
Sulfatdiazin	> 300	17 % inhibition at 300 µM
Sulfaguanidin	> 300	0 % inhibition at 300 µM
Sulfisoxazol	> 300	0 % inhibition at 300 µM
Sulfanilamid	> 300	0 % inhibition at 300 µM
Sulfadimidin	> 300	24 % inhibition at 300 µM
Sulfamoxol	> 300	37 % inhibition at 300 µM
Sulfadimethoxin	> 300	20 % inhibition at 300 µM
Sulfisomidin	> 300	0 % inhibition at 300 µM

Table 8-5 Inhibition tests of drugs and drug-like substances against Co(II)-loaded EcMetAP

Compound		IC_{50} [µM]	% inhibition (at a certain concentration)
Cyclohexanone		> 300	9 % inhibition at 100 µM[a] 9 % inhibition at 300 µM
SU6A	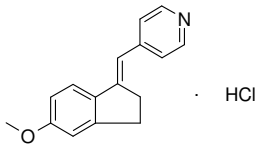	> 100	7 % inhibition at 100 µM
SU21A	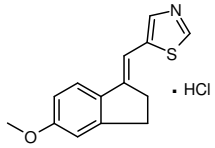	> 100	24 % inhibition at 100 µM
Thiamine dichloride	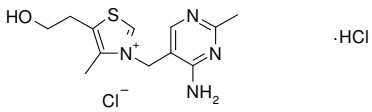	> 300	17 % inhibition at 300 µM
Isoniazid	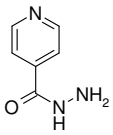	10-100	26 % inhibition at 10 µM 56 % inhibition at 100 µM
Desipramine-HCl	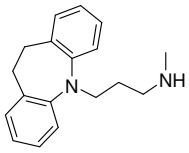	> 100	29 % inhibition at 100 µM
Nalidixic acid	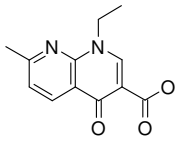	> 10	10 % inhibition at 10 µM
Niclosamid	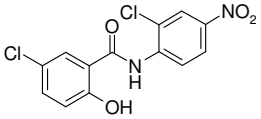	> 25	31 % inhibition at 10 µM
Salicylanilide	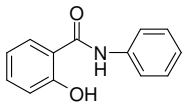	> 100	21 % inhibition at 100 µM
GK01664	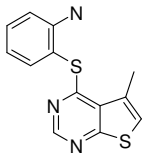	>> 1	0 % inhibition at 1 µM
SPB06965	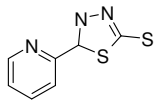	>> 1	10 % inhibition at 1 µM
Phenoxymethylpenicilline	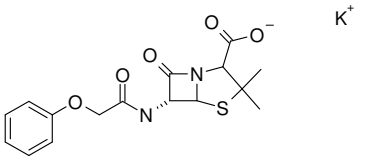	>> 10	0 % inhibition at 10 µM

a) 15 min preincubation

Table 8-6 Inhibition tests of synthetic intermediates and other small molecules against Co(II)-loaded EcMetAP

Compound			IC_{50} [µM]	% inhibition (at a certain concentration)
RS 70	1-(2-Chloro-cyclohex-2-enyl)-ethanone	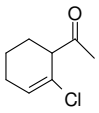	> 100	9 % inhibition at 100 µM[a] 19 % inhibition at 300 µM
RS 71	1-(1,4-Dioxa-spiro[4.5]dec-6-yl)-ethanone	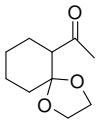	> 100	3 % inhibition at 100 µM[a] 10 % inhibition at 300 µM
RS 72	6-((E)-1-Methyl-propenyl)-1,4-dioxa-spiro[4.5]decane	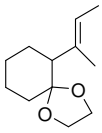	> 100	3 % inhibition at 100 µM[a] 13 % inhibition at 300 µM
RS 73	2-((E)-1-Methyl-propenyl)-cyclohexanone	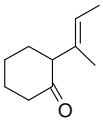	> 100	22 % inhibition at 100 µM[a] 47 % inhibition at 300 µM
RS 74	Benzoic acid 3-methyl-but-2-enyl ester	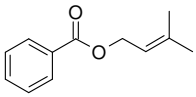	> 300	0 % inhibition at 100 µM
RS 75	4-Methyl-N-pyridin-3-yl-benzenesulfonamide	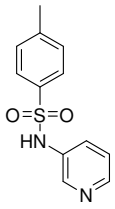	>> 10	0 % inhibition at 10 µM

a) 15 min preincubation

9 References

1. World Health Organization, *The World Health Report 2004: Changing History.* http://www.who.int/whr/2004/en/report04_en.pdf, 2004.
2. Devlin, P.E., et al., *Alteration of amino-terminal codons of human granulocyte-colony-stimulating factor increases expression levels and allows efficient processing by methionine aminopeptidase in Escherichia coli.* Gene, 1988, **65**(1), 13-22.
3. Miller, C.G., et al., *N-terminal methionine-specific peptidase in Salmonella typhimurium.* Proceedings of the National Academy of Sciences of the United States of America, 1987, **84**(9), 2718-2722.
4. Ben-Bassat, A., et al., *Processing of the initiation methionine from proteins: properties of the Escherichia coli methionine aminopeptidase and its gene structure.* Journal of Bacteriology, 1987, **169**(2), 751-757.
5. Liu, L.F., et al., *Escherichia coli methionine aminopeptidase with Tyr168 to alanine substitution can improve the N-terminal processing of recombinant proteins with valine at the penultimate position.* Analytical Biochemistry, 2004, **329**(2), 345-347.
6. Tsunasawa, S., et al., *Methionine aminopeptidase from the hyperthermophilic Archaeon Pyrococcus furiosus: molecular cloning and overexpression in Escherichia coli of the gene, and characteristics of the enzyme.* Journal of Biochemistry (Tokyo), 1997, **122**(4), 843-850.
7. Matheson, A.T., A.J. Dick, and F. Rollin, *A ribosomal-bound aminopeptidase in Escherichia coli B: substrate specificity.* Canadian Journal of Biochemistry, 1970, **48**(12), 1292-1296.
8. Vogt, V.M., *Purification and properties of an aminopeptidase from Escherichia coli.* Journal of Biological Chemistry, 1970, **245**(18), 4760-4769.
9. Kendall, R.L. and R.A. Bradshaw, *Isolation and Characterization of the Methionine Aminopeptidase from Porcine Liver Responsible for the Co-translational Processing of Proteins.* Journal of Biological Chemistry, 1992, **267**, 20667-20673.
10. Kerwar, S.S., H. Weissbach, and G.G. Glenner, *An aminopeptidase activity associated with brain ribosomes.* Archives of Biochemistry and Biophysics, 1971, **143**(1), 336-337.
11. Yoshida, A. and M. Lin, *NH 2 -terminal formylmethionine- and NH 2 -terminal methionine-cleaving enzymes in rabbits.* Journal of Biological Chemistry, 1972, **247**(3), 952-957.
12. Giglione, C., et al., *Identification of eukaryotic peptide deformylases reveals universality of N-terminal protein processing mechanisms.* EMBO Journal, 2000, **19**(21), 5916-5929.
13. Arfin, S.M., et al., *Eukaryotic methionyl aminopeptidases: two classes of cobalt-dependent enzymes.* Proceedings of the National Academy of Sciences of the United States of America, 1995, **92**(17), 7714-7718.
14. Bazan, J.F., et al., *Sequence and structure comparison suggest that methionine aminopeptidase, prolidase, aminopeptidase P, and creatinase share a common fold.* Proceedings of the National Academy of Sciences of the United States of America, 1994, **91**(7), 2473-2477.
15. Bradshaw, R.A., W.W. Brickey, and K.W. Walker, *N-terminal processing: the methionine aminopeptidase and N alpha-acetyl transferase families.* Trends in Biochemical Sciences, 1998, **23**(7), 263-267.
16. Zuo, S., et al., *Evidence that two zinc fingers in the methionine aminopeptidase from Saccharomyces cerevisiae are important for normal growth.* Molecular and General Genetics, 1995, **246**(2), 247-253.
17. Wu, S., et al., *Cloning and characterization of complementary DNA encoding the eukaryotic initiation factor 2-associated 67-kDa protein (p67).* Journal of Biological Chemistry, 1993, **268**(15), 10796-10801.
18. Datta, B. and R. Datta, *Induction of apoptosis due to lowering the level of eukaryotic initiation factor 2-associated protein, p67, from mammalian cells by antisense approach.* Experimental Cell Research, 1999, **246**(2), 376-383.
19. Datta, B., *MAPs and POEP of the roads from prokaryotic to eukaryotic kingdoms.* Biochimie, 2000, **82**(2), 95-107.

20. Ray, M.K., et al., *The eukaryotic initiation factor 2-associated 67-kDa polypeptide (p67) plays a critical role in regulation of protein synthesis initiation in animal cells.* Proceedings of the National Academy of Sciences of the United States of America, 1992, **89**(2), 539-543.
21. Endo, H., et al., *Methionine aminopeptidase 2 is a new target for the metastasis-associated protein, S100A4.* Journal of Biological Chemistry, 2002, **277**(29), 26396-26402.
22. Keeling, P.J. and W.F. Doolittle, *Methionine aminopeptidase-1: the MAP of the mitochondrion?* Trends in Biochemical Sciences, 1996, **21**(8), 285-286.
23. Kozak, M., *Comparison of initiation of protein synthesis in procaryotes, eucaryotes, and organelles.* Microbiological Reviews, 1983, **47**(1), 1-45.
24. Leon, M., et al., *Recognition of tRNA Trp by initiation factors from Escherichia coli.* European Journal of Biochemistry, 1979, **98**(1), 149-154.
25. Lucas-Lenard, J. and F. Lipmann, *Initiation of polyphenylalanine synthesis by N-acetylphenylalanyl-SRNA.* Proceedings of the National Academy of Sciences of the United States of America, 1967, **57**(4), 1050-1057.
26. Varshney, U. and U.L. RajBhandary, *Initiation of protein synthesis from a termination codon.* Proceedings of the National Academy of Sciences of the United States of America, 1990, **87**(4), 1586-1590.
27. Sasaki, J. and N. Nakashima, *Methionine-independent initiation of translation in the capsid protein of an insect RNA virus.* Proceedings of the National Academy of Sciences of the United States of America, 2000, **97**(4), 1512-1515.
28. Old, I.G., et al., *Regulation of methionine biosynthesis in the Enterobacteriaceae.* Progress in Biophysics and Molecular Biology, 1991, **56**(3), 145-185.
29. Meinnel, T., Y. Mechulam, and S. Blanquet, *Methionine as translation start signal: a review of the enzymes of the pathway in Escherichia coli.* Biochimie, 1993, **75**(12), 1061-1075.
30. Waller, J.P., *The Nh2-Terminal Residues Of The Proteins From Cell-Free Extracts Of E. Coli.* Journal of Molecular Biology, 1963, **62**, 483-496.
31. Arfin, S.M. and R.A. Bradshaw, *Cotranslational processing and protein turnover in eukaryotic cells.* Biochemistry, 1988, **27**(21), 7979-7984.
32. Solbiati, J., et al., *Processing of the N Termini of Nascent Polypeptide Chains Requires Deformylation Prior to Methionine Removal.* Journal of Molecular Biology, 1999, **290**, 607-614.
33. Flinta, C., et al., *Sequence determinants of cytosolic N-terminal protein processing.* European Journal of Biochemistry, 1986, **154**(1), 193-196.
34. Sherman, F., J.W. Stewart, and S. Tsunasawa, *Methionine or not methionine at the beginning of a protein.* Bioessays, 1985, **3**(1), 27-31.
35. Bachmair, A., D. Finley, and A. Varshavsky, *In vivo half-life of a protein is a function of its amino-terminal residue.* Science, 1986, **234**(4773), 179-186.
36. Gonda, D.K., et al., *Universality and structure of the N-end rule.* Journal of Biological Chemistry, 1989, **264**(28), 16700-16712.
37. Peseckis, S.M., I. Deichaite, and M.D. Resh, *Iodinated fatty acids as probes for myristate processing and function. Incorporation into pp60v-src.* Journal of Biological Chemistry, 1993, **268**(7), 5107-5114.
38. Dummitt, B.W., W.S. Micka, and Y.H. Chang, *Yeast glutamine-fructose-6-phosphate amidotransferase (GFA1) requires methionine aminopeptidase activity for proper function.* Journal of Biological Chemistry, 2005.
39. Towler, D.A., et al., *The biology and enzymology of eukaryotic protein acylation.* Annual Review of Biochemistry, 1988, **57**, 69-99.
40. Dummitt, B., W.S. Micka, and Y.H. Chang, *N-terminal methionine removal and methionine metabolism in Saccharomyces cerevisiae.* Journal of Cellular Biochemistry, 2003, **89**(5), 964-974.
41. Chang, S.Y., E.C. McGary, and S. Chang, *Methionine aminopeptidase gene of Escherichia coli is essential for cell growth.* Journal of Bacteriology, 1989, **171**(7), 4071-4072.
42. Li, X. and Y.H. Chang, *Amino-terminal protein processing in Saccharomyces cerevisiae is an essential function that requires two distinct methionine aminopeptidases.* Proceedings of the National Academy of Sciences of the United States of America, 1995, **92**(26), 12357-12361.

43. Miller, C.G., et al., *pepM is an essential gene in Salmonella typhimurium.* Journal of Bacteriology, 1989, **171**(9), 5215-5217.
44. Chang, Y.H., U. Teichert, and J.A. Smith, *Molecular cloning, sequencing, deletion, and overexpression of a methionine aminopeptidase gene from Saccharomyces cerevisiae.* Journal of Biological Chemistry, 1992, **267**(12), 8007-8011.
45. Hirel, P.H., et al., *Extent of N-terminal methionine excision from Escherichia coli proteins is governed by the side-chain length of the penultimate amino acid.* Proceedings of the National Academy of Sciences of the United States of America, 1989, **86**(21), 8247-8251.
46. Utsumi, T., et al., *Amino acid residue penultimate to the amino-terminal gly residue strongly affects two cotranslational protein modifications, N-myristoylation and N-acetylation.* Journal of Biological Chemistry, 2001, **276**(13), 10505-10513.
47. Chen, S., J.A. Vetro, and Y.H. Chang, *The specificity in vivo of two distinct methionine aminopeptidases in Saccharomyces cerevisiae.* Archives of Biochemistry and Biophysics, 2002, **398**(1), 87-93.
48. Lowther, W.T., et al., *Insights into the mechanism of Escherichia coli methionine aminopeptidase from the structural analysis of reaction products and phosphorus-based transition-state analogues.* Biochemistry, 1999, **38**(45), 14810-14819.
49. Pettersen, E.F., et al., *UCSF Chimera--a visualization system for exploratory research and analysis.* Journal of Computational Chemistry, 2004, **25**(13), 1605-1612.
50. Chiu, C.H., et al., *Amino acid residues involved in the functional integrity of Escherichia coli methionine aminopeptidase.* Journal of Bacteriology, 1999, **181**(15), 4686-4689.
51. Roderick, S.L. and B.W. Matthews, *Structure of the cobalt-dependent methionine aminopeptidase from Escherichia coli: a new type of proteolytic enzyme.* Biochemistry, 1993, **32**(15), 3907-3912.
52. Lowther, W.T., et al., *Escherichia coli methionine aminopeptidase: implications of crystallographic analyses of the native, mutant, and inhibited enzymes for the mechanism of catalysis.* Biochemistry, 1999, **38**(24), 7678-7688.
53. Lowther, W.T. and B.W. Matthews, *Structure and function of the methionine aminopeptidases.* Biochimica et Biophysica Acta, 2000, **1477**(1-2), 157-167.
54. Walker, K.W. and R.A. Bradshaw, *Yeast methionine aminopeptidase I. Alteration of substrate specificity by site-directed mutagenesis.* Journal of Biological Chemistry, 1999, **274**(19), 13403-13409.
55. Li, J.Y., et al., *Mutations at the S1 site of methionine aminopeptidases from Escherichia coli and homo sapiens reveal the residues critical for substrate specificity.* Journal of Biological Chemistry, 2004, **279**(20), 21128-21134.
56. Liu, S., et al., *Structure of human methionine aminopeptidase-2 complexed with fumagillin.* Science, 1998, **282**(5392), 1324-1327.
57. Cui, Y.M., et al., *Design and synthesis of chromogenic thiopeptolide substrates as MetAPs active site probes.* Bioorganic and Medicinal Chemistry, 2004, **12**(11), 2853-2861.
58. Lowther, W.T. and B.W. Matthews, *Metalloaminopeptidases: common functional themes in disparate structural surroundings.* Chemical Reviews, 2002, **102**(12), 4581-4608.
59. Wingfield, P., et al., *Purification and characterization of a methionine-specific aminopeptidase from Salmonella typhimurium.* European Journal of Biochemistry, 1989, **180**(1), 23-32.
60. Movva, N.R., et al., *Cloning and nucleotide sequence of the Salmonella typhimurium pepM gene.* Molecular and General Genetics, 1990, **223**(2), 345-348.
61. Chang, Y.H., U. Teichert, and J.A. Smith, *Purification and characterization of a methionine aminopeptidase from Saccharomyces cerevisiae.* Journal of Biological Chemistry, 1990, **265**(32), 19892-19897.
62. Atanassova, A., et al., *Molecular cloning, expression and characterization of three distinctive genes encoding methionine aminopeptidases in cyanobacterium Synechocystis sp. strain PCC6803.* Archives of Microbiology, 2003, **180**(3), 185-193.
63. Dummitt, B., Y. Fei, and Y.H. Chang, *Functional expression of human methionine aminopeptidase type 1 in Saccharomyces cerevisiae.* Protein and Peptide Letters, 2002, **9**(4), 295-303.
64. Tahirov, T.H., *Crystallization and preliminary X-ray analysis of methionine aminopeptidase from the hyperthermophilic bacterium Pyrococcus furiosus.* Acta Crystallographica, D Biological Crystallography, 1997, **53**(Pt 6), 798-801.

65. Ogasahara, K., et al., *Electrostatic stabilization in methionine aminopeptidase from hyperthermophile Pyrococcus furiosus.* Biochemistry, 1998, **37**(17), 5939-5946.

66. Tahirov, T.H., et al., *Crystal structure of methionine aminopeptidase from hyperthermophile, Pyrococcus furiosus.* Journal of Molecular Biology, 1998, **284**, 101-124.

67. Vetro, J.A. and Y.H. Chang, *Yeast methionine aminopeptidase type 1 is ribosome-associated and requires its N-terminal zinc finger domain for normal function in vivo.* Journal of Cellular Biochemistry, 2002, **85**(4), 678-688.

68. Vetro, J.A., et al., *Evidence of a dominant negative mutant of yeast methionine aminopeptidase type 2 in Saccharomyces cerevisiae.* Journal of Cellular Biochemistry, 2004, **94**(4), 656-668.

69. Yang, G., et al., *Steady-state kinetic characterization of substrates and metal-ion specificities of the full-length and N-terminally truncated recombinant human methionine aminopeptidases (type 2).* Biochemistry, 2001, **40**(35), 10645-10654.

70. Lowther, W.T., et al., *The anti-angiogenic agent fumagillin covalently modifies a conserved active-site histidine in the Escherichia coli methionine aminopeptidase.* Proceedings of the National Academy of Sciences of the United States of America, 1998, **95**(21), 12153-12157.

71. Larrabee, J.A., T. Thamrong-nawasawat, and S.Y. Mon, *High-pressure liquid chromatographic method for the assay of methionine aminopeptidase activity: application to the study of enzymatic inactivation.* Analytical Biochemistry, 1999, **269**(1), 194-198.

72. Walker, K.W., E. Yi, and R.A. Bradshaw, *Yeast (Saccharomyces cerevisiae) methionine aminopeptidase I: rapid purification and improved activity assay.* Biotechnology and Applied Biochemistry, 1999, **29 (Pt 2)**, 157-163.

73. Zuo, S., Q. Guo, and Y.H. Chang, *A protease assay via precolumn derivatization and high-performance liquid chromatography.* Analytical Biochemistry, 1994, **222**, 514-516.

74. Cohen, S.A. and D.J. Strydom, *Amino acid analysis utilizing phenylisothiocyanate derivatives.* Analytical Biochemistry, 1988, **174**(1), 1-16.

75. Zhou, Y., et al., *Two continuous spectrophotometric assays for methionine aminopeptidase.* Analytical Biochemistry, 2000, **280**(1), 159-165.

76. Lee, H.J. and I.B. Wilson, *Enzymic parameters: measurement of V and Km.* Biochimica et Biophysica Acta, 1971, **242**(3), 519-522.

77. Copik, A.J., et al., *Kinetic and spectroscopic characterization of the H178A methionyl aminopeptidase from Escherichia coli.* Biochemistry, 2003, **42**(20), 6283-6292.

78. Oefner, C., et al., *The 1.15A crystal structure of the Staphylococcus aureus methionyl-aminopeptidase and complexes with triazole based inhibitors.* Journal of Molecular Biology, 2003, **332**(1), 13-21.

79. D'Souza V, M. and R.C. Holz, *The methionyl aminopeptidase from Escherichia coli can function as an iron(II) enzyme.* Biochemistry, 1999, **38**(34), 11079-11085.

80. D'Souza V, M., et al., *Divalent metal binding properties of the methionyl aminopeptidase from Escherichia coli.* Biochemistry, 2000, **39**(13), 3817-3826.

81. D'Souza V, M., et al., *Kinetic and structural characterization of manganese(II)-loaded methionyl aminopeptidases.* Biochemistry, 2002, **41**(43), 13096-13105.

82. Li, J.Y., et al., *Specificity for inhibitors of metal-substituted methionine aminopeptidase.* Biochemical and Biophysical Research Communications, 2003, **307**(1), 172-179.

83. Meng, L., et al., *Overexpression and divalent metal binding properties of the methionyl aminopeptidase from Pyrococcus furiosus.* Biochemistry, 2002, **41**(23), 7199-7208.

84. Walker, K.W. and R.A. Bradshaw, *Yeast methionine aminopeptidase I can utilize either Zn2+ or Co2+ as a cofactor: a case of mistaken identity?* Protein Science, 1998, **7**(12), 2684-2687.

85. Chen, L.L., et al., *Type I methionine aminopeptidase from Saccharomyces cerevisiae is a potential target for antifungal drug screening.* Acta Pharmacologica Sinica, 2004, **25**(7), 907-914.

86. Wang, J., et al., *Physiologically relevant metal cofactor for methionine aminopeptidase-2 is manganese.* Biochemistry, 2003, **42**(17), 5035-5042.

87. Li, J.Y., et al., *Characterization of full length and truncated type I human methionine aminopeptidases expressed from Escherichia coli.* Biochemistry, 2004, **43**(24), 7892-7898.

88. Albeck, A. and S. Kliper, *Mechanism of cysteine protease inactivation by peptidyl epoxides.* Biochemical Journal, 1997, **322 (Pt 3)**, 879-884.

89. BASF AG, *Verfahren zur Herstellung von Proteinen bestimmter N-terminaler Struktur mit Hilfe von Prokaryonten, Patent Number DE 3532134 A1.* Patent, 1987.
90. Sheppard, G.S., et al., *3-Amino-2-hydroxyamides and related compounds as inhibitors of methionine aminopeptidase-2.* Bioorganic and Medicinal Chemistry Letters, 2004, **14**(4), 865-868.
91. Wilce, M.C., et al., *Structure and mechanism of a proline-specific aminopeptidase from Escherichia coli.* Proceedings of the National Academy of Sciences of the United States of America, 1998, **95**(7), 3472-3477.
92. Griffith, E.C., et al., *Molecular recognition of angiogenesis inhibitors fumagillin and ovalicin by methionine aminopeptidase 2.* Proceedings of the National Academy of Sciences of the United States of America, 1998, **95**(26), 15183-15188.
93. Larsen, K.S. and D.S. Auld, *Carboxypeptidase A: mechanism of zinc inhibition.* Biochemistry, 1989, **28**(25), 9620-9625.
94. Folkman, J., *Tumor angiogenesis.* Advances in Cancer Research, 1974, **19**(0), 331-358.
95. Hanson, F.R. and T.E. Eble, *An antiphage agent isolated from aspergillussp.* Journal of Bacteriology, 1949, **58**, 527-529.
96. McCowen, M.C., M.E. Callender, and J.F. Lawlis, *Fumagillin (H-3), a New Antibiotic with Amebicidal Properties.* Science, 1951, **113**, 202-203.
97. Killough, J.H., G.B. Magill, and R.C. Smith, *The treatment of amebiasis with fumagillin.* Science, 1952, **115**(2977), 71-72.
98. Ingber, D., et al., *Synthetic analogues of fumagillin that inhibit angiogenesis and suppress tumour growth.* Nature, 1990, **348**, 555-557.
99. Dezube, B.J., et al., *Fumagillin analog in the treatment of Kaposi's sarcoma: a phase I AIDS Clinical Trial Group study. AIDS Clinical Trial Group No. 215 Team.* Journal of Clinical Oncology, 1998, **16**(4), 1444-1449.
100. Kruger, E.A. and W.D. Figg, *TNP-470: an angiogenesis inhibitor in clinical development for cancer.* Expert Opinion on Investigational Drugs, 2000, **9**(6), 1383-1396.
101. Kudelka, A.P., et al., *A phase I study of TNP-470 administered to patients with advanced squamous cell cancer of the cervix.* Clinical Cancer Research, 1997, **3**(9), 1501-1505.
102. Stadler, W.M., et al., *Multi-institutional study of the angiogenesis inhibitor TNP-470 in metastatic renal carcinoma.* Journal of Clinical Oncology, 1999, **17**(8), 2541-2545.
103. Bernier, S.G., et al., *A methionine aminopeptidase-2 inhibitor, PPI-2458, for the treatment of rheumatoid arthritis.* Proceedings of the National Academy of Sciences of the United States of America, 2004, **101**(29), 10768-10773.
104. Zhang, P., et al., *Angiogenesis inhibitors specific for methionine aminopeptidase 2 as drugs for malaria and leishmaniasis.* Journal of Biomedical Science, 2002, **9**(1), 34-40.
105. Logothetis, C.J., et al., *Phase I trial of the angiogenesis inhibitor TNP-470 for progressive androgen-independent prostate cancer.* Clinical Cancer Research, 2001, **7**(5), 1198-1203.
106. Pyun, H.J., et al., *Investigation of novel fumagillin analogues as angiogenesis inhibitors.* Bioorganic and Medicinal Chemistry Letters, 2004, **14**(1), 91-94.
107. Han, C.K., et al., *Design and synthesis of highly potent fumagillin analogues from homology modeling for a human MetAP-2.* Bioorganic and Medicinal Chemistry Letters, 2000, **10**(1), 39-43.
108. Inoue, K., et al., *Docetaxel enhances the therapeutic effect of the angiogenesis inhibitor TNP-470 (AGM-1470) in metastatic human transitional cell carcinoma.* Clinical Cancer Research, 2003, **9**(2), 886-899.
109. Tran, H.T., et al., *Clinical and pharmacokinetic study of TNP-470, an angiogenesis inhibitor, in combination with paclitaxel and carboplatin in patients with solid tumors.* Cancer Chemother Pharmacol, 2004, **54**(4), 308-314.
110. Sin, N., et al., *The anti-angiogenic agent fumagillin covalently binds and inhibits the methionine aminopeptidase, MetAP-2.* Proceedings of the National Academy of Sciences of the United States of America, 1997, **94**(12), 6099-6103.
111. Griffith, E.C., et al., *Methionine aminopeptidase (type 2) is the common target for angiogenesis inhibitors AGM-1470 and ovalicin.* Chemistry and Biology, 1997, **4**, 461-471.

112. D'Souza V, M., et al., *Characterization of the active site and insight into the binding mode of the anti-angiogenesis agent fumagillin to the manganese(II)-loaded methionyl aminopeptidase from Escherichia coli.* Journal of Biological and Inorganic Chemistry, 2004, **10**(1), 41-50.
113. Bontems, F., et al., *Homology modeling and calculation of the cobalt cluster charges of the Encephalitozoon cuniculi methionine aminopeptidase, a potential target for drug design.* Biophysical Chemistry, 2003, **105**(1), 29-43.
114. Schoellmann, G. and E. Shaw, *Direct evidence for the presence of histidine in the active center of chymotrypsin.* Biochemistry, 1963, **2**, 252-255.
115. Klein, C.D. and G. Folkers, *Understanding the selectivity of fumagillin for the methionine aminopeptidase type II.* Oncology Research, 2003, **13**(12), 513-520.
116. Brdlik, C.M. and C.M. Crews, *A single amino acid residue defines the difference in ovalicin-sensitivity between type I and II methionine aminopeptidases.* Journal of Biological Chemistry, 2003, **279**(10), 9475-9480.
117. Abe, J., et al., *A fumagillin derivative angiogenesis inhibitor, AGM-1470, inhibits activation of cyclin-dependent kinases and phosphorylation of retinoblastoma gene product but not protein tyrosyl phosphorylation or protooncogene expression in vascular endothelial cells.* Cancer Research, 1994, **54**(13), 3407-3412.
118. Wang, J., et al., *Tumor suppression by a rationally designed reversible inhibitor of methionine aminopeptidase-2.* Cancer Research, 2003, **63**(22), 7861-7869.
119. Turk, B.E., et al., *Selective inhibition of amino-terminal methionine processing by TNP-470 and ovalicin in endothelial cells.* Chemistry and Biology, 1999, **6**(11), 823-833.
120. Kanno, T., et al., *High expression of methionine aminopeptidase type 2 in germinal center B cells and their neoplastic counterparts.* Laboratory Investigation, 2002, **82**(7), 893-901.
121. Matsuzawa, T., M. Hatsugai, and K. Moriguchi, *Increase of methionine aminopeptidase activity in hyperplastic Leydig cells of rat cryptorchid testis: a histochemical study.* Journal of Veterinary Medical Science, 1992, **54**(6), 1157-1163.
122. Wang, J., P. Lou, and J. Henkin, *Selective inhibition of endothelial cell proliferation by fumagillin is not due to differential expression of methionine aminopeptidases.* Journal of Cellular Biochemistry, 2000, **77**(3), 465-473.
123. Yeh, J.R., R. Mohan, and C.M. Crews, *The antiangiogenic agent TNP-470 requires p53 and p21CIP/WAF for endothelial cell growth arrest.* Proceedings of the National Academy of Sciences of the United States of America, 2000, **97**(23), 12782-12787.
124. Towbin, H., et al., *Proteomics-based target identification: bengamides as a new class of methionine aminopeptidase inhibitors.* Journal of Biological Chemistry, 2003, **278**(52), 52964-52971.
125. Zetterberg, A., O. Larsson, and K.G. Wiman, *What is the restriction point?* Current Opinion on Cellular Biology, 1995, **7**(6), 835-842.
126. Xiong, Y., et al., *p21 is a universal inhibitor of cyclin kinases.* Nature, 1993, **366**(6456), 701-704.
127. Chun, E., et al., *Novel inhibitors targeted to methionine aminopeptidase 2 (MetAP2) strongly inhibit the growth of cancers in xenografted nude model.* International Journal of Cancer, 2005, **114**(1), 124-130.
128. Kusaka, M., et al., *Cytostatic inhibition of endothelial cell growth by the angiogenesis inhibitor TNP-470 (AGM-1470).* British Journal of Cancer, 1994, **69**(2), 212-216.
129. Catalano, A., et al., *Methionine aminopeptidase-2 regulates human mesothelioma cell survival: role of Bcl-2 expression and telomerase activity.* American Journal of Pathology, 2001, **159**(2), 721-731.
130. Wernert, N., et al., *Inhibition of Angiogenesis In Vivo by ets-1 Antisense Oligonucleotides-Inhibition of Ets-1 Transcription Factor Expression by the Antibiotic Fumagillin.* Angewandte Chemie International Edition Englisch, 1999, **38**(21), 3228-3231.
131. Sheen, I.S., et al., *Fumagillin treatment of hepatocellular carcinoma in rats: An in vivo study of antiangiogenesis.* World Journal of Gastroenterology, 2005, **11**(6), 771-777.
132. Wang, J., N. Quan, and J. Henkin, *Human endothelial cells are exceptionally sensitive to loss of methionine aminopeptidase-2 (MetAP-2).* Proceedings of the Annual Meeting of the American Association for Cancer Research, 1998, **39**, 98.
133. Kim, S., et al., *Depletion of methionine aminopeptidase 2 does not alter cell response to fumagillin or bengamides.* Cancer Research, 2004, **64**(9), 2984-2987.

134. Udagawa, T., et al., *Cytochalasin E, an Epoxide Containing Aspergillus-Derived Fungal Metabolite, Inhibits Angiogenesis and Tumor Growth.* Journal of Pharmacology and Experimental Therapeutics, 2000, **294**, 421-427.

135. Aurora, R. and S.B. Dotson, *Methionine aminopeptidase type 3, Patent Number US 6,638,750 B1.* United States Patent Office, 2003.

136. Klein, C.D., et al., *Protonation states of methionine aminopeptidase and their relevance for inhibitor binding and catalytic activity.* Journal of Biological Chemistry, 2003, **278**(48), 47862-47867.

137. Jorgensen, A.T., P.O. Norrby, and T. Liljefors, *Investigation of the metal binding site in methionine aminopeptidase by density functional theory.* Journal of Computer-Aided Molecular Design, 2002, **16**(3), 167-179.

138. Zhang, Z.Y., J.P. Davis, and R.L. Van Etten, *Covalent modification and active site-directed inactivation of a low molecular weight phosphotyrosyl protein phosphatase.* Biochemistry, 1992, **31**(6), 1701-1711.

139. Bertini, I. and C. Luchinat, *University Science Books*, in *Bioinorganic Chemistry*, I. Bertini, et al., Editors. 1994: Sausalito, CA, 37-106.

140. Suarez, D., N. Diaz, and K.M. Merz, Jr., *Molecular dynamics simulations of the dinuclear zinc-beta-lactamase from Bacteroides fragilis complexed with imipenem.* Journal of Computational Chemistry, 2002, **23**(16), 1587-600.

141. Schürer, G., et al., Journal of Physical Chemistry B., 2002, **106**, 8815-8830.

142. Keding, S.J., et al., *Synthesis of (3R)-Amino-(2S)-hydroxy Amino Acids for Inhibition of Methionine Aminopeptidase-1.* Synthetic Communications, 1998, **28**, 4463-4470.

143. Hu, X., et al., *Peptidyl hydroxamic acids as methionine aminopeptidase inhibitors.* Bioorganic and Medicinal Chemistry Letters, 2004, **14**(1), 77-79.

144. Garrabrant, T., et al., *Small molecule inhibitors of methionine aminopeptidase type 2 (MetAP-2).* Angiogenesis, 2004, **7**(2), 91-96.

145. Ye, Q.Z., et al., *Metalloform-selective inhibitors of escherichia coli methionine aminopeptidase and X-ray structure of a Mn(II)-form enzyme complexed with an inhibitor.* Journal of the American Chemical Society, 2004, **126**(43), 13940-13941.

146. Luo, Q.L., et al., *Discovery and structural modification of inhibitors of methionine aminopeptidases from Escherichia coli and Saccharomyces cerevisiae.* Journal of Medicinal Chemistry, 2003, **46**(13), 2631-2640.

147. Corporation, S.B., et al., *Compounds and methods, Patent Number WO 03/051906 A2.* International Patent, 2003.

148. Marino, J.P.J., S.K. Thompson, and D.F. Veber, *Compounds and methods, Patent Nr. PCT/US04/0116490 A1.* United States Patent Office, 2004.

149. Douangamath, A., et al., *Crystal structures of Staphylococcusaureus methionine aminopeptidase complexed with keto heterocycle and aminoketone inhibitors reveal the formation of a tetrahedral intermediate.* Journal of Medicinal Chemistry, 2004, **47**(6), 1325-1328.

150. Grover, J.K., et al., *Anthelmintics: a review.* Tropical Gastroenterology, 2001, **22**(4), 180-189.

151. Bartlett, M.S., et al., *Antimicrotubule benzimidazoles inhibit in vitro growth of Pneumocystis carinii.* Antimicrobial Agents and Chemotherapy, 1992, **36**(4), 779-782.

152. Davidse, L.C. and W. Flach, *Interaction of thiabendazole with fungal tubulin.* Biochimica et Biophysica Acta, 1978, **543**(1), 82-90.

153. Burland, T.G. and K. Gull, *Molecular and cellular aspects of the interaction of benzimidazole fungicides with tubulin and microtubules*, in *Mode of action of antifungal agents*, A.P.J. Trinci and J.F. Ryley, Editors. 1984, Cambridge University Press: Cambridge, 299-320.

154. Burland, T.G., et al., *Genetic analysis of resistance to benzimidazoles in Physarum: differential expression of beta-tubulin genes.* Genetics, 1984, **108**(1), 123-141.

155. Mendz, G.L., S.L. Hazell, and S. Srinivasan, *Fumarate reductase: a target for therapeutic intervention against Helicobacter pylori.* Archives of Biochemistry and Biophysics, 1995, **321**(1), 153-159.

156. Prichard, R.K., *Mode of action of the anthelminthic thiabendazole in Haemonchus contortus.* Nature, 1970, **228**(272), 684-685.

157. Sanchez-Moreno, M., et al., *Inhibition of superoxide dismutase from Ascaris suum by benzimidazoles and synthesized pyrimidine and glycine derivatives.* Pharmacology, 1996, **52**(1), 61-68.

158. McCracken, R.O. and W.H. Stillwell, *A possible biochemical mode of action for benzimidazole anthelmintics.* International Journal for Parasitology, 1991, **21**(1), 99-104.

159. Criado Fornelio, A., F. Rodriguez Caabeiro, and A. Jimenez Gonzalez, *The mode of action of some benzimidazole drugs on Trichinella spiralis.* Parasitology, 1987, **95 (Pt 1)**, 61-70.

160. Allen, P.M. and D. Gottlieb, *Mechanism of action of the fungicide thiabendazole, 2-(4'-thiazolyl) benzimidazole.* Applied Microbiology, 1970, **20**(6), 919-926.

161. Stutzenberger, F.J. and J.N. Parle, *Effect of 2-substituted benzimidazoles on the fungus Pithomyces chartarum.* Journal of General Microbiology, 1973, **76**(1), 197-209.

162. Brown, H.D., et al., *Antiparasitic drugs. IV. 2-(4'thiazolyl)-benzimidazole, a new anthelmintic.* Journal of the American Chemical Society, 1961, **83**, 1764-1765.

163. Staron, T. and C. Allard, *Propriétés antifongiques du 2-(4'thiazolyl)benzimidazole ou thiabendazole.* Phytiatrie-Phytopharmacie, 1964, **13**(163-168).

164. Sarcina, M. and C.W. Mullineaux, *Effects of tubulin assembly inhibitors on cell division in prokaryotes in vivo.* FEMS Microbiology Letters, 2000, **191**(1), 25-29.

165. Katz, M., *Anthelmintics.* Drugs, 1977, **13**(2), 124-136.

166. Namisato, S., et al., *Pulmonary strongyloidiasis in a patient receiving prednisolone therapy.* Internal Medicine, 2004, **43**(8), 731-736.

167. Hachim, K., et al., *[Severe strongyloidiasis in a chronic haemodialysis patient].* La Presse Medicale, 2005, **34**(2 Pt 1), 105-106.

168. Vanden Bossche, H., M. Engelen, and F. Rochette, *Antifungal agents of use in animal health--chemical, biochemical and pharmacological aspects.* Journal of Veterinary Pharmacology and Therapeutics, 2003, **26**(1), 5-29.

169. Cheng, Y. and W.H. Prusoff, *Relationship between the inhibition constant (K1) and the concentration of inhibitor which causes 50 per cent inhibition (I50) of an enzymatic reaction.* Biochemical Pharmacology, 1973, **22**(23), 3099-3108.

170. Segel, I.H., *Enzyme kinetics*. Wiley Classic Library Edition published 1993 ed. 1975: John Wiley & Sons, Inc.

171. Roderick, S.L. and B.W. Matthews, *Crystallization of Methionine Aminopeptidase from Escherichia coli.* Journal of Biological Chemistry, 1988, **263**, 16531.

172. Laskowski, R.A., et al., *PROCHECK: a program to check the stereochemical quality of protein structures.* Journal of Applied Crystallography, 1993, **26**(2), 283-291.

173. Spraggon, G., et al., *Crystal structure of a methionine aminopeptidase (TM1478) from Thermotoga maritima at 1.9 A resolution.* Proteins, 2004, **56**(2), 396-400.

174. Katz, B.A., et al., *Design of potent selective zinc-mediated serine protease inhibitors.* Nature, 1998, **391**(6667), 608-612.

175. Hisano, T., et al., *Synthesis of Benzoxazoles, Benzothiazoles, Benzimidazoles and Evaluation of their antifungal, insecticidal and herbicidal activity.* Chemical and Pharmaceutical Bulletin, 1982, **30**(8), 2996-3004.

176. Mothilal, K.K., et al., *Synthesis, X-ray crystal structure, antimicrobial activity and photodynamic effects of some thiabendazole complexes.* Journal of Inorganic Biochemistry, 2004, **98**(2), 322-332.

177. Kowala, B., et al., *Transition metal complexes of thiabendazole.* Australian Journal of Chemistry, 1971, **24**, 1369-1375.

178. Hanessian, S. and S. Johnstone, *Synthesis of hydroxamic esters via alkoxyaminocarbonylation of ß-dicarbonyl compounds.* Journal of Organic Chemistry, 1999, **64**, 5896-5903.

179. Corey, E.J., et al., *Formation of olefins via pyrolysis of sulfonate esters.* Journal of Organic Chemistry, 1989, **54**, 389-393.

180. Boyer, F.E., et al., *5,6-Dihydropyran-2-ones possessing various sulfonyl functionalities: potent nonpeptidic inhibitors of HIV protease.* Journal of Medicinal Chemistry, 2000, **43**(5), 843-858.

181. Skulnick, H.I., et al., *Structure-based design of nonpeptidic HIV protease inhibitors: The sulfonamide-substituted cyclooctylpyranones.* Journal of Medicinal Chemistry, 1997, **40**, 1149-1164.

182. Honma, T., et al., *Structure-based generation of a new class of potent Cdk4 inhibitors: new de novo design strategy and library design.* Journal of Medicinal Chemistry, 2001, **44**(26), 4615-4627.

183. Högberg, T., et al., *Synthesis of pyridylallylamines related to zimelidine and their inhibition of neuronal monoamine uptake.* Journal of Medicinal Chemistry, 1981, **24**, 1499-1507.

184. Schaefer, F.C. and G.A. Peters, *Base-Catalyzed Reaction of Nitriles with Alcohols. A Convenient Route to Imidates and Amidine Salts.* Journal of Organic Chemistry, 1960, **26**, 412-417.

185. Sprinson, B.D. and C. E., *A Study of β-Hydroxy-α-Keto Acids.* Journal of Biological Chemistry, 1946, **164**, 417-432.

186. Jagoe, C.T., Ph. D. Thesis, Boston College, 1991, 154-288.

187. Kumar, S., A.L. Pearson, and R.F. Pratt, *Design, synthesis, and evaluation of alpha-ketoheterocycles as class C beta-lactamase inhibitors.* Bioorganic and Medicinal Chemistry, 2001, **9**(8), 2035-2044.

188. Sato, N., *Studies on pyrazines. 18. A new and convenient synthesis of 2-amino-3-cyanopyrazine.* Journal of Heterocyclic Chemistry, 1989, **26**, 817-819.

189. Sato, N., N. Miwa, and N. Hirokawa, *Studies on pyrazines. Part 27. A new deoxidative nucleophilic substitution of pyrazine N-oxides; synthesis of azidopyrazines with trimethylsilylazide.* Journal of the Chemical Society, Perkin Transactions 1: Organic and Bio-Organic Chemistry, 1994, 885-888.

190. Sato, N., T. Matsuura, and N. Miwa, *Studies on pyrazines. Part 30: Synthesis of aminopyrazines from azidopyrazines.* Synthesis, 1994, **9**, 931-934.

191. Efange, S.M., et al., *N-hydroxyalkyl derivatives of 3 beta-phenyltropane and 1-methylspiro[1H-indoline-3,4'-piperidine]: vesamicol analogues with affinity for monoamine transporters.* Journal of Medicinal Chemistry, 1997, **40**(24), 3905-3914.

192. Efange, S.M., et al., *Acyclic analogues of 2-(4-phenylpiperidino)cyclohexanol (vesamicol): conformationally mobile inhibitors of vesicular acetylcholine transport.* Journal of Medicinal Chemistry, 1991, **34**(8), 2638-2643.

193. Lemini, C., et al., *Synthesis of aldehydes from oxiranes using silica gel as reactant.* Synthetic Communications, 1995, **25**(18), 2695-2702.

194. Borredon, E., M. Delmas, and A. Gaset, *Epoxydation d'aldehydes et de cetones püar un procede de transfert solide-liquide.* Tetrahedron Letters, 1982, **23**(50), 5283-5286.

195. Borredon, E., et al., *Epoxide synthesis in interfacial solid-liquid conditions.* Journal of Organic Chemistry, 1990, **55**, 501-504.

196. Bouda, H., et al., *Aldehydes and ketones epoxidation with trimethylsulfonium bromide in a slightly hydrated solid-liquid medium.* Synthetic Communications, 1987, **17**(5), 503-513.

197. Borredon, M.E., et al., *Epoxydation en milieu heterogene solide-liquide fablement hydrate I: Etude des interactions moleculaires: Sel de sulfonium-base.* Tetrahedron, 1987, **43**(18), 4141-4146.

198. Borredon, M.E., M. Delmas, and A. Gaset, *Epoxydation en milieu heterogene solide-liquide faiblement hydrate II: Rôle de l'eau et schéma réactionnel.* Tetrahedron, 1988, **44**(4), 1073-1077.

199. Nudelman, A., et al., *Hypoxic radiosensitizers: substituted styryl derivatives.* Archiv der Pharmazie (Weinheim), 1994, **327**(10), 619-625.

200. Alvarez, M., et al., *Synthesis of 2-hydroxy-2-phenylethylamino derivatives as potential a-adrenergic blocking agents.* Journal of Heterocyclic Chemistry, 1985, **22**, 745-750.

201. Neumeyer, J.L., et al., *Development of a high affinity and stereoselective photoaffinity label for the D-1 dopamine receptor: synthesis and resolution of 7-[125I]iodo-8-hydroxy-3-methyl-1-(4'-azidophenyl)-2,3,4,5-tetrahydro- 1H-3-benzazepine.* Journal of Medicinal Chemistry, 1990, **33**(2), 521-526.

202. Iwasaki, T., K. KNobuhiro, and T. Endo, *Reaction of various oxiranes and carbon dioxide. Synthesis and aminolysis of five-membered cyclic carbonates.* Bulletin of the Chemical Society of Japan, 2000, **73**, 713-719.

203. Becker, H.G., et al., *D. 7.2.8. Esterkondensation*, in *Organikum: organisch-chemisches Grundpraktikum*. 1999, Wiley-VCH: Weinheim, 512-520.

204. Becker, H.G., et al., *D. 7.2.3. Aldolreaktion*, in *Organikum: organisch-chemisches Grundpraktikum.* 1999, Wiley-VCH: Weinheim, 491-499.

205. Jonczyk, A., M. Fedorynski, and M. Makosza, *Reactions of organic anions. XLIII. Catalytic method for synthesis of glycidic nitriles in aqueous medium.* Tetrahedron Letters, 1972, **23**, 2395-2396.

206. Kochetkov, N.K., É.E. Nifant'ev, and V.N. Shibaev, *Synthesis of Acyl-2-chlorocyclohexenes-2 and ethylene ketals of 2-acylcyclohexanones.* Journal of the general chemistry of the USSR (engl. Transl. of Zhurnal Obshchei Khimii), 1960, **30**(7), 2275-2282.

207. Harvey, W.E. and J.O. Miners, *The Synthesis of Diepoxide Analogues of Fumagillin.* Australian Journal of Chemistry, 1979, **32**, 2473-2481.

208. Yasui, K., et al., *Unsymmetrical ketone synthesis via a three-component conection reaction of organozincs, allylating agents, and carbon monoxide.* Journal of Organic Chemistry, 1995, **60**, 1365-1380.

209. Clark-Lewis, J.W. and M.J. Thompson, *Methylation of 3-Aminopyridines and Preparation of 2-Amino-3-methylaminopyridine and 2:3-Diaminopyridine.* Journal of the Chemical Society, 1957, 442-446.

210. Misra, P.K., et al., *3-Hydroxypropionitrile: A new reagent for carboxyl protection in protein synthesis.* Tetrahedron Letters, 1989, **30**(27), 3569-3572.

211. Goulaouic-Dubois, C., A. Guggisberg, and M. Hesse, *Protection of amines by the pyridine-2-sulfonyl group and its cleavage under mild conditions (SmI2 or electrolysis).* Journal of Organic Chemistry, 1995, **60**, 5969-5972.

212. Caldwell, W.T. and E.C. Kornfeld, *Substituted 2-sulfonamido-5-aminopyridines.* Journal of the American Chemical Society, 1942, **64**, 1695-1698.

213. Cassidy, F., et al., *Synthesis and antihypertensive activity of 3-[(substituted-carbonyl)amino]-2H-1-benzopyrans.* Journal of Medicinal Chemistry, 1992, **35**(9), 1623-1627.

214. Hemmerich, P. and S. Fallab, *Zum Verhalten des Riboflavins und strukturverwandter Verbindungen gegeüber Metallionen.* Helvetica Chimica Acta, 1958, **41**, 498-508.

215. Lee, I.-S.H., E.H. Jeoung, and K.L. Lee, *Synthesis and tautomerism of 2-aryl and 2-heteroaryl derivatives of benzimidazole.* Journal of Heterocyclic Chemistry, 1996, **33**, 1711-1716.

216. Krishnaswamy, N.R. and C.N. Sundaresan, *5-Amino-3H-1,2,4-dithiazole-3-thione as a synthon: New synthesis of 2-thioureidobenzheteroazoles.* Heteroatom Chemistry, 1994, **5**(5/6), 567-569.

217. Jen, T., et al., *Amidines and related compounds. 6. Studies on structure-activity relationships of antihypertensive and antisecretory agents related to clonidine.* Journal of Medicinal Chemistry, 1975, **18**(1), 90-99.

218. Bergmann, F.G., M.A. Kleiner, and M. Rashi, *New Substituted Purines and Purine Derivatives, Patent Number 1,201,997A.* United States Patent Office, 1968.

219. Maynard, J.A., et al., *Reaction of 2-(4'-Thiazolyl)Benzimidazole (Thiabendazole) with alkyl halides.* Australian Journal of Chemistry, 1971, **24**, 1873-1881.

220. Haugwitz, R.D., et al., *Antiparasitic agents. 3. Synthesis and anthelmintic activities of novel 2-pyridinyl-5-isothiocyanatobenzimidazoles.* Journal of Medicinal Chemistry, 1979, **22**(9), 1113-1118.

221. Sarett, L.H. and H.D. Brown, *5-(or 6)-Halo(or Amino)benzazoles and methods for preparing same, Patent Number 3,478,046.* United States Patent Office, 1969.

222. Kim, J.S., et al., *Terbenzimidazoles: influence of 2"-, 4-, and 5-substituents on cytotoxicity and relative potency as topoisomerase I poisons.* Journal of Medicinal Chemistry, 1997, **40**(18), 2818-2824.

223. Sun, Q., et al., *Synthesis and evaluation of terbenzimidazoles as topoisomerase I inhibitors.* Journal of Medicinal Chemistry, 1995, **38**(18), 3638-3644.

224. Laemmli, U.K., *Cleavage of structural proteins during the assembly of the head of bacteriophage T4.* Nature, 1970, **227**(5259), 680-685.

225. Inoue, H., H. Nojima, and H. Okayama, *High efficiency transformation of Escherichia coli with plasmids.* Gene, 1990, **96**(1), 23-28.

226. Neumann, E., et al., *Gene transfer into mouse lyoma cells by electroporation in high electric fields.* EMBO Journal, 1982, **1**(7), 841-845.

227. Sambrook, F., E.F. Fritsch, and T. Maniatis, *Molecular Cloning. A laboratory manual.* Cold Spring Harbor Press, 1989.

228. Otwinowski, Z. and W. Minor, *Processing of X-ray Diffraction Data Collected in Oscillation Mode.* Methods in Enzymology, 1997, **276: Macromolecular Crystallography, part A**, 307-326.

229. Storoni, L.C., A.J. McCoy, and R.J. Read, *Likelihood-enhanced fast rotation functions.* Acta Crystallographica, D Biological Crystallography, 2004, **60**(Pt 3), 432-438.

230. Brunger, A.T., et al., *Crystallography & NMR system: A new software suite for macromolecular structure determination.* Acta Crystallographica, D Biological Crystallography, 1998, **54 (Pt 5)**, 905-921.

231. Sheldrick, G.M. and T.R. Schneider, *SHELXL: High resolution Refinement.* Methods in Enzymology, 1997(277B), 319-343.

232. Jones, T.A., et al., *Improved methods for building protein models in electron density maps and the location of errors in these models.* Acta Crystallographica, A Foundations of Crystallography, 1991, **47 (Pt 2)**, 110-119.

233. DeLano, W.L., The PyMOL Molecular Graphics System (2002) on World Wide Web http://www.pymol.org.

10 Abbreviations

σ	Mean deviation, measurement for the level of density
(br)	Broad
AAO	L-Amino acid oxidase
b.p.	Boiling Point
BSA	Bovine Serum Albumine
CCl_4	Tetrachlormethane
CH_2Cl_2	Dichloromethane
Da	Dalton
DMF	Dimethylformamid
DMSO	Dimetylsulfoxid
DTNB	5,5'-dithiobis(2-nitrobenzoic acid)
DTT	Dithiothreitol
EDTA	ethylene diamine tetra acetic acid
EtOH	Ethanol
Fig.	Figure
g	Gram
h	Hour
hrs	Hours
HPLC	High Pressure Liquid Chromatography (Hochdruckflüssigkeitschromatographie)
HRP	Horseradish Peroxidase
IC_{50}	Inhibitor concentration to inhibit 50 % of the enzyme activity
IPTG	Isopropyl-ß-D-thiogalactopyranosid
IR	Infra red spectroscopy
J	Coupling constant
kDa	Kilodalton
l	Liter
LB	Luria Bertani Medium
m	Meta (substituted); multiplet
M	Molar
m-CPBA	meta-Chlorperbenzoic acid (MCPBA)
MeOH	Methanol
mg	Milligramm
MGMM	NH_2-Met-Gly-Met-Met-COOH
min	Minute(s)
mM	Millimolar

m.p.	Melting point
MW	Molecular Weight
nm	Nanometer
NMR	Nuclear Magnetic Resonance Spectroscopy
OD	Optical Density
OD_{280}	Optical Density at 280 nm
OS	Octanoylsucrose
p	Page
PAGE	Polyacrylamide Gel Electrophoresis
pH	negative dekadic logarithm of the protein concentration
pKa	negative dekadic logarithm of the dissociation constants of acids
PMSF	Phenylmethylsulfonylfluoride
ppm	Parts per million
r	Korrelation coefficient
RNA	Ribonucleic Acid
SDS	Sodiumdodecylsulfat
sec	second
t-BuOOH	tert.-Butylperoxide
TFA	Trifluoro acetic acid
THF	Tetrahydrofuran
TLC	Thin Layer Chromatography
Temed	N,N,N',N'-tetramethylethylenediamine
TMS	Tetramethylsilane
Tris	2-Amino-2-Hydroxymethyl-1,3-Propandiol
U	Unit(s)
V	Volt
v/v	volume per volume
w/v	weight per volume

11 Danksagung

Ich danke:

Prof. Dr. R. W. Hartmann für das entgegengebrachte Vertrauen und die Möglichkeit, an seinem Lehrstuhl promovieren zu können.

Dr. C. D. Klein für die Vergabe eines so interessanten und heterogenen Themas sowie die gute Betreuung, die vielen hilfreichen Diskussionen bzw. die vielen wertvollen Tipps bei der Durchführung der Arbeit und die unkomplizierte sowie fruchtbare Zusammenarbeit.

Prof. Dr. A. K. Kiemer für die Übernahme des Vorsitzes in der Prüfungskommission.

Dr. B. Diesel für die Übernahme des Beisitzers in der Prüfungskommission.

Prof. Dr. G. Klebe für die Möglichkeit, mit der Kristallographie ein bis dahin für mich unbekanntes Gebiet kennen zu lernen und dem gesamten Arbeitskreis für die freundliche Aufnahme. Besonderer Dank geht an

Dr. A. Heine „Röntgengott“ für seine umfassende Hilfe in allen Fragen und seine fast unvergleichliche Art, auch einem Laien wie mir Zusammenhänge und Wissen zu vermitteln.

Christian Sohn für die nette Beratung in allen technischen Fragen.

Dr. A. Di Fenza, Dr. C. Sotriffer, Dr. P. Block, Matthias Zentgraf, Alexander Hillebrecht, Oliver Koch, Naomi Tidten, Yark Boettcher, Holger Steuber und alle anderen, die dazu beigetragen haben, dass ich mich in Marburg sehr wohl gefühlt habe.

Prof. Dr. R. Bernhard für die Bereitstellung von Geräten zur Proteinaufreinigung. Besonderer Dank geht an:

Dr. B. Schiffler und Wolfgang Reinle, die immer hilfsbereit waren, mir viele Tricks gezeigt haben und immer zur Stelle waren, wenn es nötig war. Danke.

Ich danke allen (auch ehemaligen und zukünftigen) Mitgliedern des Arbeitskreises für das unvergleichliche Arbeitsklima und die vielen netten Grillabende, insbesondere

Martina Palzer und Anja Palusczak für ihre stetige Hilfsbereitschaft und immer gute Laune.

Lothar Jager, Angelika Mohseni-Tehrani und Dr. Peter Dorfmüller für den immer prompten Einsatz in technischen Notfällen und bei der Bereitstellung von Materialien.

Dr. Thomas Bild für die lustige Zeit, auch dann, wenn es mal nicht so gelaufen ist (also ca. 4 Jahre ☺), die zeitweise Pflege der „Wallac-Maschin“ und seine Freundschaft.

Eben dieser „Wallac-Maschin“ für die Messung zahlloser Assays ohne technische Ausfälle oder Störungen.

Dr. Bärbel Panther und Dr. Peter Ehmer für die angenehmen Zusammenarbeit bei der Betreuung diverser Semester.

Dr. Sarah Ulmschneider für stetige Hilfsbereitschaft und die vielen netten Gespräche, nicht zu vergessen die leckeren Cocktails.

Elisa Winterer, Christiane Scherer, Christina Ries, Sigrid Ziegler, Ursula Müller-Viera und Patrizia Kruchten für die stets gute Laune im Computerraum.

Dr. Martin Frotscher, Dr. Kerstin Jahn-Hoffmann, Dr. Marc Bartels, Emmanuel Bey, Adriane Stroba und Erika Ziegler für die kompetente Hilfe in allen Synthese-Fragen.

Christian Grimstein, Eva Kremser, Kerstin Schlitzke und Markus Altmeyer dafür, dass sie als Projektpraktikanten im Rahmen dieser Arbeit tätig waren und einige gute Ergebnissen produziert haben. Ich hoffe, es hat neben der Arbeit auch Spaß gemacht.

Dr. Stefan Böttcher, Mariano Pinto und Marcel Holzer für die vielen netten LAN-Partys - auch wenn ich oft nur „das Opfer“ war. Ich hoffe auf Revanche.

Anke Bachelier für die Hilfe bei biochemischen Fragen und allem, was mit Gelen, Säulen und Proteinen zu tun hat.

Corina Przybyla und Dana Wienhold für die gute Laune im Sekretariat und dafür, dass sie bei Einladungen für AK-Feiern immer noch an mich denken.

Dr. Eva-Maria Müller für die Überlassung diverser Fische (ja, denen geht es immer noch gut).

Patrick Frotscher und Dirk Betscheider für den Beistand bei allen Computerproblemen (und natürlich auch deren Lösung), die Festplattenrettungsaktion und diverse Weizenbierchen.

Dr. Alex Neugebauer für die gute Zusammenarbeit bei der Entwicklung neuer Scoring-Funktionen unter Berücksichtigung von Metallionen.

Dr. Ulrich Dossou „Slayer“ für seine ungekrönten Vorstellungen bei diversen Promotionsfeiern und AK-Fahrten.

Martina einfach für alles, besonders aber dafür, dass sie mich in der Zeit des Zusammenschreibens (und nicht nur da) „ertragen“ hat und für ihre Liebe.

Meiner Familie, dass sie mich immer unterstützt haben und immer für mich da sind.

Ich danke allen, die mich während der Promotion begleitet haben und ihren Teil dazu beigetragen haben, dass ich diese Zeit in guter Erinnerung behalten werde. Bei allen, die ich vergessen haben sollte, möchte ich mich hiermit entschuldigen.

Vielen Dank für die gute Zeit und viel Glück, Rolf